N AND O ISOTOPE RATIOS OF NO_3^- AS A TRACER FOR NITROGEN CYCLING AND WATER MASS DISTRIBUTION

by

Nadine Lehmann

Submitted in partial fulfillment of the requirements
for the degree of Doctor of Philosophy

at

Dalhousie University
Halifax, Nova Scotia
October 2019

TABLE OF CONTENTS

LIST OF TABLES

LIST OF FIGURES

ABSTRACT

Nitrogen plays a central role in marine biogeochemistry. Its distribution, chemical speciation and ratio relative to other nutrients governs the presence and abundance of microbial communities, and of large scale ocean production. In this respect, my thesis examines how biochemical and physical processes regulate the distribution of different nitrogen (N) species and their transformation in various marine environments by evaluating the spatial distribution of nitrogen and oxygen isotopes of nitrate (NO_3^-), in combination with a varying set of complementary biogeochemical tracers. Chapter 2 examines the isotopic composition of NO_3^- and total dissolved inorganic carbon (DIC) to elucidate the hydrography of the Western Equatorial Pacific (WEP) and biogeochemical evolution of water masses that contribute to the Equatorial Undercurrent (EUC). Based on isotope data and water mass mixing estimates, I highlight the different biogeochemical histories of nutrients feeding the northern and southern WEP, and provide support for the theory of a predominantly Southern Ocean source of NO_3^- to the EUC. Chapter 3 focuses on Baffin Bay, which represents a major link between the high Arctic and the northwestern Atlantic, owing to its effect on the salt and nutrient budgets of the adjacent Labrador Sea and the wider Atlantic Ocean. I combine NO_3^- isotope ratios with nitrous oxide (N_2O) isotope measurements to identify the origin of the pronounced N-deficit and N_2O supersaturation prevalent in deep Baffin Bay. The set of isotopic tracers used in this study allows the identification of different, yet complementary, N transformation processes. NO_3^- isotopes reflect substantial in situ remineralization of organic matter originating from surface productivity fueled by Pacific-derived nutrients, whereas N_2O isotopomer abundances point to sedimentary denitrification as a potential source of the N-deficiency observed in the deep basin. In chapter 4, I use NO_3^- isotope ratios measured in the Canada Basin and in the Baffin Bay together with hydrographic data and nutrient ratios as a baseline to evaluate the distribution of Pacific- and Atlantic-derived water masses throughout the Arctic Archipelago. With this work, I highlight the importance and applicability of dual isotope measurements as water mass tracers and provide insights into individual processes within the N cycle.

List of Abbreviations and Symbols Used

Abbreviations	Description
AAIW	Antarctic Intermediate Water
AOU	Apparent oxygen utilization
ATCC	American Type Culture Collection
AW	Atlantic Water
BBBW	Baffin Bay Bottom Water
BBDW	Baffin Bay Deep Water
BIC	Baffin Island Current
BL	Barrier Layer
BS	Barents Sea
CAA	Canadian Arctic Archipelago
CB	Canada Basin
CCGS	Canadian Coast Guard Ship
CTD	Conductivity-temperature-depth
DIC	Dissolved inorganic carbon
DIN	Dissolved inorganic nitrogen
EAC	Eastern Australian Current
EqPIW	Equatorial Pacific Intermediate Water
EUC	Equatorial Undercurrent
FS	Fram Strait
GBRUC	Great Barrier Reef Undercurrent
HE	Halmahera Eddy
HL	Halocline layer
IAEA	International Atomic Energy Agency
IW	Intermediate water
JS	Jones Sound
LCDW	Lower Circumpolar Deep Water
LHL	Lower halocline layer

Abbreviations	Description
LLWBC	Low-Latitude Western Boundary Current
LS	Lancaster Sound
LSW	Labrador Sea Water
MC	Mindanao Current
ME	Mindanao Eddy
MUC	Mindanao Undercurrent
NB	New Britain
NBCU	New Britain Coastal Undercurrent
NCJ	North Caledonian Jet
NEADW	Northeast Atlantic Deep Water
NEC	North Equatorial Current
NECC	North Equatorial Countercurrent
NGCC	New Guinea Coastal Current
NGCUC	New Guinea Coastal Undercurrent
NH	New Hanover
NI	New Ireland
NICU	New Ireland Coastal Undercurrent
NOW	North Water polynya
NPIW	North Pacific Intermediate Water
NPTW	North Pacific Tropical Water
NS	Nares Strait
NSCC	Northern Subsurface Countercurrent
NVJ	North Vanuatu Jet
ODZ	Oxygen Deficient Zone
PDW	Pacific Deep Water
PNG	Papua New Guinea
PSW	Pacific Summer Water
PWW	Pacific Winter Water
SAMW	Subantarctic Mode Water
SCJ	South Caledonian Jet
SD	Standard deviation

Abbreviations	Description
SEC	South Equatorial Current
SECC	South Equatorial Countercurrent
SGU	St. Georges Undercurrent
SI	Solomon Islands
SICU	Solomon Island Undercurrent
SP	Site preference
SPTW	South Pacific Tropical Water
SSCC	Southern Subsurface Countercurrent
UCDW	Upper Circumpolar Deep Water
UHL	Upper halocline layer
USGS	United States Geological Survey
VSMOW	Vienna standard mean ocean water
WEP	Western Equatorial Pacific
WGC	West Greenland Current
WOCE	World Ocean Circulation Experiment
WOD	World Ocean Database
WSPCW	Western South Pacific Central Water

Greek symbol	Description	Units
α	central N atom in nitrous oxide	
β	outer N atom in nitrous oxide	
δ	relative difference of isotope ratios between sample and standard	‰
Δ	nitrate isotope anomaly	‰
ϵ	isotope effect	‰
σ_θ	sigma-theta of water	$\mathrm{kg\,m^{-3}}$
θ	potential temperature of water	°C

ACKNOWLEDGEMENTS

First and foremost I would like to thank my supervisor Markus Kienast for offering me the great opportunity to work on this project. I would also like to thank him for his advice and guidance throughout the past years, and for sharing his incredible optimism and curiosity in regard to science (and beyond).

Further, I would like to thank my committee members Carolyn Buchwald, Katja Fennel and Helmuth Thomas for many constructive comments that helped to improve my thesis.

I also want to acknowledge all collaborators involved in the different parts of this thesis. Special thanks go to Julie Granger for sharing her insights and enthusiasm for stable isotope, as well as to her and her lab members Lija Treibergs, Richard Dabundo and Danielle Boshers for their assistance in the lab and for providing such a welcoming environment during my stay in Connecticut. Thanks also go to Annie Bourbonnais for opening up her home to me during my visit in Massachusetts. Further, I thank Alfonso Mucci for generously sharing seawater isotope data collected during the 2015 Canadian GEOTRACES expedition included in chapter 3 and 4.

I gratefully acknowledge the captain and crew of the RV Sonne SO-228 for contributing to a successful expedition in the western Pacific, and the captain and crew of the *CCGS Amundsen* as well as the science crew of the Canadian Arctic GEOTRACES program for their assistance during the sampling campaign and for making two weeks being stuck in the ice a surprisingly pleasant experience.

For my research and studies, I received funding from the Natural Sciences and Engineering Research Council of Canada (NSERC) and its CREATE program (Collaborative Research and Training Experience Program) through the Transatlantic Ocean System Science and Technology (TOSST) grant.

I also want to thank current and past members of the Kienast lab - Stephanie Kienast, Stef Mellon, Diksha Bista, Jess Gould, Lauren Kipp and Erin Black - for the many interesting discussions, insightful comments and for introducing me to the 'paleo world', as well as the members of DOSA, especially Lorenza Raimondi, Christoph Renkl, Krysten Rutherford, Francisco Javier Bravo Avendaño, Jacoba Mol, Colleen Wilson, Sebastian Haas and Jenna Hare for the very social environment at Dal and for the countless coffee breaks that equally

helped me to procrastinate and to stay sane.

Last but not least, I would like to thank my family and friends for their continuing support throughout the years, as well as my partner and favorite geek Myriam for her endless support and encouragement during this long endeavor, and for all the laughs along the way.

CHAPTER 1

INTRODUCTION

1.1 The role of nitrate in the marine nitrogen cycle

Nitrogen is an essential element in the marine ecosystem, not only controlling the productivity but also the spatial and temporal distribution of marine microorganisms. In the marine environment, nitrogen (N) occurs in a number of forms (N_2, NO, NH_4^+, NO_3^-, NO_2^-, N_2O) and stable oxidation states (Figure 1.1a). Transformations between different pools are catalyzed by microorganisms, such that their distribution and activity give rise to characteristic gradients of the various N species throughout the world's oceans.

The most abundant but for the majority of marine organisms unavailable form is dinitrogen gas (N_2). It is being reduced to bioavailable ammonium (NH_4^+) by N_2-fixing bacteria and archaea (diazotrophs). Within the euphotic zone, NH_4^+ – being the most reduced and favored form of N for phytoplankton – is readily assimilated into organic matter, leading to low NH_4^+ concentrations throughout most of the sunlit surface ocean. Organic matter is either consumed by grazers, remineralized within the euphotic zone by bacteria, or exported out of the euphotic zone and respired at depth (ammonification; i.e., the release of NH_4^+ from organic matter). Below the sunlit surface layer, NH_4^+ is oxidized to nitrate (NO_3^-) – the most abundant form of fixed N in the ocean – as part of the two-step nitrification process. In the first step, NH_4^+ is oxidized to nitrite (NO_2^-) by ammonium-oxidizing bacteria and archaea (AOB, AOA). In the second step, NO_2^- is transformed into NO_3^- by NO_2^--oxidizing bacteria (Figure 1.1a). NO_3^- regenerated through nitrification eventually gets transported back into the euphotic zone through ocean mixing or upwelling processes, where it subsequently gets assimilated by phytoplankton. In this respect, the drawdown of NO_3^- at the surface and the export and remineralization of organic matter at depth result in

characteristic NO_3^- depth profiles with generally low concentrations at the surface and an accumulation in intermediate and deep waters.

Given the spatial heterogeneity of those internal transformation processes, the redistribution of NO_3^- (and other nutrients) is largely dependent on broad-scale ocean circulation, such that regions of upwelling (e.g., eastern ocean margins) are associated with high nutrient concentrations in the upper water column, sustaining enhanced primary and subsequent secondary production. In this respect, upwelling of nutrient-rich deep waters in the Southern Ocean and incomplete consumption in the area of upwelling result in a return flow of high-nutrients intermediate waters that are spreading northward and are hypothesized to dominate the resupply of lower latitude thermocline waters in the Pacific and Atlantic Ocean (e.g., *Palter et al.*, 2010; *Sarmiento et al.*, 2004; *Toggweiler et al.*, 1991).

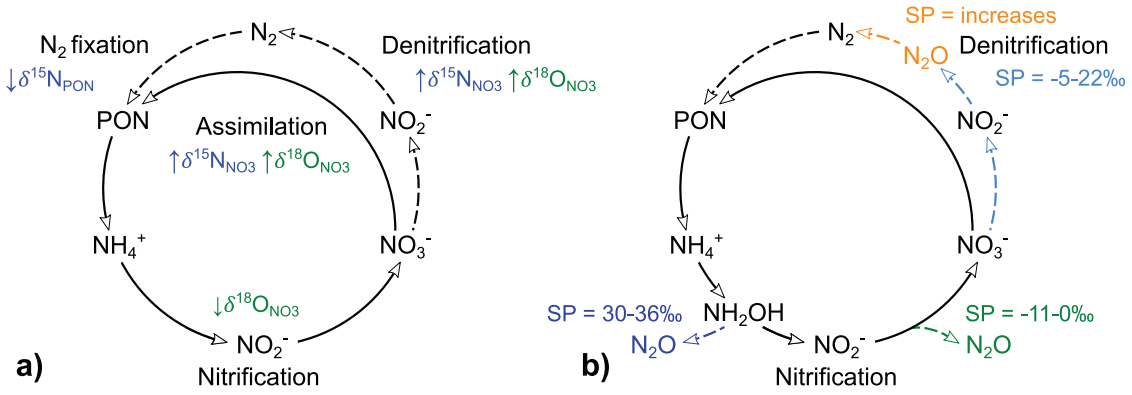

Figure 1.1: Simplified diagram illustrating (a) major microbially-mediated N transformation processes and (b) production and consumption pathways of nitrous oxide (N_2O). Sources and sinks for bioavailable N are highlighted with dashed lines, while internal cycling is indicated by solid lines. (a) The effects of individual processes on the isotopic composition of dissolved NO_3^- are highlighted by dark blue (for $\delta^{15}N$) and green ($\delta^{18}O$) arrows, respectively. (b) Process-dependent site preferences (SP) associated with N_2O production are given for nitrification (dark blue), nitrifier-denitrification (green) and denitrification (light blue), as well as N_2O consumption through denitrification (orange).

Opposing those internal N transformations (i.e., assimilation, ammonification, nitrification), the pool of bioavailable or 'fixed' nitrogen is largely driven by the input or conversion of elemental N_2 into organic material (N_2 fixation) and the removal or conversion of fixed N back to N_2 during dissimilatory NO_3^- reduction (denitrification) and anaerobic ammonium oxidation (anammox). The removal of fixed N occurs both in the

water column and sediment. Hotspots of water column denitrification include suboxic waters within the major open-ocean oxygen deficient zones (ODZs) of the eastern tropical North and South Pacific and the Arabian Sea. Up until recently, it has been hypothesized that denitrification and N_2 fixation are spatially tightly coupled due to the N-deficit in close proximity to ODZs and, hence, favorable growth conditions for diazotrophs (*Deutsch et al.*, 2007). Owing to the high iron requirement of N-fixers, their occurrence and spatial distribution, however, seems largely regulated by the availability of iron (and phosphate) (*Mills et al.*, 2004). Observations of high N_2 fixation rates in areas of elevated iron input but far off any of the major ODZs, such as the North Atlantic (*Knapp et al.*, 2008; *Moore et al.*, 2009) and the western equatorial Pacific (*Bonnet et al.*, 2009) have led to a current rethinking towards a potential spatial decoupling of the two processes (*Knapp et al.*, 2016; *Gruber*, 2016).

ODZs also represent major source regions for nitrous oxide (N_2O; e.g., *Bourbonnais et al.*, 2017; *Frame et al.*, 2014), an important greenhouse gas involved in the depletion of stratospheric ozone (*Ravishankara et al.*, 2009). Oceanic N_2O is produced during both nitrification and denitrification (Figure 1.1b; *Goreau et al.*, 1980; *Ostrom et al.*, 2000; *Santoro et al.*, 2011). In oxic systems, N_2O can be generated as a by-product during the oxidation of hydroxylamine (NH_2OH; nitrification pathway), and as an intermediate during the reduction of NO_2^- to N_2 (nitrifier-denitrification pathway). In suboxic ($O_2 < 5$ μmol L^{-1}) systems, N_2O is produced and consumed during the reduction of NO_3^- to N_2 gas (denitrification pathway).

The oceanic budget of bioavailable or fixed nitrogen, however, is still not well constrained and a topic of current research (*Gruber*, 2016), with estimates varying between roughly balanced (*Gruber*, 2004) to a net loss of $\sim$ 200 Tg N yr^{-1} (*Codispoti*, 2007). Large uncertainties are due to the spatial and temporal variability of both sources and sinks, limited spatial coverage of marine in situ measurements and corresponding problems in up-scaling from single measurements to basin-wide estimates (*Fowler et al.*, 2013; *Gruber*, 2016). Other sources of uncertainty arise from the potential impacts of global climate change – e.g., changes in microbial community composition (*Bowen et al.*, 2013) and complex biogeochemical interactions (i.e., co-limitation of iron and phosphate; *Falkowski et al.*, 1998; *Jickells et al.*, 2005; *Moore et al.*, 2013).

1.2 N and O isotope systematics and field applications

One approach that has previously been used to both resolve spatial patterns of N_2 fixation and denitrification and obtain input and removal rates is based on measured NO_3^- and phosphate (PO_4^{3-}) concentrations as well as derived [NO_3^-]-to-[PO_4^{3-}] relationships (i.e., N*, where N* = $[NO_3^-] - 16 \times [PO_4^{3-}] + 2.9$; *Deutsch et al.*, 2001; *Gruber and Sarmiento*, 1997). N transformation processes such as N_2 fixation, denitrification as well as internal N cycling (i.e., assimilation, remineralization) often occur within the same water mass. One limitation of the use of N* to estimate input and output rates is that this approach does not distinguish between the simultaneous occurrence of different N transformation processes that potentially overlap and erase one another.

N input and removal (N_2 fixation, denitrification), as well as internal N cycling (assimilation, remineralization/nitrification), however, all alter the isotopic composition of NO_3^- and other N species (e.g., NO_2^-, N_2O) in characteristic ways due to differences in fractionation arising from variations in reaction rates between the heavier and lighter isotopes (*Mariotti et al.*, 1981), thus revealing the relative contribution of individual processes to the dissolved N pool. Therefore, methodological advances allowing coupled measurements of $^{15}N/^{14}N$ and $^{18}O/^{16}O$ ratios of NO_3^- (*Sigman et al.*, 2001; *Casciotti et al.*, 2002; *McIlvin and Altabet*, 2005) as well as improved accuracy coupled with lower sample quantities necessary for adequate measurements significantly improved our understanding of the global N cycle, and helped to identify N processes that are not immediately evident from standard hydrographic measurements. In this respect, N and O isotope analyses of NO_3^- (expressed as $\delta^{15}N_{NO3}$ and $\delta^{18}O_{NO3}$, where $\delta^{15}N$ (‰) = [($^{15}N/^{14}N_{sample} \div {}^{15}N/^{14}N_{standard}$) – 1] x 1000, and $\delta^{18}O$ (‰) = [($^{18}O/^{16}O_{sample} \div {}^{18}O/^{16}O_{standard}$) – 1] $\times$ 1000, respectively), together with well-constrained process-specific fractionation factors, give insights into individual transformation processes within the N cycle.

Specifically, assimilatory NO_3^- reduction is associated with a normal isotope effect, indicating that the lighter ^{14}N and ^{16}O are preferentially assimilated by phytoplankton, which leads to an accumulation of ^{15}N and ^{18}O and an isotopic enrichment of the unconsumed residual NO_3^- pool. N and O isotope effects ($^{15}\epsilon$ and $^{18}\epsilon$, respectively; where $^{15}\epsilon$ (‰) = (($^{14}k/^{15}k - 1$) $\times$ 1000 and $^{18}\epsilon$ (‰) = (($^{16}k/^{18}k - 1$) $\times$ 1000, and k indicates the first-order rate constants of the reaction) associated with NO_3^- uptake are on the order of 5‰ (Figure 1.2; *Casciotti et al.*, 2002; *Granger et al.*, 2004, 2010).

Isotope effects associated with dissimilatory NO_3^- reduction (i.e., denitrification) range between 10 to 25‰ (e.g., *Brandes et al.*, 1998; *Granger et al.*, 2008; *Voss et al.*, 2001), with N and O isotopes being equally fractionated along a 1:1 ratio, which results in a concurrent enrichment in ^{15}N and ^{18}O of the water column dissolved NO_3^- pool (*Granger et al.*, 2008; *Sigman et al.*, 2005). This relatively high isotopic fractionation associated with water column denitrification contrasts with dissimilatory reactions within the sediment, which only impart a negligible degree of fractionation ($\epsilon \sim 0‰$) due to complete NO_3^- consumption or limited diffusive exchange of NO_3^- with the water column (Figure 1.2; *Brandes and Devol*, 1997; *Lehmann et al.*, 2005; *Sigman et al.*, 2003, 2005).

While equally fractionated during assimilatory and dissimilatory NO_3^- reduction, the remineralization of organic matter may cause a decoupling between N and O isotope ratios. In regard to N isotope ratios, the remineralization of organic matter in the ocean interior produces NO_3^- with a $\delta^{15}N$ akin to the $\delta^{15}N$ of the material exported from the sea surface, which, itself, reflects the $\delta^{15}N_{NO3}$ upwelled to the surface as well as any external N input (e.g, N_2 fixation, atmospheric input, river discharge). In this respect, the fixation of atmospheric N_2 into reactive N and its subsequent remineralization generates NO_3^- with a relatively low $\delta^{15}N$ (-1 to 0‰; *Carpenter et al.*, 1997; *Hoering and Ford*, 1960). In contrast, $\delta^{18}O$ of newly nitrified NO_3^- is independent of the isotopic signature of the recycled organic matter, but instead largely follows the $\delta^{18}O$ of ambient seawater, which generally has a value close to 0‰ (*Buchwald et al.*, 2012; *Casciotti et al.*, 2008; *Sigman et al.*, 2009b). At depth, the isotopic signature of the residual NO_3^- pool reflects an integrated signal of both N sources and sinks, thus resulting in a relatively constant $\delta^{15}N$ and $\delta^{18}O$ of 5‰ and 2‰ across much of the deep ocean (*Sigman et al.*, 2009b).

Well-constrained N and O isotope fractionation factors thus allow dual isotope measurements to be applied to specific locations of interest. For example, regional studies focusing on hotspots of water column denitrification, including suboxic waters within the major open-ocean ODZs of the eastern tropical North Pacific (*Voss et al.*, 2001; *Sigman et al.*, 2005, 2009a; *Casciotti and McIlvin*, 2007), the eastern tropical South Pacific (e.g., *Buchwald et al.*, 2012; *Bourbonnais et al.*, 2015; *Knapp et al.*, 2016) and the Arabian Sea (*Altabet et al.*, 2002; *Naqvi et al.*, 2006; *Buchwald and Casciotti*, 2013; *Martin and Casciotti*, 2017) gave new insights into the spatiotemporal extent and coupling of main processes such as denitrification and nitrification, allowing more accurate rate estimates of

individual transformations. Moreover, those regional studies helped to characterize the occurrence and importance of less constrained reactions such as anammox and dissimilatory NO_3^- reduction to ammonium (DRNA; e.g., *Kalvelage et al.*, 2013).

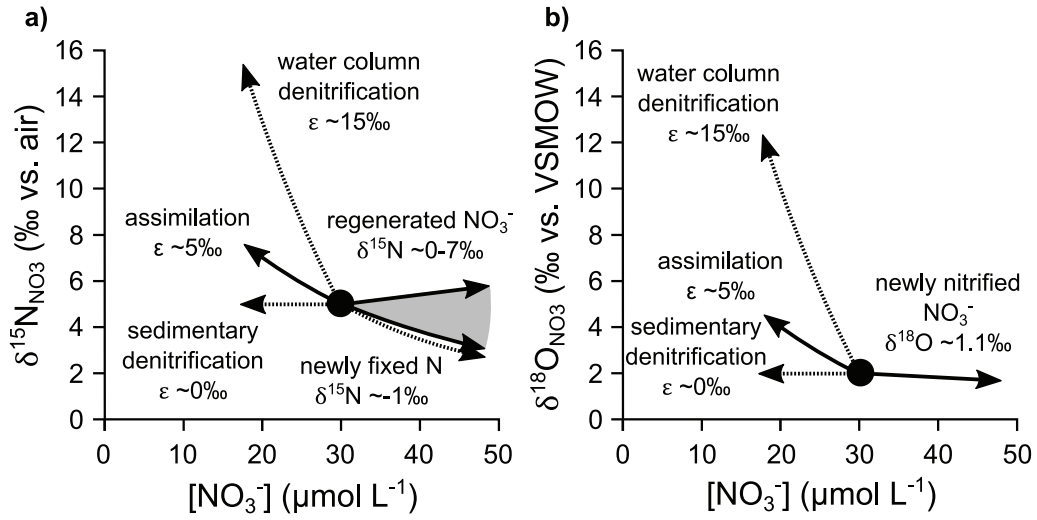

Figure 1.2: Various N transformation processes and their effect on (a) $\delta^{15}N_{NO3}$ and (b) $\delta^{18}O_{NO3}$ as a function of NO_3^- concentration. Sources and sinks for bioavailable N are highlighted with dashed lines, while internal cycling is indicated by solid lines. (After *Sigman and Fripiat*, 2019).

Besides microbially-mediated reactions, NO_3^- $\delta^{15}N$ and $\delta^{18}O$ observations are also affected by ocean circulation and mixing. Thus, by taking into account physical processes along with basin-scale circulation patterns, and by increasing the spatial extent of NO_3^- isotope observations from individual profiles to zonal/meridional transects, recent studies were able to investigate the exchange between regional N inventories and the connectivity between specific N cycling hotspots. For example, basin-wide NO_3^- isotope studies in the Pacific showed evidence for significant modifications of the return flow of high-nutrients intermediate waters spreading northward from the Southern Ocean, with isotope ratios revealing the imprint of partial utilization at the surface of the Southern Ocean, the lateral exchange with denitrified waters from the eastern margin and substantial remineralization of organic matter along the flow path (*Peters et al.*, 2018; *Rafter et al.*, 2012, 2013; *Sigman et al.*, 2009a). Similarly, N and O isotope ratios of NO_3^- measured along different transects throughout the Atlantic showed the northward spreading of isotopically enriched NO_3^-

due to partial NO_3^- assimilation in the Southern Ocean as well as a dominant imprint of remineralization and N_2 fixation in transit (*Marconi et al.*, 2015; *Tuerena et al.*, 2015). N and O isotope measurements of NO_3^- along zonal and meridional transects thus provide an important and powerful tool to study the regional variability in – and communication between – various biogeochemical processes, and, as such, evaluate the impact of local biogeochemical processes on the mean oceanic budget.

Analogous to N and O isotope ratios of NO_3^-, bulk N and O isotope ratios of N_2O ($\delta^{15}N^{bulk}$ and $\delta^{18}O_{N2O}$) in part reflect the isotopic signature of the precursory molecule (NH_4^+, NO_2^-, NO_3^-), as well as any additional fraction during its production and consumption (*Sutka et al.*, 2006; *Toyoda et al.*, 2002; *Yoshida and Toyoda*, 2000). In the absence of N_2O consumption, normal isotope effects associated with N_2O production pathways generally result in isotopically depleted N_2O compared to the precursory molecule (*Frame and Casciotti*, 2010; *Santoro et al.*, 2011; *Sutka et al.*, 2006; *Toyoda et al.*, 2005). In contrast, the preferential consumption of isotopically light N_2O during denitrification results in a concurrent enrichment in ^{15}N and ^{18}O of the unconsumed N_2O pool.

Bulk N and O isotope ratios of N_2O further allow the simultaneous analysis of isotopomer abundances, reflecting the different position of isotopic atoms within the linear asymmetric molecule ($^{14}N^{15}N^{16}O$ and $^{15}N^{14}N^{16}O$). The difference in the isotopic enrichment of the central (α) and the outer (β) N atoms in N_2O is indicated by the site preference (SP), where SP = $\delta^{15}N^{\alpha} - \delta^{15}N^{\beta}$ (*Toyoda and Yoshida*, 1999). In contrast to N_2O bulk isotope ratios, SP is thought to be process-dependent only, thus independent of the isotopic signature of the source substrate (*Sutka et al.*, 2006; *Toyoda et al.*, 2002; *Yoshida and Toyoda*, 2000). N_2O produced through NO_2^- reduction is associated with a low SP, ranging from -11 to 0‰ for the nitrifier-denitrification pathway and -5 to 22‰ for canonical denitrification (Figure 1.1b). A higher SP between 30 and 36‰ is indicative of N_2O production from NH_2OH decomposition (nitrification pathway; *Frame and Casciotti*, 2010; *Santoro et al.*, 2011; *Sutka et al.*, 2006; *Toyoda et al.*, 2005). The consumption of N_2O through denitrification further increases the SP isotopic signature of N_2O. The preferential removal of isotopically light N_2O by denitrifying bacteria in the absence of any N_2O production has been shown to occur with constant proportions between SP and $\delta^{18}O_{N2O}$ (1:2.2), as well as between $\delta^{15}N^{\alpha}$ and $\delta^{18}O_{N2O}$ (1:1.6; *Ostrom et al.*, 2007). In that sense, bulk N and O isotope ratios of N_2O and isotopomer abundances provide additional tracers to identify

the occurrence and distribution of individual N transformation processes.

1.3 Objectives

With this work, I aim to highlight the importance and applicability of coupled N and O isotope measurements of NO_3^- to identify major N transformation processes, their spatial distribution and regional differences among various marine environments. Dual NO_3^- isotope measurements complemented by ancillary hydrographic and chemical tracer data (i.e., nutrient ratios, apparent oxygen utilization) provide a powerful tool to infer integrative N transformations and water mass provenance. Specifically, coupled analyses allow the distinction between advective signals and processes imparted onto the water column in situ, thus give insight into the evolution and history of prevalent water masses. In this respect, I focus on two specific regions of the world's ocean where the lateral input of nutrient-rich, subsurface water masses plays a key role in sustaining areas of significant primary production, namely the tropical west Pacific (chapter 2) and the Canadian Arctic Ocean (chapters 3 and 4).

Specifically, chapter 2 of my thesis focuses on the Western Equatorial Pacific (WEP), a region critically important for lower latitude biogeochemistry and productivity. Nutrients in the equatorial upwelling system largely derive from the Equatorial Undercurrent (EUC), which itself is fueled by northern and southern hemisphere waters delivered through western boundary currents (e.g., *Rafter and Charles*, 2012; *Rafter and Sigman*, 2016; *Sloyan et al.*, 2010; *Toggweiler et al.*, 1991; *Wyrtki*, 1981). The relative transport of waters (and nutrients therein) from both north and south of the equator to the EUC remains elusive. Understanding the biogeochemistry and evolution of water masses that feed the EUC, however, is crucial for understanding controls on the productivity of the tropical Pacific, which itself sustains $\sim 10\%$ of global primary production (*Pennington et al.*, 2006).

In this regard, chapter 2 examines the N and O isotopic composition of NO_3^- ($^{15}N/^{14}N$ and $^{18}O/^{16}O$), nutrient ratios and hydrographic measurements at stations south and north of the equator to elucidate the hydrography of the WEP, while highlighting biogeochemical modifications of prevalent water masses along the flow path. The N* definition used in this chapter deviates slightly from the definition introduced by *Gruber and Sarmiento* (1997) for consistency with previous regional studies (e.g., *Rafter et al.*, 2012). Complementary isotope ratios of dissolved inorganic carbon ($^{13}C/^{12}C$ of DIC) are used as an additional

indicator for biological processes, signaling both surface uptake and subsurface remineralization. In chapter 2, the isotopic composition of NO_3^- and DIC coupled to standard hydrographic measurements, thus, provide a means to identify regional differences in (1) the fraction of remineralized versus preformed NO_3^-, (2) the input of newly fixed N to the dissolved NO_3^- pool, and (3) the lateral advective supply of nutrients from different ocean regions (e.g., eastern Pacific). Moreover, end-member mixing estimates using the nutrient and isotope data collected previously (e.g., *Rafter and Sigman*, 2016) and during this study (chapter 2) provide constraints on the provenance of northern and southern hemisphere water masses and their relative contribution to the EUC, which has important implications for understanding controls on the productivity of the equatorial and tropical Pacific and predicting local and regional biogeochemical variability in this region.

Chapter 3 and 4 focus on the Canadian Arctic Ocean, a major gateway between the Pacific and Atlantic Ocean due to its impact on the throughflow and export of both freshwater and nutrients to the Labrador Sea and the wider North Atlantic. In this respect, the upwelling of nutrient-rich intermediate waters in the sub-Arctic Pacific and its lateral propagation across the Bering Strait ultimately constitutes the main advective source of NO_3^- (and other nutrients) to the Arctic Ocean and ultimately the North Atlantic (*Yamamoto-Kawai et al.*, 2006). To date, only a limited number of studies have focused on N and O isotope dynamics in NO_3^- within the Canadian and US Arctic, most of which were restricted to the western Arctic and its productive continental shelves (*Brown et al.*, 2015a; *Fripiat et al.*, 2018; *Granger et al.*, 2011, 2013; *Lehmann et al.*, 2005, 2007). In chapters 3 and 4, I use N and O isotope data of NO_3^- collected during the 2015 Canadian Arctic GEOTRACES campaign to examine the lateral exchange of nutrients between the western and eastern Canadian Arctic and, thus, the connectivity between different Arctic systems and horizontal components of basinscale nutrient transport. In particular, I focus on the Canada Basin and Baffin Bay as the two deep basins in the vicinity of the North Pacific and North Atlantic (chapters 3 and 4), as well as the extensive shelf area of the Arctic Archipelago connecting the two basins (chapter 4).

Chapter 3 focuses on the surface and export production in Baffin Bay and its effect on Baffin Bay bottom water properties. Previously, the deep basin in Baffin Bay has been shown to harbor enhanced inventories of N_2O (*Fenwick et al.*, 2017; *Kitidis et al.*, 2010) and a surplus of silicic acid ($Si(OH)_4$) and PO_4^{3-} over NO_3^- in regard to general stoichiometric

expectations (e.g., *Jones et al.*, 1984; *Tremblay et al.*, 2002). Clear mechanisms leading to either of the two signals (i.e., the deficiency in NO_3^- and the supersaturation of N_2O) yet need to be identified unambiguously. In chapter 3, the differences in fractionation of N and O isotopes of NO_3^- to distinct N transformations are used to determine the spatial distribution and extent of internal N transformation (assimilation, nitrification) as well as N removal processes (anaerobic reduction) that potentially cause the observed deficit in dissolved nitrogen. The drawdown of oxygen associated with the remineralization of organic matter (i.e., ammonification and subsequent nitrification) allows the use of the apparent oxygen utilization (AOU) as an additional, independent tracer to estimate the recycled versus preformed source of nutrients in Baffin Bay. This dataset is further complemented by N_2O concentrations and the associated N_2O isotopic composition and isotopomer abundance measured along the same transects. To date, only a few N_2O profiles have been reported across the Canadian Arctic (*Kitidis et al.*, 2010; *Fenwick et al.*, 2017) and on the Chukchi Shelf (*Hirota et al.*, 2009). Accordingly, the use of N and O isotope measurements to infer N_2O cycling in the Arctic Ocean have been limited and restricted to the western part of the Arctic ecosystem (*Hirota et al.*, 2009). In this study, isotopic tracer profiles of N_2O and NO_3^- – one of the precursory molecules for N_2O production – thus are used to disentangle co-occurring N_2O production and consumption pathways and as such, evaluate the source of the previously observed N_2O accumulation in the deep Baffin Bay.

To investigate horizontal aspects of basin-scale nutrient transport and the spatial variability of Pacific-derived waters, which are considered the main advective source of fixed N for primary production in the Arctic (e.g., *Torres-Valdés et al.*, 2013; *Tremblay et al.*, 2015), chapter 4 targets the area upstream of Baffin Bay, namely the Arctic Archipelago and the Canada Basin. Accordingly, specific focus has previously been put on both the Bering and Chukchi shelf area in proximity to the Pacific water inflow. While those nutrient-rich Pacific waters support high seasonal productivity and sedimentary denitrification across those wide western Arctic shelves (e.g., *Brown et al.*, 2015a; *Chang and Devol*, 2009; *Devol et al.*, 1997; *Granger et al.*, 2011; *Tanaka et al.*, 2004), they also exert a strong impact on the Arctic further downstream by both increasing the density stratification of the Arctic water column and by fueling high primary production in areas of strong mixing and upwelling (e.g., *Cota et al.*, 1987; *Michel et al.*, 2006; *Tremblay et al.*, 2002, 2006). The Canadian Arctic Archipelago (CAA) serves as a dominant pathway for the

outflow of Pacific water (and nutrients therein) to the Labrador Sea and the wider North Atlantic (*Jones*, 2003; *Yamamoto-Kawai et al.*, 2006). However, despite its importance in distributing nutrients across the Arctic, little is known about the prevalence of individual water masses and associated nutrient distributions within the CAA.

In chapter 4, distinct nutrient signatures (e.g., N-to-P and N-to-O), characteristic for both Pacific-derived and Atlantic-derived waters, are combined with first measurements of naturally occurring stable isotope ratios of NO_3^- to trace the provenance of individual source waters and their relative distribution within the Archipelago. Isotopic end-member values measured at the entrance to the CAA both in the western Arctic (Canada Basin, this chapter) and the eastern Arctic (Baffin Bay, chapter 3) allow the distinction between biogeochemical modifications imparted on the dissolved NO_3^- pool in situ from advection and mixing processes as those waters transit through the CAA towards the North Atlantic. In that sense, variations in the isotopic composition of NO_3^-, alongside changes in nutrient and oxygen concentrations throughout the Canadian Archipelago are used to highlight the spatial variability of individual N transformations and potential input and removal processes of nutrients along the transect, and thus will help to develop a more robust understanding of N cycling in the Arctic Ocean.

CHAPTER 2

ISOTOPIC EVIDENCE FOR THE EVOLUTION OF SUBSURFACE NITRATE IN THE WESTERN EQUATORIAL PACIFIC[1]

2.1 Abstract

Subsurface waters from both hemispheres converge in the Western Equatorial Pacific (WEP), some of which form the Equatorial Undercurrent (EUC) that influences equatorial Pacific productivity across the basin. Measurements of nitrogen (N) and oxygen (O) isotope ratios in nitrate ($\delta^{15}N_{NO3}$ and $\delta^{18}O_{NO3}$), the isotope ratios of dissolved inorganic carbon ($\delta^{13}C_{DIC}$), and complementary biogeochemical tracers reveal that northern and southern WEP waters have distinct biogeochemical histories. Organic matter remineralization plays an important role in setting the nutrient characteristics on both sides of the WEP. However, remineralization in the northern WEP contributes a larger concentration of the nutrients, consistent with the older age of northern thermocline-depth and intermediate-depth waters. Remineralization introduces a relatively low $\delta^{15}N_{NO3}$ to northern waters, suggesting the production of sinking organic matter by N_2 fixation at the surface – consistent with the notion that N_2 fixation is quantitatively important in the North Pacific. In contrast,

[1]Lehmann, N., Granger, J., Kienast, M., Brown, K. S., Rafter, P. A., Martínez-Méndez, G., & Mohtadi, M. (2018). Isotopic evidence for the evolution of subsurface nitrate in the Western Equatorial Pacific. *Journal of Geophysical Research: Oceans*, 123(3), 1684–1707.
Author contribution: I analyzed the NO_3^- isotope samples in collaboration with J. Granger. G. Martínez-Méndez provided the $\delta^{13}C_{DIC}$ data and K. S. Brown contributed the mixing model calculations. I led the interpretation of the data and wrote the manuscript, with input from all co-authors.

remineralization contributes elevated $\delta^{15}N_{NO3}$ to the southern WEP thermocline, which we hypothesize to derive from the vertical flux of high-$\delta^{15}N$ material at the southern edge of the equatorial upwelling. This signal potentially masks any imprint of N_2 fixation from South Pacific waters. The observations further suggest that the intrusion of high $\delta^{15}N_{NO3}$ and $\delta^{18}O_{NO3}$ waters from the eastern margins is more prominent in the northern than southern WEP. Together, these north-south differences enable the examination of the hemispheric inputs to the EUC, which appear to derive predominantly from southern hemisphere waters.

2.2 Introduction

The Western Equatorial Pacific (WEP) is a water mass crossroad (*Fine et al.*, 1994), where northern and southern hemisphere waters delivered through western boundary currents are exported to the Indian Ocean via the Indonesian Throughflow (*Godfrey*, 1996; *Sprintall et al.*, 2014) and to the wider equatorial Pacific through the Equatorial Undercurrent (EUC; *Butt and Lindstrom*, 1994; *Johnson et al.*, 2002; *Lindstrom et al.*, 1987, Figure 2.1). As such, the WEP and its boundary currents exert an important influence on lower latitude biogeochemistry, particularly because the EUC is the source of nutrients to the equatorial Pacific surface waters (*Rafter and Charles*, 2012; *Rafter and Sigman*, 2016; *Sloyan et al.*, 2010; *Toggweiler et al.*, 1991; *Wyrtki*, 1981), fueling nearly 10% of global primary production (*Pennington et al.*, 2006).

The water masses and currents that converge at the equator at the western boundary have been investigated in a number of studies (e.g., *Bingham and Lukas*, 1995; *Fine et al.*, 1994; *Kashino et al.*, 2005; *Lindstrom et al.*, 1987; *Nie et al.*, 2016; *Toole et al.*, 1988; *Tsuchiya*, 1968). Nevertheless, the relative transports to the EUC from north and south of the equator remain subject to debate. Some studies suggest that both southern and northern hemisphere nutrients contribute substantively (*Fine et al.*, 1987; *Izumo et al.*, 2002; *Liu and Huang*, 1998), or partially ($< 20\%$; *Grenier et al.*, 2011) to the EUC, while others argue that transports from the South Pacific dominate the EUC (*Toggweiler et al.*, 1991; *Tsuchiya et al.*, 1989). In this respect, Southern Ocean nutrients are hypothesized to dominate the resupply to the lower latitude Pacific via Subantarctic Mode Water (SAMW) and WEP boundary currents (*Palter et al.*, 2010; *Sarmiento et al.*, 2004; *Toggweiler et al.*, 1991). The evolution of nutrients in SAMW from its origin in the Southern Ocean en

route to the lower latitudes of the South Pacific has been investigated recently from stable isotopes of nitrate (NO_3^-), revealing that NO_3^- in SAMW is substantially altered in transit from the Southern Ocean (*Rafter et al.*, 2013). The NO_3^- isotope ratios in SAMW bear evidence of its partial consumption at the Southern Ocean surface prior to subduction at the Subantarctic Front (*DiFiore et al.*, 2010; *Rafter et al.*, 2013; *Sigman et al.*, 1999, 2000) and lateral exchange with oxygen deficient zones at the eastern margins (*Peters et al.*, 2018; *Rafter et al.*, 2012, 2013; *Yoshikawa et al.*, 2015). Importantly, NO_3^- isotope ratios indicate that a substantial amount of NO_3^- is added to SAMW en route from the Southern Ocean to the tropics from the remineralization of organic material delivered by biological pumping (*Peters et al.*, 2018; *Rafter et al.*, 2012, 2013; *Sigman et al.*, 2009b). Thus, the nutrient content of SAMW-density waters in the tropics is influenced by surface processes in the Southern Ocean as well as by modifications along its flow path in the South Pacific. While SAMW-density waters are too deep (> 400 m) to directly upwell to the surface, diapycnal mixing between those nutrient–rich waters and overlaying NO_3^--free surface waters of the South Pacific gyre result in the resupply of lower latitude thermocline-depth nutrients (*Palter et al.*, 2010; *Rafter et al.*, 2012, 2013; *Toggweiler et al.*, 1991).

The isotopic evolution of NO_3^- in intermediate water masses of the North Pacific, which may influence the composition of the EUC, is less well characterized. Measurements of NO_3^- isotope ratios at the eastern tropical North Pacific margin have provided insights into the N biogeochemistry of oxygen deficient zones (ODZs; *Altabet et al.*, 1999; *Brandes et al.*, 1998; *Buchwald et al.*, 2015; *Sigman et al.*, 2005; *Voss et al.*, 2001). Meridional sections in the eastern tropical Pacific reveal that ODZ waters permeate westward at intermediate depths along the North Equatorial Current (NEC; *Reid*, 1965; *Reid and Mantyla*, 1978). Additionally, NO_3^- isotope profiles at station ALOHA in the North Pacific gyre bear evidence of the remineralization of N deriving from N_2 fixation in the surface gyre (*Casciotti et al.*, 2008; *Sigman et al.*, 2009a).

The WEP also appears to be a hot spot for biological N_2 fixation at the sea surface, as evidenced by measurements of total organic nitrogen (*Hansell and Feely*, 2000) and from nitrogen isotope ratios of dissolved NO_3^- (*Kienast et al.*, 2008) and settling particles (*Yoshikawa et al.*, 2005). Accordingly, $^{15}N_2$ tracer incubations off the coast of Papua New Guinea (PNG) and in the Solomon Sea indicate exceptionally high N_2 fixation rates in both areas, exceeding most estimates reported for oceanic waters (*Bonnet et al.*, 2009, 2015).

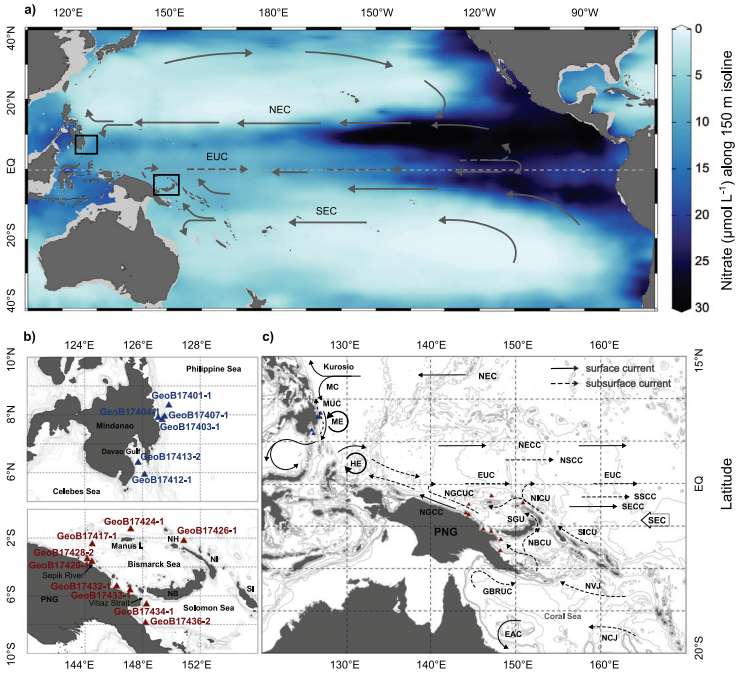

Figure 2.1: (a) Map showing simplified circulation of surface (solid line) and subsurface (dashed line) waters across the Pacific after *Talley* (1993); *Fine et al.* (1994); *Sokolov and Rintoul* (2000); *Kawabe and Fujio* (2010). Colors show NO_3^- concentrations at 150 m from the WOA13 climatology. Black squares indicate the two study areas north and south of the equator. (b) Detailed view of sampling sites (GeoB174xx) off Mindanao and Papua New Guinea (PNG), with blue colors indicating the northern stations and red colors representing the southern stations. The same color code is used throughout this study to highlight the respective hemispherical location of individual sites. (c) Illustration of major surface (solid lines) and subsurface (dashed lines) currents in the Western Equatorial Pacific (WEP) after *Lindstrom et al.* (1987); *Bingham and Lukas* (1994); *Fine et al.* (1994); *Cravatte et al.* (2011). The low-latitude western boundary currents are the Mindanao Current (MC), the New Guinea Coastal Current (NGCC) and the East Australia Current (EAC) at the surface, and the Mindanao Undercurrent (MUC), the New Guinea Coastal Undercurrent (NGCUC) and the Great Barrier Reef Undercurrent (GBRUC) at the subsurface. Additional surface currents in the WEP include the North and South Equatorial Current (NEC, SEC), and the North and South Equatorial Countercurrent (NECC and SECC). Subsurface currents include the Equatorial Undercurrent (EUC), the New Britain Coastal Undercurrent (NBCU), the North Vanuatu Jet (NVJ), the North Caledonian Jet (NCJ), the St. Georges Undercurrent (SGU), the Solomon Island Coastal Undercurrent (SICU), the New Ireland Coastal Undercurrent (NICU), and the Northern and Southern Subsurface Countercurrent (NSCC, SSCC). HE and ME indicate the Halmahera and Mindanao Eddies. Additional abbreviations indicate New Britain (NB), New Ireland (NI), New Hanover (NH), and Solomon Islands (SI).

In contrast to the WEP, $^{15}N_2$ tracer incubations in the eastern margin of the South Pacific have consistently evidenced very low N_2 fixation rates (*Knapp et al.*, 2016; *Raimbault and Garcia*, 2008), in spite of inverse model diagnoses suggesting that elevated rates of N_2 fixation may occur at the eastern gyre boundary (*Deutsch et al.*, 2007). The N isotope composition of NO_3^- correspondingly bears no clear indication of the remineralization of newly fixed N in the thermocline of the South Pacific subtropical gyre (*Peters et al.*, 2018; *Rafter et al.*, 2013), in contrast to its North Pacific equivalent (*Casciotti et al.*, 2008; *Sigman et al.*, 2009a).

Understanding the hydrography of the WEP and the biogeochemistry of water masses that feed the EUC has implications, among others, for understanding global controls on fertility and productivity of the equatorial and tropical Pacific. To this end, we examined the N and O isotopic composition of NO_3^- ($^{15}N/^{14}N$ and $^{18}O/^{16}O$), the C isotopic composition of dissolved inorganic carbon ($^{13}C/^{12}C$), and hydrographic measurements at stations south and north of the equator (Figure 2.1). Isotope ratios are reported in the delta (δ) notation, where the ratio in a sample is given relative to the ratio in a standard material and expressed in units per mil (‰):

$$\delta^{15}N_{sample} = [(^{15}N/^{14}N)_{sample}/(^{15}N/^{14}N)_{reference} - 1] \times 1000 \quad (2.1)$$

$$\delta^{18}O_{sample} = [(^{18}O/^{16}O)_{sample}/(^{18}O/^{16}O)_{reference} - 1] \times 1000 \quad (2.2)$$

$$\delta^{13}C_{sample} = [(^{13}C/^{12}C)_{sample}/(^{13}C/^{12}C)_{reference} - 1] \times 1000 \quad (2.3)$$

Measurements of coupled $\delta^{15}N$ and $\delta^{18}O$ of NO_3^- ($\delta^{15}N_{NO3}$ and $\delta^{18}O_{NO3}$) are sensitive to important biogeochemical fluxes and provide information on the origin and history of water masses (*Sigman et al.*, 2000), identifying processes that are not immediately evident from standard hydrographic measurements. The assimilation, denitrification, and production of NO_3^- (i.e., remineralization) each alter the isotopic composition in distinctive ways, thus revealing the relative contribution of different processes to the NO_3^- pool. The partial assimilation of NO_3^- at the sea surface results in a coincident enrichment of N versus O isotope ratios of the unconsumed pool with a characteristic ratio of 1 (*Casciotti et al.*, 2002; *Granger et al.*, 2004). Similarly, in oxygen deficient waters, dissimilatory NO_3^- consumption (denitrification) also imparts equivalent N versus O enrichment on residual NO_3^- (*Granger et al.*, 2008; *Sigman et al.*, 2005). In turn, the remineralization of organic

material at the subsurface, namely, the ammonification of organic nitrogen followed by its nitrification, produces NO_3^- with a $\delta^{15}N_{NO3}$ akin to that of the remineralized material, thus reflecting the $\delta^{15}N$ of material exported from the sea surface. In this respect, the fixation of atmospheric N_2 into reactive nitrogen and its subsequent remineralization generate NO_3^- with a relatively low $\delta^{15}N$ (0‰ to -1‰), deriving from the $\delta^{15}N$ of atmospheric N_2. Concurrently, the $\delta^{18}O$ of remineralized NO_3^- adopts a value near that of ambient water (*Buchwald and Casciotti*, 2010; *Buchwald et al.*, 2012; *Casciotti et al.*, 2002; *Sigman et al.*, 2009a). Interpreted in the context of hydrography and nutrient tracers, the coupled $\delta^{15}N_{NO3}$ and $\delta^{18}O_{NO3}$ thus provide a means of tracking the biogeochemical evolution of the NO_3^- pool along its flow path.

Seawater $\delta^{13}C$ in dissolved inorganic carbon (DIC; $\delta^{13}C_{DIC}$) provides additional insight into biogeochemical processing. It is not only a tracer for past water mass ventilation and air-sea gas exchange, but also an indicator of biological activity (*Kroopnick*, 1985). In the euphotic zone, the preferential removal of ^{12}C during photosynthesis leaves the residual DIC enriched in ^{13}C, while producing organic matter with a low $\delta^{13}C$. Organic matter remineralization returns ^{12}C to the ambient water, consequently decreasing the $\delta^{13}C_{DIC}$.

We thus investigate isotopic features that offer insights into distinct biogeochemical influences on NO_3^- in association with the water masses that converge in the WEP. The isotopic composition of NO_3^- and DIC, along with standard hydrographic measurements provide a means to identify the fraction of preformed NO_3^- relative to that remineralized along the flow path, and to NO_3^- advected laterally from oxygen deficient zones in the eastern Pacific (*Rafter et al.*, 2013). We also examine the degree to which the remineralization of newly fixed N imprints on the subsurface isotopic signal of NO_3^- in the two regions and consider the origins of distinct features among regional profiles. Finally, the isotopic composition of NO_3^- previously measured in the EUC (*Rafter and Sigman*, 2016) provides a basis to assess the relative contributions of northern and southern western boundary currents to the EUC. The observations reveal that stations north and south of the equator have divergent isotopic properties, suggesting limited communication and different hydrographic histories, and providing evidence of differential contributions to the EUC. These observations help elucidate the sources, transformation, and communication of subsurface nutrients in the region and are essential for predicting long-term local and regional biogeochemical variability (*Kienast et al.*, 2008).

2.3 Materials and Methods

Seawater samples were collected during the EISPAC expedition (SO-228) aboard the RV SONNE in May and June 2013 using a rosette water sampler equipped with 24 10 L Niskin bottles (*Mohtadi et al.*, 2013). Hydrographic data were obtained using a Seabird SBE911 CTD. During the cruise, a total of 18 CTD profiles were taken from 8°N and 126°E off Mindanao to 7°S and 148°E south of the Bismarck Sea (Figure 2.1). In addition to temperature, salinity and pressure, the CTD recorded oxygen concentrations using a Clark-type oxygen sensor, and turbidity and fluorescence using a fluorescence sensor. The strong surface and subsurface currents in the study area, especially off Mindanao, resulted in some difficulties in reproducing down-cast and up-cast O_2 profiles. Compared to measurements at corresponding WOCE stations, oxygen profiles showed analogous patterns to the WOCE data, but differed in terms of absolute concentrations. The oxygen profiles measured during SO-228 are thus presented as uncorrected instrumental units, and will only be referred to in terms of overall pattern rather than absolute values.

Water samples for stable isotope measurements of DIC were collected at 16 stations from the surface to a depth of around 4,000 m. A portion of the water collected in the Niskin bottles was siphoned into 100 mL glass bottles with water enough to overflow twice to avoid the formation of bubbles. The samples were poisoned with 50 μL of mercury (II) chloride ($HgCl_2$) to prevent alterations of the actual $\delta^{13}C_{DIC}$ by biological activity. The glass bottles were sealed with wax and stored at 4°C until further analysis at the MARUM isotope laboratory in Bremen. The analyses were carried out on a gas bench coupled to a Finnigan MAT 252 mass spectrometer using 1 mL of seawater. The routinely performed measurements of the internal standard SHK, which is calibrated against NBS 19 and seawater from the deep Atlantic Ocean, indicated a long-term standard deviation better than 0.1‰. The $\delta^{13}C_{DIC}$ was measured in March 2014, nearly 9 months after collection. With a few exceptions, no bubbles were present in the samples, and measured $\delta^{13}C_{DIC}$ values agree with historic WOCE values for corresponding locations and water masses.

Water samples for stable nitrogen and oxygen isotope analyses and nutrient measurements (NO_3^-, nitrite (NO_2^-), phosphate (PO_4^{3-}), silicic acid ($Si(OH)_4$) and ammonium (NH_4^+)) were collected at 12 stations. Seawater from the Niskin bottles was collected into a syringe, then filtered through a 45 μm surfactant-free cellulose acetate membrane into 15 mL high-clarity polypropylene conical tubes for nutrient measurements and into

acid-washed and prerinsed 60 mL polyethylene bottles for isotope analyses. The samples were stored at -20°C until analyses.

Nutrient analyses were conducted postcruise at the Bedford Institute of Oceanography (BIO). NO_3^- and NO_2^- in seawater were measured according to the Industrial Method 158-71W adapted from *Armstrong et al.* (1967) and *Grasshoff* (1969). The concentration of PO_4^{3-} was quantified colorimetrically using the Industrial Method 155-71W after *Murphy and Riley* (1962). For $Si(OH)_4$ measurements, the Industrial Method 186-72W was used according to *Strickland and Parsons* (1972). NH_4^+ concentrations were determined fluorometrically after *Kérouel and Aminot* (1997). Due to long-term storage, however, PO_4^{3-} and $Si(OH)_4$ concentrations at the same stations could not be reconciled with WOCE measurements at corresponding hydrographic stations.

To discern any excess or deficit of NO_3^- relative to coincident PO_4^{3-}, we exploit the semi–conservative N* tracer, defined here as N* (μM) = [NO_3^-] - 16*[PO_4^{3-}] (*Gruber and Sarmiento*, 1997). N* quantifies the concentration of reactive N added (from N_2 fixation) or lost (to denitrification) assuming that organic material is remineralized in a molar ratio of 16:1 (*Redfield*, 1934). We also refer to Si*, which corresponds to the difference between $Si(OH)_4$ and NO_3^- (Si* = [$Si(OH)_4$] - [NO_3^-]) as defined after *Sarmiento et al.* (2004). To ensure relative accuracy in calculating N* and Si*, we relied on nutrient concentrations from WOCE at corresponding stations for the end-member mixing estimates. The agreement between our measured NO_3^- concentrations and those from WOCE data provides assurance that the use of historical nutrient tracers in the mixing calculations is adequate.

To better interpret subsurface nutrient distributions, we calculated the mixed layer depth at each station using a vertical density gradient criterion defined by *Wijffels et al.* (1994), where the mixed layer depth represents the depth at which the density differs by 0.01 kg m^{-3} compared to the surface density.

NO_3^- $^{15}N/^{14}N$ and $^{18}O/^{16}O$ measurements were performed postcruise at the University of Connecticut using the denitrifier method (*Casciotti et al.*, 2002; *Sigman et al.*, 2001). This method uses denitrifying bacteria – in this case Pseudomonas chlororaphis f. sp. aureofaciens (ATCC#13985) – that lack an active nitrous oxide (N_2O) reductase, to convert NO_3^- into a nitrous oxide gas analyte. N and O isotopes in nitrous oxide were measured using a Delta V Advantage continuous flow isotope ratio mass spectrometer

interfaced with a Gas Bench II and sample preparation device, dual cold traps, and GC Pal auto-sampler. The $^{15}N/^{14}N$ reference is N_2 in air and the $^{18}O/^{16}O$ reference is Vienna Standard Mean Ocean Water (VSMOW).

NO_3^- samples were standardized to seawater-based reference material USGS-32 ($\delta^{15}N$ of 180‰ versus air; $\delta^{18}O$ of 25.7‰ versus VSMOW), USGS-34 ($\delta^{15}N$ of -1.8‰ versus air; $\delta^{18}O$ of -27.9‰ versus VSMOW), and IAEA-N3 ($\delta^{15}N$ of 4.7‰ versus air; $\delta^{18}O$ of 25.6‰ versus VSMOW) (*Böhlke et al.*, 2003; *Gonfiantini*, 1984). Standards were prepared in NO_3^--free seawater collected in the surface waters of the Sargasso Sea. Standard concentrations were adjusted to that of the corresponding samples in order to account for matrix effects on NO_3^- $\delta^{18}O$ measurements (*Weigand et al.*, 2016). Where NO_2^- was present, it was removed from samples with sulfamic acid prior to the addition of the denitrifiers according to *Granger and Sigman* (2009). Based on a minimum of triplicate measurements of individual samples, the analytical precision was 0.2‰ for $\delta^{15}N_{NO3}$ and 0.3‰ for $\delta^{18}O_{NO3}$.

To quantify the deviation from the 1:1 fractionation relationship associated with NO_3^- assimilation and denitrification, we define $\Delta(15–18)$ according to *Rafter et al.* (2013):

$$\Delta(15-18) = \delta^{15}N - ({}^{15}\varepsilon/{}^{18}\varepsilon) \times \delta^{18}O \tag{2.4}$$

where $\delta^{15}N$ and $\delta^{18}O$ are the isotopic composition of NO_3^- measured in a sample and ${}^{15}\varepsilon/{}^{18}\varepsilon$ the N-to-O isotope effect ratio of 1 (*Granger et al.*, 2004). In general terms, assimilation and denitrification do not modify $\Delta(15–18)$ from its initial value, as both impart an equivalent $\delta^{15}N_{NO3}$ and $\delta^{18}O_{NO3}$ enrichment with NO_3^- consumption. Elevated values of NO_3^- $\Delta(15–18)$ indicate a greater enrichment in $\delta^{15}N$ relative to $\delta^{18}O$ than expected for NO_3^- consumption, due to the remineralization of high-$\delta^{15}N$ material, whereas low values imply elevated $\delta^{18}O$ relative to $\delta^{15}N$ from the remineralization of isotopically light N, or from the reoxidation of NO_2^- in oxygen deficient zones (*Sigman et al.*, 2005).

To assess the relative contributions of northern and southern western boundary currents to the EUC, we compare our observations with analogous tracer measurements at 0°N/165°E (*Rafter and Sigman*, 2016). Determining the composition of a field sample based on matching a set of attributes (tracer values) in a defined set of sources (water masses) can be formulated as a linear least squares problem with both equality and inequality constraints (*Ben-David et al.*, 1997; *Mackey et al.*, 1996). Suppose we have s sources (water masses in

this case) and t tracers (potential temperature, salinity, oxygen, NO_3^-, etc.). Let $y^{t\times 1}$ be a vector of measured tracer values for a field sample of unknown composition and $x^{s\times 1}$ the set of unknown mixing fractions that must sum to one. The matrix $M^{t\times s}$ is a rectangular matrix of the measured tracer values for each of the sources (Appendix A). The unknown mixing fractions x can be obtained by solving the following linear least squares problem:

$$\underset{x}{\operatorname{argmin}} \parallel y - Mx \parallel^2 \tag{2.5}$$

$$1^T x = 1 \tag{2.6}$$

$$Ix \geq 0 \tag{2.7}$$

Equation (2.6) expresses the fact that the mixing fractions must sum to 1; 1^T is a row vector of s ones and 0 a column vector of 0s. The third inequality (equation (2.7)) states that mixing fractions must be strictly positive. In order to obtain statistically rigorous solutions to the mixing problem, we use a Monte Carlo approach to generate an ensemble of solutions (*Smith*, 1984; *Van den Meersche et al.*, 2009). The Monte Carlo method generates samples in the feasible set for the problem defined above: the feasible set consists of values for the mixing fractions that (a) add up to unity and (b) are all strictly positive. Rather than sample the feasible set uniformly, the samples are weighted by the error between the calculated tracer values from the model and the measured values y, as is standard in Markov Chain Monte Carlo calculations. We used the mirroring method described by *Van den Meersche et al.* (2009), but obtained identical results with the older, simpler sampling methods (Smith, 1984). For all the mixing models, we generated 20,000 samples and adjusted the step size in the sampling algorithm to ensure at least 30% of trial moves were accepted.

2.4 Study Area

A total of 18 hydrographic stations were visited during the EISPAC expedition (SO-228) aboard the RV SONNE in May and June 2013, off Mindanao at 8°N and 126°E and within and surrounding the Bismarck Sea at 7°S and 148°E (Figure 2.1). The complex bathymetry and hydrography of the WEP have been investigated, particularly during the Western Equatorial Pacific Observation Circulation Study (WEPOCS; e.g., *Bingham and Lukas*,

1994; *Lindstrom et al.*, 1987; *Toole et al.*, 1988; *Tsuchiya et al.*, 1989) with the overarching goal of elucidating the convoluted circulation pattern of the low-latitude western boundary currents (LLWBCs). An exhaustive list of the abbreviated names of the numerous currents and water masses of the WEP is provided in Table 2.1. These LLWBCs consist of the New Guinea Coastal Current (NGCC) and the New Guinea Coastal Undercurrent (NGCUC) in the southern hemisphere, and the Mindanao Current (MC) and Mindanao Undercurrent (MUC) in the northern hemisphere (*Lukas et al.*, 1996, Figure 2.1c).

South of the equator, the main water transport into the Bismarck Sea occurs through the Vitiaz Strait between the islands of New Guinea and New Britain (Figure 2.1b). This 1,100 m deep and $\sim$ 50 km wide sill separates the Bismarck Sea from the Solomon Sea and restricts deep and bottom water of southern origin from entering the coastal area of PNG. An additional, much smaller transport from the Solomon Sea into the Bismarck Sea has been recorded through St. Georges Channel (SGU; *Butt and Lindstrom*, 1994). The western boundary currents off PNG are fed by the broad South Equatorial Current (SEC), which crosses the Pacific at $\sim$ 3°N–20°S and brings water from the subtropical Pacific to the western boundary (Figure 2.1a). Upon reaching the western boundary, the SEC splits near 15°S into the North Vanuatu Jet (NVJ), and North and South Caledonian Jet (NCJ and SCJ, respectively). The NVJ flows directly into the Solomon Sea where it joins the NGCUC (*Cravatte et al.*, 2011), while the NCJ crosses the Coral Sea before splitting into two branches, one branch turning south into the Eastern Australian Current (EAC) and a second branch turning north into the Great Barrier Undercurrent (GBRUC) and NGCUC (Figure 2.1c; *Germineaud et al.*, 2016; *Qu and Lindstrom*, 2002). One part of the NGCUC crosses the Vitiaz Strait into the Bismarck Sea, while another part turns east south of the Bismarck Sea forming the New Britain Coastal Undercurrent (NBCU), which subsequently feeds the New Ireland Coastal Undercurrent (NICU) that flanks the eastern edge of New Ireland (NI). The NICU, in turn, bifurcates at the northern tip of NI into a western branch flowing into the Bismarck Sea and an eastward branch joining the EUC (*Butt and Lindstrom*, 1994). Subsurface waters east of NI are also influenced by a northern-more branch of the SEC at 38°S, which splits into a northern and southern branch as it approaches NI and the Solomon Islands (SI). The NICU east of NI is thus fed by waters from the NBCU, the Solomon Island Coastal Undercurrent (SICU) and the low-latitude SEC, with their relative contribution depending on the season (*Melet et al.*,

Table 2.1: Compilation of abbreviations used throughout this chapter.

	General		Currents
AOU	Apparent Oxygen Utilization	EAC	Eastern Australian Current
BL	Barrier Layer	EUC	Equatorial Undercurrent
DIC	Dissolved Inorganic Carbon	GBRUC	Great Barrier Reef Undercurrent
NB	New Britain	HE	Halmahera Eddy
NH	New Hanover	LLWBC	Low-Latitude Western Boundary Current
NI	New Ireland	MC	Mindanao Current
ODZ	Oxygen Deficient Zone	ME	Mindanao Eddy
PNG	Papua New Guinea	MUC	Mindanao Undercurrent
SI	Solomon Islands	NBCU	New Britain Coastal Undercurrent
WEP	Western Equatorial Pacific	NCJ	North Caledonian Jet
		NEC	North Equatorial Current
	Water Masses	NECC	North Equatorial Countercurrent
AAIW	Antarctic Intermediate Water	NGCC	New Guinea Coastal Current
EqPIW	Equatorial Pacific Intermediate Water	NGCUC	New Guinea Coastal Undercurrent
LCDW	Lower Circumpolar Deep Water	NICU	New Ireland Coastal Undercurrent
NPIW	North Pacific Intermediate Water	NSCC	Northern Subsurface Countercurrent
NPTW	North Pacific Tropical Water	NVJ	North Vanuatu Jet
PDW	Pacific Deep Water	SCJ	South Caledonian Jet
SAMW	Subantarctic Mode Water	SEC	South Equatorial Current
SPTW	South Pacific Tropical Water	SECC	South Equatorial Countercurrent
UCDW	Upper Circumpolar Deep Water	SGU	St. Georges Undercurrent
WSPCW	Western South Pacific Central Water	SICU	Solomon Island Undercurrent
		SSCC	Southern Subsurface Countercurrent

2010). Along the northeastern PNG coast, the surface NGCC turns to the east feeding the North Equatorial Countercurrent (NECC), while the underlying NGCUC partly turns eastward feeding the EUC (*Bingham and Lukas*, 1994) and partly crosses the equator and diverges into the Indonesian Throughflow or northward along the coast of the Philippines into the Mindanao Undercurrent (Figure 2.1c; *Qu et al.*, 2004; *Tsuchiya*, 1968). The eastward deflection of the NGCC into the NECC further results in a quasi-stationary eddy structure called the Halmahera Eddy (HE) northwest of PNG (*Fine et al.*, 1994; *Kashino et al.*, 2013).

North of the equator, the boundary currents are fed by the NEC, which crosses the Pacific at $\sim$ 10°N–20°N (Figure 2.1a). The NEC bifurcates at 14°N into two branches, the northward Kuroshio Current and the southward MC. At the southern tip of the Philippines, one branch of the MC flows southwestward into the Celebes Sea and feeds the Indonesian Throughflow (*Gordon and Fine*, 1996), while the other branch of the MC flows eastward and feeds the NECC (Figure 2.1c). The latter branch creates the persistent quasi-stationary Mindanao Eddy (ME) off the coast of the Philippines (*Fine et al.*, 1994; *Kashino et al.*, 2013; *Lukas et al.*, 1991). Both the NECC, as well as its southern counterpart the South Equatorial Countercurrent (SECC), are broad zonal surface currents in between $\sim$ 5°N–10°N and $\sim$ 3°S–10°S, respectively. Below the surface, the Northern and Southern Subsurface Countercurrents (NSCC and SSCC) flow eastward at $\sim$ 3° off the equator (Figure 2.1c).

Several water masses are associated with the LLWBCs (Figure 2.2). To the south, off PNG, subsurface water masses are composed of South Pacific Tropical Water (SPTW), apparent as a salinity maximum ($\sim$ 35.6) in the upper thermocline ($\sim 24.8\sigma_\theta$), and Western South Pacific Central Water (WSPCW) in the lower thermocline ($\sim 26.4\sigma_\theta$). SPTW originates in the oligotrophic subtropical South Pacific gyre due to high evaporation and consequent subduction of surface water (*Grenier et al.*, 2013; *Tomczak and Godfrey*, 1994). In the WEP, SPTW can further be divided into two branches, one branch reaching the Solomon Sea via the NVJ (*Germineaud et al.*, 2016; *Grenier et al.*, 2013), and a second branch entering the Solomon Sea via the GBRUC (*Gasparin et al.*, 2014). WSPCW forms seasonally through winter-convection in the subtropical convergence zone between Tasmania and New Zealand (*Grenier et al.*, 2014; *Roemmich and Cornuelle*, 1992; *Qu et al.*, 2009) and reaches the southern study site via the NCJ and GBRUC (*Gasparin et al.*, 2014).

Below the thermocline, SAMW-density water (26.8–27.1σ_θ) is discernible as a pycnostad with relatively high oxygen concentrations and a characteristically low $Si(OH)_4$-to-NO_3^- ratio (Si* minimum; *Sarmiento et al.*, 2004). The underlying Antarctic Intermediate Water (AAIW) is discernible as a salinity minimum ($\sim$ 34.4) centered around 800 m (27.2σ_θ) and extending down to $\sim$ 1,000 m. Off New Hanover (NH; GeoB1726-1), intermediate water masses are composed of Equatorial Pacific Intermediate Waters (EqPIW; $\sim$ 27.3σ_θ), permeating along the outer edge of the Bismarck Sea. These correspond to the South Pacific Tropical Intermediate Water described by *Bingham and Lukas* (1995), originating in the eastern South Pacific and reaching the study area below the EUC via the Equatorial Intermediate Current. Upper Circumpolar Deep Water (UCDW) underlies AAIW and EqPIW and forms a distinctive nearly isohaline (34.53 $\pm$ 0.03) layer between 1,200 and 2,000 m (27.3–27.7σ_θ).

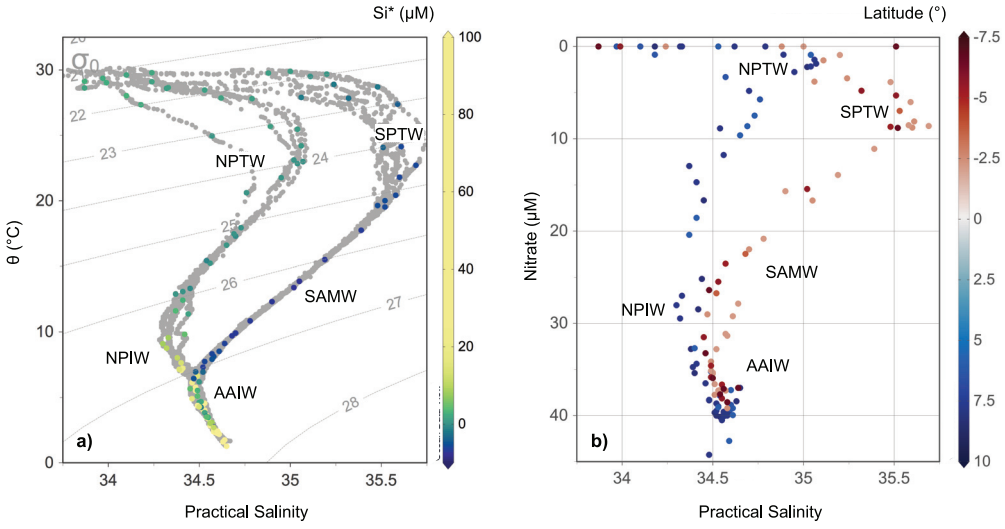

Figure 2.2: (a) Potential temperature (θ) and (b) NO_3^- concentration versus practical salinity, including summary of prevalent water masses. Gray lines (a) indicate isopycnal lines, and colors show (a) Si* ($[Si(OH)_4] - [NO_3^-]$) and (b) latitude of stations. Water masses include the North and South Pacific Tropical Water (NPTW and SPTW), Subantarctic Mode Water (SAMW), North Pacific Intermediate Water (NPIW), and Antarctic Intermediate Water (AAIW).

North of the equator off Mindanao, subsurface waters correspond to North Pacific Tropical water (NPTW) in the upper thermocline, apparent as a salinity maximum ($\sim$

34.9) centered around $\sim$ 140 m ($\sim 24.0\sigma_\theta$), and North Pacific Intermediate Water (NPIW) in the lower thermocline, with a characteristic salinity minimum ($\leq$ 34.4) centered at $\sim$ 350 m ($\sim 26.6\sigma_\theta$; Figure 2.2). NPTW forms at $\sim$ 25°N where high evaporation leads to the subduction of surface water (*Katsura et al.*, 2013; *Tsuchiya*, 1968). The salinity minimum of the NPIW is formed in the northwestern part of the subtropical gyre between the Kuroshio Extension and the Oyashio front (*Talley*, 1993). Both NPTW and NPIW are carried westward by the NEC and reach Mindanao via the MC. Pacific Deep Water (PDW), underlaying NPIW (*Kawabe and Fujio*, 2010; *Johnson and Toole*, 1993; *Wijffels et al.*, 1996), is a mixture of Antarctic Bottom Water, North Atlantic Deep Water and AAIW, and is characterized by reduced oxygen concentrations and high nutrient loads (*Tomczak and Godfrey*, 1994).

2.5 Results

2.5.1 General hydrography and water mass distribution

Hydrographic profiles reveal that stations south of the equator near PNG differ markedly from stations north of the equator off the coast of Mindanao. In general, surface and intermediate-depth waters are more saline and warmer south of equator than at corresponding depths off Mindanao (Figures 2.2 and 2.3, and Table 2.2). Both regions are characterized by relatively warm ($\geq$ 28.6°C), fresh ($\leq$ 34.0) surface waters and a shallow mixed layer ranging between $\leq$ 5 m near the coast to a maximum of 40 m further offshore (GeoB17426-1; Figures 2.2 and 2.3). Waters below the surface mixed layer correspond to the Barrier Layer (BL) of the Western Pacific Warm Pool and equatorial Pacific (*Lukas et al.*, 1991), an intermediate layer isothermal with the surface (28–30°C) that prevents heat flux through the bottom of the mixed layer into the thermocline (*Tomczak and Godfrey*, 1994).

At the southern stations off PNG, the thermocline extends from 60 to 400 m depth. Thermocline waters are comprised of SPTW ($24.8\sigma_\theta$, 19.7 $\pm$ 0.3°C), characterized by a salinity maximum of 35.51 $\pm$ 0.02 centered at $\sim$ 175 m in the upper thermocline (Figures 2.2 and 2.3, and Table 2.2), and WSPCW ($\sim 26.2\sigma_\theta$, 14.4 $\pm$ 1.4°C) in the lower thermocline. Subthermocline waters correspond to SAMW-density water ($26.8\sigma_\theta$, 7.8 $\pm$ 0.9°C), with lower salinity than overlaying tropical waters (34.53 $\pm$ 0.06) and a pronounced Si* minimum centered around $\sim$ 500 m (Figure 2.2a). AAIW is discernible as a salinity

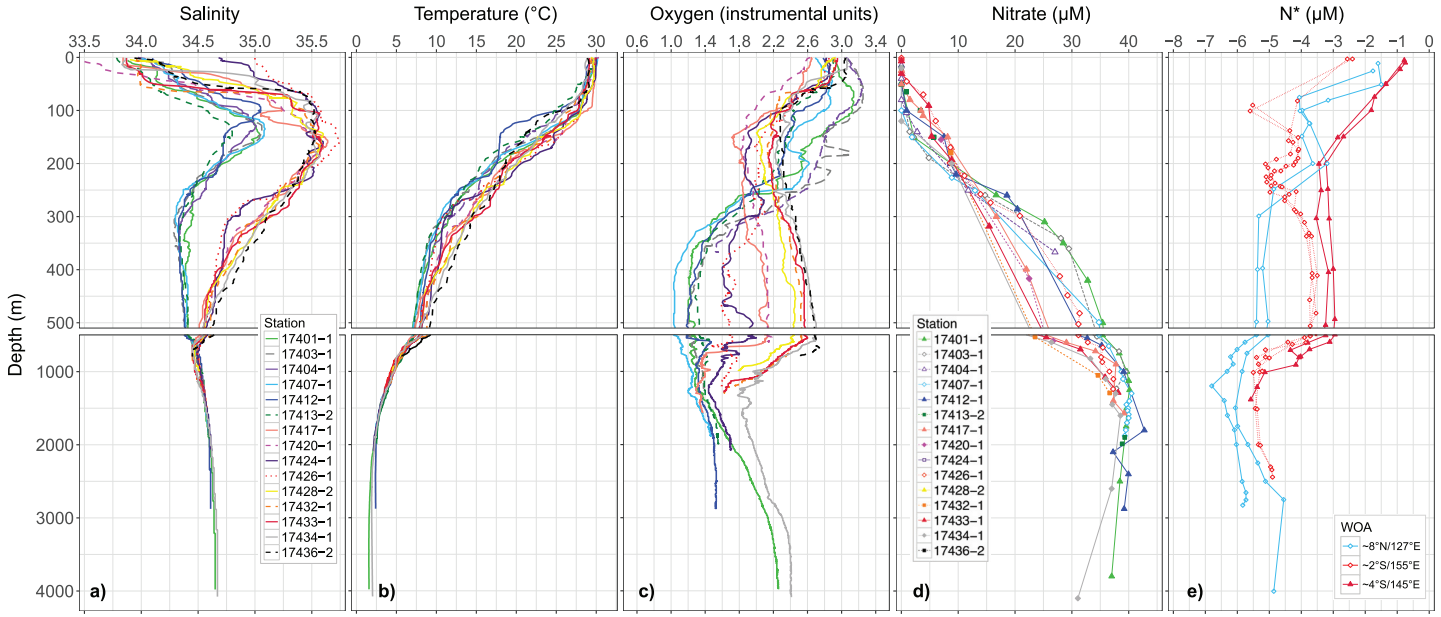

Figure 2.3: Water column profiles of (a) salinity, (b) temperature, (c) oxygen, (d) NO_3^- concentration, and (e) N* versus depth. Colors illustrate different stations with shades of blue/green indicating northern sites and shades of red showing southern sites. (e) N* values are derived from WOA13. Note variations in depth intervals on y axis.

minimum of 34.46 $\pm$ 0.01 centered around 800 m (27.2σ_θ, 5.3 $\pm$ 0.5°C) and extending down to $\sim$ 1,000 m. Below intermediate waters, salinity increases to 34.53 $\pm$ 0.03 in UCDW ($\sim$ 27.5σ_θ, 3.8 $\pm$ 0.5°C).

At the northern stations off Mindanao, the warm BL extends to the top of the thermocline at 90 m depth. The upper thermocline consists of NPTW (24.0σ_θ, 23.5 $\pm$ 1.4°C) centered at $\sim$ 140 m, with a less pronounced salinity maximum of 34.98 $\pm$ 0.08 than the corresponding SPTW. The lower thermocline corresponds to NPIW (26.6σ_θ, 9.2 $\pm$ 0.8°C), characterized by a salinity minimum ($\leq$ 34.4) centered at $\sim$ 350 m. Though not readily apparent, a slight salinity minimum ($\geq$ 27.2σ_θ) and lower temperature (0.5°C) at $\sim$ 800 m in between NPIW and the underlying PDW (27.6σ_θ; 2.7 $\pm$ 0.4°C) suggest some intrusion of AAIW reaching Mindanao from south of the equator. Below PDW ($>$ 3,000 m), salinity increases from 34.59 $\pm$ 0.02 in PDW to 34.65 $\pm$ 0.01 at $\sim$ 3,800 m.

2.5.2 NO_3^- and N* distributions

The concentration of NO_3^- is below detection in the surface mixed layer at stations north and south of the equator (Figures 2.2b and 2.3d, and Table 2.2). In both regions, NO_3^- is detectable in the BL and increases monotonically into tropical waters below: NO_3^- concentrations in SPTW (8.6 $\pm$ 0.1 μM) are higher than in NPTW (1.9 $\pm$ 0.7 μM; Figure 2.2b). At the southern stations, the concentration of NO_3^- increases in SAMW-density water to $\sim$ 25 μM off PNG and to $\sim$ 30 μM off NH (GeoB17426-1), respectively. In the underlying intermediate layer, NO_3^- concentrations average 32.4 $\pm$ 1.2 μM in AAIW off PNG and 35.7 $\pm$ 0.8 μM in EqPIW off NH (Table 2.2). At corresponding depths north of the equator, the concentration of NO_3^- in NPIW is $\sim$ 30 μM, increasing to nearly 40 μM in PDW. Bottom waters north and south of the equator have indistinguishable NO_3^- concentrations of $\sim$ 37 μM.

The N* signal, indicative of any stoichiometric excess or deficit in NO_3^- relative to PO_4^{3-}, is generally less pronounced at stations south of the equator relative to corresponding depths at northern stations (Figure 2.3e). Off PNG, N* in SPTW is –2.9 $\pm$ 0.2 μM and declines throughout the water column to $\sim$ –3.3 μM in WSPCW and SAMW-density water, –4.1 $\pm$ 0.2 μM in AAIW, and –5.4 μM in UCDW, respectively. A similar decline from the thermocline toward deep waters is apparent north of the equator off Mindanao, with N* decreasing from –3.7 $\pm$ 0.3 μM in NPTW to –5.2 $\pm$ 0.4 μM in NPIW, reaching a minimum of –6.0 $\pm$ 0.3 μM in PDW, followed by a slight increase to –5.2 $\pm$ 0.5 μM near

Table 2.2: Selected hydrographic parameters as well as NO_3^- and DIC isotope-related properties of the main water masses. Nutrient concentrations for N* values are from WOCE (MD and PNG) and WOD (NH). Oxygen concentrations for AOU calculations are from WOCE (MD and PNG) and PANDORA (NH).

	Lon (°E)	Lat (°N)	Water mass	σ_θ (kg m^{-3})	θ (°C)	Sal	[NO_3^-] (μM)	$\delta^{13}C_{DIC}$ (‰)	$\delta^{15}N_{NO3}$ (‰)	$\delta^{18}O_{NO3}$ (‰)	$\Delta(15-18)$ (‰)	N* (μM)	AOU (μmol kg^{-1})
MD	127	8	NPTW	23.0–25.0	23.5	34.98	1.9	0.6	5.7	3.5	2.3	-3.7	37.6
			SD		1.4	0.08	0.7	0.3	0.2	0.3	0.6	0.3	15.5
			NPIW	26.5–26.8	9.2	34.37	29.1	0.1	7.1	3.7	3.5	-5.2	177.9
			SD		0.8	0.04	2.5	0.0	0.1	0.2	0.2	0.4	12.9
			PDW	27.5–27.7	2.7	34.59	39.6	0.1	6.0	2.3	3.7	-6.0	218.3
			SD		0.4	0.02	0.5	0.0	0.2	0.1	0.1	0.3	3.7
			BW	>27.7	1.6	34.64	37.0	0.2	5.4	2.0	3.4	-5.2	193.4
			SD		0.1	0.01						0.5	11.5
NH	151	-2	SPTW	24.3–25.3	21.6	35.63	8.6	0.8	8.3	3.0	5.3	-4.0	92.8
			SD		1.6	0.06	0.1	0.1				0.7	8.8
			SAMW	26.8–27.1	8.2	34.57	30.5	0.8	6.9	2.7	4.2	-3.4	183.4
			SD		0.8	0.04	1.9	0.1	0.1	0.1	0.1	0.5	20.4
			EqPIW	27.2–27.4	4.7	34.50	35.7	0.6	6.3	2.3	4.0	-4.7	188.6
			SD		0.4	0.01	0.8	0.2	0.1	0.0	0.1	0.5	11.4
			UCDW	27.4–27.5	3.8	34.53	37.3	0.7	6.1	2.2	3.9	-5.2	na
			SD		0.2	0.01	0.0	0.4	0.0	0.0	0.1	0.1	
PNG	147	-6	SPTW	24.3–25.3	19.7	35.51	8.8	0.8	7.5	3.0	4.5	-2.9	57.9
			SD		0.3	0.02	0.1	0.0	0.1	0.0	0.1	0.2	7.8
			WSPCW	25.8–26.5	14.4	35.10	15.5	na	6.9	3.0	3.9	-3.4	94.2
			SD		1.4	0.12						0.2	7.0
			SAMW	26.8–27.1	7.8	34.53	25.1	1.1	6.5	2.7	3.9	-3.3	134.9
			SD		0.9	0.06	1.5	0.1	0.1	0.1	0.1	0.4	17.8
			AAIW	27.1–27.3	5.3	34.46	32.4	0.7	6.3	2.2	4.0	-4.1	160.9
			SD		0.5	0.01	1.2	0.0	0.0	0.1	0.0	0.2	7.9
			UCDW	27.3–27.7	3.8	34.53	36.8	0.4	6.0	2.1	3.9	-5.4	207.4
			SD		0.5	0.03	1.3	0.2	0.1	0.2	0.1		

the bottom.

2.5.3 NO_3^- and DIC isotope distributions

Profiles of $\delta^{15}N_{NO3}$ differ between stations north and south of the equator, particularly in the thermocline and toward the surface (Figure 2.4a). Due to NO_3^- levels below the lower limit of quantification for NO_3^- isotope ratios (< 0.5 μM), no N and O isotope data are available for surface waters. In the underlying BL, $\delta^{15}N_{NO3}$ values in a number of profiles are relatively elevated in both regions, particularly at southern stations off NH where values reach upward of 17.6‰ at 50 m depth. The $\delta^{15}N_{NO3}$ decreases progressively in the thermocline, with tropical waters being substantially more ^{15}N-enriched at southern stations (7.4–9.4‰) compared to stations off Mindanao (5.5–7.6‰). Values in SAMW-density water and NPIW below are comparable (6.5–7.2‰), albeit with slightly higher values in the core of NPIW. Among southern profiles, the $\delta^{15}N_{NO3}$ in SAMW-density water off NH (6.9 $\pm$ 0.1‰) is notably more elevated than at corresponding depths off PNG (6.5 $\pm$ 0.1‰). The $\delta^{15}N_{NO3}$ in intermediate waters are similar in both regions ($\sim$ 6‰ in AAIW and PDW) and remain comparable in deep waters (5.5‰, Figure 2.4a).

The $\delta^{18}O_{NO3}$ profiles reveal lower values at most depth intervals for stations south of the equator (Figure 2.4b). Similar to $\delta^{15}N_{NO3}$, $\delta^{18}O_{NO3}$ values are elevated in the BL at a number of stations, particularly off NH ($\leq$ 17.6‰). Below the BL, values decrease throughout the upper thermocline to an average of 3.5 $\pm$ 0.3‰ in NPTW and 3.0 $\pm$ 0.0‰ in SPTW. Values of $\delta^{18}O_{NO3}$ decrease further toward mode and intermediate waters at the southern site (2.7 $\pm$ 0.1‰ in SAMW-density water, 2.2 $\pm$ 0.1‰ in AAIW) while slightly increasing in intermediate waters off Mindanao (3.7 $\pm$ 0.2‰ in NPIW) before decreasing in PDW (2.3 $\pm$ 0.1‰). In deep waters, $\delta^{18}O_{NO3}$ values are comparable in UCDW and North Pacific bottom water averaging $\sim$ 2.1‰.

The contrasting depth distributions of $\delta^{15}N_{NO3}$ and $\delta^{18}O_{NO3}$ north and south of the equator give way to strikingly divergent profiles of Δ(15–18) between the two regions (Figure 2.4c). South of the equator, values reach maxima in SPTW ranging from 4.4‰ to 5.3‰, followed by a decrease in mode and intermediate waters ($\sim$ 4.0‰). Conversely, Δ(15–18) values show distinct minima in NPTW ($\geq$ 1.6‰) and a subsequent increase toward intermediate and deep waters (3.5 $\pm$ 0.2‰ and 3.7 $\pm$ 0.1‰ in NPIW and PDW, respectively).

Finally, $\delta^{13}C_{DIC}$ values are generally more elevated at the southern sites relative to

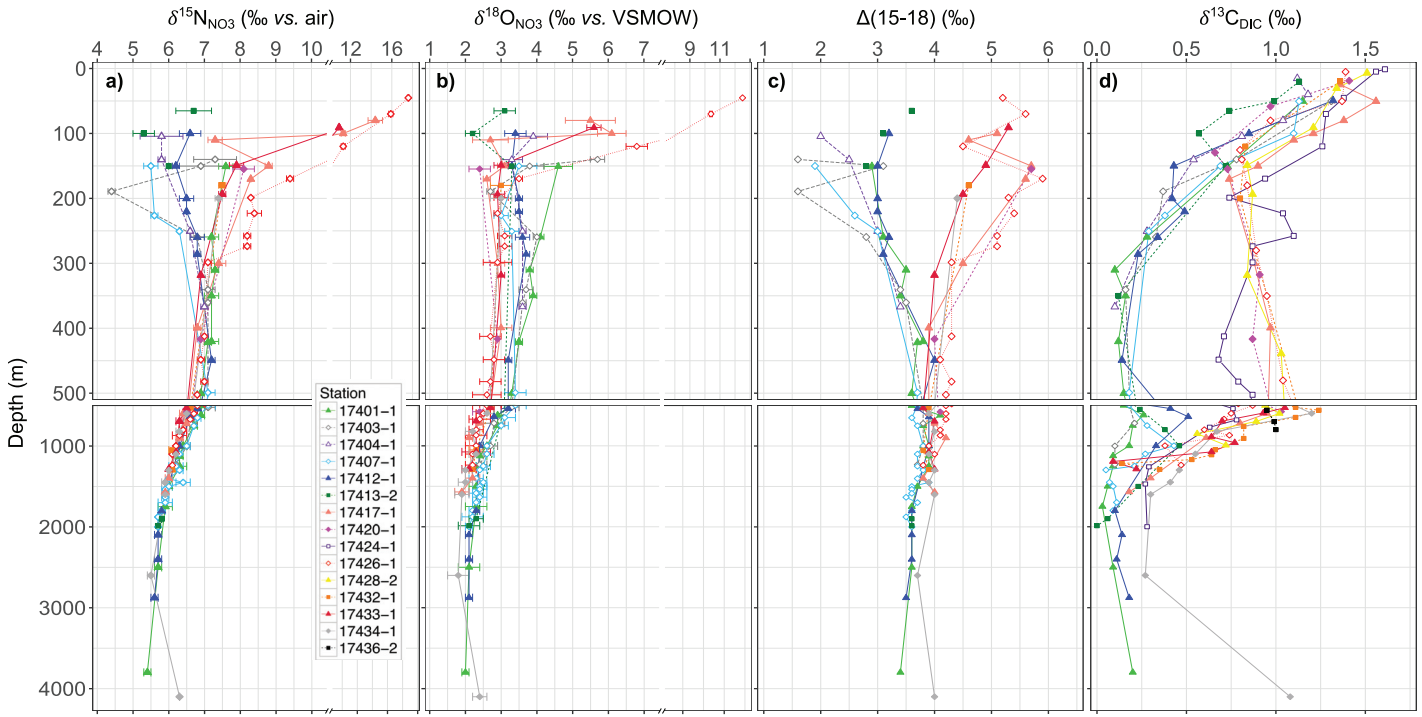

Figure 2.4: Water column profiles of (a) $\delta^{15}N_{NO3}$, (b) $\delta^{18}O_{NO3}$, (c) NO_3^- Δ(15–18), and (d) $\delta^{13}C_{DIC}$ versus depth. Note differences in intervals on x (a and b) and y axes. Colors illustrate different stations with shades of blue/green indicating northern sites and shades of red showing southern sites.

corresponding depths north of the equator (Figure 2.4d and Table 2.2). Surface values are high in both regions (1.2–1.6‰), albeit perceptibly more so at southern stations. Values of $\delta^{13}C_{DIC}$ decrease with depth reaching values of 0.8 ± 0.1‰ versus 0.6 ± 0.3‰ in SPTW and NPTW, respectively. Values decrease further to an average of 0.1 ± 0.0‰ in NPIW and in underlying PDW, whereas they increase slightly in SAMW-density water to a maximum of $\sim 1.1 \pm 0.1$‰. As with other tracers, $\delta^{13}C_{DIC}$ in SAMW-density water off NH differs from that off PNG, posting lower values of 0.8 ± 0.1‰. Below the mode water, $\delta^{13}C_{DIC}$ values are 0.7 ± 0.0‰ in AAIW, decreasing further in UCDW. A slight maximum in $\delta^{13}C_{DIC}$ at $27.1\sigma_\theta$ at stations north of the equator is evident, consistent with the intrusion of AAIW off Mindanao.

2.6 Discussion

The nutrient characteristics of WEP thermocline waters (≈100–400 m) are important because they fuel primary production locally and across the Pacific basin via the EUC (*Rafter and Sigman*, 2016; *Toggweiler et al.*, 1991). Our $\delta^{15}N_{NO3}$, $\delta^{18}O_{NO3}$, and $\delta^{13}C_{DIC}$ measurements indicate a different biogeochemical history of WEP nutrients north (Mindanao stations) versus south (PNG and NH) of the equator (Figure 2.4 and Table 2.2). Specifically, our data indicate interbasin differences in (a) the contribution of remineralization to bulk nutrients in the thermocline, (b) the $\delta^{15}N$ of organic material remineralized in the thermocline, and (c) the lateral contribution of nutrients from the eastern margins. We also identify subtle nutrient differences between PNG and NH regions south of the equator that suggest different southern pathways to the water mass crossroads of the Pacific (*Fine et al.*, 1994).

To understand the origins of these contrasting thermocline-depth nutrient characteristics, we examine our data beginning with WEP intermediate-depth (≈400–1,200 m) waters, which resupply thermocline nutrients to the respective basins via SAMW (*Palter et al.*, 2010) and NPIW. We then examine tracer distributions in the WEP thermocline and derive the $\delta^{15}N$ of sinking organic matter that is necessary to explain NO_3^- biogeochemical differences in the northern and southern WEP, which has implications for tracing the contribution of newly fixed nitrogen to the sinking organic matter flux. Finally, because nutrient characteristics of the WEP thermocline fuel equatorial Pacific primary production (*Rafter and Sigman*, 2016), we investigate the contribution of northern and southern WEP

waters to the EUC.

2.6.1 The biogeochemical history of WEP intermediate-depth waters

To a first approximation, lower oxygen concentrations, lower $\delta^{13}C_{DIC}$ values, and higher nutrient concentrations in northern WEP intermediate waters (off Mindanao; Figures 2.3c and d, and 2.4) point to a greater accumulation of remineralized material relative to the southern sites. The greater contribution of remineralized NO_3^- to the total pool at the northern sites should be reflected in the $\delta^{18}O_{NO3}$, which is sensitive to nitrification: newly nitrified NO_3^- adopts a $\delta^{18}O$ signature similar to that of ambient seawater (*Buchwald et al.*, 2012; *Casciotti et al.*, 2008; *Sigman et al.*, 2009b), thus tending to lower the $\delta^{18}O_{NO3}$ proportionally. As such, a greater contribution of remineralized NO_3^- should manifest as a lower $\delta^{18}O_{NO3}$ of subsurface NO_3^- at the northern stations. Contrary to expectations, however, the $\delta^{18}O_{NO3}$ is more elevated at the northern sites (Figure 2.4b). This difference suggests that other processes overprint the tendency toward lower $\delta^{18}O_{NO3}$ due to nitrification. Below, we examine the biogeochemical history of intermediate and mode waters in the context of their origin and circulation to explain the apparent discrepancy between $\delta^{13}C_{DIC}$ and $\delta^{18}O_{NO3}$.

2.6.1.1 The origin of southern WEP $\delta^{18}O_{NO3}$

With respect to the South Pacific, both SAMW and AAIW form due to winter cooling and deep convection of the surface layer at the Subantarctic Front of the Southern Ocean (*McCartney*, 1977; *Talley*, 1996). High surface productivity in the Southern Ocean aided by strong air-sea exchange at cold temperatures (*Bostock et al.*, 2010) imprints relatively elevated initial $\delta^{13}C_{DIC}$ values on SAMW and AAIW. In turn, the $\delta^{15}N_{NO3}$ and $\delta^{18}O_{NO3}$ in SAMW and AAIW are set by those of NO_3^- in the source waters and by biological transformations in the surface layer. In the Southern Ocean, UCDW, which upwells to the surface as part of the Southern Overturning Circulation (*Tomczak and Godfrey*, 1994), is considered as the source water of SAMW. This mechanism delivers nutrients to the surface mixed layer of the Open Antarctic Zone (*Orsi et al.*, 1995) with characteristic isotopic signatures ($\delta^{15}N_{NO3}$ of $\sim 5.0‰$, $\delta^{18}O_{NO3}$ of $\sim 2.0‰$, Table 2.3; *DiFiore et al.*, 2009; *Rafter et al.*, 2013; *Sigman et al.*, 1999, 2000). In transit from the Open Antarctic Zone and across the Subantarctic Front towards the Subantarctic Zone, isotopic discrimination

associated with the partial assimilation of NO_3^- results in the export of relatively low-$\delta^{15}N$ organic matter from the surface (*Altabet and Francois*, 1994; *Karsh et al.*, 2003; *Lourey et al.*, 2003), and a parallel increase in both the $\delta^{15}N_{NO3}$ and $\delta^{18}O_{NO3}$ remaining in surface waters that form SAMW at the Subantarctic Zone (*DiFiore et al.*, 2006; *Rafter et al.*, 2013; *Sigman et al.*, 1999; *Smart et al.*, 2015). The resulting $\delta^{15}N_{NO3}$ and $\delta^{18}O_{NO3}$ values of high latitude SAMW (51°S–41°S) and AAIW (56°S–51°S) are 6.2 ± 0.4‰ and 3.5 ± 0.7‰ and 5.5 ± 0.2‰ and 2.8 ± 0.3‰, respectively (*DiFiore et al.*, 2006; *Rafter et al.*, 2013; *Sigman et al.*, 1999; *Smart et al.*, 2015). Prior work illustrated that intermediate-depth $\delta^{18}O_{NO3}$ south of the equator is lower than its high latitude source water (SAMW) because of NO_3^- added by organic matter remineralization (*Rafter et al.*, 2013). The $\delta^{18}O_{NO3}$ values observed in SAMW-density waters of the southern WEP are similarly lower than the Southern Ocean end-member (Figure 2.5), suggesting NO_3^- was added in transit by remineralization.

To assess whether the addition of remineralized NO_3^- can similarly account for the observed decrease in $\delta^{18}O_{NO3}$ between the SAMW source and our stations south of the equator, we use a simple mass-isotope balance (*Rafter et al.*, 2013):

$$\delta^{18}O_{nitr} = (\delta^{18}O_{obs} \times [NO_3^-]_{obs} - \delta^{18}O_{source} \times [NO_3^-]_{source})/[NO_3^-]_{nitr} \quad (2.8)$$

Based on the water-mass characteristic values in Tables 2.2 and 2.3, the change in SAMW-density NO_3^- concentrations is 9.9 μM between the SAMW 50°S end-member and SAMW-density waters at the NH station. A $\delta^{18}O_{nitr}$ of 1.0‰ is necessary to explain the change in NO_3^- concentrations and $\delta^{18}O_{NO3}$ between SAMW and NH stations. This $\delta^{18}O_{nitr}$ value is in agreement with similar derivations conducted by *Rafter et al.* (2013), as well as with the empirical value for global ocean nitrification of +1.1‰ derived by *Sigman et al.* (2009b). Alternatively, we can estimate the fraction of remineralized (relative to preformed) NO_3^- using the Apparent Oxygen Utilization (AOU) and the respiration stoichiometry of *Anderson* (1995). The remineralized NO_3^- expected based on AOU is 13.3 μM, corresponding to a $\delta^{18}O_{nitr}$ of 0.8‰ (equation (6)), thus coherent with the NO_3^--based mass balance.

Another potential source of NO_3^- isotopic variability is denitrification in the eastern tropical Pacific (*Brandes et al.*, 1998; *Sigman et al.*, 2005; *Voss et al.*, 2001), which has a strong influence on N* *Gruber and Sarmiento* (1997). N* decreases from the 50°S

Table 2.3: Reference values of selected hydrographic parameters as well as NO_3^- isotope-related properties of the main water masses from *Rafter et al.* (2012, 2013); *Rafter and Sigman* (2016) and *Sigman et al.* (2009a). DIC isotope ratios are from *Bostock et al.* (2010, 2013).

	Lon	Lat	Water mass	σ_θ (kg m^{-3})	θ (°C)	Sal	$[NO_3^-]$ (μM)	$\delta^{13}C_{DIC}$ (‰)	$\delta^{15}N_{NO3}$ (‰)	$\delta^{18}O_{NO3}$ (‰)	$\Delta(15-18)$ (‰)	N* (μM)	AOU (μmol kg^{-1})
ALOHA	158°W	23°N	TW	23.0–25.0	20.6	35.19	1.9	na	4.6	3.3	1.3	-1.7	na
			SD		0.5	0.04	0.6		0.1	0.1	0	0.4	
			NPIW	26.5–26.8	7.4	34.08	28.2	-0.5	6.7	3.3	3.4	-4.9	na
			SD										
			PDW	27.5–27.7	2.5	34.6	40.9	na	5.7	2.3	3.5	-5.5	na
			SD		0.5	0.03	0.5		0.3	0.2	0.2	0.4	
			Abyssal	>27.7	1.5	34.68	37.5	na	5.1	1.9	3.2	-4	na
			SD		0.1	0.02	1.1		0.1	0.1	0.1	0.4	
EqPac	165°E–95°W	0°N	EUC	26.0	16.3	34.99	14	na	7.1	3	4.1	-5.1	na
			SD		2.6	0.12	6.5		0.3	0.3	0.3	0.9	
	110°W	5°N	NSCC	26.1	13.1	34.67	25.9	na	7.2	3.9	3.3	na	na
			SD		3.1	0.03	4.6		0.2	0.5	0.5		
	110°W	5°S	SSCC	26.4	13	34.95	28.7	na	5.8	3.5	2.3	na	na
			SD		0.5	0.03	2.2		0.6	0.3	0.7		
South Pacific	150°W	20°S	SAMW	26.8–27.1	6.1	34.37	29	na	7	2.9	4.1	-3.6	149.1
			SD		0.6	0.01	1.8		0.6	0.7	0.1	0	7.4
	150°W	20°S	AAIW	27.1–27.3	4.9	34.41	33	0.75–1.75	6.4	2.2	4.3	-4.2	321.3
			SD		0.5	0.03	1.4		0.1	0.1	0.1	0.3	3.5
Southern Ocean	150°W	51°S–41°S	SAMW	26.8–27.1	7.2	34.41	20.6	na	6.2	3.5	2.7	-2.4	58.9
			SD		0.9	0.07	3.7		0.4	0.7	0.3	0.2	18.7
	150°W	56°S–51°S	AAIW	27.1–27.3	3.3	34.19	29.8	0.85–1.6	5.5	2.8	2.7	-2.9	334.9
			SD		1	0.12	1.5		0.2	0.3	0.2	0.4	8.6
	15°W	56°S	UCDW	na	2.5	34.46	33.5	na	5	2	3	-3.5	153.3
			SD		0.2	0.14	0.7		0.1	0.3	0.2	0.3	19

SAWM end-member from -2.4 $\pm$ 0.2 to -3.4 $\pm$ 0.5 μM off NH (Table 2.3). This suggests some entrainment of ODZ water from the eastern margins, reaching the eastern coast of NI and NH via the northern branch of the SEC (*Rafter et al.*, 2012). Thus, mass balance calculations suggest that the net decrease in $\delta^{18}O_{NO3}$ at NH can largely be explained by the addition of remineralized NO_3^- in transit, countered by modest lateral entrainment of ^{18}O-enriched NO_3^- from the margins.

At stations off PNG, the SAMW-density $\delta^{18}O_{NO3}$ is identical to that off NH (2.7‰), however, the NO_3^- concentration is markedly lower (25.1 $\pm$ 1.5 μM versus 30.5 $\pm$ 1.9 μM, respectively). Repeating the δ^{18}O mass balance exercise for SAMW-density NO_3^- off PNG results in lower $\delta^{18}O_{nitr}$ values (-1.0‰ or -0.5‰ using ΔAOU) that appear inconsistent with expectations. Admittedly, these calculations are subject to large uncertainty and fail to account for a variety of processes, such as differential mixing between PNG and NH stations and end-member water mass composition. Indeed, the complex bathymetry at the western boundary off PNG reportedly fosters diapycnal mixing of intermediate water masses (*Germineaud et al.*, 2016; *Grenier et al.*, 2011; *Melet et al.*, 2011), such that the discrepancies in regenerated NO_3^- estimates between the NH and PNG stations could arise from the mixing of SAMW-density water with overlaying NO_3^--deplete gyre water, lowering the nutrient content of SAMW-density water without affecting its isotopic composition. However, hydrographic differences in other parameters such as $\delta^{15}N_{NO3}$ (discussed further below), salinity, $\delta^{13}C_{DIC}$ and oxygen concentrations argue for differences in the end-member water masses ventilating SAMW-density waters off PNG versus NH. In this respect, SAMW reaches PNG waters via the southern branch of the SEC, which may have a lesser contribution of eastern ODZ mixing relative to NH (*Rafter et al.*, 2012). Moreover, the lower thermocline of the Coral Sea is partly fed by the NCJ, which carries Central Water (WSPCW; 25.8–26.5σ_θ) originating off New Zealand (*Germineaud et al.*, 2016; *Grenier et al.*, 2013, 2014; *Roemmich and Cornuelle*, 1992).

In summary, tracer distributions and mass balance calculations suggest that the net decrease in $\delta^{18}O_{NO3}$ between the Southern Ocean source of SAMW and our southern WEP SAMW-density waters can largely be explained by the addition of remineralized NO_3^- in transit. Differential influences from the entrainment of eastern ODZ waters, diapycnal mixing, and ventilation of the PNG thermocline by WSPCW may explain tracer differences between NH and PNG intermediate water masses (further discussed below).

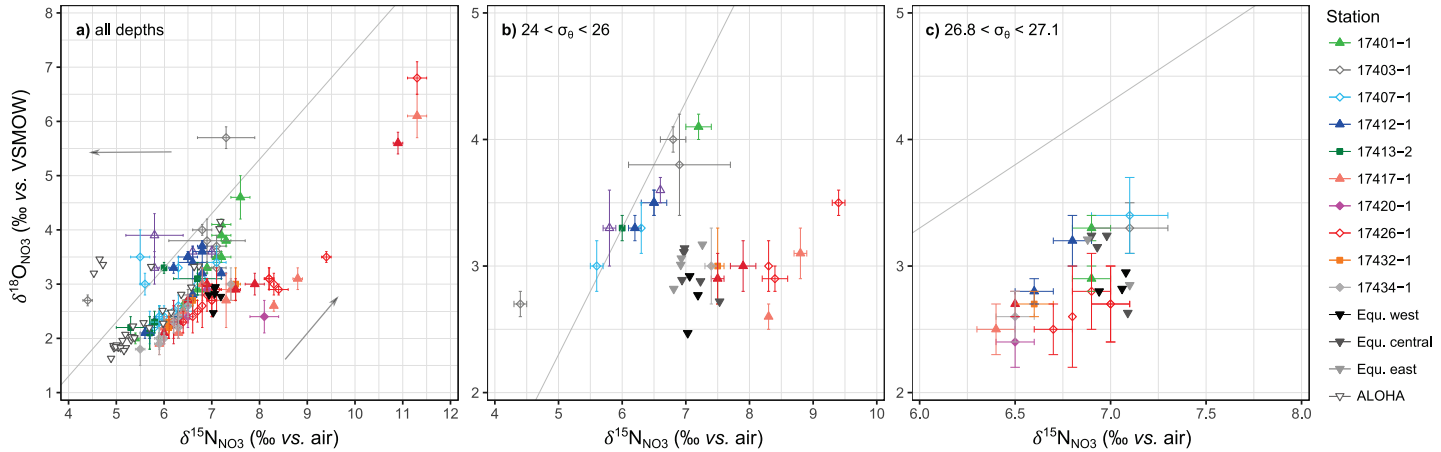

Figure 2.5: Property-property plots of $\delta^{18}O_{NO3}$ versus $\delta^{15}N_{NO3}$ including (a) all depths, and density ranges of (b) 24–26 (σ_θ) and (c) 26.8–27.1 (σ_θ). Colors represent different stations and (a) gray arrows indicate shoaling. The gray line runs through the mean $\delta^{18}O_{NO3}$ and $\delta^{15}N_{NO3}$ of the Southern Ocean SAMW end-member (3.5‰ and 6.2‰, respectively; Table 2.3), with its slope of 1 reflecting the isotopic fractionation expected from the consumption of NO_3^- through denitrification and assimilation, and any deflection from the 1:1 line indicating the remineralization of NO_3^-. Measurements from (a) station ALOHA are from *Sigman et al.* (2009a), (a, b) EUC and (a, c) SAMW data from the western (165°E to 170°W), central (140° and 155°W) and eastern (110°W) equatorial Pacific are from *Rafter et al.* (2012); *Rafter and Sigman* (2016). Note different scales on x and y axes.

2.6.1.2 The origin of northern WEP $\delta^{18}O_{NO3}$

The northern stations off Mindanao show lower $\delta^{13}C_{DIC}$ and higher nutrient concentrations in NPIW-depth and PDW-depth waters, suggesting a larger accumulation of remineralized products relative to corresponding depths south of the equator. This is consistent with the fact that – unlike SAMW and AAIW – NPIW does not outcrop at the surface in the area of formation but reflects remineralization and mixing processes along the flow path. This partly explains the higher nutrient concentrations, lower oxygen concentrations, and lower $\delta^{13}C_{DIC}$ values at intermediate depths off Mindanao. As noted above, the higher degree of remineralization would be expected to impart a lower $\delta^{18}O_{NO3}$ relative to southern stations. Yet, intermediate-depth $\delta^{18}O_{NO3}$ values are consistently higher north of the equator. The relatively elevated $\delta^{18}O_{NO3}$ may result from a larger contribution of NO_3^- advected from the eastern tropical Pacific ODZ with elevated $\delta^{18}O_{NO3}$ from denitrification (*Sigman et al.*, 2005). The larger direct contribution of waters from the eastern margin in the northern WEP is consistent with a larger N-deficit in intermediate waters north of the equator (-5.2 $\pm$ 0.4 and -4.1 $\pm$ 0.2 μM in NPIW and AAIW, respectively). The $\delta^{18}O_{NO3}$ at the WEP is also elevated (3.7 $\pm$ 0.2‰) relative to the central gyre (3.3‰, *Sigman et al.*, 2009a), further suggesting a larger lateral contribution from the eastern margin to the northern WEP. The westward movement of the denitrification signal from the eastern margin is likely propagated by the NEC, as previously inferred (*Kienast et al.*, 2008; *Rafter et al.*, 2012).

Using a mass balance to identify the $\delta^{18}O_{nitr}$ for intermediate-depth water in the northern WEP (as in section 5.1.1) is challenging because of the few dual N and O isotope measurements from the higher latitude North Pacific location of NPIW source waters. Moreover, the elevated $\delta^{18}O_{NO3}$ of WEP intermediate waters, in light of the high proportion of remineralized NO_3^-, suggests an important lateral NO_3^- input from the eastern margins – thus thwarting a single end-member mass balance exercise. The analysis of the northern WEP will be improved by upcoming high-resolution NO_3^- isotope measurements during the North Pacific GEOTRACES expedition (www.geotraces.org), which will provide fundamental constraints to elucidate the evolution of NPIW as well as other North Pacific water masses converging at the WEP.

2.6.1.3 Estimating the δ^{15}N of remineralized organic matter

The $\delta^{15}N_{NO3}$ increases in the thermocline toward the surface in the south but decreases toward the surface in the northern WEP (Figure 2.4a). The $\delta^{15}N_{NO3}$ values of southern WEP intermediate and thermocline waters are also more elevated than their high latitude source waters (Figure 2.5). The elevated $\delta^{15}N_{NO3}$ in southern WEP intermediate waters can result from either of two potential mechanisms: (1) the direct lateral advection of ^{15}N-enriched subsurface NO_3^- from the eastern margin and/or (2) the remineralization of high-δ^{15}N material (*Rafter et al.*, 2012). To a first approximation, the relatively less pronounced N* depletions in the southern WEP (-3.4 $\pm$ 0.5 μM versus -2.4 $\pm$ 0.2 μM; Table 2.2) compared to a dissolved inorganic nitrogen deficit of -23 μM within the ODZ (*Peters et al.*, 2018) indicates limited communication with the margins, suggesting the remineralization of high-δ^{15}N material as the primary origin of the high $\delta^{15}N_{NO3}$ in intermediate waters of the South Pacific. This assertion is further validated by Δ(15–18) values, which are expected to be low if contributed by the eastern ODZ (*Casciotti et al.*, 2013; *Casciotti and McIlvin*, 2007; *Granger and Wankel*, 2016; *Peters et al.*, 2018; *Rafter et al.*, 2013; *Sigman et al.*, 2005), thus not accounting for the observed increase from 2.7 $\pm$ 0.3‰ at $\sim$ 50°S to 4.2 $\pm$ 0.1‰ off NH (Tables 2.2 and 2.3). This meridional Δ(15–18) increase is otherwise consistent with the remineralization of high-δ^{15}N material in transit, which increases $\delta^{15}N_{NO3}$ while decreasing $\delta^{18}O_{NO3}$ (Figure 2.5a), thus increasing Δ(15–18). Assuming a δ^{18}O of 1.1‰ for remineralized NO_3^-, and using the following mass balance approach:

$$\delta^{15}N_{nitr} = (\Delta(15{-}18)_{obs} \times [NO_3^-]_{obs} - \Delta(15{-}18)_{source} \times [NO_3^-]_{source}) / [NO_3^-]_{nitr} + \delta^{18}O_{nitr} \quad (2.9)$$

the meridional change in Δ(15–18) can be explained by the net remineralization of material with a δ^{15}N averaging 8.1‰. Otherwise, using the isotope mass balance described above (equation (2.8)), the δ^{15}N of sinking organic matter remineralized to NO_3^- in transit from the Southern Ocean to the station off NH is on the order of 8.4‰. Previous mass balance estimates in the tropical South Pacific range between 9.0‰ (*Rafter et al.*, 2013) and 7–16‰ (*Peters et al.*, 2018). The values estimated here are in the range of δ^{15}N measured in sinking particulate material at 20°S, 100°W in the subtropical gyre (7.9 $\pm$ 2.1‰; *Knapp et al.*, 2016). As noted by others (*Rafter et al.*, 2012; *Yoshikawa et al.*, 2015), elevated δ^{15}N of sinking N in the South Pacific contradict expectations of low δ^{15}N due to N_2 fixation in the South Pacific gyre and subtropical waters. We return to this conundrum in a later

section (2.6.2.1). Off PNG, $\delta^{15}N_{NO3}$ in SAMW-density water is lower (6.5 $\pm$ 0.1‰) than off NH (Figure 2.5c), and congruent with values measured at corresponding depths further south in the Coral Sea (6.6 $\pm$ 0.5‰; *Yoshikawa et al.*, 2015). The probable influence of WSPCW in the lower thermocline off PNG precludes a parallel N isotope mass balance exercise.

Off Mindanao, NPIW-depth $\delta^{15}N_{NO3}$ (Figure 2.4a and Table 2.2) is also higher than its putative higher latitude source off Japan (7.1 $\pm$ 0.1‰ versus 6.1 $\pm$ 0.2‰; *Yoshikawa et al.*, 2006). The $\delta^{15}N_{NO3}$ at the western boundary is also higher relative to the same density interval at station ALOHA in the central gyre (6.7 $\pm$ 0.1‰; *Sigman et al.*, 2009a, Figure 2.5a). This increase in $\delta^{15}N_{NO3}$ as intermediate waters transit the North Pacific is somewhat surprising considering the widespread occurrence of N_2 fixation in the North Pacific subtropical gyre (*Karl et al.*, 1997, 2002), introducing isotopically light (lower $\delta^{15}N$) organic matter to the subsurface (*Casciotti et al.*, 2008; *Karl et al.*, 1997; *Sigman et al.*, 2009a). In this respect, the salient decrease of Δ(15–18) from intermediate waters to the subsurface (Figure 2.4c) signals the remineralization of low-$\delta^{15}N$ material north of the equator. The low-$\delta^{15}N_{NO3}$ introduced by the remineralization of newly fixed nitrogen may in part be overprinted by the lateral advection and mixing of high-$\delta^{15}N_{NO3}$ from denitrification in the ODZ of the eastern equatorial Pacific, which is consistent with the lower N*, lower Δ(15–18) and higher $\delta^{18}O_{NO3}$ values observed north compared to south of the equator (Figures 2.3 and Figure 2.4). These patterns are further consistent with the bulk of organic matter remineralization occurring in the subeuphotic zone (*Martin et al.*, 1987) – an assertion that we test in the following section by analyzing the shallower, thermocline-depth waters.

2.6.2 The biogeochemical history of WEP thermocline-depth waters

The isotope composition of NO_3^- in thermocline and near-surface waters (depths shallower than the intermediate water masses) are drastically different between the northern and southern hemisphere WEP. The most obvious difference is at $\approx$160–200 m, where the southern $\delta^{15}N_{NO3}$ is 7.5‰ (PNG) and 8.3‰ (NH), but northern $\delta^{15}N_{NO3}$ is 5.7‰ (Table 2.2). Moreover, southern WEP thermocline $\delta^{15}N_{NO3}$ is higher than the underlying intermediate water NO_3^-, whereas northern WEP NO_3^- at these depths is lower than that in waters immediately below (Table 2.2). In the next section, we examine these patterns in the southern then northern WEP thermocline.

2.6.2.1 Southern WEP NO_3^-: from the thermocline to the surface

At southern stations, thermocline depths are contiguous with SPTW, originating at $\sim 20°S$, 125°W in the subtropical gyre (*Tomczak and Godfrey*, 1994; *Tsuchiya et al.*, 1989). In this area of water mass formation, *Peters et al.* (2018) report low surface NO_3^- (< 5 μM) and a concurrent enrichment in both $\delta^{15}N_{NO3}$ and $\delta^{18}O_{NO3}$ (up to 28‰ and 25‰, respectively). They attribute these high values to the incomplete consumption of surface NO_3^- due to Fe-limitation in waters entrained from the eastern part of the upwelling system, namely, the equatorial upwelling and/or possibly upwelling at the margins. As originally proposed by *Rafter et al.* (2013), the Rayleigh distillation of NO_3^- isotopes as waters move poleward from the equatorial upwelling (*Altabet*, 2001; *Altabet and Francois*, 1994; *Rafter and Sigman*, 2016) gives way to the sinking and remineralization of high-$\delta^{15}N$ particles in SPTW, transmitting the ^{15}N-enrichment from the surface into the subsurface dissolved NO_3^- pool. This signal is evident as high-$\delta^{15}N_{NO3}$ in the tropical water along the southern WEP.

We note that SPTW entering the Bismarck Sea through the Vitiaz Strait has comparatively lower $\delta^{15}N_{NO3}$ (by 0.8‰), which can be explained by the influence of the southern branch of SPTW. The lower $\delta^{15}N_{NO3}$ of the southern SPTW branch likely reflects a regional contribution of N_2 fixation to thermocline NO_3^- (*Rafter et al.*, 2012; *Yoshikawa et al.*, 2015) and/or a diminishing influence of the northern SPTW branch.

Other ocean regions recognized to host significant in situ N_2 fixation, such as the central North Pacific gyre and the North Atlantic, are characterized by low-$\delta^{15}N_{NO3}$ in the upper thermocline, reflecting the input of isotopically light nitrogen from diazotrophy, with thermocline $\delta^{15}N_{NO3}$ as low as 1.5‰ and ~ 2.6‰ at station ALOHA and in the Sargasso Sea, respectively (*Casciotti et al.*, 2008; *Knapp et al.*, 2008). The comparative absence of an unambiguous N_2 fixation imprint in the southern WEP thermocline NO_3^- pool may owe to (i) limited remineralization of newly fixed N, and/or (ii) an overprinting by isotopically heavy NO_3^- reaching the WEP via the SEC. Against previous model predictions of high N_2 fixation rates in the eastern subtropical and tropical South Pacific (*Deutsch et al.*, 2007), *Knapp et al.* (2016) reported low (≤ 24 μmol N m^{-2} d^{-1}) to undetectable rates for that area. Limited N_2 fixation in the eastern and central South Pacific gyre may indicate a high iron requirement and the coherent iron-dependent occurrence and spatial distribution of N fixers (*Mills et al.*, 2004; *Moore and Doney*, 2007), restricting high N_2 fixation rates to

areas of elevated iron input such as the western Pacific (*Mackey et al.*, 2002; *Slemons et al.*, 2010). Conforming to these notions, elevated rates of N_2 fixation are reported for both the Solomon Sea and Bismarck Sea (*Berthelot et al.*, 2017; *Bonnet et al.*, 2009, 2015). We thus hypothesize that the relatively elevated $\delta^{15}N_{NO3}$ in the southern WEP thermocline owes primarily to the vertical flux of high-$\delta^{15}N$ material at the southern edge of the equatorial upwelling overprinting the regionally restricted influence of newly fixed nitrogen.

Within the southern WEP euphotic zone (upper $\sim$ 150 m), $\delta^{15}N_{NO3}$ increases from core SPTW toward the surface as NO_3^- concentrations decrease, reaching values upward of 17.6‰ in the BL at $\sim$ 45 m (Figure 2.6a). The approximately equivalent enrichment in $\delta^{18}O_{NO3}$ (Figure 2.6b) is consistent with NO_3^- assimilation driving the N and O isotope increases (*Casciotti et al.*, 2002; *Granger et al.*, 2004). Assuming closed-system Rayleigh dynamics, the isotope effects (ε) for NO_3^- assimilation, derived after *Mariotti et al.* (1981):

$$\varepsilon = (\delta^{15}N_{initial} - \delta^{15}N)/\ln([NO_3^-]/[NO_3^-]_{initial}) \tag{2.10}$$

are on the order of 4.1‰ (for N) and 4.2‰ (for O), in the range expected for plankton NO_3^- assimilation (*Granger and Sigman*, 2009; *Sigman et al.*, 1999, Figure 2.6).

2.6.2.2 Northern WEP NO_3^-: from the thermocline to the surface

North of the equator, NPTW, which feeds the upper thermocline, originates in the North Pacific subtropical gyre along $\sim$ 25°N between 150°E and 130°W and enters the WEP and our study site off Mindanao via the broad westward flowing NEC and MC (*Fine et al.*, 1994; *Katsura et al.*, 2013; *Nie et al.*, 2016; *Tsuchiya*, 1968). Off Mindanao, upper thermocline waters exhibit a clear minimum in $\delta^{15}N_{NO3}$, with values as low as 4.4‰. The decrease in $\delta^{15}N_{NO3}$ from intermediate waters to the lower thermocline occurs despite a coincident decrease in NO_3^- concentration (Figure 2.6a). Above the salient $\delta^{15}N_{NO3}$ minimum, a concurrent increase in both $\delta^{15}N_{NO3}$ and $\delta^{18}O_{NO3}$, along with decreasing NO_3^- concentration, suggest some degree of subsurface NO_3^- assimilation. The isotopically light thermocline NO_3^- in the NPTW and corresponding low Δ(15–18) within the same depth range suggest remineralization of organic matter with a low $\delta^{15}N$ due to N_2 fixation. This conclusion is consistent with previous studies in the area (*Kienast et al.*, 2008). Moreover, the observed $\delta^{15}N_{NO3}$ is comparable to that reported in the corresponding density range elsewhere in the subtropical North Pacific ($\sim$ 4‰ at station ALOHA, *Casciotti et al.*, 2008; *Sigman et al.*, 2009a, Figure 2.5a).

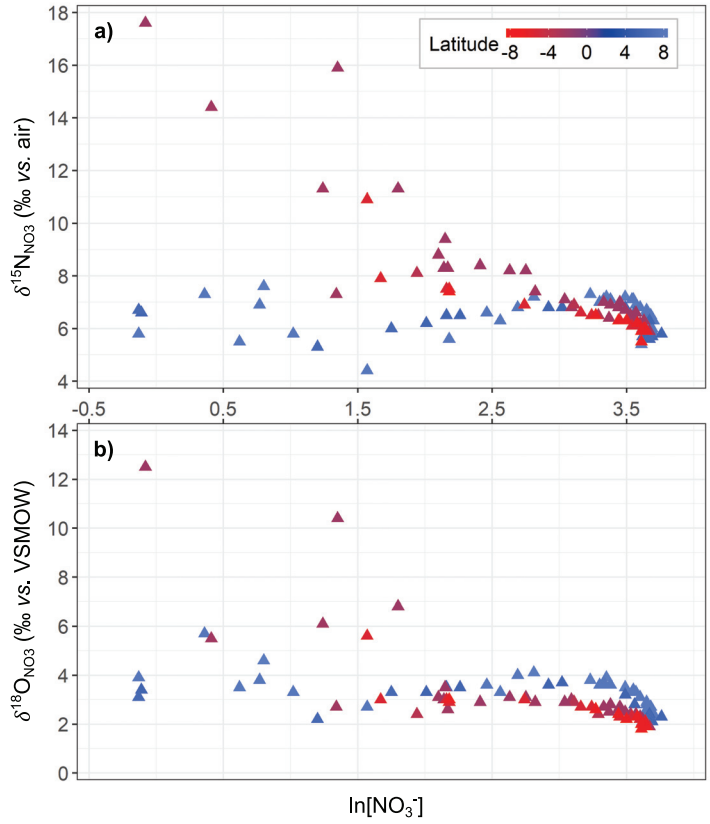

Figure 2.6: (a) $\delta^{15}N_{NO3}$ and (b) $\delta^{18}O_{NO3}$ versus the natural logarithm of [NO_3^-]. Colors show the latitude of the station, with blue colors indicating the northern site off Mindanao and red colors illustrating southern sites of PNG and NH, respectively.

While we see a clear signal of N_2 fixation in the central North Pacific and at the western boundary, explicit evidence in the South Pacific gyre seems to be missing. As pointed out above, the high δ^{15}N associated with NO_3^- advected to the surface layer of the subtropical gyres from the eastern equatorial upwelling system (*Peters et al.*, 2018; *Rafter et al.*, 2013) imprints onto the NO_3^- pool of SPTW. In contrast, this dynamic is not seen in the North Pacific gyre (*Rafter et al.*, 2013), allowing the remineralization of newly fixed N (with a low δ^{15}N) to have a larger influence on the δ^{15}N of the NO_3^- pool.

2.6.2.3 Implications for δ^{15}N of Particle Flux at the Equatorial Upwelling

An interesting implication of the apparent transport of elevated δ^{15}N NO_3^- from the low latitudes across the South Equatorial Current (SEC) into the South Pacific gyre is that this process essentially fractionates the isotopes of reactive N upwelled at the equator among regions. Incomplete consumption of NO_3^- at the equator leads to the lateral divergence of nutrients away from the equator (*Kessler*, 2006). The poleward decrease in NO_3^- and concurrent fractionation toward the lighter isotope during assimilation by phytoplankton creates an inverse correlation between NO_3^- versus the δ^{15}N of near-surface organic matter (*Altabet*, 2001; *Altabet and Francois*, 1994). This process produces an elevated δ^{15}N particle flux in the northern gyre, balanced by a lower δ^{15}N particle flux in the proximity to the upwelling system. The subsurface remineralization of the lower δ^{15}N particle flux is consistent with a zonal band of lighter δ^{15}N NO_3^- ($\sim 5‰$) focused along 3–5°S (*Rafter et al.*, 2012, 2013) within the west-to-east flowing Tsuchiya Jets (called SSCC), which flow underneath the NO_3^--rich surface waters on and south of the equator (Figure 2.1). This water mass is thought to originate in the Coral Sea, such that the associated δ^{15}N signal was initially hypothesized to reflect the transport of low-δ^{15}N NO_3^- from the remineralization of newly fixed N in the western South Pacific by the jets (*Rafter et al.*, 2012). However, as pointed out by *Yoshikawa et al.* (2015), the $\delta^{15}N_{NO3}$ in the Coral Sea thermocline is not sufficiently low to explain the signal observed in the Tsuchiya Jets off the equator. We submit that the low $\delta^{15}N_{NO3}$ transported in the jets originates from the vertical flux of low δ^{15}N generated from the partial consumption of NO_3^- in waters upwelling at and to the south of the equator (see *Rafter and Sigman*, 2016). By comparison, the Northern Subsurface Counter Current (NSCC) may have a higher $\delta^{15}N_{NO3}$ of $\geq 6‰$ (*Rafter et al.*, 2012) because it does not transit the Pacific basin underneath NO_3^-rich waters. Sinking organic matter δ^{15}N is also higher north of the equator (*Altabet et al.*, 1999), suggesting

that nitrification of this material may also elevate the $\delta^{15}N_{NO3}$ of the NSCC.

2.6.3 Quantifying the northern and southern hemisphere sources of the EUC

The eastward-flowing, thermocline-trapped EUC is the source water of the equatorial upwelling system (*Dugdale et al.*, 2002; *Rafter and Sigman*, 2016; *Wyrtki*, 1981). The EUC source region is composed of northern and southern-sourced waters (*Butt and Lindstrom*, 1994; *Fine et al.*, 1994; *Lindstrom et al.*, 1987; *Melet et al.*, 2010; *Tsuchiya et al.*, 1989; *Ueki et al.*, 2003). Estimated contributions of each hemisphere to the EUC vary among studies and investigated latitude, with some studies arguing for a dominance of the northern-sourced MC (*Fine et al.*, 1994) or southern attributions via the NGCUC and NICU (*Toggweiler et al.*, 1991; *Tsuchiya et al.*, 1989). Attributions are also divergent among modeling studies, ranging from a roughly balanced input of the southern and northern hemispheres (*Izumo et al.*, 2002) to a net dominance of southern LLWBCs (*Blanke and Raynaud*, 1997; *Fukumori et al.*, 2004; *Grenier et al.*, 2011; *Rodgers et al.*, 2003).

To a first approximation, NO_3^- isotope profiles measured at stations along the EUC (*Rafter and Sigman*, 2016) suggest a disproportionate contribution of southern hemisphere water masses to EUC NO_3^- (Figure 2.5). The N and O isotopic compositions of NO_3^- at three longitudinally distinct sections of the EUC are confined to a restricted range of 6.8–7.5‰ for $\delta^{15}N_{NO3}$ and 2.5–3.2‰ for $\delta^{18}O_{NO3}$, respectively. Compared to our stations in the southern and northern WEP, NO_3^- $\delta^{15}N$ and $\delta^{18}O$ values in the EUC appear more closely aligned with values observed at southern stations, particularly in lower density layers in the upper EUC (24–26σ_θ; Figure 2.5b): southern profiles generally show a similar range in $\delta^{18}O_{NO3}$ and somewhat higher $\delta^{15}N_{NO3}$ values relative to the upper EUC, whereas profiles at the northern sites off Mindanao indicate greater $\delta^{18}O$ values and markedly lower $\delta^{15}N$ values than at comparable densities in the EUC (Figure 2.5b). At the SAMW-density interval (26.5–27.1σ_θ), southern and northern stations are less distinct with respect to NO_3^- isotope ratios, with $\delta^{15}N_{NO3}$ and $\delta^{18}O_{NO3}$ in the EUC being slightly higher than PNG and NH, and similar to lower than values off Mindanao (Figure 2.5c). Considering that the EUC may issue from diapycnal mixing of thermocline and intermediate waters, however, the nearly uniform $\delta^{15}N_{NO3}$ and $\delta^{18}O_{NO3}$ in the EUC could arguably be explained as a mixture of upper and lower density levels of southern stations (Figure 2.5b and c).

To further interrogate the provenance of tracers in the EUC, profiles of salinity, temperature, NO_3^-, $Si(OH)_4$, oxygen, $\delta^{15}N_{NO3}$, $\delta^{18}O_{NO3}$, and $\delta^{13}C_{DIC}$ measured at 0°N/165°E (*Rafter et al.*, 2012; *Rafter and Sigman*, 2016) were used to calculate the mixture of LLWBC end-members and respective depth intervals that best account for the properties observed in the shallow and midlayer of the EUC. Individual values for each end-member are summarized in Appendix A and the results of the mixing model are illustrated in Figure 2.7, where the contribution of source waters to the upper and lower EUC is given in relation to source area and density layer, with relative proportions adding up to 1. Considering only salinity and temperature in the mixing model, the optimal solution diagnoses significant contributions to the lower and upper EUC from both hemispheres (Figure 2.7a). Putative contributions from Mindanao decrease with the addition of the isotopic tracers and NO_3^- to the mixing model (Figure 2.7b). The upper EUC then derives predominantly from the NGCUC, while the lower EUC shows significant contributions from both the NICU and NGCUC. Finally, considering $Si(OH)_4$ and oxygen concentrations in addition to the other tracers renders a solution wherein the NICU contributes dominantly to both the upper and lower EUC (Figure 2.7c). The mixing model exercise thus illustrates that the distribution of combined physical and biogeochemical tracers in the EUC is best explained by a dominance of southern WEP waters, albeit, with uncertainties regarding the differential contributions of NGCUC and NICU.

Regarding the specific provenance of NO_3^- in the EUC, the mixing model similarly indicates a disproportionate contribution from southern boundary currents ($\geq 70\%$), with the NICU accounting for $\geq 50\%$ of total EUC NO_3^- (Appendix B). Among density intervals, the model diagnoses that NO_3^- at intermediate depths (26.5–27.1σ_θ) contributes most to lower EUC NO_3^-, whereas all density intervals considered contribute comparably to upper EUC NO_3^-. In all, this analysis suggests that EUC nutrients originate predominantly from southern hemisphere boundary currents. Southern hemispheric processes that begin with Southern Ocean overturning, and include lower latitude organic matter remineralization, mixing with the eastern ODZ, and N_2 fixation, thus exert an important influence on the biogeochemical properties of waters upwelled at the equatorial Pacific.

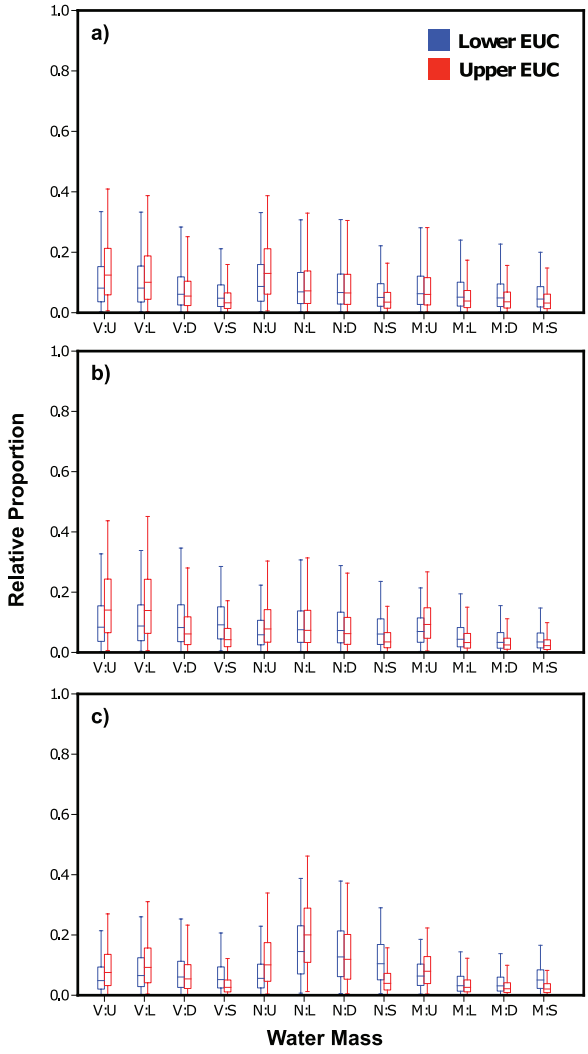

Figure 2.7: Relative contributions of different LLWBC end-members and respective density intervals to the upper EUC (24–25.5σ_θ, red) and lower EUC (25.5–26σ_θ, blue). Abbreviations on the x axis indicate the three source regions (Vitiaz Strait (V), New Hanover (N), Mindanao (M)) further divided into four density layers: upper EUC layer (U; 24–25.5σ_θ), lower EUC layer (L; 25.5–26σ_θ), deep EUC layer (D; 26–26.5σ_θ), and SAMW layer (S; 26.5–27.1σ_θ) according to the end-members listed in Appendix A. Mixing calculation include (a) salinity and temperature only, (b) salinity, temperature, NO_3^-, and isotope tracers, and (c) salinity, temperature, isotope tracers, oxygen, and nutrients (NO_3^-, $Si(OH)_4$). Solution box plots were computed from respective ensembles of solutions (see text). All boxes have a notch at the median solution value, the box covers the interquartile range, and the whiskers indicate 95% coverage intervals (e.g., 2.5–97.5 percentile).

2.7 Summary

We examined the N and O isotopic composition of NO_3^- and the distribution of complementary biogeochemical tracers to elucidate the hydrography of the WEP and the biogeochemistry and evolution of water masses that feed the EUC, which has implications for understanding controls on the productivity of the tropical Pacific. Tracer distributions reveal remarkably distinct biogeochemical features at stations north and south of the equator.

Partial assimilation along the equatorial upwelling system results in the export of high-δ^{15}N organic matter at the northern edge of the South Pacific gyre, the remineralization of which is manifested as elevated-$\delta^{15}N_{NO3}$ in SPTW advected to the western boundary – a high $\delta^{15}N_{NO3}$ signal that may overprint the influence of newly fixed nitrogen near the western boundary. The remineralization of high-δ^{15}N organic matter is further evident in underlying SAMW-density waters, which have a higher $\delta^{15}N_{NO3}$ and lower $\delta^{18}O_{NO3}$ (and thus higher Δ(15–18)) than the SAMW end-member at 50°S. Additionally, the relatively modest N* at intermediate depths further points to restricted direct lateral advection of denitrified waters from the Eastern Tropical South Pacific, and to the remineralization of high-δ^{15}N organic matter as the dominant contributor of elevated $\delta^{15}N_{NO3}$ at intermediate and thermocline depths. Differences in tracer distributions in the southern WEP thermocline off PNG compared to NH reflect the influence of waters ventilated further south, and are also consistent with diapycnal mixing of intermediate water masses. In contrast, lower $\delta^{15}N_{NO3}$ and lower Δ(15–18) in the thermocline-depth waters off Mindanao show the contribution of NO_3^- from the remineralization of newly fixed nitrogen in the North Pacific. The relatively elevated $\delta^{18}O_{NO3}$ in intermediate waters below suggests greater direct lateral contribution of NO_3^- from the eastern ODZ compared to the southern WEP. These strong hemispheric differences in WEP biogeochemical tracers allow us to place constraints on the source of EUC waters, suggesting that most EUC waters – and nutrients therein – derive from southern hemisphere sources.

CHAPTER 3

REMOTE WESTERN ARCTIC NUTRIENTS FUEL REMINERALIZATION IN DEEP BAFFIN BAY[2]

3.1 Abstract

The oceanic nitrogen cycle is critically important for the partitioning of greenhouse gases between ocean and atmosphere. Baffin Bay connects ocean regions that are major sources (North Atlantic) and sinks (North Pacific and western Arctic) of biologically available nitrogen and further harbors supersaturation of nitrous oxide and a coincident deficit in nitrate in the deep basin. Isotopic tracer profiles of both nitrogen species presented here provide novel insights into the origin and cycling of reactive nitrogen in Baffin Bay, highlighting the connectivity between different Arctic systems and horizontal components of basinscale nutrient transport. Baffin Bay bottom water properties are derived from export production in northern Baffin Bay, which is largely fueled by Pacificderived nutrients. In situ remineralization at depth gives rise to benthic denitrification, evidenced by a pronounced accumulation of nitrous oxide with a distinctively high site preference ($<44‰$) in the deep basin. Nutrients supplied to Baffin Bay are hence stripped from surface waters and trapped at depth over long timescales, where sedimentary denitrification further adds to the N removal capacity of the Arctic Ocean.

[2]Lehmann, N., Kienast, M., Granger, J., Bourbonnais, A., Altabet, M. A., & Tremblay, J.-É. (2019). Remote western Arctic nutrients fuel remineralization in deep Baffin Bay. *Global Biogeochemical Cycles*, 33, 649–667.
Author contribution: I conducted the field work and analyzed the NO_3^- and N_2O isotope samples in collaboration with J. Granger, A. Bourbonnais and M. A. Altabet. J.-É. Tremblay contributed the nutrient data. I led the interpretation of the data and wrote the manuscript, with input from all co-authors.

3.2 Introduction

Baffin Bay is one of the worlds largest marginal seas, surrounded by Greenland to the east and the Canadian Arctic Archipelago (CAA) to the west (Figure 3.1). It connects the high Arctic to the northwestern Atlantic and thus affects the salt, heat and nutrient budgets of the adjacent Labrador Sea and the wider Atlantic Ocean (*Azetsu-Scott et al.*, 2012; *Grivault et al.*, 2017; *Tang et al.*, 2004; *Yamamoto-Kawai et al.*, 2006). In addition, the recurrent and prolonged ice-free conditions of the North Water (NOW) polynya in northern Baffin Bay sustain exceptionally high primary production, making this area one of the most productive marine ecosystems in the Arctic (*Klein et al.*, 2002; *Lalande et al.*, 2009; *Tremblay et al.*, 2002). The deep ($>$ 2300 m), central Baffin Bay is surrounded by relatively narrow shelves off Baffin Island and Greenland, and separated from the Arctic Ocean and the western North Atlantic by a number of shallow channels that restrict water exchange with the Arctic and Atlantic Ocean to depths shallower than 700 m. Studies on the spatial variability of dissolved nutrient concentrations in this marginal sea have identified enhanced inventories of silicic acid ($Si(OH)_4$) and phosphate (PO_4^{3-}) in the deep Baffin Bay (*Jones et al.*, 1984; *Tremblay et al.*, 2002). A coincident deficit in nitrate (NO_3^-) in the deep Baffin Bay has been ascribed to deviations in the Redfield stoichiometry of particulate organic matter (*Jones et al.*, 1984) and the preferential remineralization of organic nitrogen in shallow waters and the subsequent export of biogenic silica to the deep basin (*Tremblay et al.*, 2002). More recently, supersaturation of nitrous oxide (N_2O) in the deep basin has also been reported (*Fenwick et al.*, 2017; *Kitidis et al.*, 2010). N_2O is a climatically active trace gas, partly responsible for the depletion of ozone (*Ravishankara et al.*, 2009). In oxic systems, N_2O is produced as a by-product during the oxidation of ammonium (NH_4^+) to nitrite (NO_2^-) (nitrification) as well as during the reduction of NO_2^- *via* nitric oxide (NO) to N_2O (nitrifier-denitrification). In suboxic ($O_2 < 5$ μmol L^{-1}) systems, N_2O is produced and consumed during the reduction of NO_3^- to N_2 gas (denitrification) (*Goreau et al.*, 1980; *Ostrom et al.*, 2000; *Santoro et al.*, 2011). While high Si:N ratios measured in sinking particulate matter in northern Baffin Bay are in line with the preferential deep accumulation of $Si(OH)_4$ over NO_3^- (*Michel et al.*, 2002), benthic denitrification may otherwise provide a sink for NO_3^-, thereby lowering the ratio of NO_3^- relative to both dissolved $Si(OH)_4$ and PO_4^{3-} in the deep basin. Thus, clear mechanisms leading to both the deficiency in NO_3^- and the supersaturation of N_2O have yet to be identified unambiguously. Global climate

change adds considerable urgency to this quest as biogeochemical fluxes in the Arctic Ocean are changing due to sea-ice retreat and consequent changes in primary production (e.g., *Arrigo et al.*, 2008; *Tremblay et al.*, 2015). While parts of the western and high Arctic may experience an increase in primary production given enhanced light penetration as a result of decreasing sea ice thickness and extent (*Ardyna et al.*, 2011; *Arrigo and van Dijken*, 2011; *Tremblay et al.*, 2015), opposing trends of declining bloom amplitudes (*Marchese et al.*, 2017) and overall decreasing primary and net community production (*Bélanger et al.*, 2013; *Bergeron and Tremblay*, 2014) are observed in the highly productive northern Baffin Bay as a potential result of increased stratification and impeded vertical nutrient supply to the surface (*Bergeron and Tremblay*, 2014). Recent temperature and salinity trends show a freshening and cooling of the surface layer (*Bergeron and Tremblay*, 2014; *Hamilton and Wu*, 2013; *Zweng and Münchow*, 2006) and a concurrent warming of the Baffin Bay intermediate layer (*Hamilton and Wu*, 2013; *Zweng and Münchow*, 2006). The extent of primary production in northern Baffin Bay is limited by nitrogen (*Tremblay et al.*, 2006; *Yamamoto-Kawai et al.*, 2006). Thus, understanding key processes affecting the distribution, chemical speciation and availability of reactive nitrogen relative to other phytoplankton nutrients in Baffin Bay has implications not only for local productivity and biogeochemical cycling, but also for nutrient inputs to the wider North Atlantic and consequent productivity therein (*Yamamoto-Kawai et al.*, 2006).

To assess prevalent N transformation processes in Baffin Bay, we present a combination of N and O isotopic compositions of both NO_3^- and N_2O collected as part of the 2015 Canadian Arctic GEOTRACES expedition (GN02). Dual N and O isotope ratios of NO_3^- ($\delta^{15}N_{NO3}$ and $\delta^{18}O_{NO3}$, where $\delta = [(R_{sample}/R_{standard} - 1] \times 1000$, and $R = {}^{15}N/{}^{14}N$ and ${}^{18}O/{}^{16}O$) are sensitive to important biogeochemical transformations and allow the identification of individual processes and their contributions to the dissolved NO_3^- pool. As such, N and O isotopes are similarly fractionated during both assimilatory NO_3^- uptake (*Casciotti et al.*, 2002; *Granger et al.*, 2004) and consumption by denitrification (*Granger et al.*, 2008; *Sigman et al.*, 2005). However, N and O isotopes are affected differentially during NO_3^- production by nitrification. While the N isotopic composition of newly nitrified NO_3^- depends on the isotopic signature of its substrate, the O isotopic composition of NO_3^- approximates the $\delta^{18}O$ of ambient water during nitrification (*Buchwald and Casciotti*, 2010; *Casciotti et al.*, 2002; *Sigman et al.*, 2005), such that it provides a tracer

of NO_3^- produced by the remineralization of organic matter at depth.

In turn, bulk N and O isotope ratios of N_2O ($\delta^{15}N^{bulk}$ and $\delta^{18}O_{N2O}$) derive from those of the precursory molecule (NH_4^+, NO_2^-, NO_3^-) and are fractionated during biological production by nitrification or denitrification and consumption by denitrification (*Sutka et al.*, 2006; *Toyoda et al.*, 2002; *Yoshida and Toyoda*, 2000). Simultaneous analyses of N_2O isotopomer abundances reflecting the different positions of isotopic atoms within the linear asymmetric molecule ($^{14}N^{15}N^{16}O$ and ($^{15}N^{14}N^{16}O$) – and of the associated site preference (SP = $\delta^{15}N^{\alpha} - \delta^{15}N^{\beta}$), corresponding to the N isotope ratios of the central (α) and the outer (β) N atoms in N_2O (*Toyoda and Yoshida*, 1999), provide additional tracers to identify the origin of N_2O. Unlike N_2O bulk isotope ratios, SP is independent of the isotopic composition of the substrate and is thought to mainly reflect the N_2O production mechanism (*Sutka et al.*, 2006; *Toyoda and Yoshida*, 1999).

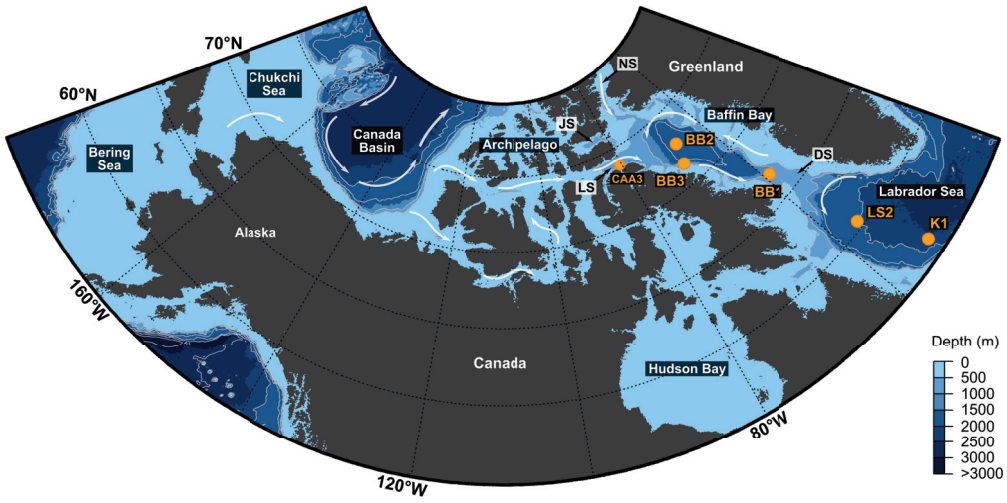

Figure 3.1: Map showing sampling sites (orange dots) in the eastern Canadian Arctic, with white arrows indicating simplified circulation pattern of surface waters (e.g., *Curry et al.*, 2011; *Muench*, 1971; *Tang et al.*, 2004; *Wu et al.*, 2012). Abbreviations indicate Lancaster Sound (LS), Jones Sound (JS), Nares Strait (NS) and Davis Strait (DS).

Below, we present NO_3^- and N_2O isotope data collected during the 2015 GEOTRACES expedition that (1) support substantial in situ remineralization of ^{15}N-enriched organic matter fueled by Pacific-derived nutrients, (2) indicate a predominantly sedimentary source of N_2O propagating well into the oxygenated water column and (3) suggest that benthic denitrification is the dominant mechanism removing dissolved inorganic nitrogen (DIN) in

the deep Baffin Bay.

3.3 Materials and Methods

3.3.1 Study site and sample collection

Data collection was conducted during the Canadian Arctic GEOTRACES expedition (GN02) in July and August 2015 aboard the *CCGS Amundsen* along a transect from 53°W, 56°N to 105°W, 69°N, covering the Labrador Sea, Baffin Bay and the eastern and central Canadian Arctic Archipelago (CAA; Figure 3.1). Seawater samples and hydrographic data were collected using a rosette of 24 x 12 L Niskin bottles mounted to a Sea-Bird SBE 911 conductivity-temperature-depth (CTD) profiler, equipped with a fluorometer and transmissometer, as well as a set of comprehensive sensors measuring dissolved oxygen, NO_3^- and light intensity (PAR). The conductivity sensor was calibrated using discrete seawater samples analyzed with a GuideLine Autosal model 8400B. The oxygen probe was calibrated using dissolved oxygen concentrations in seawater samples measured using Winkler titration (*Carpenter*, 1965).

Nutrient measurements (NH_4^+, NO_3^-, NO_2^-, PO_4^{3-}, $Si(OH)_4$) were conducted onboard following GEOTRACES protocols. NO_3^-, NO_2^-, PO_4^{3-} and $Si(OH)_4$ were analyzed according to standard colorimetric methods (Grasshoff, 1969) using a Bran+Luebbe AutoAnalyzer 3 and NH_4^+ concentrations were determined fluorometrically (Holmes et al., 1999). Seawater samples for NO_3^- isotope analyses were collected throughout the water column in pre-rinsed 60 mL high-density polyethylene bottles. Seawater samples from the upper 200 m were filtered through a 25-mm diameter 0.45 μm surfactant-free cellulose acetate membrane while samples from below 200 m depth were collected unfiltered directly into pre-rinsed 60 mL high-density polyethylene bottles. Aliquots for stable N and O isotope measurements in NO_3^- were stored immediately at –20°C.

Seawater for stable isotope analyses of N_2O was collected into 125 mL serum glass bottles via tygon tubing directly attached to the Niskin bottle. After overflowing each bottle with seawater twice to avoid any bubble formation, a small headspace was introduced by removing 1 mL of water from the top, and 0.1 mL of saturated mercury (II) chloride ($HgCl_2$) was added to suppress biological activity. Glass bottles were sealed with a butyl septum, crimped with an aluminum seal, and stored in the dark at room temperature until analysis.

3.3.2 Isotope ratio analyses of NO_3^- and N_2O

The N and O isotopic composition of NO_3^- was determined post-cruise at the University of Connecticut using the denitrifier method (*Casciotti et al.*, 2002; *Sigman et al.*, 2001). Briefly, this method uses a strain of cultured denitrifying bacteria (*Pseudomonas chlororaphis* f. sp. *aureofaciens*, ATCC# 13985) that lack the terminal N_2O reductase, hence quantitatively convert NO_3^- into N_2O gas. The product N_2O was purified and analyzed using a Thermo Delta V Advantage continuous flow isotope ratio mass spectrometer (CF-IRMS) front-loaded *via* modified Thermo Gas Bench II equipped with dual cold traps and GC Pal auto-sampler. Where NO_2^- was present, it was removed prior to isotopic analyses using sulfamic acid (*Granger and Sigman*, 2009). Samples were standardized to seawater-based reference material USGS-34 and IAEA-N3 with known δ^{15}N (vs. air) and δ^{18}O (vs. SMOW) of $-1.8‰$ and $-27.9‰$ and $4.7‰$ and $25.6‰$, respectively (*Böhlke et al.*, 2003; *Gonfiantini*, 1984). Standard deviations ($\pm$1 SD) were determined based on replicate measurements (n $\geq$ 3), yielding an analytical precision of $0.2‰$ and $0.3‰$ for δ^{15}N and δ^{18}O, respectively.

N_2O isotopomer analyses were performed post-cruise at the University of Massachusetts Dartmouth using a GV IsoPrime continuous flow isotope ratio mass spectrometer, interfaced with a multicollector and customized purge-and-trap system (*Bourbonnais et al.*, 2017). N_2O measurements were standardized and corrected for the scrambling effect (*Westley et al.*, 2007) using a set of reference N_2O gases (EMPA CB08976, EMPA CB09715, EMPA CB09766 and EMPA 53504; *Mohn et al.*, 2014) of known bulk and site-specific isotopic composition. N_2O concentrations were calculated from the N_2O peak height in a sample versus a 5°C seawater standard of known N_2O concentration (*Weiss and Price*, 1980). Seawater samples were analyzed in duplicates, and standard deviations ($\pm$1 SD) were generally $0.2‰$ for $\delta^{15}N^{bulk}$, $0.2‰$ for $\delta^{18}O_{N2O}$ and $0.7‰$ for SP. Excess N_2O, or ΔN_2O, was calculated as the difference between [N_2O] measured and [N_2O] at equilibrium, where [N_2O] at equilibrium reflects the atmospheric dry mole fraction measured in Barrow, Alaska (https://esrl.noaa.gov/gmd/).

3.4 Results and Discussion

At the time of sampling, Baffin Bay had reached nearly ice-free conditions, with ice coverage ranging from 10–30% in southern Baffin Bay (BB1) and 0–10% further north

along the shelf (BB3) and in the central basin (BB2). Surface temperature and salinity measurements evidenced seasonal signals of both surface heating and freshwater input, from sea ice meltwater and runoff, with relatively fresh (> 30.52) and warm ($< 4.8°C$) surface waters in central Baffin Bay, both increasing towards the Labrador Sea (> 33.32 and $< 6.3°C$, respectively; Figure 3.2). The broad cyclonic gyre circulation in central Baffin Bay is influenced by the West Greenland Current (WGC) entering from the Labrador Sea through Davis Strait and propagating north along the eastern side of the bay to $\sim$ 77°N where it veers to the west and joins the outflow of Nares Strait (NS), Jones Sound (JS) and Lancaster Sound (LS) to feed the southward Baffin Island Current (BIC) along the western slope off Baffin Island (Figure 3.1; *Hamilton and Wu*, 2013; *Melling et al.*, 2001; *Muench*, 1971; *Münchow et al.*, 2015; *Tang et al.*, 2004). The BIC subsequently exports relatively cold and fresh Arctic water through the western Davis Strait into the Labrador Sea where it joins the Labrador Current. Concurrently, the restricting nature of the shallow Davis Strait ($\sim$ 670 m sill depth) leads to striking differences in deep water biogeochemical properties between the Labrador Sea and Baffin Bay. Accordingly, we present hydrographic measurements from the adjacent Labrador Sea (stations K1 and LS2) that provide a reference for properties of Atlantic-derived water.

3.4.1 Origin of halocline nutrients in Baffin Bay

In Baffin Bay, a pronounced halocline ($32.8 < S < 34.2$) extends from $\sim$ 30–300 m, with uniformly cold ($-1.7°C$) water in the upper part of the halocline layer (< 200 m; Figures 3.2 and 3.3). NO_3^- and PO_4^{3-} concentrations in the halocline layer are 4–12 μmol L^{-1} and 0.7–1.0 μmol L^{-1}, respectively, decreasing progressively to below detection for NO_3^- and to 0.5 μmol L^{-1} for PO_4^{3-} near the surface layer (< 20 m; Figure 3.3 and Table 3.1). The surplus in PO_4^{3-} is consistent with the presence of Pacific-derived water and N-limitation in surface waters of western Baffin Bay (*Tremblay et al.*, 2006; *Yamamoto-Kawai et al.*, 2006) and contrasts with the concurrent depletion of both NO_3^- and PO_4^{3-} in the adjacent Labrador Sea (Figure 3.3d and e). N and O isotope ratios of NO_3^- in the halocline of central Baffin Bay (BB2) increase concurrently from minima at the center of the halocline ($\sim$ 200 m; 5.7 ± 0.1‰ and 0.5 ± 0.3‰, respectively) to peak values near the surface ($\sim$ 30 m; 8.0 ± 0.0‰ and 3.0 ± 0.2‰), signaling subsurface in situ NO_3^- consumption by phytoplankton (*Casciotti et al.*, 2002; *Granger et al.*, 2004).

The upper halocline layer (UHL, < 200 m) in the bay is comprised of Arctic waters

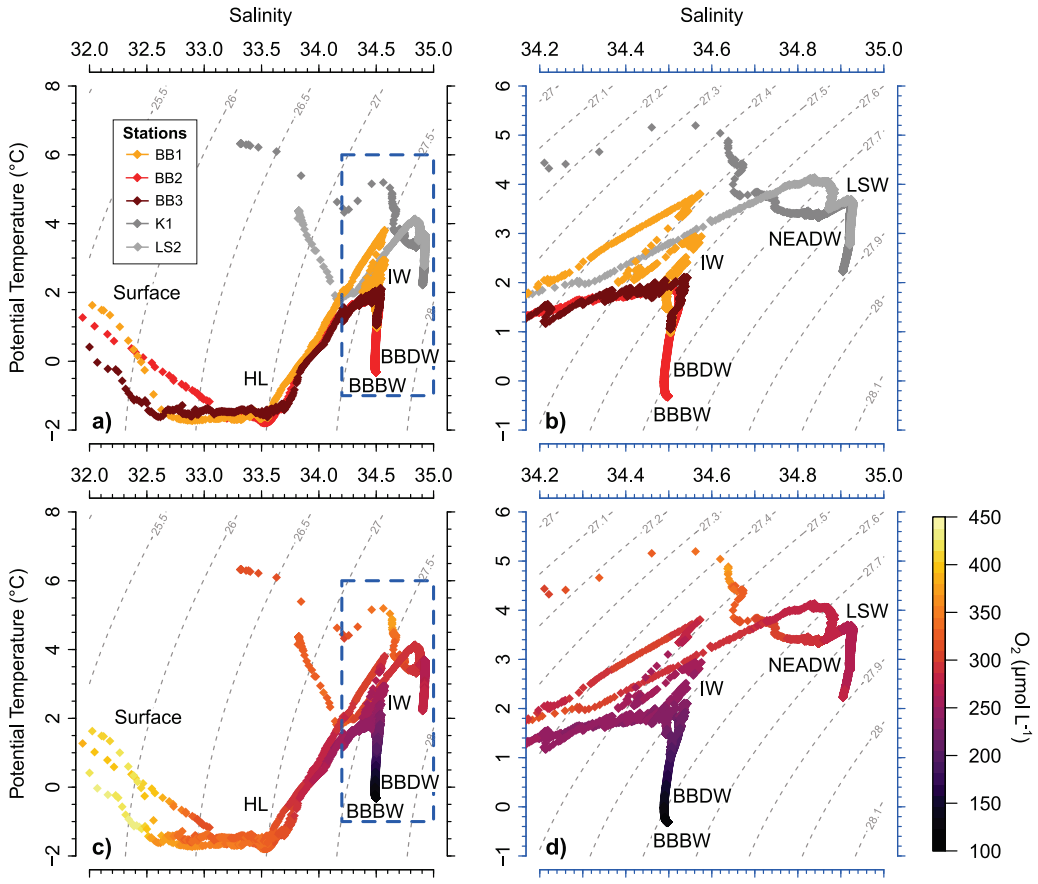

Figure 3.2: Potential temperature-salinity diagrams color-coded according to (a and b) the various stations investigated in this study and (c and d) associated oxygen (O_2) concentrations. Different stations in the Labrador Sea are indicated in shades of grey, and stations in Baffin Bay are depicted in orange and red. The dashed blue boxes (a and c) designate intermediate and deep waters enlarged in (b) and (d). Abbreviations specify the halocline layer (HL), intermediate water (IW), Baffin Bay Deep and Bottom Water (BBDW, BBBW), Labrador Sea Water (LSW), and Northeast Atlantic Deep Water (NEADW).

entering via southern Lancaster Sound, Nares Strait and Jones Sound (Figure 3.1; *Melling et al.*, 2001; *Münchow et al.*, 2007), and a remnant of the East Greenland Current (EGC) entering from the Atlantic through eastern Davis Strait, propagating northward as part of the shallower shelf component of the West Greenland Current (WGC) (*Azetsu-Scott et al.*, 2012; *Curry et al.*, 2011; *Muench*, 1971; *Tang et al.*, 2004). The Arctic-derived UHL source water shows a pronounced deficit in DIN (NH_4^+, NO_3^-, NO_2^-) below the surface layer, indicated by negative N* values of > -7.8 μmol L^{-1} (where N* = [DIN] $- 16 \times$ $[PO_4^{3-}] + 2.9$; *Deutsch et al.*, 2001; *Gruber and Sarmiento*, 1997) at $\sim$ 30 m in central Baffin Bay (BB2). These low N* values in UHL water ($\sim$ 50 m) occur in parallel with relatively elevated $\delta^{15}N_{NO3}$ ($\sim 6.2 \pm 0.2$‰) and low $\delta^{18}O_{NO3}$ ($\sim 0.8 \pm 0.1$‰). These coincident signals are largely acquired from benthic denitrification on the western Arctic continental shelf area (*Brown et al.*, 2015a; *Fripiat et al.*, 2018; *Granger et al.*, 2011), and possibly during the eastward propagation through the shallow Archipelago (*Jones*, 2003). Specifically, the elevated $\delta^{15}N$ and low $\delta^{18}O$ of NO_3^- in Pacific-origin waters derive from benthic coupled nitrification-denitrification on the Bering, Chukchi and east Siberian shelves, which increases $\delta^{15}N_{NO3}$ and lowers $\delta^{18}O_{NO3}$ compared to the open Pacific end-member (*Brown et al.*, 2015a; *Fripiat et al.*, 2018; *Granger et al.*, 2011, 2018). In keeping with the cyclonic circulation in Baffin Bay and the intrusion of Arctic water inflow (Figure 3.1), the Pacific NO_3^- signature is most pronounced in the southern Lancaster Sound (CAA3; -10.5 μmol L^{-1} for N* and $\sim 7.0 \pm 0.2$‰ for $\delta^{15}N_{NO3}$, Appendix C), indicating the eastward transport through the CAA. UHL N isotope ratios in the central basin are lower than at the entrance to Baffin Bay in Lancaster Sound but substantially more enriched than subsurface NO_3^- in the Labrador Sea (LS2, $\sim 4.8 \pm 0.1$‰; Figure 3.3g). Similarly, the subsurface N* minimum is more pronounced than at corresponding depths in the Labrador Sea (Figure 3.3f). The contribution of Pacific-derived nutrients to the central Baffin Bay is supported by modeled circulation fields in the upper water column ($<$ 200 m), showing an extension of the Baffin Island Current towards the center of the basin (*Wu et al.*, 2012), as well as previous Arctic nutrient budgets, indicating a pronounced southward transport of NO_3^- through Davis Strait (*Torres-Valdés et al.*, 2013).

The N* signal associated with Pacific-derived nutrients in Baffin Bay, however, is less pronounced than upstream in the upper halocline of the Canada Basin (-10 to -13 μmol L^{-1}). Similarly, the $\delta^{15}N_{NO3}$ is concurrently lower than in the Canada Basin (7.7–8.0‰;

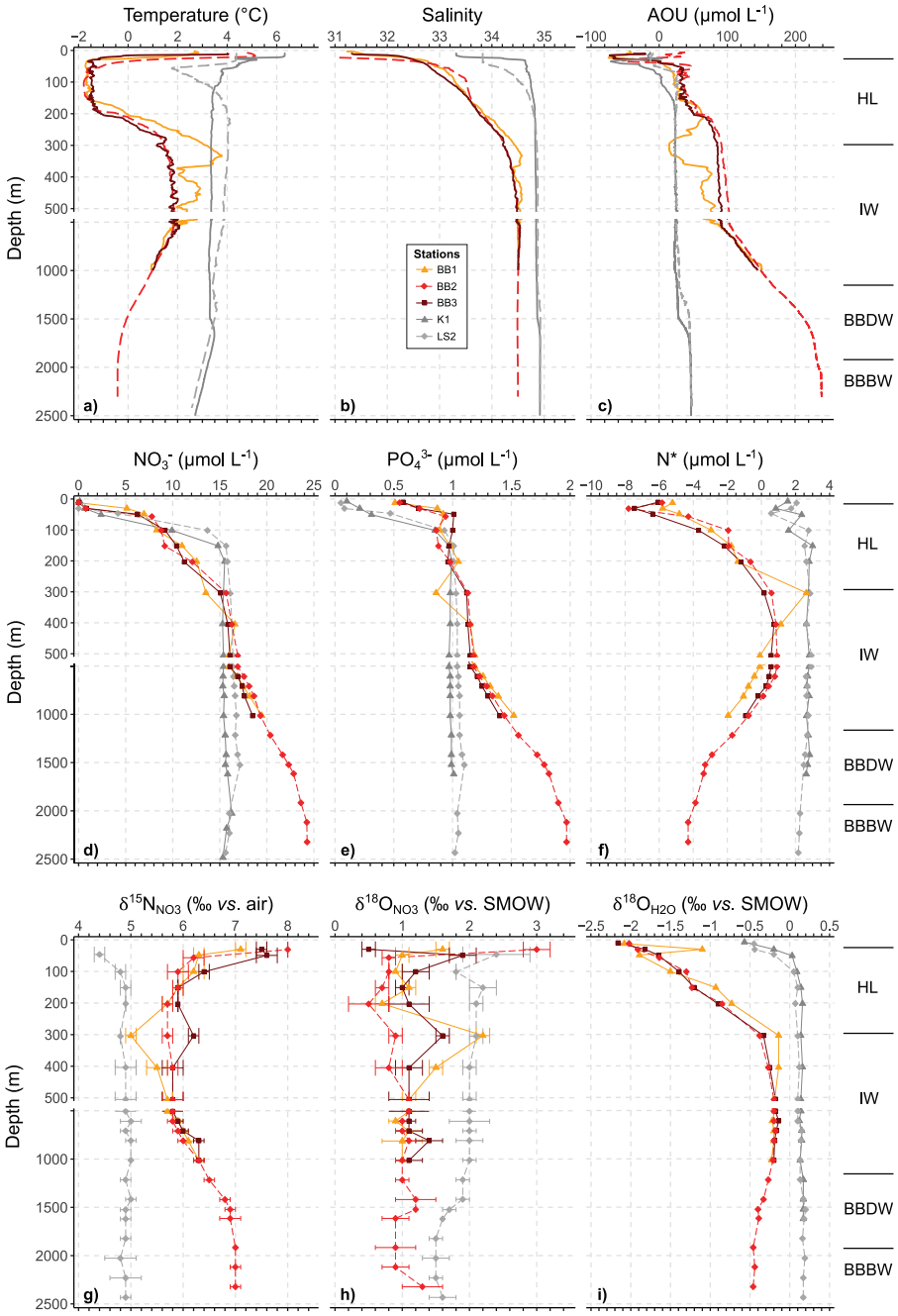

Figure 3.3: Water column profiles of (a) temperature, (b) salinity, (c) AOU, (d) NO_3^-, (e) PO_4^{3-}, (f) N*, (g) $\delta^{15}N_{NO3}$, (h) $\delta^{18}O_{NO3}$ and (i) $\delta^{18}O_{H2O}$ in Baffin Bay (orange, red) and the adjacent Labrador Sea (grey). Abbreviations indicate apparent oxygen utilization (AOU), and standard mean ocean water (SMOW) and the specific layers characterizing the water column in Baffin Bay (HL: halocline layer, IW: intermediate water, BBDW: Baffin Bay Deep Water, BBBW: Baffin Bay Bottom Water).

Brown et al., 2015a; *Granger et al.*, 2018), presumably due to vertical and tidal mixing in the area of eastern Barrow Strait (*Hughes et al.*, 2017; *Melling et al.*, 1984; *Prinsenberg and Bennett*, 1987), promoting exchange between western Arctic water and underlaying Atlantic-derived water that has a characteristic δ^{15}N of 5‰ (Figure 3.3g), as well as potential horizontal mixing with the shallow component of the WGC within Baffin Bay as part of the general cyclonic circulation in the basin (e.g., *Hamilton and Wu*, 2013; *Münchow et al.*, 2015; *Tang et al.*, 2004).

The low $\delta^{18}O_{NO3}$ (0.8‰) of the upper Baffin Bay halocline is within the range observed in the upper halocline of the western Arctic ($\sim$ 0.0–1.1‰; *Brown et al.*, 2015a; *Granger et al.*, 2018), where it is diagnostic of a highly remineralized NO_3^- reservoir from regeneration on the western Arctic shelves upstream (*Granger et al.*, 2018). The low $\delta^{18}O_{NO3}$ signal in the upper halocline of Baffin Bay may thus be entrained from the western Arctic, and may also derive from subsurface remineralization in the CAA and in situ in Baffin Bay itself. The low $\delta^{18}O_{NO3}$ values in the Baffin Bay halocline contrast with more elevated values of $\geq$ 2‰ typical of the North Atlantic thermocline (e.g., station LS2; Figure 3.3h). The latter is raised due to partial NO_3^- assimilation in the Southern Ocean (i.e., pre-formed NO_3^-), and also reflects a higher δ^{18}O of water incorporated in NO_3^- remineralized in the Atlantic compared to NO_3^- remineralized in the western Arctic, where the subsurface $\delta^{18}O_{H2O}$ is relatively low (Figure 3.3i; *Marconi et al.*, 2015; *Granger et al.*, 2018).

3.4.2 Origin of intermediate nutrients in Baffin Bay

Intermediate waters ($\sim$ 300–1200 m) in Baffin Bay are characterized by higher salinities ($>$ 34.20) and a transition to warmer temperatures ($>$ 0.4°C) than halocline waters above (Figures 3.2 and 3.3). Similarly, NO_3^- and PO_4^{3-} concentrations are higher and N* increases to positive values in intermediate waters (17.5 μmol L^{-1}, 1.2 μmol L^{-1} and 0.4 μmol L^{-1}, respectively). While these general patterns hold for the entire basin, noticeable differences are evident among stations within Baffin Bay. Specifically, in southern Baffin Bay at Davis Strait (BB1) peaks in salinity, temperature and N* (34.57, 3.8°C and 2.6 μmol L^{-1}) at $\sim$ 300 m are more pronounced than at corresponding depths in central Baffin Bay (BB2; Figure 3.3). NO_3^- and PO_4^{3-} concentrations at BB1 show respective minima at 300 m (13.5 μmol L^{-1} and 0.9 μmol L^{-1}), which remain absent in the central Baffin Bay. These nutrient minima are associated with higher O_2 concentrations (Figure 3.2) and a corresponding minimum in the apparent oxygen utilization (AOU = $[O_2]_{saturation}$

Table 3.1: Average values and standard deviations (SD) of hydrographic parameters associated with individual depth horizons/water masses. Abbreviations used in the table include: AOU, apparent oxygen utilization; BBBW, Baffin Bay Bottom Water; BBDW, Baffin Bay Deep Water; HL, halocline layer; IW, intermediate water; na, not available.

		σ_θ (kg m^{-3})	Temp. (°C)	Salinity	$[NO_3^-]$ (μmol L^{-1})	$[PO_4^{3-}]$ (μmol L^{-1})	N* (μmol L^{-1})	AOU (μmol L^{-1})
Surface (< 30 m)	Ave	24.60	4.0	31.01	0.0	0.5	-5.8	6.3
	SD		1.5	0.51	na	na	na	27.1
HL (30 - 300 m)	Ave	27.04	-0.6	33.66	7.7	0.9	-3.3	53.9
	SD		1.2	0.40	4.2	0.1	2.8	27.5
IW (300 - 1200 m)	Ave	27.61	1.3	34.49	17.5	1.2	0.4	129.5
	SD		0.4	0.06	1.3	0.1	0.6	26.2
BBDW (1200 - 1800 m)	Ave	27.71	-0.1	34.49	21.8	1.7	-2.8	215.7
	SD		0.2	0.00	1.1	0.1	0.8	14.8
BBBW (1800 - 2300 m)	Ave	27.73	-0.4	34.50	24.0	1.9	-4.2	237.5
	SD		0.0	0.00	0.4	0.0	0.2	2.2

– $[O_2]_{measured}$). A corresponding minimum in AOU is not apparent in the central bay (Figure 3.3c). Finally, the isotope ratios of NO_3^- at BB1 exhibit a prominent minimum in $\delta^{15}N_{NO3}$ ($5.0 \pm 0.1‰$) and a corresponding local maximum in $\delta^{18}O_{NO3}$ ($2.2 \pm 0.1‰$) at $\sim$ 300 m. Conversely, in central Baffin Bay (BB2), a corresponding $\delta^{15}N_{NO3}$ minimum remains absent ($5.7 \pm 0.1‰$ at 300 m), whereas the local maximum in $\delta^{18}O_{NO3}$ ($1.0 \pm 0.2‰$) is consistent with the southern Baffin Bay, although less pronounced than at BB1 (Figure 3.3, Table 3.2).

Below 300 m, hydrographic properties become more uniform among stations. $\delta^{15}N_{NO3}$ values show a progressive increase from the base of the halocline to the lower intermediate layer (6.3‰ at 1000 m), and $\delta^{18}O_{NO3}$ decrease to relatively constant values of $\sim 1.0‰$ in the deeper layer.

Intermediate waters in Baffin Bay are partially comprised of warm and saline Irminger Water ($\sim$ 5.0°C and $\sim$ 35.0; *Garcia-Ibanez et al.*, 2018), which enters Baffin Bay at the eastern side of Davis Strait via the lower slope branch of the WGC ($<$ 600 m) and mixes with adjacent Arctic waters as it propagates north and recirculates within the basin (*Azetsu-Scott et al.*, 2012; *Curry et al.*, 2011; *Rudels*, 1986; *Tang et al.*, 2004). Arctic waters therein are thought to derive from water circulated within Canada Basin lower halocline waters (*Bailey*, 1956), ultimately originating in the Barents Sea winter branch in the Eurasian Basins (*Rudels et al.*, 2004) and partly entering Baffin Bay from the north through Nares Strait (*Rudels*, 1986; *Rudels et al.*, 2004). In the Canada Basin, this Barents Sea branch centers at a salinity of $\sim$ 34.3 and temperature of ~ -0.6°C.

The pronounced peaks in temperature and salinity in southern Baffin Bay coincide with the inflow of Irminger Water through Davis Strait. Less pronounced maxima in both parameters relative to the Irminger Basin are consistent with previous measurements at Davis Strait (*Azetsu-Scott et al.*, 2012; *Tang et al.*, 2004), reflecting a progressive cooling and freshening as Irminger Water propagates northward in the WGC (*Yashayaev*, 2007). NO_3^- concentrations (13.5 μmol L^{-1}) are slightly lower while O_2 concentrations (309.5 μmol L^{-1}) increase relative to previous measurements further downstream ($\sim$ 14 μmol L^{-1} and $<$ 290 μmol L^{-1}, respectively; *Castrillejo et al.*, 2018; *Garcia-Ibanez et al.*, 2018), opposing the general expectation of decreasing O_2 and increasing nutrients as the water mass ages. While potential mixing with overlaying water along transit in the WGC could result in the observed nutrient and O_2 distribution, the depth of the warm and saline

Table 3.2: Average values and standard deviations (SD) of H_2O, NO_3^-, and N_2O isotope and isotopomer parameters associated with individual depth horizons/water masses. Abbreviations used in the table include: BBBW, Baffin Bay Bottom Water; BBDW, Baffin Bay Deep Water; HL, halocline layer; IW, intermediate water; na, not available; SP, N_2O site-preference.

		$\delta^{18}O_{H2O}$ (‰)	$\delta^{15}N_{NO3}$ (‰)	$\delta^{18}O_{NO3}$ (‰)	$[N_2O]$ (nmol L^{-1})	$\delta^{15}N^{bulk}$ (‰)	$\delta^{15}N^{\alpha}$ (‰)	$\delta^{15}N^{\beta}$ (‰)	$\delta^{18}O_{N2O}$ (‰)	SP (‰)
Surface ($<$ 30 m)	Ave	-2.02	na	na	13.1	6.5	19.9	-6.9	44.6	26.7
	SD	na	na	na	0.0	0.3	0.3	0.9	0.6	1.2
HL (30 - 300 m)	Ave	-1.39	6.0	0.7	15.4	6.7	17.7	-4.3	45.2	21.9
	SD	0.41	0.9	1.0	0.6	0.2	0.6	0.5	0.4	1.0
IW (300 - 1200 m)	Ave	-0.24	5.9	1.0	15.3	7.2	22.3	-8.0	51.1	30.3
	SD	0.07	0.2	0.2	0.7	0.3	2.0	1.7	3.6	3.7
BBDW (1200 - 1800 m)	Ave	-0.35	6.8	1.1	17.7	8.5	30.5	-13.6	67.7	44.1
	SD	0.06	0.2	0.2	0.4	0.3	2.2	1.8	4.0	3.9
BBBW (1800 - 2300 m)	Ave	-0.45	7.0	1.0	na	na	na	na	na	na
	SD	0.01	0.1	0.3	na	na	na	na	na	na

Irminger core – with maxima in T and S at 333 m – does not coincide with the observed AOU minimum at 296 m (Figure 3.3). The AOU minimum at 296 m may otherwise derive from the sinking and intrusion of recently ventilated surface waters of Atlantic origin, with low nutrients at intermediate depth signaling assimilation at the surface and/or dilution in the WGC. The local minima in $\delta^{15}N_{NO3}$ and $\delta^{18}O_{NO3}$ are consistent with the dilution of NO_3^--depleted surface waters in the WGC as mixing with zero or low NO_3^- concentrations would largely converge the NO_3^- isotopic signature towards the high-NO_3^- mixing end-member. While such cascading of increasingly dense water has not been reported for this area, it has recently been suggested by model analyses, simulating the sinking of brine-enriched Greenland Shelf waters at Davis Strait and the propagation of those waters northward into Baffin Bay (*Marson et al.*, 2017).

In the central bay, hydrographic properties at BB2 fall between values of Arctic and Atlantic/Irminger end-members, thus reflecting the recirculation of intermediate waters within the basin and associated mixing between the WGC and northern source waters (*Muench*, 1971; *Rudels*, 1986; *Tang et al.*, 2004). Previous estimates of northern vs. southern contribution to intermediate waters range from a small but significant fraction ($\sim$ 20%; *Azetsu-Scott et al.*, 2012) to a predominantly ($<$ 80%; *Rudels*, 1986) Arctic contribution. Mean nutrient concentrations at BB2 (Table 3.1) are comparable to peak values associated with the WGC recorded at Davis Strait (*Torres-Valdés et al.*, 2013). Given the lower nutrient content of the western Arctic end-member ($\sim$ 12 μmol L^{-1} and $\sim$ 0.8 μmol L^{-1} in the Canada Basin lower halocline; Granger2018) and evidenced mixing between Arctic and Atlantic waters, we would expect the nutrient concentrations at BB2 to reflect an intermediate between the two end-members. The relatively high nutrient concentrations in the central bay thus suggest some additional nutrient input from remineralization in situ or in transit from the Canada Basin to Baffin Bay. This is further substantiated by an increase in AOU and $\delta^{15}N_{NO3}$ ($\sim$ 129.5 μmol L^{-1} and 5.9‰ at BB2) relative to measurements in the Canada Basin (65 μmol L^{-1} and 5.6‰) and in southern Baffin Bay (Figure 3.3), supporting some remineralization of high-^{15}N organic matter (see section below for details).

3.4.3 Origin of deep and bottom nutrients in Baffin Bay

The deep water column in Baffin Bay is comprised of Baffin Bay Deep Water (BBDW), corresponding to a salinity of 34.49 near the 0°C isotherm ranging from $\sim$ 1200–1800

m, and Baffin Bay Bottom Water (BBBW) at $>$ 1800 m with low temperatures ($-0.4°$C) and a slightly higher salinity (34.50). To date, the origin of Baffin Bay deep and bottom waters is not settled unequivocally. Recent studies point to a northern origin via the Smith Sound in Nares Strait (*Bailey*, 1956; *Bourke and Paquette*, 1991; *Muench*, 1971; *Rudels*, 1986; *Tan and Strain*, 1980), where different proposed mechanisms, including winter cooling and brine rejection in Nares Strait, lead to an increase in density and thus sinking of those waters to depth. Based on some studies (*Bailey*, 1956; *Rudels et al.*, 2004), BBDW and BBBW are ventilated by the same Barents Sea branch present in the lower Canada Basin halocline that potentially feeds the Baffin Bay intermediate layer. $\delta^{18}O_{H2O}$ in BBBW ($-0.45‰$, Figure 3.3i) are lower compared to the Canada Basin lower halocline ($-0.2‰$; *Granger et al.*, 2018). These lower values in BBBW, in agreement with values previously measured in the deep basin (*Tan and Strain*, 1980), may thus reflect brine rejection associated with its formation prior to sinking. BBDW and BBBW may have long residence times, with wide-ranging estimates of 77–1450 years (*Top et al.*, 1980; *Wallace*, 1985). Residence time estimates for Baffin Bay are based on different box model approaches and ^{3}He/Tritium data (*Top et al.*, 1980) versus chlorofluoromethane measurements (*Wallace*, 1985). In both approaches, the age estimates largely depend on the source water and renewal mechanisms of BBDW and BBBW. However, given that these supply mechanisms still remain to be fully resolved, large uncertainties are associated with estimated deep water renewal times.

Nutrient profiles reveal a gradual increase in both NO_3^- and PO_4^{3-} from BBDW to BBBW (24.0 μmol L^{-1} and 1.9 mol L^{-1} in BBBW), which coincides with decreasing O_2 concentrations to 113 μmol L^{-1} (32% saturation, where % saturation reflects the [O_2] measured relative to the [O_2] at equilibrium calculated using in situ temperature and salinity (after *Garcia and Gordon*, 1992) at the bottom of the bay (Figure 3.2). Nutrients may thus have accrued in the basin over indeterminate yet potentially long timescales. Based on the organic matter respiration stoichiometry (170 O_2: 1 P; *Anderson and Sarmiento*, 1994) and assuming that the Canada Basin lower halocline ventilates BBDW and BBBW – thus only accounting for the increase in AOU from the source towards Baffin Bay – we estimate that $\sim$ 1/2 of the deep dissolved PO_4^{3-} pool derives from remineralization in transit from the Canada Basin or in situ in Baffin Bay. The low $\delta^{18}O_{NO3}$ values (1.0 $\pm$ 0.3‰), which are among the lowest recorded in deep ocean waters, corroborate the

notion that a substantial fraction of the nutrients in deep Baffin Bay are regenerated, as newly nitrified NO_3^- adopts a $\delta^{18}O$ value that $\sim$ +1.1‰ more enriched relative to ambient seawater (*Buchwald et al.*, 2012; *Casciotti et al.*, 2008; *Sigman et al.*, 2009a, $\delta^{18}O_{H2O}$ of -0.45‰ in BBBW, Figure 3.3i). Based on regenerated PO_4^{3-} from AOU, we estimate a concurrent addition of 16.2 μmol L^{-1} of NO_3^- assuming Redfield stoichiometry, a value larger than the observed increase in NO_3^- (+12.0 μmol L^{-1}) between the Canada Basin end-member and BBBW. This lower observed value, however, is consistent with the N* minimum (-4.2 μmol L^{-1}) observed in the deep basin (Figure 3.3f), which we interpret to signal N loss from benthic denitrification. This prominent N-deficit has otherwise been ascribed to either a modified Redfield stoichiometry of sinking particles stemming from assimilation in N-depleted waters at the surface (N:P ratio of 9.6 as a result of surface N-depletion; *Jones et al.*, 1984), or from the preferential remineralization of particulate organic carbon and nitrogen in the upper water column ($<$ 100 m) and subsequent export of biogenic silica to depth (*Michel et al.*, 2002; *Tremblay et al.*, 2002). The $\delta^{15}N_{NO3}$ in BBBW (7.0 $\pm$ 0.1‰) is more akin to the Pacific-derived nutrients entering Baffin Bay in the UHL in Lancaster Sound compared to the Canada Basin lower halocline NO_3^- (5.6 $\pm$ 0.1‰; *Granger et al.*, 2018), thus further validating the notion that a high proportion of nutrients in BBBW are remineralized in situ, from primary production at the surface that is largely fueled by Pacific-derived NO_3^-. This inference is also supported by observations of a ^{15}N-enrichment in particulate organic matter and high export production in the western part of the NOW polynya (*Tremblay et al.*, 2002, 2006). In spite of a striking N* minimum, the apparent $\delta^{15}N$ increase from mid-depth to BBDW persisting into BBBW is specifically not attributable to water column denitrification, given the elevated O_2 concentrations and the absence of a parallel $\delta^{18}O_{NO3}$ increase (*Granger et al.*, 2008; *Sigman et al.*, 2005). Based on regenerated NO_3^- from AOU and using the following mass balance

$$\delta_{nitr} \times [NO_3^-]_{nitr} = \delta_{obs} \times [NO_3^-]_{obs} - \delta_{background} \times [NO_3^-]_{background} \qquad (3.1)$$

we approximate the $\delta^{15}N$ of remineralized NO_3^- added to BBBW to be 8.0‰, a value within the range of ^{15}N-enrichement in particulate organic matter in northern Baffin Bay (*Tremblay et al.*, 2002).

Given that a substantially lower fraction of sinking organic material is expected to remineralize in deep and bottom waters compared to the intermediate layer and above,

the higher nutrient concentrations and higher $\delta^{15}N_{NO3}$ in bottom waters compared to intermediate depths is explained by (a) a substantially longer residence time of deeper basin waters compared to intermediate waters above (5–20 yrs; *Rudels*, 1986; *Top et al.*, 1980), as well as (b) a contribution of Atlantic-derived water with a lower $\delta^{15}N_{NO3}$ at intermediate depths.

In situ remineralization of ^{15}N-enriched organic matter, in and of itself, does not explain the apparent N* minimum of BBBW. Although water column denitrification can be ruled out, dissimilatory NO_3^- consumption in the sediment likely acts as a substantial sink for DIN. Sediment denitrification is expected to impart negligible isotopic discrimination on $\delta^{15}N_{NO3}$ and $\delta^{18}O_{NO3}$ in the overlying water column due to complete consumption or diffusion limitation of NO_3^- from the sediment and a subsequent suppression of the organism-level isotope effect (ε close to 0‰; *Brandes and Devol*, 1997; *Lehmann et al.*, 2005; *Sigman et al.*, 2003, 2005). In this context, we estimate the denitrification rates necessary to explain the observed N* minimum in the deep basin from the N* difference between the Barents Sea source water and Baffin Bay deep and bottom water, integrated from 1200 m to the bottom. We account for the sediment surface area, extracted from the GEBCO_2014 30 arc-second dataset (version 20150318, www.gebco.net), and an upper and lower range of water residence time estimates (1450 vs. 77 years; *Top et al.*, 1980; *Wallace*, 1985), yielding denitrification rates ranging from 10.1 to 190.8 μmol L^{-1} m^{-2} d^{-1}, with lower-end estimates similar to the deep Canada Basin (*Granger et al.*, 2018) and upper-end estimates on the same order as reported for the deep Bering Sea (*Lehmann et al.*, 2005). The wide range in estimated denitrification rates reflects the large uncertainty associated with bottom water residence times. More precise age estimates, which would significantly improve our estimates of denitrification rates, are still pending for the deep Baffin Bay. The incident N_2O in the deep basin could thus originate in part or dominantly from sediment denitrification (see section 3.4.5).

3.4.4 Undersaturation and isotopically light N_2O in the shallow water column

Shallow N_2O concentrations in Baffin Bay are concordant ($< 6\%$ deviation) with previous measurements conducted during the same 2015 GEOTRACES cruise using discrete samples and independent gas chromatograph mass spectrometry (*Fenwick et al.*, 2017, Figure 3.4a). N_2O data show low concentrations at the surface (13.3 $\pm$ 0.0 nmol L^{-1})

which increase to a subsurface peak (16.3 ± 0.0 nmol L^{-1}) at $\sim$ 30 m (Figure 3.4a). Excess N_2O, or ΔN_2O, in the upper 30 m corresponds to values close to equilibrium with the atmosphere (-0.3 ± 0.0 nmol L^{-1}). N_2O isotope ratios at the surface (6.5 ± 0.3‰ and 44.7 ± 0.6‰ for $\delta^{15}N^{bulk}$ and ‰ for $\delta^{18}O_{N2O}$, Figure 3.4b) are similar to tropospheric N_2O values ($\sim$ 6.6‰ and 44.2‰; *Toyoda et al.*, 2013). The low N_2O concentrations close to equilibrium with the atmosphere at BB2 contrast previous findings associated with the Baffin Bay marginal ice zone, where a pronounced shallow (13 m) N_2O maximum (28.1 nmol L^{-1}, 179% saturation) has been ascribed to local N_2O production *via* nitrification (*Kitidis et al.*, 2010).

Below the surface layer, N_2O concentrations show a decrease throughout the halocline layer (15.1 ± 0.1 nmol L^{-1} at $\sim$ 100 m), which corresponds to a deficit in N_2O relative to equilibrium ($\Delta N_2O <$ -1.8 $\pm$ 0.1 nmol L^{-1}). In contrast, the Pacific-derived source waters of the Baffin Bay UHL show a pronounced N_2O supersaturation in the western Arctic ($\leq$ 148%) coincident with the N* minimum (*Fenwick et al.*, 2017; *Hirota et al.*, 2009; *Zhang et al.*, 2015). In line with the negative N* and elevated $\delta^{15}N_{NO3}$ in Pacific-derived waters, the N_2O supersaturation is largely acquired from benthic denitrification on the western Arctic continental shelf area (*Fenwick et al.*, 2017). Subsequently, the progressive decrease in N_2O from west to east through the Archipelago, reaching values close to equilibrium toward Baffin Bay, has been explained both by sea-air exchange and mixing with low-N_2O waters (i.e., sea ice meltwater, river water) (*Fenwick et al.*, 2017). N_2O isotope abundances in Pacific Winter Water in the western Arctic (5.7‰, 47.9‰ and 22.6‰ for $\delta^{15}N^{bulk}$, $\delta^{18}O_{N2O}$ and SP; Table 3.3) are comparable to those in the Baffin Bay subsurface peak (6.6 ± 0.1‰, 45.5 ± 0.1‰ and 22.1 ± 1.2‰; Figure 3.4), consistent with a dilution by sea ice meltwater as N_2O gets expelled from sea ice during its formation (*Randall et al.*, 2012; *Zhang et al.*, 2015). Sea-air exchange and mixing with low-N_2O waters (i.e., sea ice meltwater, river water) have been invoked to explain a progressive decrease in N_2O in transit through the Archipelago, reaching values close to equilibrium toward Baffin Bay (*Fenwick et al.*, 2017). In this respect, the slightly higher $\delta^{15}N^{bulk}$ and concurrently lower $\delta^{18}O_{N2O}$ and SP in Baffin Bay observed in this study relative to the western Arctic may then reflect some imprint of atmospheric N_2O as values approach a tropospheric isotopic signature (Figure 3.4), in agreement with a general negative net N_2O sea-air flux (*Fenwick et al.*, 2017).

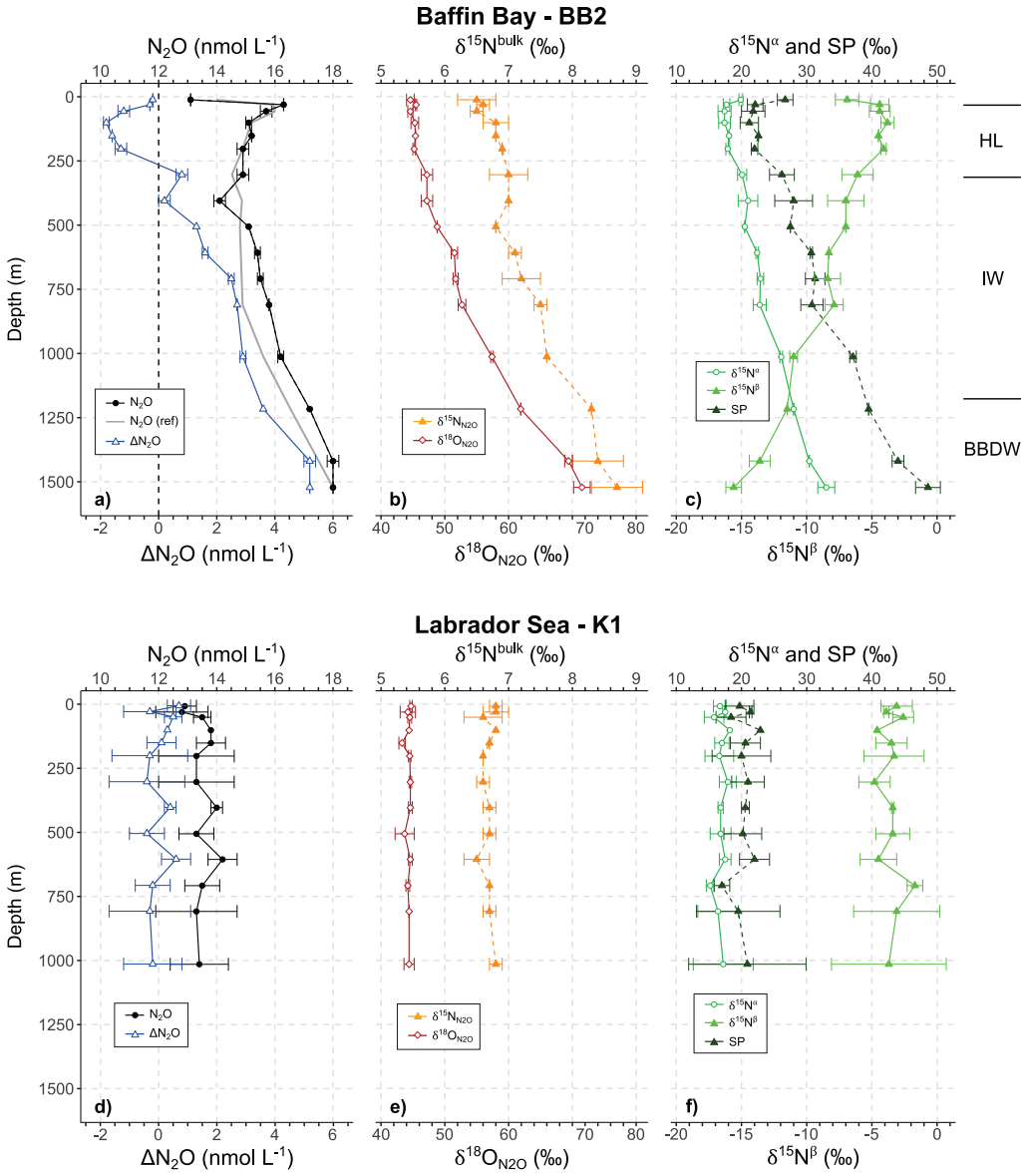

Figure 3.4: Water column profiles of N_2O concentrations and isotopomer abundances in the top 1500 m of the water column in (a, b and c) Baffin Bay (BB2) and (d, e and f) Labrador Sea (K1). (a) N_2O reference concentrations (grey line) represent independent measurements from the same 2015 GEOTRACES expedition at station BB2 in Baffin Bay (*Fenwick et al.*, 2017). The black dashed line (a) marks the N_2O equilibrium with the atmosphere. Abbreviations indicate the specific layers characterizing the water column in Baffin Bay (HL, halocline layer; IW, intermediate water; BBDW, Baffin Bay Deep Water).

Table 3.3: Reference values of selected hydrographic parameters as well as nutrient and isotope data associated with Pacific Winter Water (PWW) and the Lower Halocline Layer (LHL) in the Canada Basin. Nutrient and NO_3^- isotope data were collected during the 2009 Canada International Polar Year GEOTRACES program (*Granger et al.*, 2018) and N_2O concentrations and isotopomer values are from the 2015 US Arctic GEOTRACES campaign (data provided by A. Bourbonnais).

	Temp. (°C)	Salinity	$[NO_3^-]$ (μmol L^{-1})	$[PO_4^{3-}]$ (μmol L^{-1})	N* (μmol L^{-1})	AOU (μmol L^{-1})	$\delta^{18}O_{H2O}$ (‰)
PWW	-1.5	31.1	16	1.9	-13	95	-1.2
LHL	-0.6	34.3	12	0.8	0	65	-0.2

	$\delta^{15}N_{NO3}$ (‰)	$\delta^{18}O_{NO3}$ (‰)	$[N_2O]$ (nmol L^{-1})	ΔN_2O (μmol L^{-1})	$\delta^{15}N^{bulk}$ (μmol L^{-1})	$\delta^{18}O_{N2O}$ (‰)	SP (‰)
PWW	8.0 ± 0.1	0.0 ± 0.3	21.5	4.8	5.7	47.9	22.6
LHL	5.6 ± 0.1	0.9 ± 0.3	16.1	0.6	7.2	50.5	24.8

We note that the ΔN_2O minimum in the Baffin Bay halocline specifically does not arise from lower tropospheric N_2O levels when those waters were last in contact with the atmosphere on the Chukchi and East Siberian shelves and a prolonged transit time of Pacific-derived waters through the Arctic. Considering a transit time of $\sim$ 10–15 years (*Aksenov et al.*, 2016; *Nguyen et al.*, 2011) and accounting for the associated atmospheric N_2O mixing ratio (315.9 ppb; https://esrl.noaa.gov/gmd/) still results in a ΔN_2O minimum (-1.2 ± 0.1 nmol L^{-1}) at $\sim$ 100 m, supporting the notion of mixing and sea-air flux as the driving forces leading to the undersaturation in Baffin Bay halocline waters.

3.4.5 N_2O supersaturation in the deep basin

N_2O concentrations increase progressively from the halocline to respective maxima at the deepest depth sampled (N_2O of 18.0 ± 0.0 nmol L^{-1} at $\sim$ 1500 m), in agreement with previous observations (*Fenwick et al.*, 2017; *Kitidis et al.*, 2010) and contrasting with relatively constant values in the deep Labrador Sea (Figure 3.4d). Accounting for the potentially long residence times of BBDW (*Top et al.*, 1980; *Wallace*, 1985) and corresponding preindustrial atmospheric N_2O mixing ratios (270 ppb; *Flückiger et al.*, 1999), ΔN_2O increases similarly towards the deep basin (5.2 ± 0.0 nmol L^{-1}).

The pronounced accumulation of N_2O in deep Baffin Bay also contrasts with other Arctic deep basins (e.g., Canada Basin), where N_2O concentrations are close to equilibrium when considering the ventilation age and corresponding preindustrial atmospheric N_2O levels (*Fenwick et al.*, 2017; *Zhan et al.*, 2015). N_2O at depth is also considerably greater than the Barents Sea branch end-member in the lower halocline of the Canada Basin (0.6 nmol L^{-1}; Table 3.3). The N_2O in deep Baffin Bay thus likely originated in situ, from water column and sedimentary nitrification and/or denitrification. AOU and ΔN_2O in BBDW are positively correlated below 500 m (Figure 3.5a), a correlation that is typically interpreted as evidence for nitrification as the dominant source of N_2O – given the consumption of O_2 during oxic remineralization (*Cohen and Gordon*, 1978). Assuming Redfield stoichiometry, wherein 17% of the O_2 ascribed to remineralization is consumed by NH_4^+ oxidation (*see Ward*, 2008), the slope of the observed linear relationship suggests that 0.035 nmol N_2O were produced per μmol O_2 consumed, resulting in a N_2O yield of 0.021% from nitrification. This estimate is close to values reported for oxic intermediate waters of the subarctic Pacific Ocean (0.028%; *Grundle et al.*, 2012). By further assuming the nitrification of 13.9 μmol L^{-1} of NH_4^+, derived from the increase in AOU between the

Canada Basin lower halocline and BBDW, in situ nitrification would add a maximum of 2.9 nmol L^{-1} to the water-column ΔN_2O, accounting for $\sim$ ½ of the observed 5.2 nmol L^{-1} at 1500 m. This estimate, however, must be considered as an upper limit for N_2O produced through nitrification in the water column, given that the potential incidence of benthic denitrification, as suggested by a strong inverse correlation between ΔN_2O and N* (Figure 3.5b), would also manifest as a positive correlation between N_2O and AOU (*Nevison et al.*, 2003; *Yamagishi et al.*, 2005). Regardless, this approximation suggests that an additional production pathway is needed to explain the N_2O supersaturation at depth.

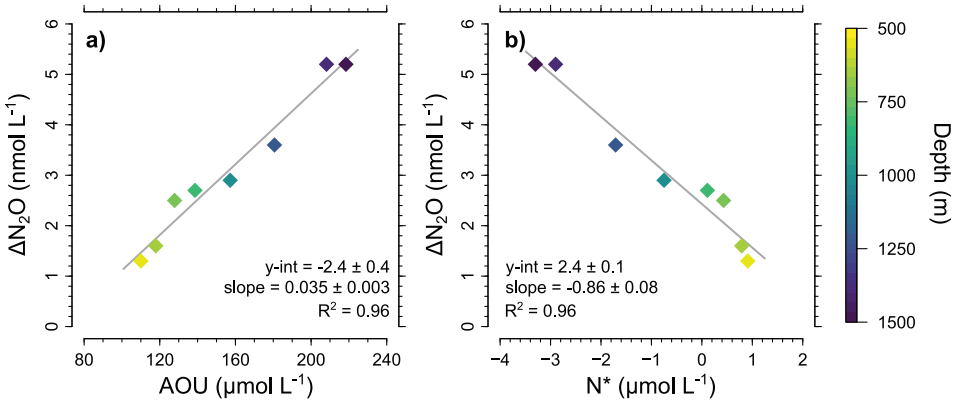

Figure 3.5: Property-property plot of ΔN_2O *vs.* (a) AOU and (b) N* in central Baffin Bay (BB2), color-coded against depth. Grey lines indicate linear regression analyses.

To further assess the contribution of additional N_2O production pathways to the observed deep N_2O signal, we investigate bulk isotope distributions and isotopomer abundances associated with the N_2O supersaturation in Baffin Bay. The accumulation of N_2O at depth is associated with progressive increases in $\delta^{15}N^{bulk}$, $\delta^{18}O_{N2O}$ and SP (8.7 $\pm$ 0.4‰, 71.5 $\pm$ 1.3‰ and 48.6 $\pm$ 1.9‰) in BBDW at 1500 m (Figure 3.4), contrasting Labrador Sea profiles which show little variation with depth (Figure 3.4) and ratios within error of tropospheric N_2O ($\sim$ 6.6‰, 44.2‰ and 18.4‰ for $\delta^{15}N^{bulk}$, $\delta^{18}O_{N2O}$ and SP, respectively; *Toyoda et al.*, 2013). Bulk isotope ratios and associated SP in BBDW are also distinctively larger than those in Barents Sea source waters in the Canada Basin (7.2‰, 50.5‰and 24.8‰ for $\delta^{15}N^{bulk}$, $\delta^{18}O_{N2O}$ and SP; Table 3.3). To obtain an approximation of the isotopic signature of the N_2O produced in the deep basin, we apply a two component mixing model and a set of mass balance estimates similar to equation 3.1, where the N_2O observed

represents a mixture between a constant N_2O background and the N_2O produced in situ (*Casciotti et al.*, 2018). Using the Keeling plot method (*Keeling*, 1961), the isotopic signature of the N_2O produced can then be estimated from the intercept of the linear regression of isotope ratios *vs*. the inverse of the measured N_2O concentration (Figure 3.6). Based on the linear regressions, the N_2O added to bottom waters has moderately elevated $\delta^{15}N^{bulk}$ ($16.7 \pm 1.5‰$), highly elevated $\delta^{18}O_{N2O}$, $\delta^{15}N^{\alpha}$, and SP ($168.1 \pm 9.5‰$, $86.1 \pm 6.1‰$ and $138.1 \pm 11.6‰$, respectively), and a very low $\delta^{15}N^{\beta}$ ($-52.2 \pm 5.8‰$).

The estimated $\delta^{15}N^{bulk}$ added to the basin is more elevated than the $\delta^{15}N^{bulk}$ expected from N_2O production through nitrification. Given normal isotope effects associated with N_2O production from nitrification (*Frame and Casciotti*, 2010; *Santoro et al.*, 2011; *Sutka et al.*, 2006; *Toyoda et al.*, 2005), the $\delta^{15}N^{bulk}$ of N_2O produced would be equal to or lower than the $\delta^{15}N$ of the NH_4^+ substrate. The precursory NH_4^+, in turn, derives from the ammonification of sinking organic material ($< 9‰$ in northern Baffin Bay; *Tremblay et al.*, 2006).

In the absence of N_2O consumption, N_2O production *via* denitrification is expected to produce $\delta^{15}N^{bulk}$ that is equal to or lower than the $\delta^{15}N$ of NO_3^- overlaying the sediment ($7.0‰$). The elevated expected $\delta^{15}N^{bulk}$ indicates that the N_2O added to the deep basin has been fractionated by partial N_2O consumption in the sediment, as isotopically light N_2O is preferentially reduced to N_2. Likewise, relatively elevated $\delta^{18}O_{N2O}$ and $\delta^{15}N^{\alpha}$ also suggest isotopic discrimination from N_2O reduction. Thus, N_2O in deep Baffin Bay largely originates from the sediment where it is partially reduced by denitrification. Considering the source of N_2O, the most parsimonious explanation is then that it, too, originates from benthic denitrification, namely, from NO_3^- reduction to N_2O, rather than from nitrification in the sediments or overlying water column. To test whether benthic denitrification accounts for observed N_2O isotope ratios, we first consider the expected isotopic composition of N_2O produced by denitrification, assuming steady state production and reduction of N_2O in the sediments. Given an initial $\delta^{15}N_{NO3}$ of $7.0‰$ in the overlying water column, we make the simplifying assumption that the $\delta^{15}N^{bulk}$ generated at the sediment depth of denitrification converges on a value of $7.0‰$, as NO_3^- is completely consumed within sediments (*Lehmann et al.*, 2005). Given little or no site preference from N_2O production during denitrification (*Sutka et al.*, 2006), the $\delta^{15}N^{\alpha}$ (and $\delta^{15}N^{\beta}$) produced are thus equivalently $7.0‰$. The $\delta^{15}N^{\alpha}$ returned from the Keeling plot ($86.1‰$) then

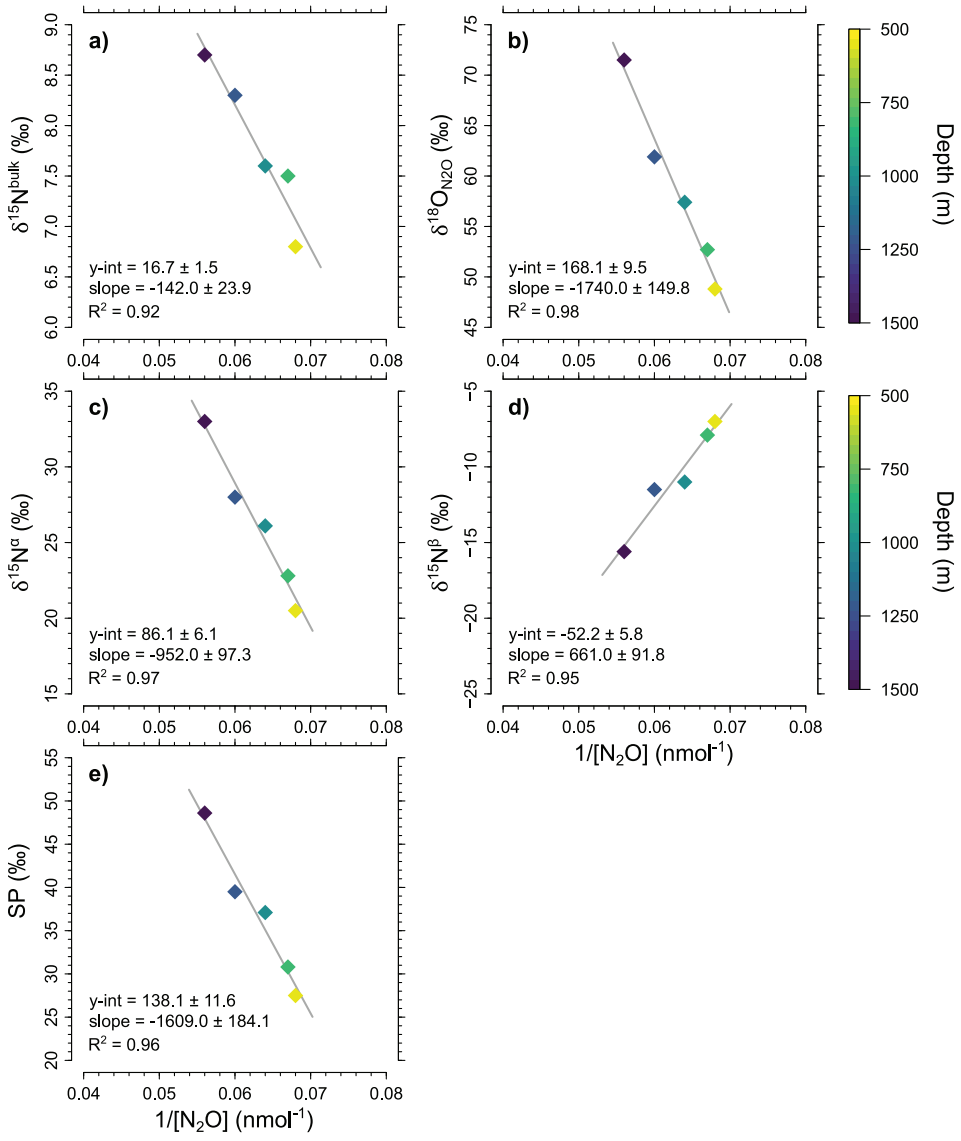

Figure 3.6: Keeling plots showing (a) $\delta^{15}N^{bulk}$, (b) $\delta^{18}O_{N2O}$, (c) $\delta^{15}N^{\alpha}$, (d) $\delta^{15}N^{\beta}$ and (e) site-preference (SP) against the inverse of the independently measured N_2O concentration (*Fenwick et al.*, 2017) in central Baffin Bay (BB2) where depth $>$ 500 m. The intercept of the linear regression (grey line) indicates the isotopic signature of the N_2O produced in situ.

suggests that the δ^{15}N increase of N_2O was incurred by its reduction (catalytic breakage of the N^{α}-O bond of N_2O), increasing $\delta^{15}N^{\alpha}$ by approximately $86.1‰ - 7.0‰ = 79.1‰$. Given an invariant $\delta^{18}O_{N2O}$ *vs.* $\delta^{15}N^{\alpha}$ ratio of 1.6 evidenced from denitrifier culture studies (*Ostrom et al.*, 2007), the expected ^{18}O-enrichment from N_2O reduction should then be 126.5‰ ($\delta^{15}N^{\alpha} \times 1.6‰ = \delta^{18}O_{N2O}$). From the Keeling plot, the $\delta^{18}O_{N2O}$ added to the bottom water is on the order of 168.1‰, thus an approximated 167.1‰ greater than the δ^{18}O of NO_3^- in the overlying water column (1.0‰). If N_2O reduction accounts for 126.5‰ of this $\delta^{18}O_{N2O}$ increase, the remaining 40.6‰ is then consistent with expectations of branching O isotope effects for NO_3^- and NO_2^- reduction. Branching effects are manifested onto $\delta^{18}O_{N2O}$ from the preferential abstraction of the lighter O isotope during both the reduction of NO_3^- to NO_2^- ($^{18}\varepsilon \approx -25$ to $-30‰$; *Casciotti and McIlvin*, 2007) and NO_2^- reduction to N_2O ($^{18}\varepsilon \approx -8$ to $-12‰$; *Casciotti and McIlvin*, 2007; *Frame and Casciotti*, 2010), producing N_2O with a δ^{18}O nearly 40‰ greater than the δ^{18}O of NO_3^-, barring isotopic equilibration of the NO_2^- intermediate with water (*Casciotti and McIlvin*, 2007). Thus, both the $\delta^{15}N^{\alpha}$ and $\delta^{18}O_{N2O}$ derived from Keeling plots are consistent with the N_2O efflux from the benthos, wherein it is produced and consumed by denitrification.

Neither of the scenarios above, however, explains the SP of 138.1‰ derived from the Keeling plots. SP is thought to be process-dependent, with values for individual production processes ranging from -11 to 0‰ for nitrifier-denitrification, -5 to 22‰ for canonical denitrification and 30 to 36‰ for NH_2OH decomposition (*Frame and Casciotti*, 2010; *Santoro et al.*, 2011; *Sutka et al.*, 2006; *Toyoda et al.*, 2005). Assuming little or no site preference imparted during the production of N_2O *via* denitrification, SP is influenced only by the reduction of N_2O, increasing in a ratio of 0.45 relative to $\delta^{18}O_{N2O}$ (*Ostrom et al.*, 2007). The SP imparted to N_2O from its reduction would then be 56.9‰ ($\delta^{18}O_{N2O}$ x 0.45 = SP), a value substantially lower than the inferred SP of 138.1‰. Alternatively, invoking a SP of 36‰ for N_2O produced from hydroxylamine oxidation or by fungal denitrification does not explain the observed SP either ($56.9‰ + 36‰ = 92.9‰$). The SP of N_2O produced in sediments thus cannot be straight-forwardly reconciled from the accepted isotope systematics of N_2O production and consumption.

The disproportionate SP extrapolated from the Keeling plot derives in part from the correspondingly low extrapolated $\delta^{15}N^{\beta}$ ($-52.2‰$), which amplifies the SP signal. Analogously low $\delta^{15}N^{\beta}$ of N_2O have been observed in core oxygen deficient zones (ODZs) at

continental margins (*Bourbonnais et al.*, 2017; *Casciotti et al.*, 2018; *Farías et al.*, 2009). These negative $\delta^{15}N^{\beta}$ excursions have been explained by N_2O reduction in excess of its production, thus breaking the steady-state assumption which would otherwise yield a lower SP (*Bourbonnais et al.*, 2017; *Farías et al.*, 2009). This explanation, however, does not reconcile the observations herein, given that our extrapolated SP is too elevated relative to $\delta^{15}N^{\alpha}$ and $\delta^{18}O_{N2O}$ to be imparted solely by N_2O reduction. The consumption of N_2O could only explain a low $\delta^{15}N^{\beta}$ if the associated isotope effect on $\delta^{15}N^{\beta}$ were inverse, thus further decreasing $\delta^{15}N^{\beta}$ relative to $\delta^{15}N^{\alpha}$ as a function of N_2O reduced, which is contrary to observations of a modest yet positive N isotope effect (*Ostrom et al.*, 2007), presumably from secondary isotope effects from bond breakage of the N^{α}-O bond of N_2O.

If not from N_2O reduction, the low $\delta^{15}N^{\beta}$ must be imparted during N_2O formation from NO, which agrees with similar conclusions drawn from N_2O isotopomer measurements in the South Pacific ODZ (*Casciotti et al.*, 2018). Based on previous work (*Schmidt et al.*, 2004), a high SP is expected from the preferential breakage of the N-O bond in the symmetric intermediate at the NO reductase site (NOR) preceding N_2O formation from NO, which is also associated with the prediction of an inverse isotope effect on $\delta^{15}N^{\alpha}$ atom of NO incorporated into N_2O. While such dynamics could explain the low $\delta^{15}N^{\beta}$ and high $\delta^{15}N^{\alpha}$ here, the normal and inverse isotope effects on respective N^{β} and N^{α} of N_2O during its reduction, and by extension the SP, would have to be considerable to explain the current data. We thus surmise that the NO intermediate during denitrification may be subject to competing inorganic reactions in the sediments, potentially resulting in disproportionate SP compared to culture observations. As such, potentially elevated levels of Fe(II) and Mn(II) associated with sedimentary redox-reactions in deep Baffin Bay may fuel competing chemical denitrification processes with associated SP values generally being elevated relative to N_2O production via bacterial denitrification (*Grabb et al.*, 2017). Regardless, contrary to the current dogma, the N_2O SP is not unequivocally indicative of the origin of N_2O from nitrification or denitrification echoing a sentiment also expressed by others (*Schmidt et al.*, 2004). As such, the isotopic signatures of NO_3^- and N_2O in deep Baffin Bay are consistent with N_2O production and reduction by benthic denitrification, a conclusion consistent with considerable N* decrease toward the benthos.

3.4.6 Alternative mechanisms evoked for N loss in Baffin Bay deep and bottom waters

Even though both the isotopic signature of dissolved NO_3^- as well as N_2O isotopomers are consistent with benthic denitrification, we examine whether other processes may explain the negative N* values in deep Baffin Bay. The N* minimum along with the $\delta^{15}N_{NO3}$ enrichment could be advected signals of benthic denitrification in the source region(s) of BBDW and BBBW. In this regard, the Barents Sea halocline branch upstream in the Canada Basin does not show an analogous signal of denitrification in the dissolved NO_3^- pool (*Granger et al.*, 2018). While significant denitrification associated with water column particles has been observed in ODZs (*Ganesh et al.*, 2015), we deem this scenario unlikely in deep Baffin Bay, given the relatively elevated O_2 concentration in the deep basin, as well as the decreasing size of particles with depth, likely resulting in a diffusive O_2 flux to particles that exceeds the associated oxidant demand (*Bianchi et al.*, 2018). If the denitrification signal (e.g., N* minimum and ^{15}N-enrichment) originates from brine-enriched waters accumulating at the bottom of the shelf in Nares Strait, this signal would need to be significantly higher than the signal we see in deep Baffin Bay to withstand dilution and mixing during its slow descent towards the bottom (*Bourke and Paquette*, 1991). Moreover, assuming that Nares Strait water feeds into intermediate and deep/bottom waters of Baffin Bay (*Rudels*, 1986), we would expect a signal of DIN removal and elevated $\delta^{15}N_{NO3}$ and AOU to be evident in intermediate waters. While the lower residence time of Baffin Bay intermediate waters plus an additional inflow of Atlantic water at $\sim$ 300 m from the south could potentially dilute such a signal in the upper water column, it does not explain the more pronounced signal towards the bottom of Baffin Bay. As such, the prevalent decrease of N* with depth in light of increasing nutrient concentration strongly suggests that the distinct negative N* incurred largely in the deep basin. In that sense, the relatively isolated deeper portion of Baffin Bay and the resultant limited horizontal advection of nutrients, complemented by the comparably low NO_3^- in the Barents Sea source water, argues for the predominantly local regeneration of NO_3^- as the main source for benthic denitrification, further supported by the N and O isotope ratios of dissolved NO_3^- isotopes.

3.5 Summary and concluding remarks

Tracer profiles presented here provide insights into the origins and cycling of reactive nitrogen in Baffin Bay, while highlighting the connectivity between different Arctic systems and horizontal components of large-scale nutrient transport. Baffin Bay provides a link between the higher Arctic and the North Atlantic. The enclosed nature of the deep basin and thus long residence time of deep and bottom waters enable a pronounced accumulation of Pacific-origin nutrients along with a drawdown of O_2 and supersaturation in N_2O. Bottom water properties are thus predominantly driven by export production in northern Baffin Bay and the highly productive North Water region which is largely fueled by Pacific-derived nutrients. Substantial in situ remineralization supports denitrification in the sediment, evident by a pronounced accumulation of N_2O with a prominent sedimentary isotope signature in well-oxygenated BBDW and BBBW. Nutrients supplied to the NOW hence are removed from surface waters and trapped in deep Baffin Bay over potentially long timescales.

Primary production in the NOW polynya is largely driven by nutrients supplied vertically from the halocline layer (*Tremblay et al.*, 2002) such that any changes in source water properties and/or vertical mixing will potentially affect the extent of production and subsequent export into the deep basin. Given that the upper boundary yield of primary production and export is set by new nutrients supplied to the surface (*Tremblay et al.*, 2015), enhanced productivity over the shallow western Arctic shelf (*Arrigo and van Dijken*, 2011) where Pacific-derived waters and nutrients therein ventilate the Arctic upper halocline (*Brown et al.*, 2015a; *Granger et al.*, 2018) has the potential to reduce production and subsequent export in northern Baffin Bay. Moreover, prolonged open water conditions upstream of Baffin Bay along the transect north of and through the Archipelago may further strip nutrients from the UHL, given predicted ice retreat and augmented vertical mixing in areas currently shielded by ice cover. Increased vertical stratification (*Bergeron and Tremblay*, 2014) and recent decline in the overall bloom amplitude (*Marchese et al.*, 2017) in the NOW polynya may further affect nutrient and carbon export and subsequently impede remineralization and storage at depth, which may further translate into a reduction in denitrification and N_2O flux from deep Baffin Bay. Ultimately, this study shows that the Baffin Bay's potential to store carbon and nutrients over prolonged timescales is largely determined by the productivity of the northern basin and complex processes affecting

nutrient drawdown further upstream in the higher Arctic.

CHAPTER 4

NITRATE ISOTOPE DISTRIBUTIONS ALONG THE CANADIAN ARCTIC GEOTRACES TRANSECT: IMPLICATIONS FOR HIGH LATITUDE N CYCLING

4.1 Abstract

The Canadian Arctic Ocean plays a key role in the marine nitrogen cycle. It provides a connection between the North Pacific, which hosts regions of denitrifcation, and the North Atlantic, an area of extensive N_2 fixation. Water column measurements of nitrogen (N) and oxygen (O) isotope ratios of nitrate ($\delta^{15}N_{NO3}$ and $\delta^{18}O_{NO3}$) collected during the Canadian Arctic GEOTRACES expedition in 2015 throughout the Canadian Archipelago shed light on both the origin and internal cycling of NO_3^- in the Canadian Arctic.

NO_3^- isotope values in the Canada Basin and western Archipelago show a relative enrichment in ^{15}N and a coincident minimum in $\delta^{18}O$ associated with the nutrient-rich Pacific Winter Water (PWW) in the upper halocline layer. Together with a pronounced N deficit, these isotope ratios are indicative of both benthic denitrification upstream on the Bering and Chukchi shelves and remineralization along the transit. A largely preserved subsurface peak in $\delta^{15}N_{NO3}$ and a minimum in $\delta^{18}O_{NO3}$ west of Barrow Strait suggest little biogeochemical and physical modifications of PWW in the western Archipelago. These observations contrast with more turbulent conditions east of Barrow Strait that lead to a modest decrease in $\delta^{15}N_{NO3}$ and increase in $\delta^{18}O_{NO3}$ towards Baffin Bay - consistent with

the mixing of PWW and underlying Atlantic-derived waters in the eastern Archipelago. Underlying Atlantic-derived waters, entering the Archipelago from both the Canada Basin in the west and Baffin Bay in the east show evidence of the remineralization of organic matter enriched in ^{15}N, indicative of a predominant Pacific-derived nutrient source.

4.2 Introduction

The Arctic Ocean is hydrographically complex, with substantial regional and seasonal variability. Waters in the Arctic Ocean are of both Atlantic and Pacific origin, with Atlantic waters entering the Arctic from the east through the Barents Sea and Fram Strait while Pacific waters propagate through the Bering Strait in the west (e.g., *Aagaard et al.*, 1981; *Coachman and Barnes*, 1961; *Rudels et al.*, 1994). Differences in the hydrographic properties of those source waters result in a distinct layering of the water column, where relatively fresh waters, consisting of river discharge, ice melt, precipitation and Pacific water, overlay warm and more saline Atlantic water. The strength of this salinity-driven stratification varies regionally, depending on both the relative contribution of individual water masses as well as modifications by river input, the formation and melting of sea ice and shelf interactions along the transit through the Arctic. Particularly shallow continental shelves, making up about 50% of the area of Arctic Ocean, have been shown to be able to modify the physical as well as biogeochemical properties of those waters as they circulate through the Arctic. Prior studies have focused on the western Arctic shelf area, where nutrient-rich Pacific water transits across the wide Bering and Chukchi shelves ($<$ 200 m) and fuel high seasonal productivity in the water column and denitrification in the sediment (e.g., *Brown et al.*, 2015a; *Chang and Devol*, 2009; *Devol et al.*, 1997; *Granger et al.*, 2011; *Tanaka et al.*, 2004). By subsequently ventilating the upper halocline layer of the western Arctic, this relatively fresh and nutrient-enriched Pacific water exerts a profound impact on the Arctic Ocean not only by acting as a density barrier restraining the heat transfer from the warm and dense Atlantic water towards the surface (e.g., *Aagaard et al.*, 1981), but further by fueling Arctic productivity downstream in areas where this subsurface nutrient pool becomes accessible to surface and subsurface primary producers (e.g., *Codispoti et al.*, 2013; *Cota et al.*, 1987; *Michel et al.*, 2006; *Tremblay et al.*, 2002, 2006).

Little is known about the prevalence and biogeochemical modification of these nutrient-rich Pacific-derived waters within the Canadian Arctic Archipelago (CAA) further downstream of the western Arctic shelves and the Canada Basin. The CAA encompasses the vast and complex Arctic continental shelf area bordered by the Beaufort Sea in the west, the Arctic Ocean in the north and Baffin Bay in the east (Figure 4.1), and makes up $\sim 20\%$ of the total shelf area in the Arctic (*Carmack et al.*, 2006). Numerous channels between the collection of islands that shape the CAA allow the propagation of Arctic water eastward towards the Labrador Sea. At the same time, the shallow bathymetry ($\geq$ 125 m) of the CAA prevents intermediate and deep water flow towards the Atlantic (*Melling et al.*, 1984; *Prinsenberg and Bennett*, 1987). Thus, while Fram Strait provides the only throughflow for intermediate and deep water to circulate back to the North Atlantic, both Fram Strait and the CAA serve as dominant pathways for the outflow of Pacific water to the Labrador Sea and the wider North Atlantic (*Azetsu-Scott et al.*, 2012; *Jones*, 2003; *Jones and Coote*, 1980; *Yamamoto-Kawai et al.*, 2006). The overall oceanography of the region shows strong annual/interannual fluctuations in freshwater input and ice cover, which affects light penetration, stratification, nutrient supply and ultimately productivity. To date, only a few studies have focused on the spatial and temporal variability of nutrients in that region and their impact on primary production, emphasizing the importance of both remineralization in the euphotic zone versus upwelling of halocline nutrients from the Pacific layer as a means to modulate surface production (*Codispoti et al.*, 2013; *Cota et al.*, 1987; *Martin et al.*, 2010; *Michel et al.*, 2006; *Tremblay et al.*, 2008, 2015).

Previous studies focusing on the hydrography and tracer distribution in the western and central Canadian Arctic have identified waters of Pacific origin based on the characteristic surplus of silicic acid ($Si(OH)_4$) and a concurrent deficit in nitrate (NO_3^-) over phosphate (PO_4^{3-}; *Codispoti et al.*, 2005; *Ekwurzel et al.*, 2001; *Jones et al.*, 1998; *Reeve et al.*, 2019; *Yamamoto-Kawai et al.*, 2008). This characteristic nutrient signature is imparted onto Pacific-derived waters as a consequence of denitrification in the Pacific Ocean (*Lehmann et al.*, 2005, 2007) and en route towards the Canada Arctic on the extensive Bering, Chukchi and East Siberian shelf (*Brown et al.*, 2015a; *Chang and Devol*, 2009; *Devol et al.*, 1997; *Fripiat et al.*, 2018; *Granger et al.*, 2011; *Tanaka et al.*, 2004), which results in the reduction of NO_3^- to N_2 and, as such, the removal of fixed nitrogen (N) relative to other

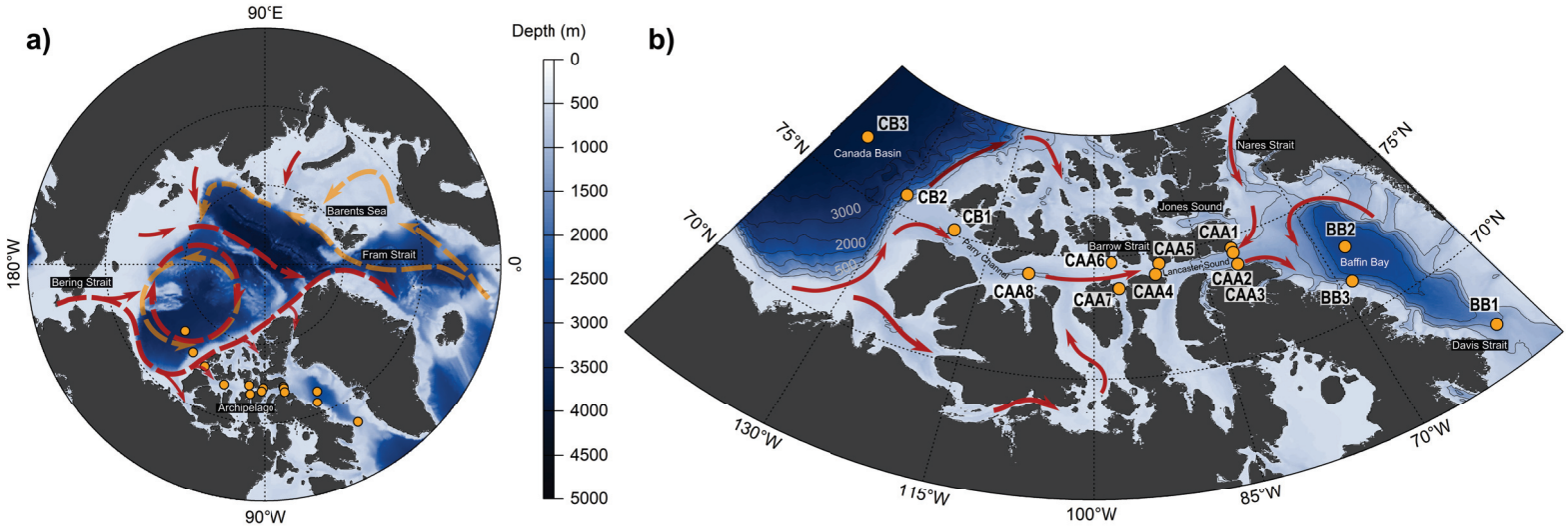

Figure 4.1: Maps showing the surface/subsurface (red) and intermediate (orange) circulation in the (a) central Arctic and (b) the Canadian Arctic Archipelago (after *Aagaard et al.*, 1981; *McLaughlin et al.*, 2004; *Rudels et al.*, 1994). (a) highlights the inflow of Pacific water through Bering Strait versus Atlantic water inflow through both Barents Sea and Fram Strait and illustrates the largescale circulation in the Beaufort Sea, characterized by the clockwise gyre movement at the surface and reversed counter-clockwise flow at the subsurface (Beaufort Undercurrent; *Carmack and McLaughlin*, 2011). (b) In the CAA, water consists of Canada Basin water entering via numerous straits along the Queen Elisabeth Islands, the Amundsen Gulf and the M'Clure Strait, as well as Makarov and Lincoln Sea water entering through Nares Strait (*McLaughlin et al.*, 2004). Orange dots indicate sampling sites during the 2015 GEOTRACES campaign (stations BB1-BB3 were discussed in the previous chapter (*Lehmann et al.*, 2019)). Specific areas covered are the central Canada Basin (CB3), M'Clure Strait (CB1), Viscount Melville Sound (CAA8), Barrow Strait (CAA6) and Lancaster Sound (CAA1, CAA2, CAA3).

nutrients. Thus, nutrient ratios provide a robust tool to distinguish Pacific- from Atlantic-influenced waters in the Arctic, especially in more remote areas (e.g., eastern Canadian Arctic/Lancaster Sound; *Jones*, 2003) where any distinction based on temperature and salinity data reaches its limitations. One limitation associated with the use of nutrient stoichiometric tracers such as N* (where N* = $[NO_3^-] - 16 \times [PO_4^{3-}] + 2.9$; *Deutsch et al.*, 2001; *Gruber and Sarmiento*, 1997) as both water mass tracer and to estimate sources and sinks of bioavailable N arises from the alteration of those values due to potential stoichiometric deviations during remineralization and/or assimilation. Moreover, nutrient ratios do not account for overlapping input and removal processes that have the potential to erase one another. In this respect, using N* measurements as a tracer for Pacific-derived waters in the Arctic is subject to some uncertainty due to the potential occurrence of local sedimentary denitrification downstream to the Pacific water inflow (e.g., *Alkire et al.*, 2019; *Bauch et al.*, 2011).

Coupled measurements of $^{15}N/^{14}N$ and $^{18}O/^{16}O$ ratios of NO_3^- (expressed as $\delta^{15}N_{NO3}$ and $\delta^{18}O_{NO3}$) can address those shortcomings due to their complementary sensitivity to individual processes affecting the marine N cycle. The uptake of NO_3^- due to both phytoplankton assimilation at the sea surface and denitrification (i.e., the reduction of NO_3^- to N_2) at the subsurface result in a coincident increase in the N and O isotope ratio of the unconsumed NO_3^- along a characteristic 1:1 ratio (*Casciotti et al.*, 2002; *Granger et al.*, 2004, 2008; *Sigman et al.*, 2005). In turn, the remineralization of organic material at the subsurface, namely, the ammonification of organic nitrogen followed by nitrification (i.e., the oxidation of NH_4^+ to nitrite (NO_2^-) and NO_3^-), produces NO_3^- with a $\delta^{15}N$ akin to that of the remineralized material, thus reflecting the $\delta^{15}N$ of material exported from the sea surface. In contrast, the $\delta^{18}O$ of newly nitrified NO_3^- is independent of its source substrate but rather approaches the isotope signature of ambient water (*Buchwald and Casciotti*, 2010; *Casciotti et al.*, 2002; *Sigman et al.*, 2005). Given their differential sensitivities to respective biogeochemical transformations, the coupled N and O isotope ratios of NO_3^- provide an integrative tool to study coincident processes within the N cycle.

To date, the use of N and O isotope measurements to infer NO_3^- cycling and N transformation processes in the Arctic Ocean has been limited and mostly restricted to the western part of the Arctic ecosystem (*Brown et al.*, 2015a; *Fripiat et al.*, 2018; *Granger et al.*, 2011, 2013, 2018; *Lehmann et al.*, 2005, 2007). These studies revealed a pronounced

relative enrichment in ^{15}N and a coinciding minimum in $\delta^{18}O$ associated with the dissolved NO_3^- pool in Pacific-derived waters in the western Arctic. While sedimentary denitrification results in a negligible imprint of isotopic fractionation to the overlying water column (*Brandes and Devol*, 1997; *Lehmann et al.*, 2005, 2007), it has been shown that coupled nitrification-denitrification in the sediment of the western Arctic continental shelves prompts the efflux of ^{15}N-enriched NH_4^+ (*Brown et al.*, 2015a; *Granger et al.*, 2011). Subsequent water column nitrification introduces this high-^{15}N signature into the dissolved NO_3^- pool, while concurrently providing isotopically light $\delta^{18}O_{NO3}$ (*Brown et al.*, 2015a; *Fripiat et al.*, 2018; *Granger et al.*, 2011, 2018). The isotopic evolution of NO_3^- across the Canadian Archipelago, connecting the western Canadian Arctic with the eastern Arctic Baffin Bay and Labrador Sea, however, remains elusive. Here, we combine basic hydrographic variables, oxygen concentrations and nutrient ratios with first measurements of naturally occurring stable isotope ratios of NO_3^- throughout the Canadian Archipelago to elucidate (1) the distribution of prevalent water masses in the CAA, (2) biogeochemical modifications of those waters due to both mixing and biological production, and (3) potential input and removal processes of nutrients along the flow path. Moreover, the comparison to previous studies of NO_3^- N and O isotopes at both ends of the transect (*Brown et al.*, 2015a; *Granger et al.*, 2011, 2018; *Lehmann et al.*, 2019) will provide a distinction between local processes imparted on the isotopic composition of NO_3^- and advection and mixing signals, which is crucial to better understand marine biogeochemical cycling in the Arctic Ocean.

4.3 Materials and Methods

Hydrographic data and seawater samples were collected as part of the Canadian Arctic GEOTRACES effort in 2015 (July – September) aboard the *CCGS Amundsen* during two consecutive legs (GN02 and GN03), at hydrographic stations spanning from 56°N and 53°W in the Labrador Sea to 78°N and 150°W in the Canada Basin. Hydrographic data were obtained using a conductivity-temperature-depth profiler (CTD; Sea-Bird SBE-9plus), equipped with an oxygen sensor (Sea-Bird SBE-43), a chlorophyll fluorometer (Seapoint), a transmissometer (WET Labs C-Star), and a PAR sensor (Biosperical/LI-COR). The conductivity probe was calibrated against discrete salinity samples analyzed on a GuideLine Autosal 8400B. The oxygen sensor was calibrated with direct measurements

of dissolved oxygen concentrations in seawater samples analyzed by Winkler titration (*Carpenter*, 1965).

Discrete seawater samples were collected throughout the water column using a rosette water sampler equipped with 24 x 12 L Niskin bottles mounted to the CTD. Concentrations of NO_3^-, nitrite (NO_2^-), PO_4^{3-} and $Si(OH)_4$ were measured onboard using an automated nutrient analyzer (Bran+Luebbe Autoanalyzer 3). Ammonium (NH_4^+) concentrations were determined by fluorometry according to the method of *Holmes et al.* (1999). The surplus or deficit of dissolved inorganic nitrogen (DIN; NO_3^-, NO_2^-, NH_4^+) relative to PO_4^{3-} was evaluated according to *Gruber and Sarmiento* (1997) and *Deutsch et al.* (2001), where N* = [DIN] - 16 x [PO_4^{3-}] + 2.9, assuming Redfield remineralization stoichiometry. To further quantify the fraction of regenerated relative to total nutrients, we determine the apparent oxygen utilization (AOU; *Broecker and Peng*, 1982), where AOU = $[O_2]_{\text{saturation}}$ - $[O_2]_{\text{measured}}$. The saturation concentration of O_2 was derived using in situ oxygen, temperature and salinity values (*Garcia and Gordon*, 1992).

For NO_3^- isotope analyses, seawater from $>$ 200 m depth was collected directly from the Niskin bottles into pre-rinsed 60 mL high-density polyethylene bottles, without filtration. Seawater from $<$ 200 m depth was filtered through a 0.45-μm pore-size surfactant-free cellulose acetate membrane prior to the collection into 60 mL bottles. The samples were stored frozen at -20°C until further analyses. Measurements of dual N and O isotope ratios ($^{15}N/^{14}N$ and $^{18}O/^{16}O$) in NO_3^- were performed at the University of Connecticut using the denitrifier method (*Casciotti et al.*, 2002; *Sigman et al.*, 2001). This method uses cultured denitrifying bacteria (*Pseudomonas chlororaphis* f. sp. *aureofaciens*, ATCC# 13985) that lack the terminal N_2O reductase, which allows the quantitative conversion of NO_3^- in a sample into a N_2O gas analyte. The product N_2O was extracted, concentrated and purified using a custom-built Thermo Gas Bench II equipped with a GC Pal auto-sampler and dual cold traps and analyzed on a Thermo Delta V Advantage continuous flow isotope ratio mass spectrometer (*Casciotti et al.*, 2002; *McIlvin and Casciotti*, 2011). Isotope ratios are expressed in units of per mil (‰) and reported using the delta (δ) notation:

$$\delta^{15}N_{sample} = [(^{15}N/^{14}N)_{sample}/(^{15}N/^{14}N)_{reference} - 1] \times 1000 \quad (4.1)$$

$$\delta^{18}O_{sample} = [(^{18}O/^{16}O)_{sample}/(^{18}O/^{16}O)_{reference} - 1] \times 1000 \quad (4.2)$$

Samples were referenced to air for δ^{15}N and to Vienna Standard Mean Ocean Water (VSMOW) for δ^{18}O, and standardized using the seawater-based reference material IAEA-N3 (4.7‰ and 25.6‰ for δ^{15}N and δ^{18}O) and USGS-34 (-1.8‰ and -27.9‰ for δ^{15}N and δ^{18}O; *Böhlke et al.*, 2003; *Gonfiantini*, 1984). To account for potential matrix effects on $\delta^{18}O_{NO3}$ measurements, NO_3^- concentrations in the standard material were adjusted by diluting with NO_3^--free seawater to bracket NO_3^- concentrations in our seawater samples (*Weigand et al.*, 2016). Where NO_2^- was present, it was removed prior to isotope analyses by adding sulfamic acid to avoid any interference with NO_3^- (*Granger and Sigman*, 2009). Replicate measurements (n $\geq$ 3) of all samples yield an average analytical precision ($\pm$1 SD) of 0.2‰ for δ^{15}N and of 0.3‰ for δ^{18}O, respectively.

To identify any influence of nitrification processes and to quantify the deviation from the 1:1 fractionation relationship associated with NO_3^- assimilation, we define Δ(15-18) according to *Rafter et al.* (2013):

$$\Delta(15-18) = \delta^{15}\mathrm{N} - ({}^{15}\varepsilon/{}^{18}\varepsilon) \times \delta^{18}\mathrm{O} \tag{4.3}$$

where δ^{15}N and δ^{18}O are the isotopic composition of NO_3^- measured in a sample and ${}^{15}\epsilon/{}^{18}\epsilon$ is the N-to-O isotope effect ratio for NO_3^- assimilation, which according to *Granger et al.* (2004) equals 1.

4.4 Results

4.4.1 Hydrographic properties

4.4.1.1 Central Canada Basin

Temperature and salinity measurements reveal a characteristic layering of the water column in the central Canada Basin (Station CB3; Figure 4.2). Surface waters are relatively cold (-1.3°C) and fresh (S $\geq$ 26.7) due to a seasonal signal of sea ice melt and the accumulation of river water in the Beaufort Gyre (e.g., *Macdonald et al.*, 1999; *Yamamoto-Kawai et al.*, 2009). Below the influence of winter mixing ($\sim$ 40 m), salinity increases progressively with depth, characteristic for the Arctic halocline layer (Figure 4.2). Therein, the relatively warm ($\leq$ -0.1°C) upper layer with its core at $\sim$ 60 m (σ_θ: $\sim$ 24.9) designates Pacific Summer Water (PSW; *Steele et al.*, 2004). The shallow depth of the temperature maximum and the associated low salinity ($\sim$ 31.1) suggests that the PSW originates from the Alaskan

coast (as Alaskan Coastal Water), entering the Canada Basin from Barrow Canyon on the eastern Chukchi Shelf (*Coachman et al.*, 1975; *Timmermans et al.*, 2014). A prominent temperature maximum slightly deeper in the water column ($\sim$ 120 m), generally observed in the Canada Basin and representative of summer Bering Sea Water (sBSW; e.g., *Steele et al.*, 2004), is notably absent here, in agreement with recent findings reporting the absence of sBWS in the central Canada Basin in recent years (*Timmermans et al.*, 2014). Below PSW, temperatures decrease to a minimum ($\geq$ -1.44°C) at $\sim$180 m, indicating the presence of Pacific Winter Water (PWW) centered at a salinity of 33.1 (σ_θ: $\sim$ 26.6; Figure 4.2; *Coachman and Barnes*, 1961). PWW is formed in the Chukchi Sea winter mixed layer as a result of cooling and brine rejection during seasonal ice formation, followed by the lateral intrusion into the Canada Basin upper halocline layer down to depth of neutral buoyancy (e.g., *Aagaard et al.*, 1981).

Below the Pacific-influenced upper halocline layer (UHL), both the lower halocline layer (LHL) and the intermediate layer of the Canada Basin are comprised of Atlantic-derived waters. Atlantic waters originating from the Barents Sea (AW_{BS}) in the eastern Arctic (*Jones and Anderson*, 1986) are centered at $\sim$ 220-250 m and a salinity of 34.1 (σ_θ: $\sim$ 27.4) underlying PWW. A prominent temperature maximum ($\leq$ 0.8°C) centered at $\sim$ 480 m (σ_θ: $\sim$ 27.9) underlying the Barents Sea branch is consistence with the presence of Atlantic Water entering the Arctic at Fram Strait (AW_{FS}; *Coachman and Barnes*, 1961; *Jones et al.*, 1998; *Rudels et al.*, 1996).

4.4.1.2 Western Canadian Archipelago

Shelf stations CB2 and CB1 show a hydrographic structure analogous to the water column of the central basin, albeit with evident shoaling of surface, halocline and intermediate Atlantic waters inshore (eastward; Figure 4.2). The surface mixed layer progressively shoals from M'Clure Strait (CB1; $\sim$ 12 m) into Viscount Melville Sound (CAA8; $<$ 8 m). Surface waters become more saline and warmer towards the shelf, with evidently limited input of sea ice melt (and freshwater) to the surface layer, in contrast to the central basin (Figure 4.2a and b). The temperature maximum of PSW is colder (-0.3°C) and shallower (54 m) at shelf stations (CB2 and CB1), and is largely absent at the adjacent western CAA stations (Figure 4.2b). The temperature minimum of PWW shoals inshore from $\sim$ 150 m at CB2 to $\sim$ 90 m at CAA8, while becoming concurrently warmer ($>$ -1.38°C). Correspondingly, the AW_{FS} temperature maximum shoals towards the shelf break, from

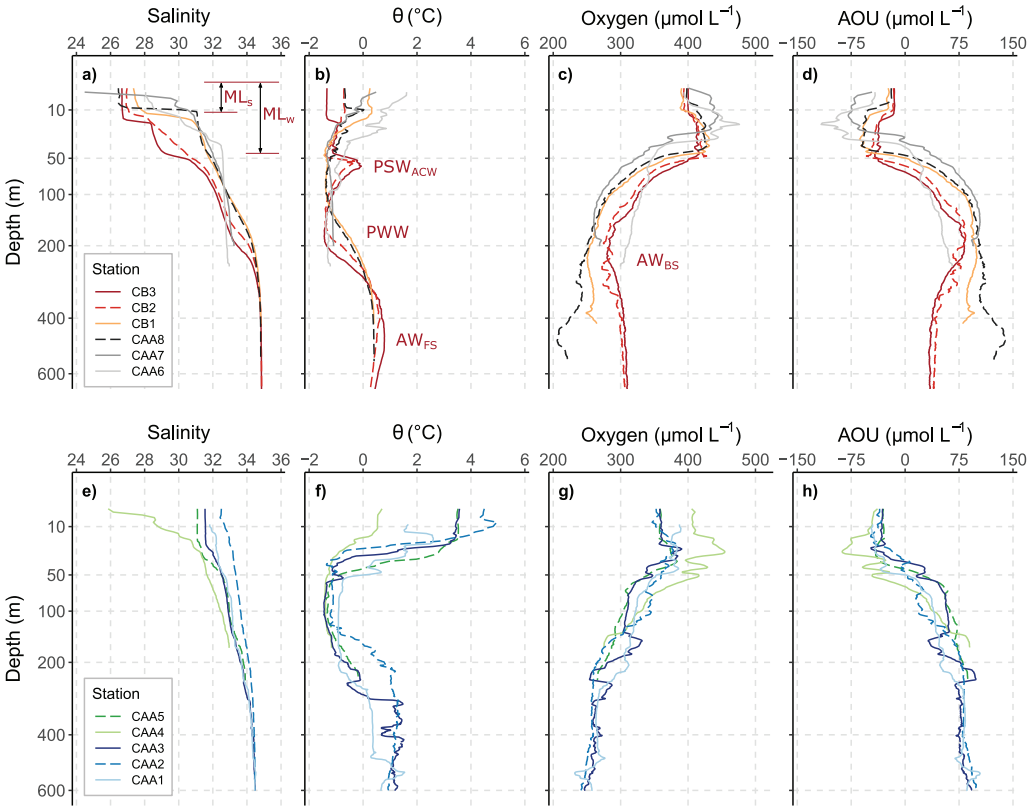

Figure 4.2: Water column profiles of (a, e) salinity, (b, f) potential temperature, (c, g) oxygen and (d, h) AOU at stations in the western CAA and Barrow Strait (top panels) and in the eastern CAA (bottom panels). Water masses defined in the central Canada Basin are highlighted in red (top panels). Abbreviations indicate apparent oxygen utilization (AOU), the summer and winter mixed layer (ML_S and ML_W), Pacific Summer Water originating from Alaskan Coastal waters (PSW_{ACW}), Pacific Winter Water (PWW) and Atlantic waters originating from the Barents Sea (AW_{BS}) and Fram Strait (AW_{FS}).

$\sim$ 480 m in the central basin to $\sim$ 410 m at CB1, followed by an increase in depth to $\sim$ 560 m in the western CAA (CAA8). Simultaneously, core AW_{FS} waters become colder in M'Clure Strait and Viscount Melville Sound ($\leq$ 0.4°C at CAA8). Concordant with the sill depth of $\sim$ 375 m at the western entrance of M'Clure Strait, AW_{FS} waters are the densest waters entering the CAA from the Canada Basin to the west (Figure 4.2).

4.4.1.3 Central Canadian Archipelago

In the central CAA, a shallow $\sim$ 125 m sill at Barrow Strait causes enhanced mixing of subsurface waters, while preventing the intrusion of AW_{FS} into the eastern CAA and further into Baffin Bay (Figure 4.2b; *Hughes et al.*, 2017; *Melling et al.*, 1984; *Prinsenberg and Bennett*, 1987). Accordingly, temperature at CAA6 decreases from the surface maximum of 1.6°C to -0.6°C at 40 m, followed by a relatively muted decrease to a minimum of -1.4°C at $\sim$ 150 m and a slight subsequent increase at the bottom (-1.2°C at 250 m). Concurrently, salinity increases from 28.1 at the surface to 32.5 at $\sim$ 40 m and 32.9 at $\sim$ 250 m (Figure 4.2). CAA7 to the south of CAA6 shows a decrease in temperature from a surface maximum of 0.5°C to a relatively shallow minimum of -1.3°C at 46 m, followed by an increase to -1.1°C at $\sim$ 200 m. Salinity at CAA7 increases continuously from 24.5 at the surface to 32.0 at the temperature minimum and 33.2 at depth ($\sim$ 200 m).

4.4.1.4 Eastern Canadian Archipelago

Hydrographic stations in eastern Lancaster Sound (CAA1-3) indicate some distinct variability in water column properties between the northern and southern sound. The general circulation in Lancaster Sound is dominated by an eastward flux of Arctic waters at the southern shore towards Baffin Bay and westward counter-currents at the northern side bringing waters from Baffin Bay into the sound (*Prinsenberg and Bennett*, 1987).

Accordingly, hydrographic profiles in southern Lancaster Sound (CAA3) show a distinct vertical zonation, roughly analogous to the central Canada Basin and western CAA (Figure 4.2). Surface waters are warmer ($\geq$ 1.5°C) and more saline ($\geq$ 31.5) than west of Barrow Strait. The subsurface temperature minimum (-1.5°C) in the upper halocline is less saline (32.9) and shallower in the water column (centered at $\sim$ 90 m; σ_θ: $\sim$ 26.4) than at the western end of the transect. Below this UHL minimum, temperature increases to a pronounced maximum of $\leq$ 1.5°C centered at 420 m (σ_θ: $\sim$ 27.5; Figure 4.2f). This temperature maximum is warmer and more saline ($\sim$ 34.4) than AW_{FS} in the central

Canada Basin and western CAA, consistent with Atlantic water entering the study area from the east rather than from the Canada Basin (*Prinsenberg and Hamilton*, 2005). This Atlantic end-member originates in the Irminger Sea, enters Baffin Bay through Davis Strait and propagates north via the West Greenland Current (*Azetsu-Scott et al.*, 2012; *Hamilton and Wu*, 2013; *Münchow et al.*, 2015; *Tang et al.*, 2004).

In northern Lancaster Sound (CAA1-2), the UHL temperature minimum is warmer ($\geq$ -1.4°C at CAA2 and $\geq$ -0.9°C at CAA1) and more saline ($\geq$ 33.2 at CAA2 and $\geq$ 33.1 at CAA1) in comparison to the southern station (CAA3). Temperature values associated with the underlying AW temperature maximum are comparable among stations in eastern Lancaster Sound, albeit the vertical extent of the maximum shows some variability, with a general broader extent at CAA2 contrasting a relatively restricted peak at CAA1 (Figure 4.2).

4.4.2 Nutrient concentrations and isotope ratios

4.4.2.1 Central Canada Basin

In the central Canada Basin (CB3), NO_3^- is below detection from the surface to the base of the winter mixed layer ($\sim$ 40 m), whereas PO_4^{3-} and $Si(OH)_4$ concentrations are $\leq$ 0.6 μmol L^{-1} and $\leq$ 2.8 μmol L^{-1}, respectively (Figure 4.3a-c). The excess in PO_4^{3-} over NO_3^- translates into a negative N* value (-5.1 μmol L^{-1}) at the surface (Figure 4.3d). Below the remnant of winter mixing, nutrient concentrations progressively increase to peak values at $\sim$ 180 m in core PWW (e.g., *Coachman and Barnes*, 1961; *Cooper et al.*, 1997; *Jones and Anderson*, 1986; *McLaughlin et al.*, 1996; *Reeve et al.*, 2019), reaching 15.8 μmol L^{-1}, 1.8 μmol L^{-1} and 36.6 μmol L^{-1} for NO_3^-, PO_4^{3-} and $Si(OH)_4$, respectively. Concurrently, a pronounced deficit in DIN relative to PO_4^{3-} is evident as a prominent N* minimum (-10.5 μmol L^{-1}) at the depth of PWW (Figure 4.3d). [O_2] progressively decreases from a subsurface maximum of $\sim$ 416 μmol L^{-1} at the bottom of the winter mixed layer to characteristically low concentrations in PWW (*Jones and Anderson*, 1986), reaching $\sim$ 288 μmol L^{-1} at the temperature minimum (Figure 4.2c). Accordingly, AOU increases from a subsurface minimum ($\sim$ -42 μmol L^{-1}) at $\sim$ 40 m to a maximum ($\sim$ 84 μmol L^{-1}) in PWW (Figure 4.2d).

Below the upper halocline, both [NO_3^-] and [O_2] decrease to slight minima (11.9 μmol L^{-1} for NO_3^- and $\sim$ 280 μmol L^{-1} for O_2) in AW_{BS} at $\sim$ 220-250 m. These relatively low NO_3^- concentrations and the concurrent O_2 minimum in the lower halocline result in a

prominent minimum in NO (394 μmol L^{-1}, where NO = 9 $\times[NO_3^-]+[O_2]$; *Broecker*, 1974) characteristic of AW_{BS} (Figure 4.4d; *Jones and Anderson*, 1986). $[NO_3^-]$ subsequently increases to 12.4 μmol L^{-1} at the AW_{FS} temperature maximum. $[PO_4^{3-}]$ and $[Si(OH)_4]$ show a concurrent decrease below PWW, reaching minimum values (0.8 μmol L^{-1} and 6.2 μmol L^{-1}) in the core of AW_{FS} ($\sim$ 480 m; σ_θ: $\sim$ 27.9), followed by increasing concentrations with depth. N* increases below the minimum in PWW to slightly positive values in the lower halocline ($\sim$ 0.2 μmol L^{-1}) and underlying AW_{FS} (2.8 μmol L^{-1}; Figure 4.3b). $[O_2]$ increases from the minimum in AW_{BS} to $\sim$ 305 μmol L^{-1} at the core of the AW_{FS} temperature maximum. AOU slightly decreases from the PWW maximum ($\sim$ 84 μmol L^{-1}) to $\sim$ 79 μmol L^{-1} in AW_{BS}, followed by a more pronounced decrease to $\sim$ 35 μmol L^{-1} in AW_{FS} (Figure 4.2d).

Depth distributions of NO_3^- isotope ratios in the central basin (CB3) are analogous to those described previously at the more southern Canada Basin stations in the southeastern Beaufort Sea (*Granger et al.*, 2018). Values of $\delta^{15}N_{NO3}$ are relatively constant at $\sim$ 7.9‰ from the base of PSW ($\sim$ 75 m) to the PWW temperature minimum ($\sim$ 180 m; Figure 4.5a). Conversely, $\delta^{18}O_{NO3}$ increases from a minimum of -0.2 $\pm$ 0.1‰ at 100 m to $\sim$0.5‰ in the core of PWW (Figure 4.5b). Above 100 m, both $\delta^{15}N_{NO3}$ and $\delta^{18}O_{NO3}$ increase with decreasing $[NO_3^-]$ to $\sim$ 40 m (where NO_3^- is no longer detected), consistent with isotope fractionation from partial NO_3^- assimilation. However, a decrease in Δ(15-18) from PWW (8.0‰ at 120 m) towards the base of the winter mixed layer (7.2‰ at $\sim$ 60 m; Figure 4.4h) indicates a proportionally greater increase in $\delta^{18}O_{NO3}$ than $\delta^{15}N_{NO3}$, contrary to expectations of equivalent N and O isotope fractionation during its assimilation (*Casciotti et al.*, 2002; *Granger et al.*, 2004).

Below the UHL, $\delta^{15}N_{NO3}$ progressively decreases to 6.1 $\pm$ 0.1‰ in AW_{BS}, and to 5.2 $\pm$ 0.1‰ in AW_{FS} below. In contrast, $\delta^{18}O_{NO3}$ values increase from the local minimum in PWW to 0.7 $\pm$ 0.2‰ in AW_{BS} and to 1.6 $\pm$ 0.1‰ in AW_{FS}. The divergent trends in $\delta^{15}N_{NO3}$ and $\delta^{18}O_{NO3}$ translate into a gradual decrease in Δ(15-18) from values of 7.4‰ in core PWW to 3.6‰ at the AW_{FS} temperature maximum. Concurrently, $\delta^{18}O_{H2O}$ ratios, which influence the $\delta^{18}O$ of remineralized NO_3^-, progressively increase with depth, from $\sim$ -3.6‰ in the surface layer to -1.4‰ in PWW and 0.2‰ in AW_{FS} (Figure 4.5c).

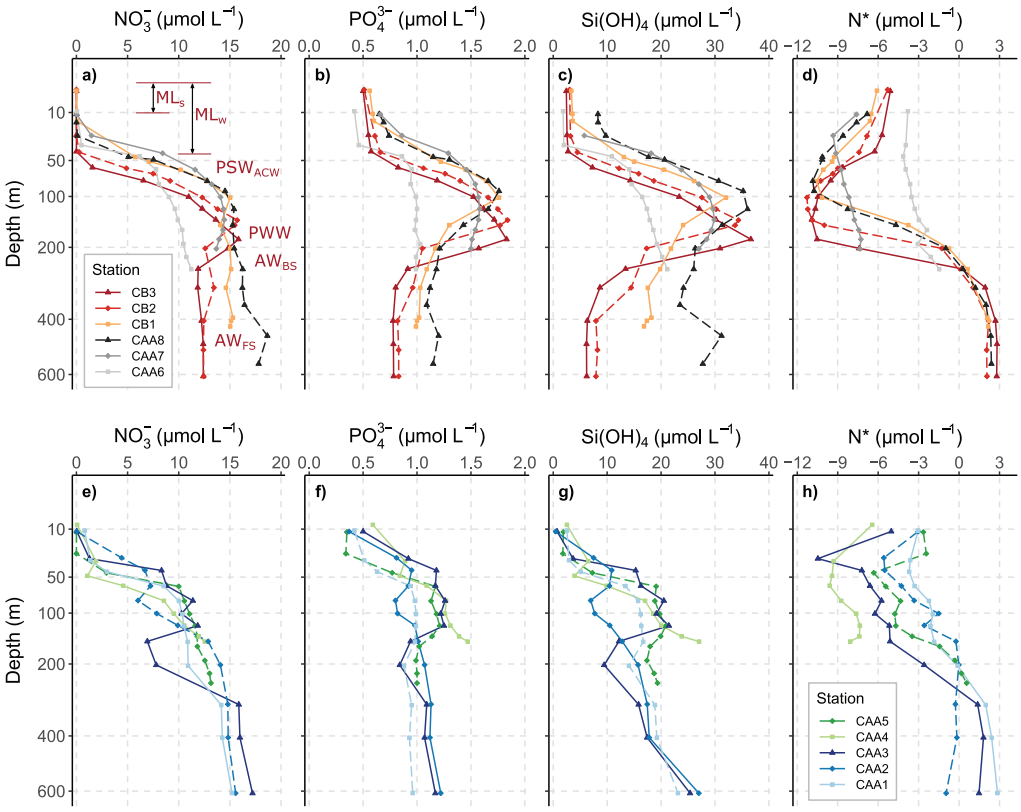

Figure 4.3: Water column profiles of (a, e) NO_3^-, (b, f) PO_4^{3-}, (c, g) $Si(OH)_4$ and (d, h) N* at stations in the western CAA and Barrow Strait (top panels) and in the eastern CAA (bottom panels). Water masses defined in the central Canada Basin are highlighted in red (top panels). Abbreviations indicate the summer and winter mixed layer (ML_S and ML_W), Pacific Summer Water originating from Alaskan Coastal waters (PSW_{ACW}), Pacific Winter Water (PWW) and Atlantic waters originating from the Barents Sea (AW_{BS}) and Fram Strait (AW_{FS}).

4.4.2.2 Western Canadian Archipelago

Nutrient profiles show a decrease in the depth of the NO_3^--depleted surface layer from the central basin ($\sim$ 40 m) to the western CAA ($<$ 15 m at CAA8) and a concurrent increase in surface [PO_4^{3-}] ($\leq$ 0.7 μmol L^{-1}) and [$Si(OH)_4$] ($\leq$ 8.3 μmol L^{-1}). The shallower nitracline (defined as maximum change in [NO_3^-] over given depth interval) in the western CAA is consistent with the shoaling of subsurface water masses evident in temperature and salinity profiles. Accordingly, underlying nutrient maxima and N* minimum are as shallow as $\sim$ 75 m in the western CAA in comparison to $\sim$ 180 m in the central basin. Nutrient concentrations, N* values and [O_2] associated with the temperature minimum are comparable between the central Canada Basin and the western CAA (Figure 4.4b, c and e).

Nutrient concentrations in the underlying AW_{BS} increase from the central basin on-shelf to 16.2 μmol L^{-1}, 1.1 μmol L^{-1} and 24.2 μmol L^{-1} at CAA8 for [NO_3^-], [PO_4^{3-}] and [$Si(OH)_4$], respectively. The minimum in NO_3^- shoals towards the shelf break ($\sim$ 200 m), while being no longer detectable in the western CAA (CAA8) in accordance with the steady increase in NO_3^- westward (Figure 4.3a). [O_2] decreases westward to $\sim$ 235 μmol L^{-1} at CAA8, whereas AOU increases to $\sim$ 110 μmol L^{-1} along the same transect. Concurrently, the minimum in NO shoals to 200 m at the shelf break, followed by a subsequent increase in depth to $\sim$ 250-300 m in the western CAA (Figure 4.4d). N* values are comparable between the central basin and the western Archipelago (Figure 4.4e). Nutrients in core AW_{FS} increase on-shelf to 17.8 μmol L^{-1}, 1.2 μmol L^{-1} and 27.7 μmol L^{-1} at CAA8 for [NO_3^-], [PO_4^{3-}] and [$Si(OH)_4$]), respectively. Accordingly, [O_2] in core AW_{FS} decreases on-shelf to $\sim$ 220 μmol L^{-1} at CAA8, whereas AOU increases to $\sim$ 123 μmol L^{-1} (Figure 4.2c and d). In contrast, N* values in core AW_{FS} remain similar to corresponding values in the central basin.

NO_3^- isotope ratios at the shelf break and in the western CAA show a concurrent enrichment in $\delta^{15}N_{NO3}$ and $\delta^{18}O_{NO3}$ above PWW, similar to the central basin. In underlying PWW, N and O isotope ratios indicate a slight decrease in $\delta^{15}N_{NO3}$ on-shelf to 7.5‰ associated with the temperature minimum at CAA8 and an enrichment of the $\delta^{18}O_{NO3}$ minimum to 0.1‰. AW_{BS} shows a small increase in both $\delta^{15}N_{NO3}$ and $\delta^{18}O_{NO3}$ towards Viscount Melville Sound (6.3‰ and 1.0‰ at CAA8). Diverging trends between N and O isotope ratios are observed in the underlying AW_{FS}, with $\delta^{15}N_{NO3}$ becoming isotopically enriched while $\delta^{18}O_{NO3}$ decreases along the same transect ($\delta^{15}N_{NO3}$ of 6.3‰ and 1.1‰

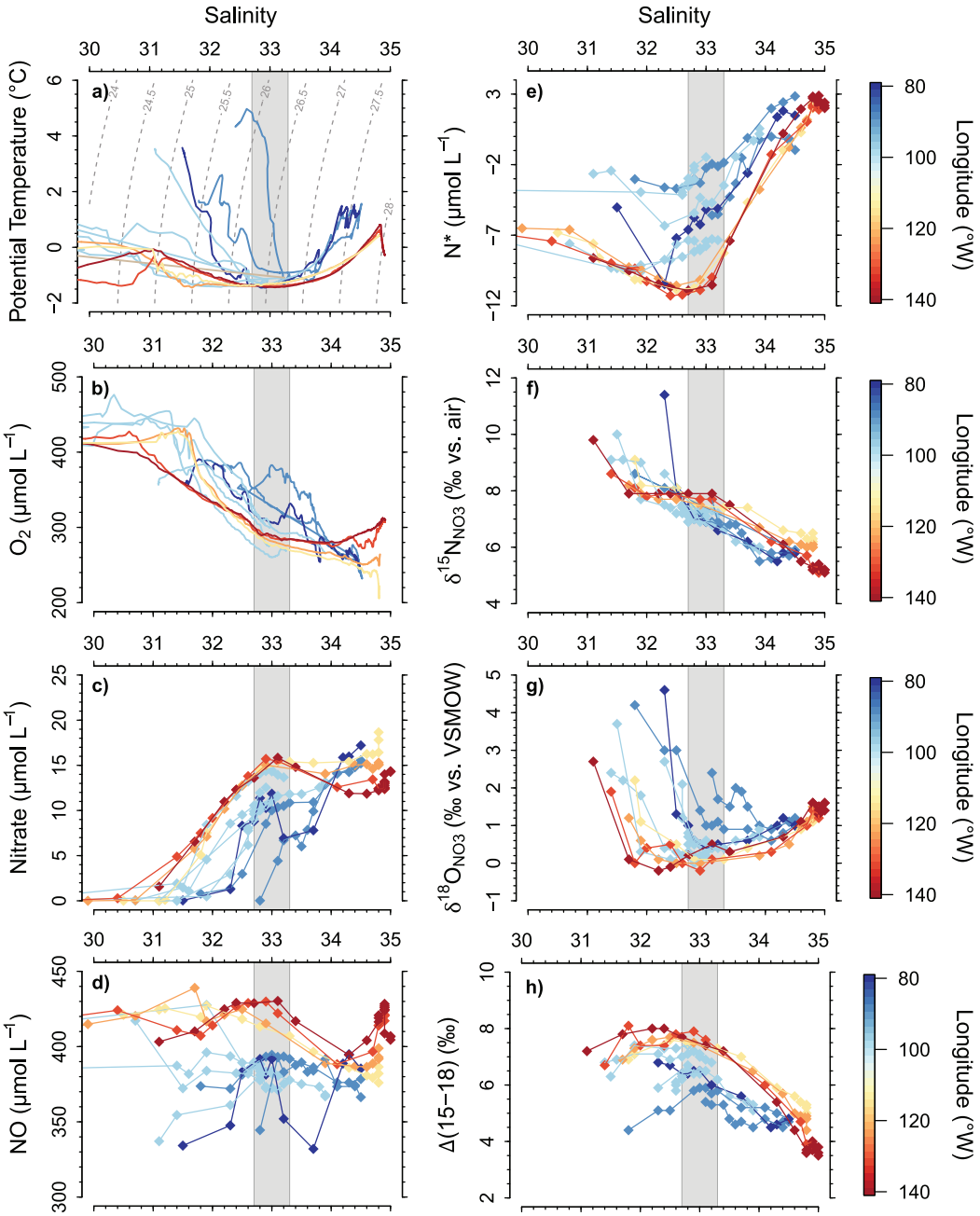

Figure 4.4: (a) Potential temperature-salinity diagram and tracer concentrations of (b) O_2, (c) NO_3^-, (d) NO, (e) N*, (f) $\delta^{15}N_{NO3}$, (g) $\delta^{18}O_{NO3}$ and (h) Δ(15-18) plotted as a function of salinity. Colors show the longitude of the hydrographic stations, with warmer colors (shades of red) highlighting stations west of Barrow Strait and colder colors (shades of blue) indicate stations east of Barrow Strait in Lancaster Sound. The grey shaded area designates the salinity range ($32.7 < S < 33.3$) representing the core of Pacific Winter Water (PWW) in the western CAA.

at CAA8). The diverging trends in $\delta^{15}N_{NO3}$ and $\delta^{18}O_{NO3}$ are reflected in an increase in Δ(15-18) from the Canada Basin towards Viscount Melville Sound ($\sim$ 5.2‰; Figure 4.4h).

4.4.2.3 Central Canadian Archipelago

The station east of Viscount Melville Sound near northern Barrow Strait (CAA6) is marked by an absence of pronounced nutrient maxima associated with PWW, otherwise revealing relatively continuous increases in [NO_3^-], [PO_4^{3-}] and [$Si(OH)_4$] below $\sim$ 45 m (Figure 4.3a-c). Accordingly, [O_2] shows a relatively muted decrease from 360 to 300 μmol L^{-1} between 40 m and bottom depths at 250 m, while AOU increases from 0 μmol L^{-1} to 66 μmol L^{-1} for the same depth interval (Figure 4.2c and d). A comparable N* minimum designating PWW at the western stations remains absent at CAA6, with values only slightly decreasing from -3.8 μmol L^{-1} at the surface to -4.1 μmol L^{-1} at 45 m and a relatively uniform increase to -1.5 μmol L^{-1} at the bottom.

The N isotope ratios of NO_3^- show relatively little variation with depth. $\delta^{15}N_{NO3}$ decreases from a maximum of 7.8‰ at 45 m to a weak minimum of 6.9‰ at $\sim$ 120 m and increases to 7.1‰ at 250 m (Figure 4.5a). $\delta^{18}O_{NO3}$ decreases from 2.1‰ at 45 m to comparably constant values of $\sim$ 0.5‰ between 140 m and the bottom (Figure 4.5b).

In contrast, nutrient concentrations at CAA7 to the south of CAA6 show some distinct maxima at $\sim$ 120 m, albeit less pronounced than stations further to the western (Figure 4.3a-c). In this respect, [NO_3^-], [PO_4^{3-}] and [$Si(OH)_4$] increase from 1.5 μmol L^{-1}, 0.9 μmol L^{-1} and 5.8 μmol L^{-1} at 25 m to 14.4 μmol L^{-1}, 1.6 μmol L^{-1} and 29.7 at the nutrient maxima, followed by a decrease to 13.7 μmol L^{-1}, 1.5 μmol L^{-1} and 27.0 μmol L^{-1} at depths (200 m). Similarly, AOU increases from -55 μmol L^{-1} at the surface to a maximum of 120 μmol L^{-1} associated with the nutrient maxima, and decreases to 111 μmol L^{-1} at 200 m. N* values decrease from a surface maximum of -7.6 μmol L^{-1} to a subsurface minimum of -9.3 μmol L^{-1} at 25 m and increase to -7.3 μmol L^{-1} at the bottom (Figure 4.3d).

N and O isotope ratios at CAA7 increase concurrently with decreasing [NO_3^-] from $\sim$ 60 m to the shallowest depth (25 m) where NO_3^- is detectable. Below this subsurface enrichment, $\delta^{15}N_{NO3}$ is relatively constant, decreasing only slightly from 7.4‰ at the temperature minimum ($\sim$ 60 m) to 7.2‰ at 200 m. $\delta^{18}O_{NO3}$ decreases from 0.1‰ at 60 m to a minimum of 0.0‰ at 100 m, followed by an increase to 0.4‰ at bottom depths. Δ(15-18) shows a similar pattern as station CAA8 west of Barrow Strait, indicating a

pronounced minimum (6.3‰) at 25 m, an increase to maximum values ($\sim$ 7.4‰) between $\sim$ 40-100 m, and a subsequent decrease towards the bottom (6.8‰ at 200 m).

4.4.2.4 Eastern Canadian Archipelago

At the eastern end of the CAA transect in southern Lancaster Sound (CAA3), moderate nutrient maxima (11.9 μmol L^{-1}, 1.3 μmol L^{-1}, 21.5 μmol L^{-1} for $[NO_3^-]$, $[PO_4^{3-}]$ and $[Si(OH)_4]$) at $\sim$ 80-120 m and coinciding negative N* values indicating the presence of PWW (*Jones and Coote*, 1980; *Jones*, 2003). N* associated with the nutrient maxima, however, is less negative (-6.2 to -5.2 μmol L^{-1}) than corresponding values in the central Archipelago (CAA7) and western Lancaster Sound ($\sim$ -7.4 μmol L^{-1} at CAA4; Figure 4.3h). $[O_2]$ decreases from a subsurface maximum of 390 μmol L^{-1} to 290 μmol L^{-1} at the nutrient maximum, a value in line with concentrations measured in PWW in the western CAA (Figure 4.2g).

Below PWW, $[NO_3^-]$, $[PO_4^{3-}]$ and $[Si(OH)_4]$ decrease to subsurface minima of 6.9 μmol L^{-1}, 0.8 μmol L^{-1} and 9.5 μmol L^{-1} between 150-200 m (σ_θ: 26.7-27.1), thus resembling the nutrient minima observed in AW_{BS} in the Canada Basin. NO values at the nutrient maxima are equivalently low, with the NO minimum (332 μmol L^{-1}) at $\sim$ 200 m being lower than corresponding minima in the western CAA (Figure 4.4d). While the shallow sill at Barrow Strait prevents any propagation of waters $> \sim$ 125 m eastward, previous studies suggested the propagation of AW_{BS} through Nares Strait into northern Baffin Bay (*Rudels*, 1986; *Rudels et al.*, 2004). In AW below, nutrient concentrations are higher in comparison to AW_{FS} in the western CAA, reaching values of 16.0 μmol L^{-1} for $[NO_3^-]$, 1.1 μmol L^{-1} for $[PO_4^{3-}]$ and 17.4 μmol L^{-1} for $[Si(OH)_4]$. Concurrently, N* increases from negative values in the halocline layer to peak values of 1.8 μmol L^{-1} associated with the AW temperature maximum, whereas $[O_2]$ decreases to $\sim$ 260 μmol L^{-1}. Thus, N* and $[O_2]$ associated with the temperature maximum are lower than corresponding values in the Canada Basin.

NO_3^- isotope ratios in PWW in southern Lancaster Sound show a similar distribution to the western CAA and CAA7 in central CAA, however, with $\delta^{15}N_{NO3}$ being slightly lower ($\sim$ 7.0‰) and the $\delta^{18}O_{NO3}$ minimum heavier ($\sim$ 0.4‰ at 120 m) than further to the west. Below PWW, $\delta^{15}N_{NO3}$ decreases to 6.2‰ at 200 m (σ_θ: $\sim$ 27.1), an isotopic signature similar to AW_{BS} in the Canada Basin (Figure 4.5d and e). $\delta^{18}O_{NO3}$ increases from its minimum in PWW to 0.6‰, thus is slightly more enriched compared to AW_{BS}. NO_3^- in

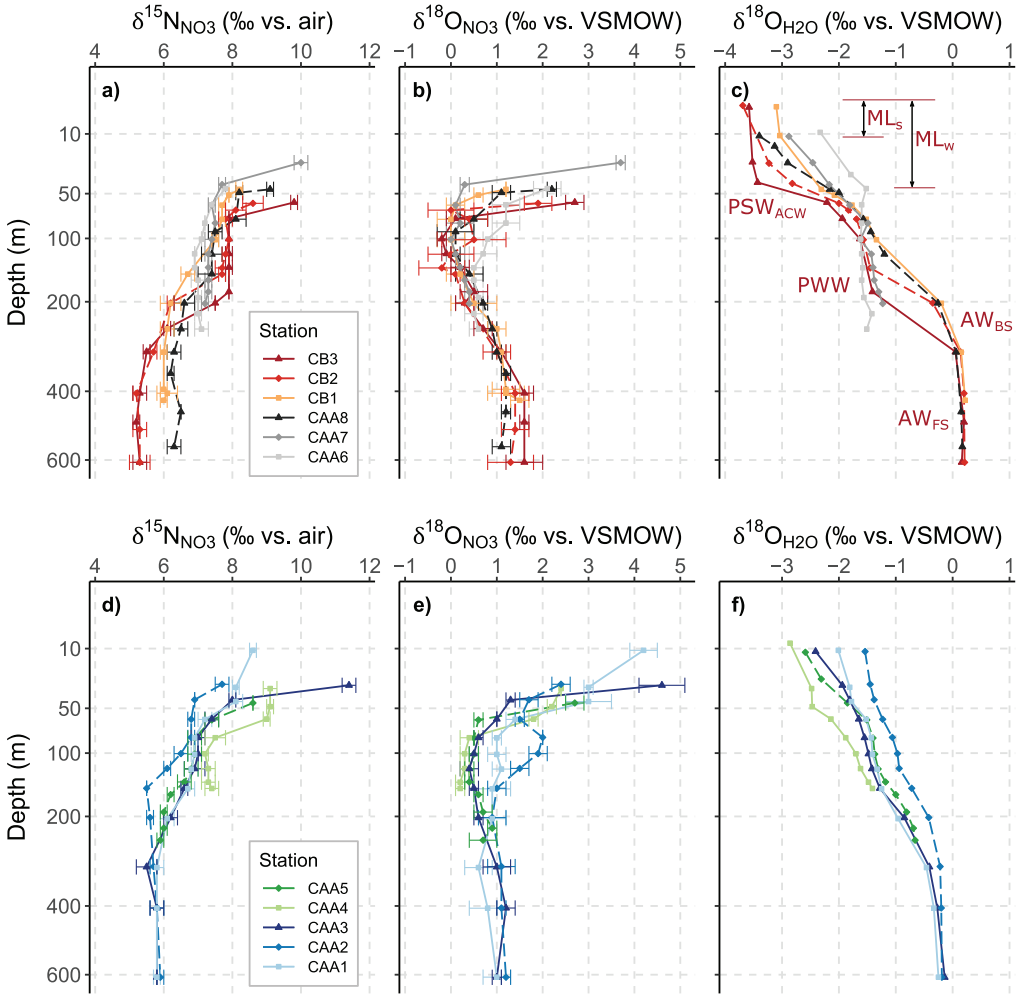

Figure 4.5: Water column profiles of (a, d) $\delta^{15}N_{NO3}$, (b, e) $\delta^{18}O_{NO3}$ and (c, f) $\delta^{18}O_{H2O}$ at stations in the western CAA and Barrow Strait (top panels) and in the eastern CAA (bottom panels). Water masses defined in the central Canada Basin are highlighted in red (top panels). Abbreviations indicate the summer and winter mixed layer (ML_S and ML_W), Pacific Summer Water originating from Alaskan Coastal waters (PSW_{ACW}), Pacific Winter Water (PWW) and Atlantic waters originating from the Barents Sea (AW_{BS}) and Fram Strait (AW_{FS}).

the underlying Atlantic end-member deriving from Baffin Bay is enriched in regard to ^{15}N ($\sim 5.5‰$) and depleted in ^{18}O ($\sim 1.0‰$) in comparison to AW_{FS} in the central Canada Basin.

The spatial variability observed in the hydrographic profiles between southern and northern Lancaster Sound is further evident in nutrient and isotope distributions. Accordingly, nutrient maxima associated with the halocline layer are less pronounced, while N* is less negative in northern Lancaster Sound (CAA2 and CAA1; Figure 4.3e-h). Below the cold upper halocline layer, distinct nutrient minima are also present at CAA2 and CAA1 between 100-200 m (σ_θ: ~ 27.1). $\delta^{15}N_{NO3}$ shows a similar enrichment ($\sim 6.9‰$) in the upper halocline layer of CAA 2 and CAA1, whereas a comparable $\delta^{18}O_{NO3}$ minimum in the same layer remains absent. NO_3^- isotope ratios associated with the AW temperature maximum are analogous between southern and northern Lancaster Sound (Figure 4.5d and e).

4.5 Discussion

The CAA is an important pathway for both nutrients and freshwater from the western Arctic to the North Atlantic. The flow through the CAA is affected by a number of sills, most notably Barrow Strait ($\sim$ 125 m sill depth) in central CAA (Figure 4.1), which allows the propagation of surface and upper halocline waters while simultaneously restricting the eastward flow of dense Atlantic water from the Canada Basin (*Melling et al.*, 1984; *Prinsenberg and Bennett*, 1987). In this respect, we discuss hydrographic and biogeochemical tracer distributions according to their relative location to Barrow Strait and, accordingly, divide them into western and eastern profiles. In accordance with the general westward propagation of PWW and AW along the southern slope of the Canada Basin (Figure 4.1; *Melling et al.*, 1984), the eastward modifications of individual density layers throughout the Archipelago will be examined relative to end-member values recorded at the Canada Basin shelf station CB2, which is deemed representative of the water masses entering the CAA at its western side.

4.5.1 Assimilation signal in near-surface waters

Surface waters in our study area show the persistent N-limited conditions characteristic of the Pacific-influenced western Arctic surface layer (*Yamamoto-Kawai et al.*, 2006;

Tremblay et al., 2008). Underlying this N-depleted surface layer, a progressive shoaling of the nitracline along a west-east transect largely coincides with the depth of the subsurface chlorophyll maximum (SCM; i.e., the depth of the fluorescence maximum; Figure 4.6a). The SCM is a persistent feature throughout our study area and reflects the year-round limited replenishment of nutrients in the surface layer due to the impact of sea ice and enhanced stratification (e.g., *Ahmed et al.*, 2019; *Martin et al.*, 2010). In this respect, the SCM designates pronounced phytoplankton growth below the mixed layer where sufficient light from above coincides with enhanced nutrient supply from below (*Brown et al.*, 2015b; *Martin et al.*, 2010; *Tremblay et al.*, 2008). The variability in SCM characteristics is generally well explained by regional differences in stratification at the depth of the SCM (*Martin et al.*, 2010). Thus, the deeper nitracline and the relatively weak development of the SCM in the central Canada Basin (CB3) reflect the relatively thick low-salinity, low-density polar mixed layer and perennially low surface [NO_3^-] due to low wintertime replenishment (*Brown et al.*, 2015b; *Codispoti et al.*, 2005; *Martin et al.*, 2010; *Tremblay et al.*, 2008). This relatively stable upper water column evident at the western stations contrasts with the central and eastern CAA where a more turbulent regime induced by a strong tidal flow and wind-induced mixing (*Hughes et al.*, 2017; *Melling et al.*, 1984; *Prinsenberg and Bennett*, 1987) leads to an increase in the vertical flux of nutrients and, correspondingly, a shallower nitracline and more pronounced SCM (Figure 4.6; e.g., *Cota and Horne*, 1989).

In accordance with the variability seen in the nitracline and SCM distribution, we observe some regional differences in the weak accumulation of NO_2^- (≤ 0.24 μmol L^{-1}) and NH_4^+ (≤ 0.78 μmol L^{-1}) between the western and eastern CAA (Figure 4.6). The buildup of NH_4^+ generally just below the SCM reflects the remineralization of sinking organic matter, where light inhibits subsequent nitrification. The co-occurrence of small NO_2^- maxima and a relatively weak SCM at stations in the western CAA suggests that NO_2^- likely derives from partial assimilatory reduction of NO_3^- and the excretion of NO_2^- by phytoplankton – a mechanism previously suggested to occur in the Beaufort Sea (*Tremblay et al.*, 2008). Conversely, the more pronounced SCM at and east of Barrow Strait is associated with more diffuse peaks in NO_2^- deeper in the water column, and below the SCM and subsurface NH_4^+ peak. This sequential accumulation of NH_4^+ and NO_2^- below the SCM thus suggests an imprint of organic matter remineralization (*Santoro et al.*, 2013).

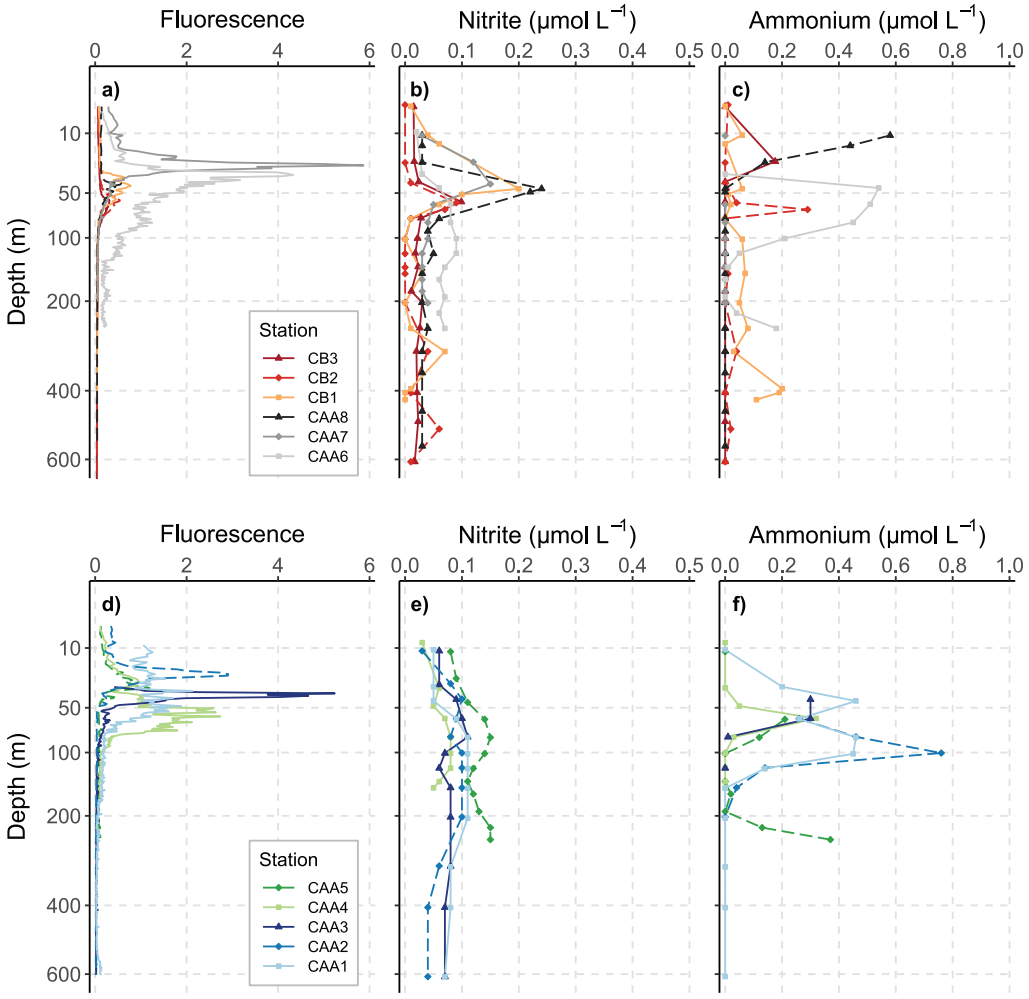

Figure 4.6: Water column profiles of (a, d) fluorescence, (b, e) NO_2^- and (c, f) NH_4^+ at stations in the western CAA and Barrow Strait (top panels) and in the eastern CAA (bottom panels).

N and O isotope ratios of NO_3^- in the nitracline increase concurrently from the base of the nitracline toward the NO_3^--depleted surface layer, consistent with the uptake of NO_3^- by phytoplankton associated with the SCM. NO_3^- assimilation in the absence of other processes results in a 1:1 enrichment in N and O isotope ratios of the dissolved NO_3^- pool (*Casciotti et al.*, 2002; *Granger et al.*, 2004). The stronger increase in $\delta^{18}O_{NO3}$ relative to $\delta^{15}N_{NO3}$ throughout the transect, highlighted by an upward decrease in Δ(15-18) throughout the nitracline (Figure 4.4h), may reflect co-occurring N transformations that either result in an input of isotopically low $\delta^{15}N$ or an enhanced enrichment in $\delta^{18}O$ of NO_3^-. Estimated open-system isotope effects (ϵ; where ϵ = ($\delta^{15}N$ - $\delta^{15}N_{initial}$) / 1 - [NO_3^-] / [NO_3^-]$_{initial}$; *Mariotti et al.*, 1981), a means to indicate the degree of fractionation between the heavier and the lighter isotope, range between 2.1-5.5‰ for $^{18}\epsilon$ versus 1.2-4.4‰ for $^{15}\epsilon$ along the transect. These values are lower than expected based on both culture experiments and field studies (Figure 4.7a and b; e.g., *Casciotti et al.*, 2002; *Granger et al.*, 2004, 2010; *Sigman et al.*, 2005), further substantiating a possible impact of overlapping processes throughout the nitracline.

Along the western stations, the strongest assimilation signal can be observed in the central Canada Basin, followed by a progressive decrease towards the shelf and into the western CAA (Figure 4.4f and g). Given the low surface and SCM productivity previously reported for the central basin (e.g., *Wallace et al.*, 1987) and indicated by relatively weak fluorescence peaks (Figure 4.6), the concurrent subsurface enrichment in both N and O isotope ratios evident in the central Canada Basin and towards the western CAA may be entrained from the western Arctic rather than produced locally in the upper water column. Bottom waters over the southern Chukchi Shelf carry a strong signal of enhanced NO_3^- utilization during summer, leading to a concurrent enrichment of both $\delta^{15}N_{NO3}$ and $\delta^{18}O_{NO3}$ (reaching values of $\leq$ 13‰ and $\leq$ 11‰, respectively; *Brown et al.*, 2015a). In this respect, the observed assimilation signal may reflect the remote imprint of nutrient-deprived PSW penetrating the subsurface layer ($\sim$ 50 m) of the Canada Basin rather than a local NO_3^- uptake signal. The lower enrichment towards the shelf and into the western CAA thus may be explained by the dilution of the PSW signal, as indicated by the temperature profiles, and a potential input of low $\delta^{15}N_{NO3}$. The allochthonous input of reactive N through river discharge is generally considered minor throughout the central channel of the Archipelago (*Ahmed et al.*, 2019). The southern Beaufort Sea and western CAA, however, have been

shown to carry some freshwater imprint from the nearby Mackenzie River (*Shadwick et al.*, 2011), which thus potentially acts as a source of low-^{15}N NO_3^- to the upper water column. Another process potentially introducing isotopically light N the dissolved NO_3^- pool is N_2 fixation. Although N_2 fixation has been reported in the Canada Basin (*Blais et al.*, 2012; *Harding et al.*, 2018; *Sipler et al.*, 2017), little is known about the potential occurrence and rates throughout different Arctic environments. While still considered a minor input, prior studies have found higher rates associated with the Mackenzie River plume and negligible rates throughout the CAA (*Blais et al.*, 2012).

In the eastern CAA, both river input and rates of N_2 fixation are deemed negligible and unlikely to explain the observed lower enrichment in δ^{15}N over δ^{18}O. However, the co-occurrence of nitrification as part of organic matter remineralization in the vicinity of the SCM has the potential to introduce low-^{15}N to the dissolved NO_3^- pool, due to the comparably high isotopic fractionation associated with incomplete NH_4^+ oxidation compared to NH_4^+ assimilation (e.g., *Casciotti et al.*, 2003; *DiFiore et al.*, 2009; *Fawcett et al.*, 2011), thus potentially acting as a source for the observed decrease in Δ(15-18) towards the surface.

4.5.2 Modifications of PWW throughout the Canadian Archipelago

The PWW temperature minimum of the UHL shoals from the Canada Basin on-shelf and further into the Archipelago. Nutrient concentrations and $\delta^{15}N_{NO3}$ generally decrease, while N* and $\delta^{18}O_{NO3}$ increase along the west-east transect (Figure 4.4).

To a first approximation, the nutrient maxima and NO_3^- isotope ratios of PWW observed at the westernmost stations are concordant with those observed in PWW of the southern Canada Basin (*Brown et al.*, 2015a; *Granger et al.*, 2018). The origin of biogeochemical tracers in PWW have been discussed in previous studies. Briefly, the nutrient and AOU maxima in PWW derive from remineralization on the shallow Chukchi shelf (e.g., *Granger et al.*, 2018; *Jones and Anderson*, 1986; *Shimada et al.*, 2005). The low $\delta^{18}O_{NO3}$, which mirrors $\delta^{18}O_{H2O}$ (*Buchwald et al.*, 2012; *Casciotti et al.*, 2008; *Sigman et al.*, 2009a), further indicates that NO_3^- is entirely nitrified (remineralized). The elevated $\delta^{15}N_{NO3}$ of PWW, in turn, results from coupled nitrification-denitrification of Pacific-derived NO_3^- on the Bering and Chukchi shelves, which increases δ^{15}N in proportion to the benthic N loss (quantified by N*; *Brown et al.*, 2015a; *Fripiat et al.*, 2018; *Granger et al.*, 2011, 2018). Accordingly, the newly remineralized nature of UHL NO_3^- is reflected in the low

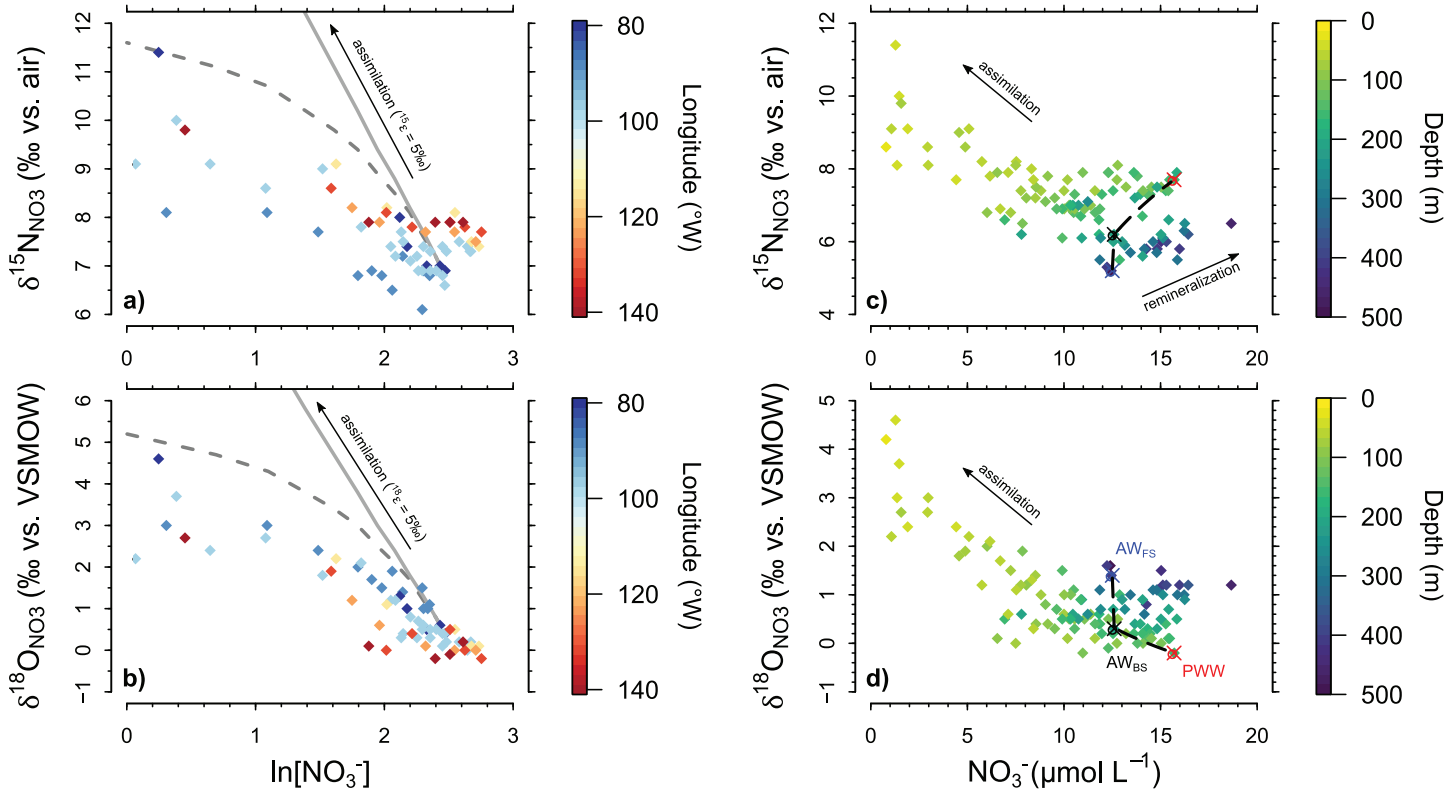

Figure 4.7: δ^{15}N and δ^{18}O of NO_3^- plotted against (a and b) the negative logarithm of NO_3^- and (c and d) NO_3^- concentrations. Colors show (a and b) the longitude of the hydrographic stations, with warmer colors (shades of red) highlighting stations west of Barrow Strait and colder colors (shades of blue) indicate stations east of Barrow Strait towards Baffin Bay, and (c and d) the water depth of the individual data point. Only isotope data from depths of $\leq$ 150 m are included in a and b. Grey lines indicate Rayleigh closed system (solid line) and open system (dashed line) estimates for NO_3^- assimilation, assuming a $^{15}\epsilon$ and $^{18}\epsilon$ of 5‰ (*Granger et al.*, 2004, 2010). End-member values are highlighted in red (Pacific Winter Water; PWW), black (Barents Sea Atlantic Water; AW_{BS}) and blue (Fram Strait Atlantic Water; AW_{FS}). Mixing lines between end-members are indicated in black.

$\delta^{18}O_{NO3}$ evidenced at CB2 and CB3 (Figure 4.5e). By taking into account the $\delta^{18}O_{H2O}$ ($\sim$ -1.4‰) associated with the nutrient maximum, we estimate an expected $\delta^{18}O_{NO3}$ for newly nitrified NO_3^- on the order of $\sim$ -0.3‰, a value well aligned with measurements in the central and eastern Canada Basin.

From the Canada Basin, Pacific-derived waters enter the western CAA via the Amundsen Gulf adjacent to the southeastern Beaufort Sea and at M'Clure Strait at station CB1 (Figure 4.1). A progressive warming of the upper halocline in the western CAA is attributed to an absence of lateral intrusions of cold shelf waters and an upward flux of heat from the warmer Atlantic layer underlying PWW (*Melling et al.*, 1984). The small increase in $\delta^{18}O_{NO3}$ and decrease in $\delta^{15}N_{NO3}$ are in line with the imprint of underlying AW_{BS} with a lower $\delta^{15}N_{NO3}$ and concurrently higher $\delta^{18}O_{NO3}$. Concurrently, the slight increase in $\delta^{18}O_{NO3}$ (+ 0.3‰) alongside a constantly low $\delta^{18}O_{H2O}$ (-1.4‰) supports the notion of negligible remineralization in PWW in the western CAA. While both hydrographic parameters and biogeochemical tracers indicate some diapycnal mixing between the upper and lower halocline on-shelf, the maintenance of pronounced peaks associated with individual water masses indicate a relatively stable water column in the western CAA (Figures 4.2 and 4.3; *Hughes et al.*, 2017; *Martin et al.*, 2010).

In the central CAA, the variability in nutrient distributions and NO_3^- isotope ratios largely reflects the general circulation pattern in Barrow Strait, with a dominant eastward flux of Arctic waters centered at the southern shore towards Lancaster Sound (*Prinsenberg and Bennett*, 1987). Previous studies investigating the fractional contribution of both Pacific and Atlantic water to the water column of the CAA concluded that Barrow Strait waters down to a depth of $\sim$ 140 m are almost entirely ($\geq$ 95%) of Pacific origin (*Jones*, 2003; *Shadwick et al.*, 2011). Thus, the shallow bathymetry in Barrow Strait enhances vertical mixing which leads to the perturbation of the halocline layer and the broadening of the Pacific core, while concurrently impeding the propagation of underlying AW_{BS} and AW_{FS} across the shallow sill (*Melling et al.*, 1984; *Prinsenberg and Bennett*, 1987). The restricted influence of AW is most apparent in the cold and fresh ($\theta \leq$ -1.1°C, S $\leq$ 33.2) water extending to depth ($\sim$ 200 m) at CAA7. Concurrently, negative N* values ($\leq$ -7.3 μmol L^{-1}) throughout the water column associated with relatively elevated $\delta^{15}N_{NO3}$ ($\geq$ 7.2‰) and low $\delta^{18}O_{NO3}$ ($\leq$ 0.4‰) in between $\sim$ 80 m and 200 m argue for a predominantly Pacific origin at CAA7. However, while both N* and NO_3^- isotope ratios carry a prevailing

Pacific signature in southern Barrow Strait, tracer distributions in northern Barrow Strait (CAA6) are notably different from both the Pacific signature recorded in Viscount Melville Sound (CAA8) and southern Barrow Strait (CAA7). In this regard, the higher N* values throughout the water column associated with lower $\delta^{15}N_{NO3}$ and higher $\delta^{18}O_{NO3}$ at CAA6 are in line with the admixture of water from northwestern Lancaster Sound (CAA5) and, thus, from Baffin Bay entering Lancaster Sound as part of the westward counter-currents at the northern side of the sound.

East of Barrow Strait, the contribution of Pacific water to the water column inherits some significant regional variability as the eastward flow of waters from the Canada Basin is largely centered in the upper water column ($\leq$ 120 m) at the southern shore of Lancaster Sound (*Prinsenberg and Hamilton*, 2005). Accordingly, while vertical and tidal mixing in the vicinity of Barrow Strait largely erode the distinct layering of the water column, we again observe a cold halocline underlain by warm and more saline waters of Atlantic origin (Figure 4.2d and e; see section below for details). Previous hydrographic studies in Lancaster Sound suggested an active regeneration of the temperature minimum ($\geq$ -1.7°C) in the upper halocline east of Barrow Strait, contrasting the western CAA where a similar regeneration remains absent (*Lemon and Fissel*, 1982; *Melling et al.*, 1984; *Prinsenberg and Hamilton*, 2005). During the 2015 transect, relatively shallow nutrient maxima, negative N* values and a corresponding isotopic enrichment in N isotope ratios of NO_3^- depict a distinct Pacific influence on the upper halocline layer of the western (CAA4 and CAA5) and eastern Lancaster Sound (CAA 1-3; Figures 4.3 and 4.4), substantiating previous findings of dominant Pacific-derived nutrient ratios in the eastern CAA (e.g., *Jones*, 2003). The degree of isotopic enrichment in $\delta^{15}N_{NO3}$ and coincident negative N* values are consistent with a dominant eastward flow of Arctic waters in southern Lancaster Sound towards Baffin Bay (*Prinsenberg and Bennett*, 1987). Accordingly, we observe a stronger Pacific-derived signal in southern Lancaster Sound relative to the northern side and, concurrently, a progressive weakening of both ^{15}N-enrichment and negative N* from the southwestern Lancaster Sound (CAA4) to the southeastern part of the sound (CAA3). The notably weaker Pacific signal in the eastern Lancaster Sound compared to the central CAA (CAA7) points to the mixing between the eastward flowing PWW and underlying Atlantic-derived waters with a characteristic lighter $\delta^{15}N_{NO3}$ ($\sim$ 5‰; *Lehmann et al.*, 2019) entering Lancaster Sound from Baffin Bay.

4.5.3 Eastward modifications of Atlantic-derived waters

The NO_3^- isotope ratios measured in AW_{BS} in the central basin are indistinguishable from corresponding values reported previously at more southern stations of the Beaufort Gyre (*Granger et al.*, 2018). The values in AW_{BS} (6.1 $\pm$ 0.1‰ for $\delta^{15}N_{NO3}$ and 0.7 $\pm$ 0.2‰ for $\delta^{18}O_{NO3}$) derive dominantly from mixing of PWW and AW_{FS} end-members, given the inherently low [NO_3^-] in the Barents Sea branch (*Granger et al.*, 2018). NO_3^- isotope ratios in AW_{FS} measured in the Canada Basin (5.2 $\pm$ 0.1‰ for $\delta^{15}N_{NO3}$ and 1.6 $\pm$ 0.1‰ for $\delta^{18}O_{NO3}$) are well in agreement with previous measurements in the southwestern Canada Basin and southeastern Beaufort Sea ($\delta^{15}N_{NO3}$ of 5.3 $\pm$ 0.3‰ and $\delta^{18}O_{NO3}$ of 1.5-2.1‰; *Brown et al.*, 2015a; *Granger et al.*, 2018) and close to values characterizing North Atlantic Deep Water (4.9‰ and 1.7‰ for $\delta^{15}N_{NO3}$ and $\delta^{18}O_{NO3}$, respectively; *Marconi et al.*, 2015). The AW_{FS} $\delta^{15}N_{NO3}$ thus reflect the isotopic signature of NO_3^- imported from the sub-Arctic North Atlantic, while the relatively low $\delta^{18}O_{NO3}$ suggests pronounced mid-depth remineralization in the Nordic Seas (*Granger et al.*, 2018).

From the Canada Basin, AW_{BS} becomes warmer, more saline and less oxygenated in transit to Viscount Melville Sound (Figure 4.2). Correspondingly, nutrient concentrations and N* increase, concurrent with an enrichment in $\delta^{15}N_{NO3}$ and $\delta^{18}O_{NO3}$ (by $\sim$ 0.1‰ for $\delta^{15}N_{NO3}$ and $\sim$ 0.7‰ for $\delta^{18}O_{NO3}$, respectively). In contrast, the underlying temperature maximum designating AW_{FS} becomes colder, less oxygenated and accumulates nutrients in transit from the Canada Basin to Viscount Melville Sound. Concurrently, $\delta^{15}N_{NO3}$ increases by 1.1‰ whereas $\delta^{18}O_{NO3}$ decreases by 0.3‰. To a first approximation, the increase in temperature, salinity and N* in the Barents Sea branch are consistent with mixing between the lower halocline and the underlying Fram Strait branch. The higher [O_2] in both the underlying AW_{FS} and overlying PWW, however, suggests some concurrent local imprint of remineralization on AW_{BS}. Based on the change in AOU between the Canada Basin shelf and Viscount Melville Sound and taking into account the oxygen-to-nutrient stoichiometry of organic matter respiration (*Anderson and Sarmiento*, 1994), we approximate an addition of remineralized of PO_4^{3-} of 0.2 μmol L^{-1} along the western transect. By assuming Redfield stoichiometry (*Redfield et al.*, 1963), this regenerated PO_4^{3-} further translates into a concurrent addition of NO_3^- of 3.0 μmol L^{-1} from remineralization in transit, a value close to the observed increase in NO_3^- (+ 3.6 μmol L^{-1}) along the same transect. Alternatively, we can estimate the concentration of regenerated NO_3^- using a

simplified isotope mass balance:

$$[NO_3^-]_{reg} = (\delta^{15}N_{total} \times [NO_3^-]_{total} - \delta^{15}N_{source} \times [NO_3^-]_{source})/[NO_3^-]_{reg} \quad (4.4)$$

where we account for the prevalent changes in $\delta^{15}N_{NO3}$ and $[NO_3^-]$ between the Canada Basin shelf (source) and Viscount Melville Sound (total). The complete consumption of NO_3^- in the surface layer results in a $\delta^{15}N$ of the organic matter akin to the isotopic signature of the NO_3^- supplied to the surface. Assuming that surface production and the subsequent export of organic matter is largely fueled by PWW – i.e., a $\delta^{15}N_{org}$ of 7.5-7.7‰ – we calculate an addition of 3.1-3.2 μmol L^{-1} NO_3^- added to the LHL, in good agreement with estimated + 3.0 μmol L^{-1} from AOU. In contrast to expected lower $\delta^{18}O_{NO3}$ in the presence of remineralization, the observed increase in $\delta^{18}O_{NO3}$ in the LHL is consistent with nitrification as its enrichment largely mirrors the concurrent increase in $\delta^{18}O_{H2O}$ (Figure 4.5).

In the underlying AW_{FS}, AOU increases from 41.0 μmol L^{-1} at the shelf break to 122.8 μmol L^{-1} at CAA8, coinciding with an increase in $[NO_3^-]$ and $[PO_4^{3-}]$ of 5.4 μmol L^{-1} and 0.3 μmol L^{-1}, respectively. Regenerated nutrients expected from the AOU difference between CB2 and CAA8 are 7.7 μmol L^{-1} for $[NO_3^-]$ and 0.5 μmol L^{-1} for $[PO_4^{3-}]$, thus slightly higher than observed. Based on this AOU relationship, the estimated fraction of regenerated nutrients to total nutrients increases from 0.3 at the Canada Basin shelf to 0.6 in Viscount Melville Sound. The impact of organic matter remineralization is similarly reflected in the $\delta^{15}N$ and $\delta^{18}O$ of NO_3^-, where an increase $\delta^{15}N_{NO3}$ and a decrease in $\delta^{18}O_{NO3}$ translates into a minimum in Δ(15-18) in the core of AW_{FS} (Figure 4.4). Specifically, the ammonification and subsequent nitrification of high-^{15}N organic matter exported from the surface translates into a high $\delta^{15}N$ of the dissolved NO_3^- pool at depth. Accordingly, given that newly nitrified $\delta^{18}O_{NO3}$ approaches a value close to ambient seawater (*Buchwald et al.*, 2012; *Casciotti et al.*, 2008; *Sigman et al.*, 2005), the observed decrease in $\delta^{18}O_{NO3}$ largely mirrors the imprint of isotopically light seawater, with the measured $\delta^{18}O_{NO3}$ (1.1‰) close to the value expected from $\delta^{18}O_{H2O}$ (0.2‰ + 1.1‰).

Using the isotope mass balance above (Equation 4.4) and an equally enriched $\delta^{15}N$ of the organic matter (7.5-7.7‰), we estimate an addition of 6.2-6.3 μmol L^{-1} of NO_3^- to AW_{FS}, a value between observed nutrient concentrations and estimated concentrations based on organic matter respiration stoichiometry and isotope mass balance. Slight discrepancies

between measured and estimated values may result from mixing between the Atlantic-derived LHL and AW_{FS} as suggested by observed changes in temperature and salinity. The effect of mixing processes between two end-members (e.g., LHL and AW_{FS}) can be addressed using a simplified mixing model:

$$\delta_{mix} C_{mix} = \delta_a C_a X_a + \delta_b C_b X_b \tag{4.5}$$

taking into account the NO_3^- concentration (C), the isotopic signature (δ) and the fraction (X) of the individual end-member (a and b). These mixing estimates generally result in curved mixing line between the two end-members, reflecting the stronger impact of the high-NO_3^- mixing end-member (Figure 4.7).

As indicated in the previous section, the eastward propagation of Atlantic-derived waters is largely inhibited by the shallow sill at Barrow Strait. As such, the temperature maximum underlying PWW in Lancaster Sound designates an Atlantic end-member entering from Baffin Bay through Davis Strait and propagating north along the West Greenland shelf (*Azetsu-Scott et al.*, 2012; *Hamilton and Wu*, 2013; *Münchow et al.*, 2015; *Tang et al.*, 2004). In comparison to the Fram Strait end-member, Atlantic waters entering from Baffin Bay are relatively enriched in regard to ^{15}N ($\sim$ 5.5‰) and depleted in ^{18}O ($\sim$ 1.0‰). This difference in the AW end-member NO_3^- isotopic signature derives from the remineralization of high-^{15}N organic matter in transit through Baffin Bay (*Lehmann et al.*, 2019), consistent with the overall higher nutrient concentrations in Lancaster Sound versus the Canada Basin.

In addition to the westward intrusion of AW from Baffin Bay, some striking minima in NO and nutrient concentrations between PWW and the AW temperature maximum in southern and central Lancaster Sound resembles the nutrient characteristics that designate Atlantic-derived lower halocline waters east of Barrow Strait. While a comparable signal remains absent in the central CAA, the nutrient and isotope signal in Lancaster Sound may thus reflect the westward intrusion of lower halocline water from the Barents Sea that has previously been suggested to enter Baffin Bay via Nares Strait (e.g., *Münchow et al.*, 2007; *Rudels et al.*, 2004). Accordingly, while NO_3^- isotope ratios are largely consistent with these findings, with $\delta^{15}N_{NO3}$ and $\delta^{18}O_{NO3}$ in the Canada Basin LHL and in Lancaster Sound being similar within uncertainty, a closer comparison between the Lancaster Sound and Atlantic waters entering through Nares Strait remains challenging due to missing

end-member values from Nares Strait.

4.6 Summary

In this study, we examined water column natural abundance N and O isotope ratios of NO_3^- collected during the 2015 Canadian Arctic GEOTRACES along a transect from the Canada Basin through the Canadian Archipelago and towards Baffin Bay.

Isotope values at the western end of the transect show a pronounced enrichment in $\delta^{15}N_{NO3}$ and a coincident minimum in $\delta^{18}O_{NO3}$ in the Canada Basin upper halocline layer, indicative of both benthic denitrification upstream on the Bering and Chukchi shelves and remineralization processes along the transit. This subsurface peak in $\delta^{15}N$ of NO_3^- designates the presence of cold Pacific-derived halocline throughout the west-to-east transect from the Canada Basin towards Baffin Bay. This high-^{15}N NO_3^- indicates a relatively stable water column and little modification of the Pacific-derived UHL in the western CAA, contrasting with more turbulent conditions and mixing with underlying Atlantic water in the eastern CAA. N and O isotope ratios in the underlying water column show evidence of remineralization of ^{15}N-enriched organic matter in both the Atlantic end-member originating from Fram Strait and evident in the western CAA, as well as Atlantic waters originating in the Irminger Sea and present in Lancaster Sound.

The spatial variability of NO_3^- and N and O isotope ratios throughout the CAA reflect the distribution of Pacific- and Atlantic-derived waters, and hence the proximity to the western Arctic area of inflow. Isotope data presented here thus shed light on both the origin and internal cycling of NO_3^- in the Canadian Arctic, while providing insight into horizontal aspects of inter-basin nutrient transport.

CHAPTER 5

CONCLUSIONS

This thesis aimed to highlight the importance and applicability of dual N and O isotope measurements of NO_3^- to identify major N transformation processes, their spatial distribution and regional differences among various marine environments. When combined with hydrographic and nutrient data, coupled analyses of $^{15}N/^{14}N$ and $^{18}O/^{16}O$ ratios of NO_3^- – allowing the distinction between concurrent transformation processes due to process-dependent differences in fractionation – give valuable insight not only into major in situ N transformations but further into regional circulation patterns and water mass provenance.

Specifically, I examined the N and O isotopic composition of NO_3^- and the distribution of complementary biogeochemical tracers (e.g., Si*, N*, $\delta^{13}C$ of DIC) to gain insight into the complex hydrography of the western equatorial Pacific and the biogeochemical modifications of the prevalent water masses that feed the EUC and ultimately the equatorial upwelling system (chapter 2). While the hydrographic features of the region have been studied previously, in particular during the Western Equatorial Pacific Observation Circulation Study (WEPOCS; e.g., *Bingham and Lukas*, 1994; *Lindstrom et al.*, 1987; *Toole et al.*, 1988; *Tsuchiya et al.*, 1989), little is know about the biogeochemistry in this region, despite its importance in shaping lower latitude biogeochemistry and productivity along the equator. Although it has long been suggested that nutrients in the equatorial Pacific largely originate from the Southern Ocean (*Toggweiler et al.*, 1991), few studies have attempted to quantify the relative contribution to the EUC and upper equatorial Pacific.

Using a combination of chemical tracers ($\delta^{15}N_{NO3}$, $\delta^{18}O_{NO3}$, and $\delta^{13}C_{DIC}$, nutrient ratios), I provide evidence for the different biogeochemical histories of nutrients feeding

the northern and southern WEP. Specifically, key findings drawn from these data include pronounced regional differences between the northern and southern WEP in regard to (i) the relative contribution of remineralization to total dissolved nutrients, (ii) the derived isotopic signature of the remineralized organic matter, and (iii) the lateral contribution of nutrients from the eastern margins. Particularly, by putting our measurements into a basin-wide context and applying them – alongside previously published data from both source regions in the North and South Pacific (*Rafter et al.*, 2012, 2013; *Sigman et al.*, 2009a) – in a set of isotope mass balance calculations, I showed that the net decrease in $\delta^{18}O_{NO3}$ between the Southern Ocean source of SAMW and our southern WEP intermediate waters may largely derive from the addition of newly nitrified NO_3^- added by organic matter remineralization in transit, and that the derived N isotopic composition of this remineralized organic matter needs to be relatively enriched (8.1-8.4‰) in order to explain the observed meridional variability of the dissolved NO_3^- pool. These observations based on mass balance estimates and nutrient ratios substantiate previous findings from the eastern and central Pacific (*Peters et al.*, 2018; *Rafter et al.*, 2012, 2013), suggesting that the prevalent ^{15}N-enrichment throughout the South Pacific intermediate layer may predominantly reflect an imprint from the remineralization of high-^{15}N organic matter stemming from the incomplete utilization of NO_3^- along the equatorial upwelling system rather than a pronounced entrainment of denitrified NO_3^- originating at the eastern margins.

One interesting conundrum remains from this study in regard to the imprint of N_2 fixation on the N isotopic composition of thermocline NO_3^-. Based on NO_3^- $\delta^{15}N$ and $\delta^{18}O$, I showed evidence for the remineralization of newly fixed N_2 north of the equator. Simultaneously, a comparable imprint of N_2 fixation on the dissolved NO_3^- remains absent in the southern WEP, despite convincing evidence of substantial N_2 fixation in both the Solomon Sea and Bismarck Sea (*Berthelot et al.*, 2017; *Bonnet et al.*, 2009, 2015). The relatively elevated $\delta^{15}N_{NO3}$ in the southern WEP potentially reflects the overprinting of this isotopically light signature from N_2 fixation by the advection of ^{15}N-enriched thermocline waters. Additional aspects that may lead to this observed discrepancy are the hydrographic complexity of the region, the potential regional heterogeneity of the N_2 fixation signal and a potentially high degree of export relative to shallow remineralization, as recently observed further to the south (*Knapp et al.*, 2018). Increased sampling, both spatially and temporally, may provide constraints on those uncertainties and the relative impact of N_2

fixation on the EUC nutrient pool.

Another important conclusion from this study comes from mixing model estimates, that – based on subsurface measurements of N and O isotope ratios of NO_3^- along with nutrient and oxygen measurements – investigate the relative contribution of both northern and southern boundary currents to the upper and lower EUC. This exercise, indicating that $\geq$ 70% of EUC nutrients derive from the southern boundary currents, provides support to the theory of a predominantly Southern Ocean source of NO_3^- to the equatorial upwelling system. This regional study thus helped to unravel the sources, transformations and communication of subsurface nutrients, which is highly relevant for predicting local and regional biogeochemical variability in this region.

Simultaneously, this study highlights the importance of baseline $\delta^{15}N_{NO3}$ and $\delta^{18}O_{NO3}$ measurements conducted on a regional scale in order to evaluate the impact of local biogeochemical processes on the mean ocean budget. These N and O isotope data applied to a varying set of mass balance equations and put into context with the wider circulation pattern act as a powerful diagnostic tool to, in this specific case, untangle Southern hemispheric N transformation processes that include lower latitude organic matter remineralization, mixing with the eastern ODZ, and N_2 fixation. Comparable interpretations and mass balance estimates are currently still challenging in the North Pacific. The only few dual N and O isotope measurements from the higher latitude North Pacific make an accurate characterization of North Pacific water mass end-members difficult and highlight the need for high-resolution NO_3^- isotope measurements throughout the North Pacific. Investigating spatial distributions and regional differences in N transformations and nutrient supply is greatly facilitated by zonal and meridional transects (such as CLIVAR P16S, GEOTRACES Pandora (GP12) and US GEOTRACES Eastern Pacific Zonal Transect (GP16) throughout the South Pacific), allowing to investigate the communication between different ocean regions and the connectivity between various N cycling hotspots. Although the main mandate of the GEOTRACES program is the study of input, removal and cycling of trace elements and isotopes in the water column, the inclusion of macro-nutrients and their isotopes as part of their regular sampling strategy has provided a unique opportunity to investigate the internal cycling and the spatial variability in sources and sinks, which is critically important not only to improve current flux and budget estimates, but further to help locate areas previous overlooked in regard to specific N cycling processes.

In this respect, chapters 3 and 4 investigated NO_3^- isotope data collected during the 2015 Canadian Arctic GEOTRACES campaign, which included two consecutive cruises covering stations from the western Beaufort Sea to the southern Labrador Sea. Specific focus was put on the distribution and lateral propagation of nutrient-rich Pacific-origin water through the Canadian Arctic (chapter 3 and 4) and its regional impact on productivity and water column N inventory (chapter 3).

In chapter 3, I showed the significance of coupled NO_3^- and N_2O isotope measurements in providing constraints on different, yet complementary, N transformation processes that could not be detected based on individual isotope systems alone. In that sense, one important conclusion from this chapter derives from the O isotopic composition of NO_3^-, which indicated the highly remineralized nature of deep and bottom water nutrients in Baffin Bay. This key finding allowed us to ascribe the observed enrichment in the N isotopic composition of NO_3^- to the isotopic signature of particulate organic matter exported from the surface and, as such, identify the source of subsurface NO_3^- that ultimately supports this export production. In the absence of complementary $\delta^{18}O$ measurements, this ^{15}N-enrichment may otherwise have been ascribed to dissimilatory NO_3^- reduction which would similarly lead to an enrichment in ^{15}N (and ^{18}O) of the residual NO_3^- pool. By further combining our NO_3^- isotope data with isotope ratios and isotopomer abundance of N_2O, I provided first evidence for the origin of N_2O accumulating in the deep basin, and showed that sedimentary denitrification may act as a dominant source of the observed deficit in bioavailable N in the deep Baffin Bay. The large range of derived N*-based denitrification rate estimates thus clearly highlights the need for improved estimates of water residence time and source water contributions.

Little is still known about the origin of deep and bottom waters in Baffin Bay, with current mechanisms suggested for deep water formation being relatively hypothetical. Increased sampling along the shelves and along submarine canyons, specifically, may help to gain further insights into deep water formation and source water contributions by putting constraints on the spatial occurrence and extent of cascading events that potentially ventilate the deeper water column in Baffin Bay. Moreover, an increased spatial extent of NO_3^- isotope observations along the shelves would allow to better characterize and quantify nutrient inputs associated with increased meltwater fluxes from Greenland – a process that is not well understood yet and will become increasingly important with ongoing

climate change. Although both the isotopic signature of NO_3^- as well as N_2O isotopomers are consistent with the remineralization of ^{15}N-enriched organic matter and sedimentary denitrification, an increased resolution of bottom water isotope data (especially of N_2O) would further aid to develop a more robust and holistic understanding of bottom water N cycling.

Data presented in this chapter have shown that Baffin Bay bottom water properties are derived from export production in northern Baffin Bay, which is largely fueled by Pacific-derived nutrients advected from the western Arctic. Aspects of this lateral nutrient transport have been investigated in chapter 4, where I examined water column natural abundance N and O isotope ratios of NO_3^- collected during the 2015 Canadian Arctic GEOTRACES along a transect from the Canada Basin through the Canadian Archipelago and towards Baffin Bay. The spatial variability of NO_3^- and N and O isotope ratios revealed distinct west-to-east gradients throughout the Archipelago associated with the distribution of Pacific- and Atlantic-derived waters, and thus the proximity to the western Arctic area of inflow and regions of upwelling. Understanding the distribution and spatial variability of the nutrient-rich halocline layer is specifically important given its impact on both the stability and density structure of the water column (e.g., *Aagaard et al.*, 1981), and Arctic productivity downstream in areas where this subsurface nutrient pool becomes accessible to primary producers. As such, chapter 3 and 4 helped to tease apart locally generated NO_3^- isotope signals versus water mass transport and mixing processes, which is crucial for understanding N cycle processes on a local and basin scale. The data described here (chapter 3 and 4) represent the first NO_3^- and N_2O isotope data for the eastern and central Canadian Arctic to date. While this study only provides a snapshot of N transformations affecting the N inventory of the shallow Archipelago and the deep Baffin Bay, it improved our understanding of current processes and provides a baseline to evaluate changes over time.

Changes in the Arctic due to climate impacts are already affecting shelf-basin interactions, freshwater storage, and nutrient distribution and availability in the Arctic. Specifically, biogeochemical fluxes in the Arctic Ocean are changing due to sea-ice retreat and increased stratification, with associated changes in both light intensity and nutrient supply leading to opposing trends in primary production (e.g., *Arrigo et al.*, 2008; *Tremblay et al.*, 2015). Additional measurements to resolve seasonal patterns of nutrient supply

and the relative contribution of remineralization versus new production would be highly beneficial to better constrain nutrient inventories and fluxes relevant for primary production in different Arctic environments. One aspect that is currently highly understudied in regard to its impact on different N species and their isotope systems is the presence and formation/melt of sea ice, and specific case studies such as for Southern Ocean (e.g., *Fripiat et al.*, 2014) are currently still missing for the Arctic Ocean. In this regard, little is known about the presence and abundance of ice algae, which likely impact isotope ratios associated with both the upper water column dissolved N pool as well as export production and remineralization at depth.

NO_3^- isotope data in the Arctic are still few and far between. As such, recent NO_3^- $\delta^{15}N$ and $\delta^{18}O$ measurements as part of multiple GEOTRACES expeditions critically increased the number of profiles throughout the Arctic (and globally) and thus will help to develop a coherent understanding of N cycling, in particular, and marine biogeochemistry, more generally, on a regional scale and globally.

Overall, this project provides critically important baseline isotope constraints not only on the convoluted water mass composition of both the western equatorial Pacific and the Canadian Arctic that were previously difficult to resolve based on physical parameters alone, but also on nutrient biogeochemistry locally and on a regional scale. The three independent chapters of this thesis each highlight the tight coupling of the biogeochemical and the physical environment, and thus emphasize the importance of – and need for – multi-tracer studies able to bridge between biogeochemical cycling and physical forcing.

APPENDIX A

WEP MIXING MODEL END-MEMBERS

Table A.1: End-members used in three-component mixing model.

			σ_θ (kg m^{-3})	[NO_3^-] (μM)	$\delta^{15}N_{NO3}$ (‰)	$\delta^{18}O_{NO3}$ (‰)	Sal	θ (°C)	O_2 (μmol kg^{-1})	$\delta^{13}C_{DIC}$ (‰)	[$Si(OH)_4$] (μM)
MD	Ave	Upper EUC	24–25.5	4.1	5.5	3.1	34.86	20.1	177	0.43	5.6
	SD			1.7	0.2	0.1	0.02	2.2	9	0.03	0.3
	Ave	Lower EUC	25.5–26	13	6.6	3.7	34.47	14	172	0.36	11.9
	SD			0	0	0	0	0	3	0	0.5
	Ave	Deepest EUC	26–26.5	20.6	7	3.8	34.41	11.8	145	0.19	25
	SD			na	na	na	na	na	na	na	na
	Ave	SAMW	26.5–27.1	33.8	7	3.3	34.4	7.4	89	0.19	45.2
	SD			3.4	0.1	0.2	0.05	1.2	11	0.22	8.2
NH	Ave	Upper EUC	24–25.5	8.6	8.9	3.3	35.64	21.6	124	0.94	3.7
	SD			0.1	0.8	0.4	0.08	1.6	7	0.14	1.2
	Ave	Lower EUC	25.5–26	12.5	8.3	3	35.29	16.7	104	1.1	6.6
	SD			2	0.1	0.1	0.14	1.6	2	0.04	1.1
	Ave	Deepest EUC	26–26.5	13.6	8.3	3	35.16	15.2	102	1.1	11.1
	SD			2.3	0.1	0.1	0.25	2.7	3	0.12	2.9
	Ave	SAMW	26.5–27.1	29.8	6.9	2.6	34.6	8.3	106	0.71	25.5
	SD			4.6	0.2	0.2	0.09	1.5	16	0.08	7.5
PNG	Ave	Upper EUC	24–25.5	7.6	7.6	3	35.5	21.3	165	0.83	2.8
	SD			2.9	0.9	0.4	0.23	3.5	10	0.21	1.7
	Ave	Lower EUC	25.5–26	8.8	7.5	2.9	35.52	19.6	153	0.87	5.6
	SD			3	0.6	0.5	0.08	1.2	11	0.04	2.8
	Ave	Deepest EUC	26–26.5	15.5	6.9	3	35.02	13.4	154	0.84	8.2
	SD			7.2	0.3	0.3	0.08	2.2	9	0.09	1.2
	Ave	SAMW	26.5–27.1	26.7	6.5	2.6	34.51	7.2	156	0.98	22.9
	SD			2.6	0.2	0.3	0.05	1	14	0.11	5.1
EUC	Ave	Upper EUC	24–25.5	11.5	7	2.9	35.2	20.2	125	0.9	7
	SD			2.3	0.3	0.2	0.08	2.8	5	0.1	2.2
	Ave	Lower EUC	25.5–26	15.8	7.1	3	35.2	16.3	123	0.92	12.6
	SD			2.2	0.2	0.3	0.22	2	5	0.1	3.1

APPENDIX B

WEP MIXING MODEL OUTPUT

Table B.1: Mean NO_3^- estimates derived from model simulations indicating the contribution (in μM) of individual sources to upper (24–25.5σ_θ) and lower (25.5–26σ_θ) EUC NO_3^-.

			σ_θ (kg m^{-3})	Upper EUC [NO_3^-] (μM)	Lower EUC [NO_3^-] (μM)
MD	Ave	Upper EUC	24–25.5	0.385	0.295
	SD			0.253	0.213
	Ave	Lower EUC	25.5–26	0.456	0.555
	SD			0.415	0.497
	Ave	Deepest EUC	26–26.5	0.571	0.818
	SD			0.518	0.768
	Ave	SAMW	26.5–27.1	0.878	2.089
	SD			0.758	1.539
NH	Ave	Upper EUC	24–25.5	0.962	0.641
	SD			0.726	0.539
	Ave	Lower EUC	25.5–26	2.885	1.944
	SD			1.521	1.293
	Ave	Deepest EUC	26–26.5	1.758	1.928
	SD			1.419	1.389
	Ave	SAMW	26.5–27.1	1.454	3.497
	SD			1.227	2.353
PNG	Ave	Upper EUC	24–25.5	0.652	0.481
	SD			0.527	0.412
	Ave	Lower EUC	25.5–26	0.947	0.749
	SD			0.742	0.634
	Ave	Deepest EUC	26–26.5	1.074	1.267
	SD			0.955	1.078
	Ave	SAMW	26.5–27.1	0.900	1.728
	SD			0.809	1.405

APPENDIX C

WATER COLUMN PROFILES IN LANCASTER SOUND AND THE LABRADOR SEA

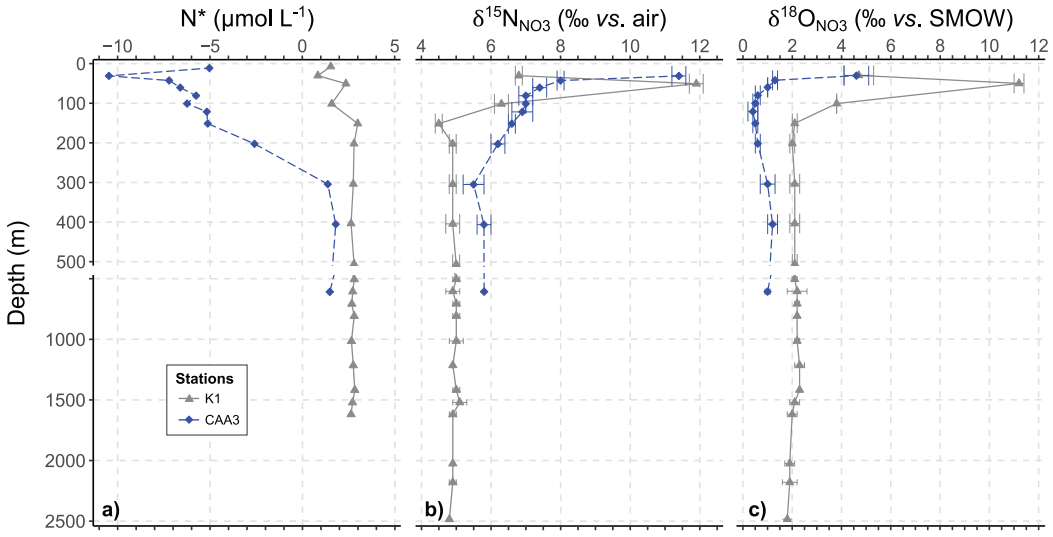

Figure C.1: Water column profiles of (a) N*, (b) $\delta^{15}N_{NO3}$ and (c) $\delta^{18}O_{NO3}$ in Lancaster Sound (blue) and Labrador Sea (grey). Abbreviation indicates standard mean ocean water (SMOW).

APPENDIX D

COPYRIGHT AGREEMENTS

JOHN WILEY AND SONS LICENSE TERMS AND CONDITIONS

Aug 06, 2019

This Agreement between Nadine Lehmann ("You") and John Wiley and Sons ("John Wiley and Sons") consists of your license details and the terms and conditions provided by John Wiley and Sons and Copyright Clearance Center.

License Number	4642801060162
License date	Aug 05, 2019
Licensed Content Publisher	John Wiley and Sons
Licensed Content Publication	Journal of Geophysical Research: Oceans
Licensed Content Title	Isotopic Evidence for the Evolution of Subsurface Nitrate in the Western Equatorial Pacific
Licensed Content Author	Mahyar Mohtadi, Gema Martínez-Méndez, Patrick A. Rafter, et al
Licensed Content Date	Mar 2, 2018
Licensed Content Volume	123
Licensed Content Issue	3
Licensed Content Pages	24
Type of use	Dissertation/Thesis
Requestor type	Author of this Wiley article
Format	Print and electronic
Portion	Full article
Will you be translating?	No
Title of your thesis / dissertation	N and O isotope ratios of NO3- as a tracer for nitrogen cycling and water mass distribution
Expected completion date	Oct 2019
Expected size (number of pages)	200
Requestor Location	Nadine Lehmann LSC Ocean Wing 1355 Oxford St Halifax, NS B3H 4R2 Canada Attn: Nadine Lehmann
Publisher Tax ID	EU826007151
Total	0.00 CAD
Terms and Conditions	

TERMS AND CONDITIONS

This copyrighted material is owned by or exclusively licensed to John Wiley & Sons, Inc. or one of its group companies (each a"Wiley Company") or handled on behalf of a society with which a Wiley Company has exclusive publishing rights in relation to a particular work (collectively "WILEY"). By clicking "accept" in connection with completing this licensing transaction, you agree that the following terms and conditions apply to this transaction (along with the billing and payment terms and conditions established by the Copyright

Clearance Center Inc., ("CCC's Billing and Payment terms and conditions"), at the time that you opened your RightsLink account (these are available at any time at http://myaccount.copyright.com).

Terms and Conditions

- The materials you have requested permission to reproduce or reuse (the "Wiley Materials") are protected by copyright.

- You are hereby granted a personal, non-exclusive, non-sub licensable (on a stand-alone basis), non-transferable, worldwide, limited license to reproduce the Wiley Materials for the purpose specified in the licensing process. This license, **and any CONTENT (PDF or image file) purchased as part of your order,** is for a one-time use only and limited to any maximum distribution number specified in the license. The first instance of republication or reuse granted by this license must be completed within two years of the date of the grant of this license (although copies prepared before the end date may be distributed thereafter). The Wiley Materials shall not be used in any other manner or for any other purpose, beyond what is granted in the license. Permission is granted subject to an appropriate acknowledgement given to the author, title of the material/book/journal and the publisher. You shall also duplicate the copyright notice that appears in the Wiley publication in your use of the Wiley Material. Permission is also granted on the understanding that nowhere in the text is a previously published source acknowledged for all or part of this Wiley Material. Any third party content is expressly excluded from this permission.

- With respect to the Wiley Materials, all rights are reserved. Except as expressly granted by the terms of the license, no part of the Wiley Materials may be copied, modified, adapted (except for minor reformatting required by the new Publication), translated, reproduced, transferred or distributed, in any form or by any means, and no derivative works may be made based on the Wiley Materials without the prior permission of the respective copyright owner.**For STM Signatory Publishers clearing permission under the terms of the STM Permissions Guidelines only, the terms of the license are extended to include subsequent editions and for editions in other languages, provided such editions are for the work as a whole in situ and does not involve the separate exploitation of the permitted figures or extracts,** You may not alter, remove or suppress in any manner any copyright, trademark or other notices displayed by the Wiley Materials. You may not license, rent, sell, loan, lease, pledge, offer as security, transfer or assign the Wiley Materials on a stand-alone basis, or any of the rights granted to you hereunder to any other person.

- The Wiley Materials and all of the intellectual property rights therein shall at all times remain the exclusive property of John Wiley & Sons Inc, the Wiley Companies, or their respective licensors, and your interest therein is only that of having possession of and the right to reproduce the Wiley Materials pursuant to Section 2 herein during the continuance of this Agreement. You agree that you own no right, title or interest in or to the Wiley Materials or any of the intellectual property rights therein. You shall have no rights hereunder other than the license as provided for above in Section 2. No right, license or interest to any trademark, trade name, service mark or other branding ("Marks") of WILEY or its licensors is granted hereunder, and you agree that you shall not assert any such right, license or interest with respect thereto

- NEITHER WILEY NOR ITS LICENSORS MAKES ANY WARRANTY OR REPRESENTATION OF ANY KIND TO YOU OR ANY THIRD PARTY, EXPRESS, IMPLIED OR STATUTORY, WITH RESPECT TO THE MATERIALS

OR THE ACCURACY OF ANY INFORMATION CONTAINED IN THE MATERIALS, INCLUDING, WITHOUT LIMITATION, ANY IMPLIED WARRANTY OF MERCHANTABILITY, ACCURACY, SATISFACTORY QUALITY, FITNESS FOR A PARTICULAR PURPOSE, USABILITY, INTEGRATION OR NON-INFRINGEMENT AND ALL SUCH WARRANTIES ARE HEREBY EXCLUDED BY WILEY AND ITS LICENSORS AND WAIVED BY YOU.

- WILEY shall have the right to terminate this Agreement immediately upon breach of this Agreement by you.

- You shall indemnify, defend and hold harmless WILEY, its Licensors and their respective directors, officers, agents and employees, from and against any actual or threatened claims, demands, causes of action or proceedings arising from any breach of this Agreement by you.

- IN NO EVENT SHALL WILEY OR ITS LICENSORS BE LIABLE TO YOU OR ANY OTHER PARTY OR ANY OTHER PERSON OR ENTITY FOR ANY SPECIAL, CONSEQUENTIAL, INCIDENTAL, INDIRECT, EXEMPLARY OR PUNITIVE DAMAGES, HOWEVER CAUSED, ARISING OUT OF OR IN CONNECTION WITH THE DOWNLOADING, PROVISIONING, VIEWING OR USE OF THE MATERIALS REGARDLESS OF THE FORM OF ACTION, WHETHER FOR BREACH OF CONTRACT, BREACH OF WARRANTY, TORT, NEGLIGENCE, INFRINGEMENT OR OTHERWISE (INCLUDING, WITHOUT LIMITATION, DAMAGES BASED ON LOSS OF PROFITS, DATA, FILES, USE, BUSINESS OPPORTUNITY OR CLAIMS OF THIRD PARTIES), AND WHETHER OR NOT THE PARTY HAS BEEN ADVISED OF THE POSSIBILITY OF SUCH DAMAGES. THIS LIMITATION SHALL APPLY NOTWITHSTANDING ANY FAILURE OF ESSENTIAL PURPOSE OF ANY LIMITED REMEDY PROVIDED HEREIN.

- Should any provision of this Agreement be held by a court of competent jurisdiction to be illegal, invalid, or unenforceable, that provision shall be deemed amended to achieve as nearly as possible the same economic effect as the original provision, and the legality, validity and enforceability of the remaining provisions of this Agreement shall not be affected or impaired thereby.

- The failure of either party to enforce any term or condition of this Agreement shall not constitute a waiver of either party's right to enforce each and every term and condition of this Agreement. No breach under this agreement shall be deemed waived or excused by either party unless such waiver or consent is in writing signed by the party granting such waiver or consent. The waiver by or consent of a party to a breach of any provision of this Agreement shall not operate or be construed as a waiver of or consent to any other or subsequent breach by such other party.

- This Agreement may not be assigned (including by operation of law or otherwise) by you without WILEY's prior written consent.

- Any fee required for this permission shall be non-refundable after thirty (30) days from receipt by the CCC.

- These terms and conditions together with CCC's Billing and Payment terms and conditions (which are incorporated herein) form the entire agreement between you and WILEY concerning this licensing transaction and (in the absence of fraud) supersedes

all prior agreements and representations of the parties, oral or written. This Agreement may not be amended except in writing signed by both parties. This Agreement shall be binding upon and inure to the benefit of the parties' successors, legal representatives, and authorized assigns.

- In the event of any conflict between your obligations established by these terms and conditions and those established by CCC's Billing and Payment terms and conditions, these terms and conditions shall prevail.

- WILEY expressly reserves all rights not specifically granted in the combination of (i) the license details provided by you and accepted in the course of this licensing transaction, (ii) these terms and conditions and (iii) CCC's Billing and Payment terms and conditions.

- This Agreement will be void if the Type of Use, Format, Circulation, or Requestor Type was misrepresented during the licensing process.

- This Agreement shall be governed by and construed in accordance with the laws of the State of New York, USA, without regards to such state's conflict of law rules. Any legal action, suit or proceeding arising out of or relating to these Terms and Conditions or the breach thereof shall be instituted in a court of competent jurisdiction in New York County in the State of New York in the United States of America and each party hereby consents and submits to the personal jurisdiction of such court, waives any objection to venue in such court and consents to service of process by registered or certified mail, return receipt requested, at the last known address of such party.

WILEY OPEN ACCESS TERMS AND CONDITIONS

Wiley Publishes Open Access Articles in fully Open Access Journals and in Subscription journals offering Online Open. Although most of the fully Open Access journals publish open access articles under the terms of the Creative Commons Attribution (CC BY) License only, the subscription journals and a few of the Open Access Journals offer a choice of Creative Commons Licenses. The license type is clearly identified on the article.

The Creative Commons Attribution License

The Creative Commons Attribution License (CC-BY) allows users to copy, distribute and transmit an article, adapt the article and make commercial use of the article. The CC-BY license permits commercial and non-

Creative Commons Attribution Non-Commercial License

The Creative Commons Attribution Non-Commercial (CC-BY-NC)License permits use, distribution and reproduction in any medium, provided the original work is properly cited and is not used for commercial purposes.(see below)

Creative Commons Attribution-Non-Commercial-NoDerivs License

The Creative Commons Attribution Non-Commercial-NoDerivs License (CC-BY-NC-ND) permits use, distribution and reproduction in any medium, provided the original work is properly cited, is not used for commercial purposes and no modifications or adaptations are made. (see below)

Use by commercial "for-profit" organizations

Use of Wiley Open Access articles for commercial, promotional, or marketing purposes requires further explicit permission from Wiley and will be subject to a fee.

Further details can be found on Wiley Online Library

http://olabout.wiley.com/WileyCDA/Section/id-410895.html

Other Terms and Conditions:

v1.10 Last updated September 2015

Questions? customercare@copyright.com or +1-855-239-3415 (toll free in the US) or +1-978-646-2777.

JOHN WILEY AND SONS LICENSE TERMS AND CONDITIONS

Aug 06, 2019

This Agreement between Nadine Lehmann ("You") and John Wiley and Sons ("John Wiley and Sons") consists of your license details and the terms and conditions provided by John Wiley and Sons and Copyright Clearance Center.

License Number	4642801354594
License date	Aug 05, 2019
Licensed Content Publisher	John Wiley and Sons
Licensed Content Publication	Global Biogeochemical Cycles
Licensed Content Title	Remote Western Arctic Nutrients Fuel Remineralization in Deep Baffin Bay
Licensed Content Author	N. Lehmann, M. Kienast, J. Granger, et al
Licensed Content Date	Jun 7, 2019
Licensed Content Volume	33
Licensed Content Issue	6
Licensed Content Pages	19
Type of use	Dissertation/Thesis
Requestor type	Author of this Wiley article
Format	Print and electronic
Portion	Full article
Will you be translating?	No
Title of your thesis / dissertation	N and O isotope ratios of NO3- as a tracer for nitrogen cycling and water mass distribution
Expected completion date	Oct 2019
Expected size (number of pages)	200
Requestor Location	Nadine Lehmann LSC Ocean Wing 1355 Oxford St Halifax, NS B3H 4R2 Canada Attn: Nadine Lehmann
Publisher Tax ID	EU826007151
Total	0.00 CAD
Terms and Conditions	

TERMS AND CONDITIONS

This copyrighted material is owned by or exclusively licensed to John Wiley & Sons, Inc. or one of its group companies (each a"Wiley Company") or handled on behalf of a society with which a Wiley Company has exclusive publishing rights in relation to a particular work (collectively "WILEY"). By clicking "accept" in connection with completing this licensing transaction, you agree that the following terms and conditions apply to this transaction (along with the billing and payment terms and conditions established by the Copyright

Clearance Center Inc., ("CCC's Billing and Payment terms and conditions"), at the time that you opened your RightsLink account (these are available at any time at http://myaccount.copyright.com).

Terms and Conditions

- The materials you have requested permission to reproduce or reuse (the "Wiley Materials") are protected by copyright.

- You are hereby granted a personal, non-exclusive, non-sub licensable (on a stand-alone basis), non-transferable, worldwide, limited license to reproduce the Wiley Materials for the purpose specified in the licensing process. This license, **and any CONTENT (PDF or image file) purchased as part of your order,** is for a one-time use only and limited to any maximum distribution number specified in the license. The first instance of republication or reuse granted by this license must be completed within two years of the date of the grant of this license (although copies prepared before the end date may be distributed thereafter). The Wiley Materials shall not be used in any other manner or for any other purpose, beyond what is granted in the license. Permission is granted subject to an appropriate acknowledgement given to the author, title of the material/book/journal and the publisher. You shall also duplicate the copyright notice that appears in the Wiley publication in your use of the Wiley Material. Permission is also granted on the understanding that nowhere in the text is a previously published source acknowledged for all or part of this Wiley Material. Any third party content is expressly excluded from this permission.

- With respect to the Wiley Materials, all rights are reserved. Except as expressly granted by the terms of the license, no part of the Wiley Materials may be copied, modified, adapted (except for minor reformatting required by the new Publication), translated, reproduced, transferred or distributed, in any form or by any means, and no derivative works may be made based on the Wiley Materials without the prior permission of the respective copyright owner.**For STM Signatory Publishers clearing permission under the terms of the STM Permissions Guidelines only, the terms of the license are extended to include subsequent editions and for editions in other languages, provided such editions are for the work as a whole in situ and does not involve the separate exploitation of the permitted figures or extracts,** You may not alter, remove or suppress in any manner any copyright, trademark or other notices displayed by the Wiley Materials. You may not license, rent, sell, loan, lease, pledge, offer as security, transfer or assign the Wiley Materials on a stand-alone basis, or any of the rights granted to you hereunder to any other person.

- The Wiley Materials and all of the intellectual property rights therein shall at all times remain the exclusive property of John Wiley & Sons Inc, the Wiley Companies, or their respective licensors, and your interest therein is only that of having possession of and the right to reproduce the Wiley Materials pursuant to Section 2 herein during the continuance of this Agreement. You agree that you own no right, title or interest in or to the Wiley Materials or any of the intellectual property rights therein. You shall have no rights hereunder other than the license as provided for above in Section 2. No right, license or interest to any trademark, trade name, service mark or other branding ("Marks") of WILEY or its licensors is granted hereunder, and you agree that you shall not assert any such right, license or interest with respect thereto

- NEITHER WILEY NOR ITS LICENSORS MAKES ANY WARRANTY OR REPRESENTATION OF ANY KIND TO YOU OR ANY THIRD PARTY, EXPRESS, IMPLIED OR STATUTORY, WITH RESPECT TO THE MATERIALS

OR THE ACCURACY OF ANY INFORMATION CONTAINED IN THE MATERIALS, INCLUDING, WITHOUT LIMITATION, ANY IMPLIED WARRANTY OF MERCHANTABILITY, ACCURACY, SATISFACTORY QUALITY, FITNESS FOR A PARTICULAR PURPOSE, USABILITY, INTEGRATION OR NON-INFRINGEMENT AND ALL SUCH WARRANTIES ARE HEREBY EXCLUDED BY WILEY AND ITS LICENSORS AND WAIVED BY YOU.

- WILEY shall have the right to terminate this Agreement immediately upon breach of this Agreement by you.

- You shall indemnify, defend and hold harmless WILEY, its Licensors and their respective directors, officers, agents and employees, from and against any actual or threatened claims, demands, causes of action or proceedings arising from any breach of this Agreement by you.

- IN NO EVENT SHALL WILEY OR ITS LICENSORS BE LIABLE TO YOU OR ANY OTHER PARTY OR ANY OTHER PERSON OR ENTITY FOR ANY SPECIAL, CONSEQUENTIAL, INCIDENTAL, INDIRECT, EXEMPLARY OR PUNITIVE DAMAGES, HOWEVER CAUSED, ARISING OUT OF OR IN CONNECTION WITH THE DOWNLOADING, PROVISIONING, VIEWING OR USE OF THE MATERIALS REGARDLESS OF THE FORM OF ACTION, WHETHER FOR BREACH OF CONTRACT, BREACH OF WARRANTY, TORT, NEGLIGENCE, INFRINGEMENT OR OTHERWISE (INCLUDING, WITHOUT LIMITATION, DAMAGES BASED ON LOSS OF PROFITS, DATA, FILES, USE, BUSINESS OPPORTUNITY OR CLAIMS OF THIRD PARTIES), AND WHETHER OR NOT THE PARTY HAS BEEN ADVISED OF THE POSSIBILITY OF SUCH DAMAGES. THIS LIMITATION SHALL APPLY NOTWITHSTANDING ANY FAILURE OF ESSENTIAL PURPOSE OF ANY LIMITED REMEDY PROVIDED HEREIN.

- Should any provision of this Agreement be held by a court of competent jurisdiction to be illegal, invalid, or unenforceable, that provision shall be deemed amended to achieve as nearly as possible the same economic effect as the original provision, and the legality, validity and enforceability of the remaining provisions of this Agreement shall not be affected or impaired thereby.

- The failure of either party to enforce any term or condition of this Agreement shall not constitute a waiver of either party's right to enforce each and every term and condition of this Agreement. No breach under this agreement shall be deemed waived or excused by either party unless such waiver or consent is in writing signed by the party granting such waiver or consent. The waiver by or consent of a party to a breach of any provision of this Agreement shall not operate or be construed as a waiver of or consent to any other or subsequent breach by such other party.

- This Agreement may not be assigned (including by operation of law or otherwise) by you without WILEY's prior written consent.

- Any fee required for this permission shall be non-refundable after thirty (30) days from receipt by the CCC.

- These terms and conditions together with CCC's Billing and Payment terms and conditions (which are incorporated herein) form the entire agreement between you and WILEY concerning this licensing transaction and (in the absence of fraud) supersedes

all prior agreements and representations of the parties, oral or written. This Agreement may not be amended except in writing signed by both parties. This Agreement shall be binding upon and inure to the benefit of the parties' successors, legal representatives, and authorized assigns.

- In the event of any conflict between your obligations established by these terms and conditions and those established by CCC's Billing and Payment terms and conditions, these terms and conditions shall prevail.

- WILEY expressly reserves all rights not specifically granted in the combination of (i) the license details provided by you and accepted in the course of this licensing transaction, (ii) these terms and conditions and (iii) CCC's Billing and Payment terms and conditions.

- This Agreement will be void if the Type of Use, Format, Circulation, or Requestor Type was misrepresented during the licensing process.

- This Agreement shall be governed by and construed in accordance with the laws of the State of New York, USA, without regards to such state's conflict of law rules. Any legal action, suit or proceeding arising out of or relating to these Terms and Conditions or the breach thereof shall be instituted in a court of competent jurisdiction in New York County in the State of New York in the United States of America and each party hereby consents and submits to the personal jurisdiction of such court, waives any objection to venue in such court and consents to service of process by registered or certified mail, return receipt requested, at the last known address of such party.

WILEY OPEN ACCESS TERMS AND CONDITIONS

Wiley Publishes Open Access Articles in fully Open Access Journals and in Subscription journals offering Online Open. Although most of the fully Open Access journals publish open access articles under the terms of the Creative Commons Attribution (CC BY) License only, the subscription journals and a few of the Open Access Journals offer a choice of Creative Commons Licenses. The license type is clearly identified on the article.

The Creative Commons Attribution License

The Creative Commons Attribution License (CC-BY) allows users to copy, distribute and transmit an article, adapt the article and make commercial use of the article. The CC-BY license permits commercial and non-

Creative Commons Attribution Non-Commercial License

The Creative Commons Attribution Non-Commercial (CC-BY-NC)License permits use, distribution and reproduction in any medium, provided the original work is properly cited and is not used for commercial purposes.(see below)

Creative Commons Attribution-Non-Commercial-NoDerivs License

The Creative Commons Attribution Non-Commercial-NoDerivs License (CC-BY-NC-ND) permits use, distribution and reproduction in any medium, provided the original work is properly cited, is not used for commercial purposes and no modifications or adaptations are made. (see below)

Use by commercial "for-profit" organizations

Use of Wiley Open Access articles for commercial, promotional, or marketing purposes requires further explicit permission from Wiley and will be subject to a fee.

Further details can be found on Wiley Online Library

http://olabout.wiley.com/WileyCDA/Section/id-410895.html

Other Terms and Conditions:

v1.10 Last updated September 2015

Questions? customercare@copyright.com or +1-855-239-3415 (toll free in the US) or +1-978-646-2777.

BIBLIOGRAPHY

Aagaard, K., L. K. Coachman, and E. Carmack, On the halocline of the Arctic Ocean, *Deep Sea Research Part A. Oceanographic Research Papers*, *28*, 529–545, 1981.

Ahmed, M., B. G. T. Else, T. M. Burgers, and T. Papakyriakou, Variability of surface water pCO_2 in the Canadian Arctic Archipelago from 2010 to 2016, *Journal of Geophysical Research: Oceans*, *124*, 1876–1896, 2019.

Aksenov, Y., M. Karcher, A. Proshutinsky, R. Gerdes, B. De Cuevas, E. Golubeva, F. Kauker, A. T. Nguyen, G. A. Platov, and M. Wadley, Arctic pathways of Pacific Water: Arctic Ocean Model Intercomparison experiments, *Journal of Geophysical Research: Oceans*, *121*, 27–59, 2016.

Alkire, M. B., R. Rember, and I. Polyakov, Discrepancy in the identification of the Atlantic/Pacific front in the central Arctic Ocean: NO versus nutrient relationships, *Geophysical Research Letters*, *46*, 3843–3852, 2019.

Altabet, M. A., Nitrogen isotopic evidence for micronutrient control of fractional NO_3^- utilization in the equatorial Pacific, *Limnology and Oceanography*, *46*, 368–380, 2001.

Altabet, M. A., and R. Francois, Sedimentary nitrogen isotopic ratio as a recorder for surface ocean nitrate utilization, *Global Biogeochemical Cycles*, *8*, 103–116, 1994.

Altabet, M. A., C. Pilskaln, R. Thunell, C. Pride, D. M. Sigman, F. Chavez, and R. Francois, The nitrogen isotope biogeochemistry of sinking particles from the margin of the eastern North Pacific, *Deep-Sea Research Part I: Oceanographic Research Papers*, *46*, 655–679, 1999.

Altabet, M. A., M. J. Higginson, and D. W. Murray, The effect of millennial-scale changes in Arabian Sea denitrification on atmospheric CO_2, *Nature*, *415*, 159–162, 2002.

Anderson, L. A., On the hydrogen and oxygen content of marine phytoplankton, *Deep Sea Research Part I: Oceanographic Research Papers*, *42*, 1675–1680, 1995.

Anderson, L. A., and J. L. Sarmiento, Redfield ratios of remineralization determined by nutrient data analysis, *Global biogeochemical cycles*, *8*, 65–80, 1994.

Ardyna, M., M. Gosselin, C. Michel, M. Poulin, and J.-É. Tremblay, Environmental forcing of phytoplankton community structure and function in the Canadian High Arctic: Contrasting oligotrophic and eutrophic regions, *Marine Ecology Progress Series*, *442*, 37–57, 2011.

Armstrong, F. A. J., C. R. Stearns, and J. D. H. Strickland, The measurement of upwelling and subsequent biological process by means of the Technicon Autoanalyzer and associated equipment, *Deep Sea Research*, *14*, 381–389, 1967.

Arrigo, K. R., and G. L. van Dijken, Secular trends in Arctic Ocean net primary production, *Journal of Geophysical Research: Oceans*, *116*, 2011.

Arrigo, K. R., G. van Dijken, and S. Pabi, Impact of a shrinking Arctic ice cover on marine primary production, *Geophysical Research Letters*, *35*, 2008.

Azetsu-Scott, K., B. Petrie, P. Yeats, and C. Lee, Composition and fluxes of freshwater through Davis Strait using multiple chemical tracers, *Journal of Geophysical Research: Oceans*, *117*, 2012.

Bailey, W. B., On the origin of deep Baffin Bay water, *Journal of the Fisheries Board of Canada*, *13*, 303–308, 1956.

Bauch, D., M. R. van der Loeff, N. Andersen, S. Torres-Valdes, K. Bakker, and E. P. Abrahamsen, Origin of freshwater and polynya water in the Arctic Ocean halocline in summer 2007, *Progress in Oceanography*, *91*, 482–495, 2011.

Bélanger, S., M. Babin, and J.-É. Tremblay, Increasing cloudiness in Arctic damps the increase in phytoplankton primary production due to sea ice receding, *Biogeosciences*, *10*, 4087–4101, 2013.

Ben-David, M., T. A. Hanley, D. R. Klein, and D. M. Schell, Seasonal changes in diets of coastal and riverine mink: the role of spawning Pacific salmon, *Canadian Journal of Zoology*, *75*, 803–811, 1997.

Bergeron, M., and J.-É. Tremblay, Shifts in biological productivity inferred from nutrient drawdown in the southern Beaufort Sea (2003–2011) and northern Baffin Bay (1997–2011), Canadian Arctic, *Geophysical Research Letters*, *41*, 3979–3987, 2014.

Berthelot, H., M. Benavides, P. H. Moisander, O. Grosso, and S. Bonnet, High-nitrogen fixation rates in the particulate and dissolved pools in the Western Tropical Pacific (Solomon and Bismarck Seas), *Geophysical Research Letters*, *44*, 8414–8423, 2017.

Bianchi, D., T. S. Weber, R. Kiko, and C. Deutsch, Global niche of marine anaerobic metabolisms expanded by particle microenvironments, *Nature Geoscience*, *11*, 263–268, 2018.

Bingham, F. M., and R. Lukas, The southward intrusion of North Pacific Intermediate Water along the Mindanao Coast, *Journal of Physical Oceanography*, *24*, 141–154, 1994.

Bingham, F. M., and R. Lukas, The distribution of intermediate water in the western equatorial Pacific during January–February 1986, *Deep Sea Research Part I: Oceanographic Research Papers*, *42*, 1545–1573, 1995.

Blais, M., J.-É. Tremblay, A. D. Jungblut, J. Gagnon, J. Martin, M. Thaler, and C. Lovejoy, Nitrogen fixation and identification of potential diazotrophs in the Canadian Arctic, *Global Biogeochemical Cycles*, *26*, 2012.

Blanke, B., and S. Raynaud, Kinematics of the Pacific Equatorial Undercurrent: An Eulerian and Lagrangian approach from GCM results, *Journal of Physical Oceanography*, *27*, 1038–1053, 1997.

Böhlke, J. K., S. J. Mroczkowski, and T. B. Coplen, Oxygen isotopes in nitrate: new reference materials for ^{18}O:^{17}O:^{16}O measurements and observations on nitrate-water equilibration, *Rapid Communications in Mass Spectrometry*, *17*, 1835–1846, 2003.

Bonnet, S., I. C. Biegala, P. Dutrieux, L. O. Slemons, and D. G. Capone, Nitrogen fixation in the western equatorial Pacific: Rates, diazotrophic cyanobacterial size class distribution, and biogeochemical significance, *Global Biogeochemical Cycles*, *23*, 2009.

Bonnet, S., M. Rodier, K. A. TurkKubo, C. Germineaud, C. Menkes, A. Ganachaud, S. Cravatte, P. Raimbault, E. Campbell, and F. Quéroué, Contrasted geographical distribution of N_2 fixation rates and nifH phylotypes in the Coral and Solomon Seas (southwestern Pacific) during austral winter conditions, *Global Biogeochemical Cycles*, *29*, 1874–1892, 2015.

Bostock, H. C., B. N. Opdyke, and M. J. Williams, Characterising the intermediate depth waters of the Pacific Ocean using $\delta^{13}C$ and other geochemical tracers, *Deep Sea Research Part I: Oceanographic Research Papers*, *57*, 847–859, 2010.

Bostock, H. C., P. J. Sutton, M. J. M. Williams, and B. N. Opdyke, Reviewing the circulation and mixing of Antarctic Intermediate Water in the South Pacific using evidence from geochemical tracers and Argo float trajectories, *Deep-Sea Research Part I: Oceanographic Research Papers*, *73*, 84–98, 2013.

Bourbonnais, A., M. A. Altabet, C. N. Charoenpong, J. Larkum, H. Hu, H. W. Bange, and L. Stramma, Nloss isotope effects in the Peru oxygen minimum zone studied using a mesoscale eddy as a natural tracer experiment, *Global Biogeochemical Cycles*, *29*, 793–811, 2015.

Bourbonnais, A., R. T. Letscher, H. W. Bange, V. Échevin, J. Larkum, J. Mohn, N. Yoshida, and M. A. Altabet, N_2O production and consumption from stable isotopic and concentration data in the Peruvian coastal upwelling system, *Global Biogeochemical Cycles*, *31*, 678–698, 2017.

Bourke, R. H., and R. G. Paquette, Formation of Baffin Bay bottom and deep waters, in *Elsevier Oceanography Series*, vol. 57, pp. 135–155, Elsevier, 1991.

Bowen, J. L., P. J. Kearns, M. Holcomb, and B. B. Ward, Acidification alters the composition of ammonia-oxidizing microbial assemblages in marine mesocosms, *Marine Ecology Progress Series*, *492*, 1–8, 2013.

Brandes, J. A., and A. H. Devol, Isotopic fractionation of oxygen and nitrogen in coastal marine sediments, *Geochimica et Cosmochimica Acta*, *61*, 1793–1801, 1997.

Brandes, J. A., A. H. Devol, T. Yoshinari, D. A. Jayakumar, and S. W. A. Naqvi, Isotopic composition of nitrate in the central Arabian Sea and eastern tropical North Pacific: A tracer for mixing and nitrogen cycles, *Limnology and Oceanography*, *43*, 1680–1689, 1998.

Broecker, W. S., NO, a conservative water-mass tracer, *Earth and Planetary Science Letters*, *23*, 100–107, 1974.

Broecker, W. S., and T.-H. Peng, *Tracers in the a Sea*, Lamont-Doherty Geological Observatory, Columbia University, Palisades, New York, 1982.

Brown, Z. W., K. L. Casciotti, R. S. Pickart, J. H. Swift, and K. R. Arrigo, Aspects of the marine nitrogen cycle of the Chukchi Sea shelf and Canada Basin, *Deep Sea Research Part II: Topical Studies in Oceanography*, *118*, 73–87, 2015a.

Brown, Z. W., K. E. Lowry, M. A. Palmer, G. L. van Dijken, M. M. Mills, R. S. Pickart, and K. R. Arrigo, Characterizing the subsurface chlorophyll a maximum in the Chukchi Sea and Canada Basin, *Deep Sea Research Part II: Topical Studies in Oceanography*, *118*, 88–104, 2015b.

Buchwald, C., and K. L. Casciotti, Oxygen isotopic fractionation and exchange during bacterial nitrite oxidation, *Limnology and Oceanography*, *55*, 1064–1074, 2010.

Buchwald, C., and K. L. Casciotti, Isotopic ratios of nitrite as tracers of the sources and age of oceanic nitrite, *Nature Geoscience*, *6*, 308–313, 2013.

Buchwald, C., A. E. Santoro, M. R. McIlvin, and K. L. Casciotti, Oxygen isotopic composition of nitrate and nitrite produced by nitrifying cocultures and natural marine assemblages, *Limnology and Oceanography*, *57*, 1361–1375, 2012.

Buchwald, C., A. E. Santoro, R. H. R. Stanley, and K. L. Casciotti, Nitrogen cycling in the secondary nitrite maximum of the eastern tropical North Pacific off Costa Rica, *Global Biogeochemical Cycles*, *29*, 2061–2081, 2015.

Butt, J., and E. Lindstrom, Currents off the east coast of New Ireland, Papua New Guinea, and their relevance to regional undercurrents in the Western Equatorial Pacific Ocean, 1994.

Carmack, E., D. Barber, J. Christensen, R. Macdonald, B. Rudels, and E. Sakshaug, Climate variability and physical forcing of the food webs and the carbon budget on panarctic shelves, *Progress in Oceanography*, *71*, 145–181, 2006.

Carmack, E. C., and F. A. McLaughlin, Towards recognition of physical and geochemical change in Subarctic and Arctic Seas, *Progress in Oceanography*, *90*, 90–104, 2011.

Carpenter, E. J., H. Harvey, B. Fry, and D. G. Capone, Biogeochemical tracers of the marine cyanobacterium Trichodesmium, *Deep Sea Research Part I: Oceanographic Research Papers*, *44*, 27–38, 1997.

Carpenter, J. H., The Chesapeake Bay Institute Technique for the Winkler dissolved oxygen method, *Limnology and Oceanography*, *10*, 141–143, 1965.

Casciotti, K. L., and M. R. McIlvin, Isotopic analyses of nitrate and nitrite from reference mixtures and application to Eastern Tropical North Pacific waters, *Marine Chemistry*, *107*, 184–201, 2007.

Casciotti, K. L., D. M. Sigman, M. G. Hastings, J. K. Böhlke, and A. Hilkert, Measurement of the oxygen isotopic composition of nitrate in seawater and freshwater using the denitrifier method, *Analytical Chemistry*, *74*, 4905–4912, 2002.

Casciotti, K. L., D. M. Sigman, and B. B. Ward, Linking diversity and stable isotope fractionation in ammonia-oxidizing bacteria, *Geomicrobiology Journal*, *20*, 335–353, 2003.

Casciotti, K. L., T. W. Trull, D. M. Glover, and D. Davies, Constraints on nitrogen cycling at the subtropical North Pacific Station ALOHA from isotopic measurements of nitrate and particulate nitrogen, *Deep Sea Research Part II: Topical Studies in Oceanography*, *55*, 1661–1672, 2008.

Casciotti, K. L., C. Buchwald, and M. McIlvin, Implications of nitrate and nitrite isotopic measurements for the mechanisms of nitrogen cycling in the Peru oxygen deficient zone, *Deep Sea Research Part I: Oceanographic Research Papers*, *80*, 78–93, 2013.

Casciotti, K. L., M. Forbes, J. Vedamati, B. D. Peters, T. S. Martin, and C. W. Mordy, Nitrous oxide cycling in the Eastern Tropical South Pacific as inferred from isotopic and isotopomeric data, *Deep Sea Research Part II: Topical Studies in Oceanography*, 2018.

Castrillejo, M., N. Casacuberta, M. Christl, C. Vockenhuber, H.-A. Synal, M. I. García-Ibáñez, P. Lherminier, G. Sarthou, J. Garcia-Orellana, and P. Masqué, Tracing water masses with ^{129}I and ^{236}U in the subpolar North Atlantic along the GEOTRACES GA01 section, *Biogeosciences*, *15*, 5545–5564, 2018.

Chang, B. X., and A. H. Devol, Seasonal and spatial patterns of sedimentary denitrification rates in the Chukchi sea, *Deep-Sea Research Part II: Topical Studies in Oceanography*, *56*, 1339–1350, 2009.

Coachman, L. K., and C. A. Barnes, The contribution of Bering Sea water to the Arctic Ocean, *Arctic*, *14*, 147–161, 1961.

Coachman, L. K., K. Aagaard, and R. B. Tripp, *Bering Strait: the regional physical oceanography*, Seattle, University of Washington Press, 1975.

Codispoti, L. A., An oceanic fixed nitrogen sink exceeding 400 Tg N a^{-1} vs the concept of homeostasis in the fixed-nitrogen inventory, *Biogeosciences Discussions*, *3*, 1203–1246, 2007.

Codispoti, L. A., C. Flagg, V. Kelly, and J. H. Swift, Hydrographic conditions during the 2002 SBI process experiments, *Deep Sea Research Part II: Topical Studies in Oceanography*, *52*, 3199–3226, 2005.

Codispoti, L. A., V. Kelly, A. Thessen, P. Matrai, S. Suttles, V. Hill, M. Steele, and B. Light, Synthesis of primary production in the Arctic Ocean: III. Nitrate and phosphate based estimates of net community production, *Progress in Oceanography*, *110*, 126–150, 2013.

Cohen, Y., and L. I. Gordon, Nitrous oxide in the oxygen minimum of the eastern tropical North Pacific: Evidence for its consumption during denitrification and possible mechanisms for its production, *Deep Sea Research*, *25*, 509–524, 1978.

Cooper, L. W., T. E. Whitledge, J. M. Grebmeier, and T. Weingartner, The nutrient, salinity, and stable oxygen isotope composition of Bering and Chukchi Seas waters in and near the Bering Strait, *Journal of Geophysical Research: Oceans*, *102*, 12563–12573, 1997.

Cota, G. F., and E. P. W. Horne, Physical control of Arctic ice algal production, *Marine Ecology Progress Series*, *52*, 111–121, 1989.

Cota, G. F., S. J. Prinsenberg, E. B. Bennett, J. W. Loder, M. R. Lewis, J. L. Anning, N. H. F. Watson, and L. R. Harris, Nutrient fluxes during extended blooms of Arctic ice algae, *Journal of Geophysical Research: Oceans*, *92*, 1951–1962, 1987.

Cravatte, S., A. Ganachaud, Q.-P. P. Duong, W. S. Kessler, G. Eldin, and P. Dutrieux, Observed circulation in the Solomon Sea from SADCP data, *Progress in Oceanography*, *88*, 116–130, 2011.

Curry, B., C. M. Lee, and B. Petrie, Volume, freshwater, and heat fluxes through Davis Strait, 2004–05, *Journal of Physical Oceanography*, *41*, 429–436, 2011.

Deutsch, C., N. Gruber, R. M. Key, J. L. Sarmiento, and A. Ganachaud, Denitrification and N_2 fixation in the Pacific Ocean, *Global Biogeochemical Cycles*, *15*, 483–506, 2001.

Deutsch, C., J. L. Sarmiento, D. M. Sigman, N. Gruber, and J. P. Dunne, Spatial coupling of nitrogen inputs and losses in the ocean, *Nature*, *445*, 163–167, 2007.

Devol, A. H., L. A. Codispoti, and J. P. Christensen, Summer and winter denitrification rates in western Arctic shelf sediments, *Continental Shelf Research*, *17*, 1029–1050, 1997.

DiFiore, P. J., D. M. Sigman, T. W. Trull, M. J. Lourey, K. Karsh, G. Cane, and R. Ho, Nitrogen isotope constraints on subantarctic biogeochemistry, *Journal of Geophysical Research: Oceans*, *111*, 2006.

DiFiore, P. J., D. M. Sigman, and R. B. Dunbar, Upper ocean nitrogen fluxes in the Polar Antarctic Zone: Constraints from the nitrogen and oxygen isotopes of nitrate, *Geochemistry, Geophysics, Geosystems*, *10*, 2009.

DiFiore, P. J., D. M. Sigman, K. L. Karsh, T. W. Trull, R. B. Dunbar, and R. S. Robinson, Poleward decrease in the isotope effect of nitrate assimilation across the Southern Ocean, *Geophysical Research Letters*, *37*, 2010.

Dugdale, R. C., A. G. Wischmeyer, F. P. Wilkerson, R. T. Barber, F. Chai, M.-S. Jiang, and T.-H. Peng, Meridional asymmetry of source nutrients to the equatorial Pacific upwelling ecosystem and its potential impact on ocean–atmosphere CO_2 flux; a data and modeling approach, *Deep Sea Research Part II: Topical Studies in Oceanography*, *49*, 2513–2531, 2002.

Ekwurzel, B., P. Schlosser, R. A. Mortlock, R. G. Fairbanks, and J. H. Swift, River runoff, sea ice meltwater, and Pacific water distribution and mean residence times in the Arctic Ocean, *Journal of Geophysical Research: Oceans*, *106*, 9075–9092, 2001.

Falkowski, P. G., R. T. Barber, and V. Smetacek, Biogeochemical controls and feedbacks on ocean primary production, *Science*, *281*, 200–206, 1998.

Farías, L., M. Castro-González, M. Cornejo, J. Charpentier, J. Faúndez, N. Boontanon, and N. Yoshida, Denitrification and nitrous oxide cycling within the upper oxycline of the eastern tropical South Pacific oxygen minimum zone, *Limnology and Oceanography*, *54*, 132–144, 2009.

Fawcett, S. E., M. W. Lomas, J. R. Casey, B. B. Ward, and D. M. Sigman, Assimilation of upwelled nitrate by small eukaryotes in the Sargasso Sea, *Nature Geoscience*, *4*, 717–722, 2011.

Fenwick, L., D. Capelle, E. Damm, S. Zimmermann, W. J. Williams, S. Vagle, and P. D. Tortell, Methane and nitrous oxide distributions across the North American Arctic Ocean during summer, 2015, *Journal of Geophysical Research: Oceans*, *122*, 390–412, 2017.

Fine, R. A., W. H. Peterson, and H. G. Ostlund, The penetration of tritium into the Tropical Pacific, *Journal of Physical Oceanography*, *17*, 553–564, 1987.

Fine, R. A., R. Lukas, F. M. Bingham, M. J. Warner, and R. H. Gammon, The western equatorial Pacific: A water mass crossroads, *Journal of Geophysical Research: Oceans*, *99*, 25063–25080, 1994.

Flückiger, J., A. Dällenbach, T. Blunier, B. Stauffer, T. F. Stocker, D. Raynaud, and J.-M. Barnola, Variations in atmospheric N_2O concentration during abrupt climatic changes, *Science*, *285*, 227–230, 1999.

Fowler, D., M. Coyle, U. Skiba, M. A. Sutton, J. N. Cape, S. Reis, L. J. Sheppard, A. Jenkins, B. Grizzetti, J. N. Galloway, P. Vitousek, A. Leach, A. F. Bouwman, K. Butterbach-Bahl, F. Dentener, D. Stevenson, M. Amann, and M. Voss, The global nitrogen cycle in the twenty-first century, *Philosophical Transactions of the Royal Society B: Biological Sciences*, *368*, 2013.

Frame, C. H., and K. L. Casciotti, Biogeochemical controls and isotopic signatures of nitrous oxide production by a marine ammonia-oxidizing bacterium, *Biogeosciences*, *7*, 2695–2709, 2010.

Frame, C. H., E. Deal, C. D. Nevison, and K. L. Casciotti, N_2O production in the eastern South Atlantic: Analysis of N_2O stable isotopic and concentration data, *Global Biogeochemical Cycles*, *28*, 1262–1278, 2014.

Fripiat, F., D. M. Sigman, S. E. Fawcett, P. A. Rafter, M. A. Weigand, and J.-L. Tison, New insights into sea ice nitrogen biogeochemical dynamics from the nitrogen isotopes, *Global Biogeochemical Cycles*, *28*, 115–130, 2014.

Fripiat, F., M. Declercq, C. J. Sapart, L. G. Anderson, V. Bruechert, F. Deman, D. FonsecaBatista, C. Humborg, A. Roukaerts, I. P. Semiletov, and F. Dehairs, Influence of the bordering shelves on nutrient distribution in the Arctic halocline inferred from water column nitrate isotopes, *Limnology and Oceanography*, *63*, 2154–2170, 2018.

Fukumori, I., T. Lee, B. Cheng, and D. Menemenlis, The origin, pathway, and destination of Niño-3 water estimated by a simulated passive tracer and its adjoint, *Journal of Physical Oceanography*, *34*, 582–604, 2004.

Ganesh, S., L. A. Bristow, M. Larsen, N. Sarode, B. Thamdrup, and F. J. Stewart, Size-fraction partitioning of community gene transcription and nitrogen metabolism in a marine oxygen minimum zone, *The Isme Journal*, *9*, 2682–2696, 2015.

Garcia, H. E., and L. I. Gordon, Oxygen solubility in seawater: Better fitting equations, *Limnology and Oceanography*, *37*, 1307–1312, 1992.

Garcia-Ibanez, M. I., F. F. Pérez, P. Lherminier, P. Zunino, H. Mercier, and P. Tréguer, Water mass distributions and transports for the 2014 GEOVIDE cruise in the North Atlantic, *Biogeosciences*, *15*, 2075–2090, 2018.

Gasparin, F., C. Maes, J. Sudre, V. Garcon, and A. Ganachaud, Water mass analysis of the Coral Sea through an optimum multiparameter method, *Journal of Geophysical Research: Oceans*, *119*, 7229–7244, 2014.

Germineaud, C., A. Ganachaud, J. Sprintall, S. Cravatte, G. Eldin, M. S. Alberty, and E. Privat, Pathways and water mass properties of the thermocline and intermediate waters in the Solomon Sea, *Journal of Physical Oceanography*, *46*, 3031–3049, 2016.

Godfrey, J. S., The effect of the Indonesian throughflow on ocean circulation and heat exchange with the atmosphere: A review, *Journal of Geophysical Research: Oceans*, *101*, 12217–12237, 1996.

Gonfiantini, R., Stable isotope reference samples for geochemical and hydrological investigations, *The International Journal of Applied Radiation and Isotopes*, *35*, 1984.

Gordon, A. L., and R. a. Fine, Pathways of water between the Pacific and Indian oceans in the Indonesian seas, *Nature*, *379*, 146–149, 1996.

Goreau, T. J., W. A. Kaplan, S. C. Wofsy, M. B. McElroy, F. W. Valois, and S. W. Watson, Production of NO_2^- and N_2O by nitrifying bacteria at reduced concentrations of oxygen, *Applied and Environmental Microbiology*, *40*, 526–532, 1980.

Grabb, K. C., C. Buchwald, C. M. Hansel, and S. D. Wankel, A dual nitrite isotopic investigation of chemodenitrification by mineral-associated Fe(II) and its production of nitrous oxide, *Geochimica et Cosmochimica Acta*, *196*, 388–402, 2017.

Granger, J., and D. M. Sigman, Removal of nitrite with sulfamic acid for nitrate N and O isotope analysis with the denitrifier method, *Rapid Communications in Mass Spectrometry*, *23*, 3753–3762, 2009.

Granger, J., and S. D. Wankel, Isotopic overprinting of nitrification on denitrification as a ubiquitous and unifying feature of environmental nitrogen cycling, *Proceedings of the National Academy of Sciences of the United States of America*, *113*, E6391–E6400, 2016.

Granger, J., D. M. Sigman, J. A. Needoba, and P. J. Harrison, Coupled nitrogen and oxygen isotope fractionation of nitrate during assimilation by cultures of marine phytoplankton, *Limnology and Oceanography*, *49*, 1763–1773, 2004.

Granger, J., D. M. Sigman, M. F. Lehmann, and P. D. Tortell, Nitrogen and oxygen isotope fractionation during dissimilatory nitrate reduction by denitrifying bacteria, *Limnology and Oceanography*, *53*, 2533–2545, 2008.

Granger, J., D. M. Sigman, M. Rohde, M. T. Maldonado, and P. D. Tortell, N and O isotope effects during nitrate assimilation by unicellular prokaryotic and eukaryotic plankton cultures, *Geochimica et Cosmochimica Acta*, *74*, 1030–1040, 2010.

Granger, J., M. G. Prokopenko, D. M. Sigman, C. W. Mordy, Z. M. Morse, L. V. Morales, R. N. Sambrotto, and B. Plessen, Coupled nitrification-denitrification in sediment of the eastern Bering Sea shelf leads to ^{15}N enrichment of fixed N in shelf waters, *Journal of Geophysical Research: Oceans*, *116*, 2011.

Granger, J., M. G. Prokopenko, C. W. Mordy, and D. M. Sigman, The proportion of remineralized nitrate on the ice-covered eastern Bering Sea shelf evidenced from the oxygen isotope ratio of nitrate, *Global Biogeochemical Cycles*, *27*, 962–971, 2013.

Granger, J., D. M. Sigman, J. Gagnon, J.-E. Tremblay, and A. Mucci, On the properties of the Arctic halocline and deep water masses of the Canada Basin from nitrate isotope ratios, *Journal of Geophysical Research: Oceans*, *123*, 5443–5458, 2018.

Grasshoff, K., A simultaneous multiple channel system for nutrient analysis in seawater with analog and digital analog record, *Advances in Automated Analysis, Technicon International Conference*, *11*, 133–145, 1969.

Grenier, M., S. Cravatte, B. Blanke, C. Menkes, A. KochLarrouy, F. Durand, A. Mélet, and C. Jeandel, From the western boundary currents to the Pacific Equatorial Undercurrent: Modeled pathways and water mass evolutions, *Journal of Geophysical Research: Oceans*, *116*, 2011.

Grenier, M., C. Jeandel, F. Lacan, D. Vance, C. Venchiarutti, A. Cros, and S. Cravatte, From the subtropics to the central equatorial Pacific Ocean: Neodymium isotopic composition and rare earth element concentration variations, *Journal of Geophysical Research: Oceans*, *118*, 592–618, 2013.

Grenier, M., C. Jeandel, and S. Cravatte, From the subtropics to the equator in the Southwest Pacific: Continental material fluxes quantified using neodymium data along modeled thermocline water pathways, *Journal of Geophysical Research: Oceans*, *119*, 3948–3966, 2014.

Grivault, N., X. Hu, and P. G. Myers, Evolution of Baffin Bay water masses and transports in a numerical sensitivity experiment under enhanced Greenland melt, *Atmosphere - Ocean*, *55*, 169–194, 2017.

Gruber, N., The dynamics of the marine nitrogen cycle and its influence on atmospheric CO2 variations, in *The ocean carbon cycle and climate*, pp. 97–148, Springer, 2004.

Gruber, N., Elusive marine nitrogen fixation, *Proceedings of the National Academy of Sciences*, *113*, 4246–4248, 2016.

Gruber, N., and J. L. Sarmiento, Global patterns of marine nitrogen fixation and denitrification, *Global Biogeochemical Cycles*, *11*, 235–266, 1997.

Grundle, D. S., R. Maranger, and S. K. Juniper, Upper water column nitrous oxide distributions in the northeast subarctic Pacific Ocean, *Atmosphere - Ocean*, *50*, 475–486, 2012.

Hamilton, J., and Y. Wu, *Synopsis and trends in the physical environment of Baffin Bay and Davis Strait*, Ocean and Ecosystem Sciences Division, Maritimes Region, Fisheries and Oceans Canada, 2013.

Hansell, D. A., and R. A. Feely, Atmospheric intertropical convergence impacts surface ocean carbon and nitrogen biogeochemistry in the western tropical Pacific, *Geophysical Research Letters*, *27*, 1013–1016, 2000.

Harding, K., K. A. Turk-Kubo, R. E. Sipler, M. M. Mills, D. A. Bronk, and J. P. Zehr, Symbiotic unicellular cyanobacteria fix nitrogen in the Arctic Ocean, *Proceedings of the National Academy of Sciences*, *115*, 13371–13375, 2018.

Hirota, A., A. Ijiri, D. D. Komatsu, S. B. Ohkubo, F. Nakagawa, and U. Tsunogai, Enrichment of nitrous oxide in the water columns in the area of the Bering and Chukchi Seas, *Marine Chemistry*, *116*, 47–53, 2009.

Hoering, T. C., and H. T. Ford, The isotope effect in the fixation of nitrogen by azotobacter, *Journal of the American Chemical Society*, *82*, 376–378, 1960.

Holmes, R. M., A. Aminot, R. Kérouel, B. A. Hooker, and B. J. Peterson, A simple and precise method for measuring ammonium in marine and freshwater ecosystems, *Canadian Journal of Fisheries and Aquatic Sciences*, *56*, 1801–1808, 1999.

Hughes, K. G., J. M. Klymak, X. Hu, and P. G. Myers, Water mass modification and mixing rates in a 1/12° simulation of the Canadian Arctic Archipelago, *Journal of Geophysical Research: Oceans*, *122*, 803–820, 2017.

Izumo, T., J. Picaut, and B. Blanke, Tropical pathways, equatorial undercurrent variability and the 1998 La Niña, *Geophysical research letters*, *29*, 2002.

Jickells, T. D., Z. S. An, K. K. Andersen, A. R. Baker, G. Bergametti, N. Brooks, J. J. Cao, P. W. Boyd, R. A. Duce, K. A. Hunter, H. Kawahata, N. Kubilay, J. LaRoche, P. S. Liss, N. Mahowald, J. M. Prospero, A. J. Ridgwell, I. Tegen, and R. Torres, Global iron connections between desert dust, ocean biogeochemistry, and climate, *Science*, *308*, 67–71, 2005.

Johnson, G. C., and J. M. Toole, Flow of deep and bottom waters in the Pacific at 10°N, *Deep Sea Research Part I: Oceanographic Research Papers*, *40*, 371–394, 1993.

Johnson, G. C., B. M. Sloyan, W. S. Kessler, and K. E. McTaggart, Direct measurements of upper ocean currents and water properties across the tropical Pacific during the 1990s, *Progress in Oceanography*, *52*, 31–61, 2002.

Jones, E. P., Tracing Pacific water in the North Atlantic Ocean, *Journal of Geophysical Research*, *108*, 3116, 2003.

Jones, E. P., and L. G. Anderson, On the origin of the chemical properties of the Arctic Ocean halocline, *Journal of Geophysical Research: Oceans*, *91*, 10759–10767, 1986.

Jones, E. P., and A. R. Coote, Nutrient distributions in the Canadian Archipelago: Indicators of summer water mass and flow characteristics, *Canadian Journal of Fisheries and Aquatic Sciences*, *37*, 589–599, 1980.

Jones, E. P., D. Dyrssen, and A. R. Coote, Nutrient regeneration in deep Baffin Bay with consequences for measurements of the conservative tracer NO and fossil fuel CO_2 in the oceans, *Canadian Journal of Fisheries and Aquatic Sciences*, *41*, 30–35, 1984.

Jones, E. P., L. G. Anderson, and J. H. Swift, Distribution of Atlantic and Pacific waters in the upper Arctic Ocean: Implications for circulation, *Geophysical Research Letters*, *25*, 765–768, 1998.

Kalvelage, T., G. Lavik, P. Lam, S. Contreras, L. Arteaga, C. R. Löscher, A. Oschlies, A. Paulmier, L. Stramma, and M. M. M. Kuypers, Nitrogen cycling driven by organic matter export in the South Pacific oxygen minimum zone, *Nature Geoscience*, *6*, 228–234, 2013.

Karl, D., R. Letelier, L. Tupas, J. Dore, J. Christian, and D. Hebel, The role of nitrogen fixation in biogeochemical cycling in the subtropical North Pacific Ocean, *Nature*, *388*, 533–538, 1997.

Karl, D., A. Michaels, B. Bergman, D. Capone, E. Carpenter, R. Letelier, F. Lipschultz, H. Paerl, D. Sigman, and L. Stal, Dinitrogen fixation in the world's oceans, *Biogeochemistry*, *57*, 47–98, 2002.

Karsh, K. L., T. W. Trull, M. J. Lourey, and D. M. Sigman, Relationship of nitrogen isotope fractionation to phytoplankton size and iron availability during the Southern Ocean Iron RElease Experiment (SOIREE), *Limnology and Oceanography*, *48*, 1058–1068, 2003.

Kashino, Y., A. Ishida, and Y. Kuroda, Variability of the Mindanao Current: Mooring observation results, *Geophysical research letters*, *32*, 2005.

Kashino, Y., A. Atmadipoera, and Y. Kuroda, Observed features of the Halmahera and Mindanao Eddies, *Journal of Geophysical Research: Oceans*, *118*, 6543–6560, 2013.

Katsura, S., E. Oka, B. Qiu, and N. Schneider, Formation and subduction of North Pacific tropical water and their interannual variability, *Journal of Physical Oceanography*, *43*, 2400–2415, 2013.

Kawabe, M., and S. Fujio, Pacific ocean circulation based on observation, *Journal of Oceanography*, *66*, 389–403, 2010.

Keeling, C. D., The concentration and isotopic abundances of carbon dioxide in rural and marine air, *Geochimica et Cosmochimica Acta*, *24*, 277–298, 1961.

Kérouel, R., and A. Aminot, Fluorometric determination of ammonia in sea and estuarine waters by direct segmented flow analysis, *Marine Chemistry*, *57*, 265–275, 1997.

Kessler, W. S., The circulation of the eastern tropical Pacific: A review, *Progress in Oceanography*, *69*, 181–217, 2006.

Kienast, M., M. F. Lehmann, A. Timmermann, E. Galbraith, T. Bolliet, A. Holbourn, C. Normandeau, and C. Laj, A mid-Holocene transition in the nitrogen dynamics of the western equatorial Pacific: Evidence of a deepening thermocline?, *Geophysical Research Letters*, *35*, 2008.

Kitidis, V., R. C. Upstill-Goddard, and L. G. Anderson, Methane and nitrous oxide in surface water along the North-West Passage, Arctic Ocean, *Marine Chemistry*, *121*, 80–86, 2010.

Klein, B., B. LeBlanc, Z.-P. Mei, R. Beret, J. Michaud, C.-J. Mundy, C. H. von Quillfeldt, M.-È. Garneau, S. Roy, and Y. Gratton, Phytoplankton biomass, production and potential export in the North Water, *Deep Sea Research Part II: Topical Studies in Oceanography*, *49*, 4983–5002, 2002.

Knapp, A. N., P. J. DiFiore, C. Deutsch, D. M. Sigman, and F. Lipschultz, Nitrate isotopic composition between Bermuda and Puerto Rico: Implications for N_2 fixation in the Atlantic Ocean, *Global Biogeochemical Cycles*, *22*, 2008.

Knapp, A. N., K. L. Casciotti, W. M. Berelson, M. G. Prokopenko, and D. G. Capone, Low rates of nitrogen fixation in eastern tropical South Pacific surface waters, *Proceedings of the National Academy of Sciences*, *113*, 4398–4403, 2016.

Knapp, A. N., K. M. McCabe, O. Grosso, N. Leblond, T. Moutin, and S. Bonnet, Distribution and rates of nitrogen fixation in the western tropical South Pacific Ocean constrained by nitrogen isotope budgets, *Biogeosciences*, *15*, 2619–2628, 2018.

Kroopnick, P. M., The distribution of ^{13}C of ΣCO_2 in the world oceans, *Deep Sea Research Part A. Oceanographic Research Papers*, *32*, 57–84, 1985.

Lalande, C., A. Forest, D. G. Barber, Y. Gratton, and L. Fortier, Variability in the annual cycle of vertical particulate organic carbon export on Arctic shelves: Contrasting the Laptev Sea, Northern Baffin Bay and the Beaufort Sea, *Continental Shelf Research*, *29*, 2157–2165, 2009.

Lehmann, M. F., D. M. Sigman, D. C. McCorkle, B. G. Brunelle, S. Hoffmann, M. Kienast, G. Cane, and J. Clement, Origin of the deep Bering Sea nitrate deficit: Constraints from the nitrogen and oxygen isotopic composition of water column nitrate and benthic nitrate fluxes, *Global Biogeochemical Cycles*, *19*, 2005.

Lehmann, M. F., D. M. Sigman, D. C. McCorkle, J. Granger, S. Hoffmann, G. Cane, and B. G. Brunelle, The distribution of nitrate $^{15}N/^{14}N$ in marine sediments and the impact of benthic nitrogen loss on the isotopic composition of oceanic nitrate, *Geochimica et Cosmochimica Acta*, *71*, 5384–5404, 2007.

Lehmann, N., M. Kienast, J. Granger, A. Bourbonnais, M. A. Altabet, and J.-É. Tremblay, Remote western Arctic nutrients fuel remineralization in deep Baffin Bay, *Global Biogeochemical Cycles*, 2019.

Lemon, D. D., and D. B. Fissel, Seasonal variations in currents and water properties in northwestern Baffin Bay, 1978–1979, *Arctic*, *35*, 211–218, 1982.

Lindstrom, E., R. Lukas, R. Fine, E. Firing, S. Godfrey, G. Meyers, and M. Tsuchiya, The western equatorial Pacific Ocean circulation study, *Nature*, *330*, 533–537, 1987.

Liu, Z., and B. Huang, Why is there a tritium maximum in the central equatorial Pacific thermocline?, *Journal of Physical Oceanography*, *28*, 1527–1533, 1998.

Lourey, M. J., T. W. Trull, and D. M. Sigman, Sensitivity of $\delta^{15}N$ of nitrate, surface suspended and deep sinking particulate nitrogen to seasonal nitrate depletion in the Southern Ocean, *Global Biogeochemical Cycles*, *17*, 2003.

Lukas, R., E. Firing, P. Hacker, P. L. Richardson, C. A. Collins, R. Fine, and R. Gammon, Observations of the Mindanao Current during the western equatorial Pacific Ocean circulation study, *Journal of Geophysical Research: Oceans*, *96*, 7089–7104, 1991.

Lukas, R., T. Yamagata, and J. P. McCreary, Pacific lowlatitude western boundary currents and the Indonesian throughflow, *Journal of Geophysical Research: Oceans*, *101*, 12209–12216, 1996.

Macdonald, R. W., E. C. Carmack, F. A. McLaughlin, K. K. Falkner, and J. H. Swift, Connections among ice, runoff and atmospheric forcing in the Beaufort Gyre, *Geophysical Research Letters*, *26*, 2223–2226, 1999.

Mackey, D. J., J. E. O. O'Sullivan, and R. J. Watson, Iron in the western Pacific: A riverine or hydrothermal source for iron in the Equatorial Undercurrent?, *Deep Sea Research Part I: Oceanographic Research Papers*, *49*, 877–893, 2002.

Mackey, M. D., D. J. Mackey, H. W. Higgins, and W. S. W., CHEMTAX - a program for estimating class abundances from chemical markers: Application to HPLC measurements of phytoplankton, *Marine Ecology Progress Series*, *144*, 265–283, 1996.

Marchese, C., C. Albouy, J.-É. Tremblay, D. Dumont, F. D'Ortenzio, S. Vissault, and S. Bélanger, Changes in phytoplankton bloom phenology over the North Water (NOW) polynya: A response to changing environmental conditions, *Polar Biology*, *40*, 1721–1737, 2017.

Marconi, D., M. A. Weigand, P. A. Rafter, M. R. McIlvin, M. Forbes, K. L. Casciotti, and D. M. Sigman, Nitrate isotope distributions on the US GEOTRACES North Atlantic cross-basin section: Signals of polar nitrate sources and low latitude nitrogen cycling, *Marine Chemistry*, *177*, 143–156, 2015.

Mariotti, A., J. C. Germon, P. Hubert, P. Kaiser, R. Letolle, A. Tardieux, and P. Tardieux, Experimental determination of nitrogen kinetic isotope fractionation: Some principles; illustration for the denitrification and nitrification processes, *Plant and Soil*, *62*, 413–430, 1981.

Marson, J. M., P. G. Myers, X. Hu, B. Petrie, K. Azetsu-Scott, and C. M. Lee, Cascading off the West Greenland Shelf: A numerical perspective, *Journal of Geophysical Research: Oceans*, *122*, 5316–5328, 2017.

Martin, J., J.-É. Tremblay, J. Gagnon, G. Tremblay, A. Lapoussière, C. Jose, M. Poulin, M. Gosselin, Y. Gratton, and C. Michel, Prevalence, structure and properties of subsurface chlorophyll maxima in Canadian Arctic waters, *Marine Ecology Progress Series*, *412*, 69–84, 2010.

Martin, J. H., G. A. Knauer, D. M. Karl, and W. W. Broenkow, VERTEX: Carbon cycling in the northeast Pacific, *Deep Sea Research Part A. Oceanographic Research Papers*, *34*, 267–285, 1987.

Martin, T. S., and K. L. Casciotti, Paired N and O isotopic analysis of nitrate and nitrite in the Arabian Sea oxygen deficient zone, *Deep Sea Research Part I: Oceanographic Research Papers*, *121*, 121–131, 2017.

McCartney, M. S., Subantarctic Mode Water, 1977.

McIlvin, M. R., and M. A. Altabet, Chemical conversion of nitrate and nitrite to nitrous oxide for nitrogen and oxygen isotopic analysis in freshwater and seawater, *Analytical Chemistry*, *77*, 5589–5595, 2005.

McIlvin, M. R., and K. L. Casciotti, Technical updates to the bacterial method for nitrate isotopic analyses, *Analytical Chemistry*, *83*, 1850–1856, 2011.

McLaughlin, F., E. Carmack, R. Ingram, W. Williams, and C. Michel, Oceanography of the Northwest Passage, in *The Sea*, edited by A. Robinson and K. Brink, pp. 1211–1242, New York, NY: Harvard university Press, 2004.

McLaughlin, F. A., E. C. Carmack, R. W. Macdonald, and J. K. B. Bishop, Physical and geochemical properties across the Atlantic/Pacific water mass front in the southern Canadian Basin, *Journal of Geophysical Research: Oceans*, *101*, 1183–1197, 1996.

Melet, A., L. Gourdeau, W. S. Kessler, J. Verron, and J.-M. Molines, Thermocline circulation in the Solomon Sea: A modeling study, *Journal of Physical Oceanography*, *40*, 1302–1319, 2010.

Melet, A., J. Verron, L. Gourdeau, and A. Koch-Larrouy, Equatorward pathways of Solomon Sea water masses and their modifications, *Journal of Physical Oceanography*, *41*, 810–826, 2011.

Melling, H., R. A. Lake, D. R. Topham, and D. B. Fissel, Oceanic thermal structure in the western Canadian Arctic, *Continental Shelf Research*, *3*, 233–258, 1984.

Melling, H., Y. Gratton, and G. Ingram, Ocean circulation within the North Water polynya of Baffin Bay, *Atmosphere-Ocean*, *39*, 301–325, 2001.

Michel, C., M. Gosselin, and C. Nozais, Preferential sinking export of biogenic silica during the spring and summer in the North Water polynya (northern Baffin Bay): Temperature or biological control?, *Journal of Geophysical Research*, *107*, 2002.

Michel, C., R. G. Ingram, and L. R. Harris, Variability in oceanographic and ecological processes in the Canadian Arctic Archipelago, *Progress in Oceanography*, *71*, 379–401, 2006.

Mills, M. M., C. Ridame, M. Davey, J. La Roche, and R. J. Gelder, Iron and phosphorus co-limit nitrogen fixation in the eastern tropical North Atlantic, *Nature*, *429*, 292–294, 2004.

Mohn, J., B. Wolf, S. Toyoda, C. T. Lin, M. C. Liang, N. Brüggemann, H. Wissel, A. E. Steiker, J. Dyckmans, L. Szwec, N. E. Ostrom, K. L. Casciotti, M. Forbes, A. Giesemann, R. Well, R. R. Doucett, C. T. Yarnes, A. R. Ridley, J. Kaiser, and N. Yoshida, Interlaboratory assessment of nitrous oxide isotopomer analysis by isotope ratio mass spectrometry and laser spectroscopy: Current status and perspectives, *Rapid Communications in Mass Spectrometry*, *28*, 1995–2007, 2014.

Mohtadi, M., F. Bergmann, R. V. C. Blanquera, J. Buleka, J. W. M. Carag, J. Carriérre-Garwood, E. P. Dassié, A. G. S. Fernando, F. Gernhardt, and H. Ghasemifard, Report and preliminary results of RV SONNE cruise SO-228, Kaohsiung-Townsville, 04.05.2013–23.06.2013, EISPAC-WESTWIND-SIODP, *Tech. rep.*, 2013.

Moore, C. M., M. M. Mills, E. P. Achterberg, R. J. Geider, J. LaRoche, M. I. Lucas, E. L. McDonagh, X. Pan, A. J. Poulton, M. J. A. Rijkenberg, D. J. Suggett, S. J. Ussher, and E. M. S. Woodward, Large-scale distribution of Atlantic nitrogen fixation controlled by iron availability, *Nature Geoscience*, *2*, 867–871, 2009.

Moore, C. M., M. M. Mills, K. R. Arrigo, I. Berman-Frank, L. Bopp, P. W. Boyd, E. D. Galbraith, R. J. Geider, C. Guieu, S. L. Jaccard, T. D. Jickells, J. La Roche, T. M. Lenton, N. M. Mahowald, E. Maranon, I. Marinov, J. K. Moore, T. Nakatsuka, A. Oschlies, M. A. Saito, T. F. Thingstad, A. Tsuda, and O. Ulloa, Processes and patterns of oceanic nutrient limitation, *Nature Geoscience*, *6*, 701–710, 2013.

Moore, J. K., and S. C. Doney, Iron availability limits the ocean nitrogen inventory stabilizing feedbacks between marine denitrification and nitrogen fixation, *Global Biogeochemical Cycles*, *21*, 2007.

Muench, R. D., The Physical Oceanography of the Northern Baffin Bay Region, *Tech. rep.*, 1971.

Münchow, A., K. K. Falkner, and H. Melling, Spatial continuity of measured seawater and tracer fluxes through Nares Strait, a dynamically wide channel bordering the Canadian Archipelago, *Journal of Marine Research*, *65*, 759–788, 2007.

Münchow, A., K. K. Falkner, and H. Melling, Baffin island and west Greenland current systems in northern Baffin bay, *Progress in Oceanography*, *132*, 305–317, 2015.

Murphy, J., and J. P. Riley, A modified single solution method for the determination of phosphate in natural waters, *Analytica Chimica Acta*, *27*, 31–36, 1962.

Naqvi, S. W. A., H. Naik, A. Pratihary, W. D'Souza, P. V. Narvekar, D. A. Jayakumar, A. H. Devol, T. Yoshinari, and T. Saino, Coastal versus open-ocean denitrification in the Arabian Sea, *Biogeosciences*, *3*, 621–633, 2006.

Nevison, C. D., J. H. Butler, and J. W. Elkins, Global distribution of N_2O and the ΔN_2O-AOU yield in the subsurface ocean, *Global Biogeochemical Cycles*, *17*, 2003.

Nguyen, A. T., D. Menemenlis, and R. Kwok, Arctic iceocean simulation with optimized model parameters: Approach and assessment, *Journal of Geophysical Research: Oceans*, *116*, 2011.

Nie, X., S. Gao, F. Wang, and T. Qu, Subduction of North Pacific Tropical Water and its equatorward pathways as shown by a simulated passive tracer, *Journal of Geophysical Research: Oceans*, *121*, 8770–8786, 2016.

Orsi, A. H., T. Whitworth, and W. D. Nowlin, On the meridional extent and fronts of the Antarctic Circumpolar Current, *Deep Sea Research Part I: Oceanographic Research Papers*, *42*, 641–673, 1995.

Ostrom, N. E., M. E. Russ, B. Popp, T. M. Rust, and D. M. Karl, Mechanisms of nitrous oxide production in the subtropical North Pacific based on determinations of the isotopic abundances of nitrous oxide and di-oxygen, *Chemosphere - Global Change Science*, *2*, 281–290, 2000.

Ostrom, N. E., A. Piit, R. L. Sutka, P. H. Ostrom, A. S. Grandy, K. M. Huizinga, and G. P. Robertson, Isotopologue effects during N_2O reduction in soils and in pure cultures of denitrifiers, *Journal of Geophysical Research: Biogeosciences*, *112*, 2007.

Palter, J. B., J. L. Sarmiento, A. Gnanadesikan, J. Simeon, and R. D. Slater, Fueling export production: Nutrient return pathways from the deep ocean and their dependence on the Meridional Overturning Circulation, *Biogeosciences*, *7*, 3549–3568, 2010.

Pennington, J. T., K. L. Mahoney, V. S. Kuwahara, D. D. Kolber, R. Calienes, and F. P. Chavez, Primary production in the eastern tropical Pacific: A review, *Progress in Oceanography*, *69*, 285–317, 2006.

Peters, B. D., P. J. Lam, and K. L. Casciotti, Nitrogen and oxygen isotope measurements of nitrate along the US GEOTRACES Eastern Pacific Zonal Transect (GP16) yield insights into nitrate supply, remineralization, and water mass transport, *Marine Chemistry*, *201*, 137–150, 2018.

Prinsenberg, S. J., and E. B. Bennett, Mixing and transports in Barrow Strait, the central part of the Northwest Passage, *Continental Shelf Research*, *7*, 913–935, 1987.

Prinsenberg, S. J., and J. Hamilton, Monitoring the volume, freshwater and heat fluxes passing through Lancaster sound in the Canadian Arctic Archipelago, *Atmosphere-Ocean*, *43*, 1–22, 2005.

Qu, T., and E. J. Lindstrom, A climatological interpretation of the circulation in the western South Pacific, *Journal of Physical Oceanography*, *32*, 2492–2508, 2002.

Qu, T., E. J. Lindstrom, I. Pacific, E. S. Technology, and N. Aeronautics, Northward intrusion of Antarctic Intermediate Water in the western Pacific, *Journal of Physical Oceanography*, *34*, 2104–2118, 2004.

Qu, T., S. Gao, I. Fukumori, R. A. Fine, and E. J. Lindstrom, Origin and pathway of equatorial 13°C water in the Pacific identified by a simulated passive tracer and its adjoint, *Journal of Physical Oceanography*, *39*, 1836–1853, 2009.

Rafter, P. A., and C. D. Charles, Pleistocene equatorial Pacific dynamics inferred from the zonal asymmetry in sedimentary nitrogen isotopes, *Paleoceanography*, *27*, 2012.

Rafter, P. A., and D. M. Sigman, Spatial distribution and temporal variation of nitrate nitrogen and oxygen isotopes in the upper equatorial Pacific Ocean, *Limnology and Oceanography*, *61*, 14–31, 2016.

Rafter, P. a., D. M. Sigman, C. D. Charles, J. Kaiser, and G. H. Haug, Subsurface tropical Pacific nitrogen isotopic composition of nitrate: Biogeochemical signals and their transport, *Global Biogeochemical Cycles*, *26*, 2012.

Rafter, P. A., P. J. DiFiore, and D. M. Sigman, Coupled nitrate nitrogen and oxygen isotopes and organic matter remineralization in the Southern and Pacific Oceans, *Journal of Geophysical Research: Oceans*, *118*, 4781–4794, 2013.

Raimbault, P., and N. Garcia, Evidence for efficient regenerated production and dinitrogen fixation in nitrogen-deficient waters of the South Pacific Ocean: Impact on new and export production estimates, *Biogeosciences*, *5*, 323–338, 2008.

Randall, K., M. Scarratt, M. Levasseur, S. Michaud, H. Xie, and M. Gosselin, First measurements of nitrous oxide in Arctic sea ice, *Journal of Geophysical Research: Oceans*, *117*, 2012.

Ravishankara, A. R., J. S. Daniel, and R. W. Portmann, Nitrous oxide (N_2O): The dominant ozone-depleting substance emitted in the 21st century, *Science*, *326*, 123–125, 2009.

Redfield, A. C., On the proportions of organic derivatives in sea water and their relation to the composition of plankton, 1934.

Redfield, A. C., B. H. Ketchum, and F. A. Richard, The influence of organisms on the composition of seawater, in *The Sea*, edited by M. N. Hill, vol. 2 ed., pp. 26–77, Wiley-Interscience, New York, New York, 1963.

Reeve, J. L., R. C. Hamme, and W. J. Williams, Tracing denitrification in the Canada Basin: N_2 loss to the atmosphere on the Chukchi Shelf and benthic inputs in deep waters, *Deep Sea Research Part I: Oceanographic Research Papers*, *143*, 127–138, 2019.

Reid, J. L., Intermediate waters of the Pacific Ocean, *John Hopkins Oceanographic Studies*, *2*, 1965.

Reid, J. L., and A. W. Mantyla, On the mid-depth circulation of the North Pacific Ocean, *Journal of Physical Oceanography*, *8*, 946–951, 1978.

Rodgers, K. B., B. Blanke, G. Madec, O. Aumont, P. Ciais, and J. Dutay, Extratropical sources of equatorial Pacific upwelling in an OGCM, *Geophysical research letters*, *30*, 2003.

Roemmich, D., and B. Cornuelle, The subtropical mode waters of the South Pacific Ocean, *Journal of Physical Oceanography*, *22*, 1178–1187, 1992.

Rudels, B., The outflow of polar water through the Arctic Archipelago and the oceanographic conditions in Baffin Bay, *Polar Research*, *4*, 161–180, 1986.

Rudels, B., E. P. Jones, L. G. Anderson, and G. Kattner, On the intermediate depth waters of the Arctic Ocean, 1994.

Rudels, B., L. G. Anderson, and E. P. Jones, Formation and evolution of the surface mixed layer and halocline of the Arctic Ocean, *Journal of Geophysical Research: Oceans*, *101*, 8807–8821, 1996.

Rudels, B., E. P. Jones, U. Schauer, and P. Eriksson, Atlantic sources of the Arctic Ocean surface and halocline waters, *Polar Research*, *23*, 181–208, 2004.

Santoro, A. E., C. Buchwald, M. R. McIlvin, and K. L. Casciotti, Isotopic signature of N_2O produced by marine ammonia-oxidizing archaea, *Science*, *333*, 1282–1285, 2011.

Santoro, A. E., C. M. Sakamoto, J. M. Smith, J. N. Plant, A. L. Gehman, A. Z. Worden, K. S. Johnson, C. A. Francis, and K. L. Casciotti, Measurements of nitrite production in and around the primary nitrite maximum in the central California Current, *Biogeosciences*, *10*, 7395–7410, 2013.

Sarmiento, J. L., N. Gruber, M. A. Brzezinski, and J. P. Dunne, High-latitude controls of thermocline nutrients and low latitude biological productivity, *Nature*, *427*, 56–60, 2004.

Schmidt, H. L., R. A. Werner, N. Yoshida, and R. Well, Is the isotopic composition of nitrous oxide an indicator for its origin from nitrification or denitrification? A theoretical approach from referred data and microbiological and enzyme kinetic aspects, *Rapid Communications in Mass Spectrometry*, *18*, 2036–2040, 2004.

Shadwick, E. H., H. Thomas, Y. Gratton, D. Leong, S. A. Moore, T. Papakyriakou, and A. E. F. Prowe, Export of Pacific carbon through the Arctic Archipelago to the North Atlantic, *Continental Shelf Research*, *31*, 806–816, 2011.

Shimada, K., M. Itoh, S. Nishino, F. McLaughlin, E. Carmack, and A. Proshutinsky, Halocline structure in the Canada Basin of the Arctic Ocean, *Geophysical Research Letters*, *32*, 2005.

Sigman, D. M., and F. Fripiat, Nitrogen isotopes in the Ocean, pp. 263–278, Academic Press, Oxford, 2019.

Sigman, D. M., M. A. Altabet, D. C. McCorkle, R. Francois, and G. Fischer, The δ^{15}N of nitrate in the southern ocean: Consumption of nitrate in surface waters, *Global Biogeochemical Cycles*, *13*, 1149–1166, 1999.

Sigman, D. M., M. A. Altabet, D. C. McCorkle, R. Francois, and G. Fischer, The δ^{15}N of nitrate in the Southern Ocean: Nitrogen cycling and circulation in the ocean interior, *Journal of Geophysical Research: Oceans*, *105*, 19599–19614, 2000.

Sigman, D. M., K. L. Casciotti, M. Andreani, C. Barford, M. Galanter, and J. K. Böhlke, A bacterial method for the nitrogen isotopic analysis of nitrate in seawater and freshwater, *Analytical Chemistry*, *73*, 4145–4153, 2001.

Sigman, D. M., R. Robinson, A. N. Knapp, A. Van Geen, D. C. McCorkle, J. A. Brandes, and R. C. Thunell, Distinguishing between water column and sedimentary denitrification in the Santa Barbara Basin using the stable isotopes of nitrate, *Geochemistry, Geophysics, Geosystems*, *4*, 2003.

Sigman, D. M., J. Granger, P. J. DiFiore, M. M. Lehmann, R. Ho, G. Cane, and A. van Geen, Coupled nitrogen and oxygen isotope measurements of nitrate along the eastern North Pacific margin, *Global Biogeochemical Cycles*, *19*, 2005.

Sigman, D. M., P. J. DiFiore, M. P. Hain, C. Deutsch, and D. M. Karl, Sinking organic matter spreads the nitrogen isotope signal of pelagic denitrification in the North Pacific, *Geophysical Research Letters*, *36*, 2009a.

Sigman, D. M., P. J. DiFiore, M. P. Hain, C. Deutsch, Y. Wang, D. M. Karl, A. N. Knapp, M. F. Lehmann, and S. Pantoja, The dual isotopes of deep nitrate as a constraint on the cycle and budget of oceanic fixed nitrogen, *Deep Sea Research Part I: Oceanographic Research Papers*, *56*, 1419–1439, 2009b.

Sipler, R. E., D. Gong, S. E. Baer, M. P. Sanderson, Q. N. Roberts, M. R. Mulholland, and D. A. Bronk, Preliminary estimates of the contribution of Arctic nitrogen fixation to the global nitrogen budget, *Limnology and Oceanography Letters*, *2*, 159–166, 2017.

Slemons, L. O., J. W. Murray, J. Resing, B. Paul, and P. Dutrieux, Western Pacific coastal sources of iron, manganese, and aluminum to the Equatorial Undercurrent, *Global Biogeochemical Cycles*, *24*, 2010.

Sloyan, B. M., L. D. Talley, T. K. Chereskin, R. Fine, and J. Holte, Antarctic Intermediate Water and Subantarctic Mode Water formation in the southeast Pacific: The role of turbulent mixing, *Journal of physical oceanography*, *40*, 1558–1574, 2010.

Smart, S. M., S. E. Fawcett, S. J. Thomalla, M. A. Weigand, C. J. C. Reason, and D. M. Sigman, Isotopic evidence for nitrification in the Antarctic winter mixed layer, *Global Biogeochemical Cycles*, *29*, 427–445, 2015.

Smith, R. L., Efficient Monte Carlo procedures for generating points uniformly distributed over bounded regions, *Operations Research*, *32*, 1296–1308, 1984.

Sokolov, S., and S. Rintoul, Circulation and water masses of the southwest Pacific: WOCE Section P11, Papua New Guinea to Tasmania, *Journal of Marine Research*, *58*, 223–268, 2000.

Sprintall, J., A. L. Gordon, A. Koch-Larrouy, T. Lee, J. T. Potemra, K. Pujiana, and S. E. Wijffels, The Indonesian seas and their role in the coupled ocean–climate system, *Nature Geoscience*, *7*, 487–492, 2014.

Steele, M., J. Morison, W. Ermold, I. Rigor, M. Ortmeyer, and K. Shimada, Circulation of summer Pacific halocline water in the Arctic Ocean, *Journal of Geophysical Research: Oceans*, *109*, 2004.

Strickland, J. D. H., and T. R. Parsons, A practical handbook of seawater analysis, *Fisheries Research Board of Canada, Ottawa*, 1972.

Sutka, R. L., N. E. Ostrom, P. H. Ostrom, J. A. Breznak, H. Gandhi, A. J. Pitt, and F. Li, Distinguishing nitrous oxide production from nitrification and denitrification on the basis of isotopomer abundances, *Applied and Environmental Microbiology*, *72*, 638–644, 2006.

Talley, L. D., Distribution and formation of North Pacific Intermediate Water, 1993.

Talley, L. D., Antarctic Intermediate Water in the South Atlantic, in *The South Atlantic*, pp. 219–238, Springer, 1996.

Tan, F. C., and P. M. Strain, The distribution of sea ice meltwater in the eastern Canadian Arctic, *Journal of Geophysical Research: Oceans*, *85*, 1925–1932, 1980.

Tanaka, T., L. Guo, C. Deal, N. Tanaka, T. Whitledge, and A. Murata, N deficiency in a well-oxygenated cold bottom water over the Bering Sea shelf: influence of sedimentary denitrification, *Continental Shelf Research*, *24*, 1271–1283, 2004.

Tang, C. C. L., C. K. Ross, T. Yao, B. Petrie, B. M. DeTracey, and E. Dunlap, The circulation, water masses and sea-ice of Baffin Bay, *Progress in Oceanography*, *63*, 183–228, 2004.

Timmermans, M.-L., A. Proshutinsky, E. Golubeva, J. M. Jackson, R. Krishfield, M. McCall, G. Platov, J. Toole, W. Williams, T. Kikuchi, and S. Nishino, Mechanisms of Pacific Summer Water variability in the Arctic's Central Canada Basin, *Journal of Geophysical Research: Oceans*, *119*, 7523–7548, 2014.

Toggweiler, J. R., K. Dixon, and W. S. Broecker, The Peru upwelling and the ventilation of the South Pacific thermocline, *Journal of Geophysical Research: Oceans*, *96*, 20467–20497, 1991.

Tomczak, M., and J. S. Godfrey, *Regional oceanography: An introduction*, Pergamon, Tarrytown, N.Y., 1994.

Toole, J. M., E. Zou, and R. C. Millard, On the circulation of the upper waters in the western equatorial Pacific Ocean, *Deep Sea Research Part A. Oceanographic Research Papers*, *35*, 1451–1482, 1988.

Top, Z., W. B. Clarke, W. C. Eismont, and E. P. Jones, Radiogenic helium in Baffin Bay bottom water, *JOURNAL OF MARINE RESEARCH*, *38*, 435–452, 1980.

Torres-Valdés, S., T. Tsubouchi, S. Bacon, A. C. NaveiraGarabato, R. Sanders, F. A. McLaughlin, B. Petrie, G. Kattner, K. AzetsuScott, and T. E. Whitledge, Export of nutrients from the Arctic Ocean, *Journal of Geophysical Research: Oceans*, *118*, 1625–1644, 2013.

Toyoda, S., and N. Yoshida, Determination of nitrogen isotopomers of nitrous oxide on a modified isotope ratio mass spectrometer, *Analytical Chemistry*, *71*, 4711–4718, 1999.

Toyoda, S., N. Yoshida, T. Miwa, Y. Matsui, H. Yamagishi, U. Tsunogai, Y. Nojiri, and N. Tsurushima, Production mechanism and global budget of N_2O inferred from its isotopomers in the western North Pacific, *Geophysical research letters*, *29*, 2002.

Toyoda, S., H. Mutobe, H. Yamagishi, N. Yoshida, and Y. Tanji, Fractionation of N_2O isotopomers during production by denitrifier, *Soil Biology and Biochemistry*, *37*, 1535–1545, 2005.

Toyoda, S., N. Kuroki, N. Yoshida, K. Ishijima, Y. Tohjima, and T. Machida, Decadal time series of tropospheric abundance of N_2O isotopomers and isotopologues in the northern hemisphere obtained by the longterm observation at Hateruma Island, Japan, *Journal of Geophysical Research: Atmospheres*, *118*, 3369–3381, 2013.

Tremblay, J.-É., Y. Gratton, E. C. Carmack, C. D. Payne, and N. M. Price, Impact of the large-scale Arctic circulation and the North Water polynya on nutrient inventories in Baffin Bay, *Journal of Geophysical Research*, *107*, 2002.

Tremblay, J.-É., C. Michel, K. A. Hobson, M. Gosselin, and N. M. Price, Bloom dynamics in early opening waters of the Arctic Ocean, *Limnology and Oceanography*, *51*, 900–912, 2006.

Tremblay, J.-É., K. Simpson, J. Martin, L. Miller, Y. Gratton, D. Barber, and N. M. Price, Vertical stability and the annual dynamics of nutrients and chlorophyll fluorescence in the coastal, southeast Beaufort Sea, *Journal of Geophysical Research: Oceans*, *113*, 2008.

Tremblay, J.-É., L. G. Anderson, P. Matrai, P. Coupel, S. Bélanger, C. Michel, and M. Reigstad, Global and regional drivers of nutrient supply, primary production and CO_2 drawdown in the changing Arctic Ocean, *Progress in Oceanography*, *139*, 171–196, 2015.

Tsuchiya, M., Upper waters of the intertropical Pacific Ocean, *Johns Hopkins Press, Baltimore*, *4*, 50, 1968.

Tsuchiya, M., R. Lukas, R. A. Fine, E. Firing, and E. Lindstrom, Source waters of the Pacific Equatorial Undercurrent, *Progress in Oceanography*, *23*, 101–147, 1989.

Tuerena, R. E., R. S. Ganeshram, W. Geibert, A. E. Fallick, J. Dougans, A. Tait, S. F. Henley, and E. M. S. Woodward, Nutrient cycling in the Atlantic basin: The evolution of nitrate isotope signatures in water masses, *Global Biogeochemical Cycles*, *29*, 1830–1844, 2015.

Ueki, I., Y. Kashino, and Y. Kuroda, Observation of current variations off the New Guinea coast including the 1997–1998 El Niño period and their relationship with Sverdrup transport, *Journal of Geophysical Research: Oceans*, *108*, 2003.

Van den Meersche, K., K. Soetaert, and D. Van Oevelen, xsample(): An R function for sampling linear inverse problems, *Journal of Statistical Software*, *30*, 2009.

Voss, M., J. W. Dippner, and J. P. Montoya, Nitrogen isotope patterns in the oxygen-deficient waters of the Eastern Tropical North Pacific Ocean, *Deep Sea Research Part I: Oceanographic Research Papers*, *48*, 1905–1921, 2001.

Wallace, D. W. R., A study of the ventilation of Arctic waters using chlorofluoromethanes as tracers, Ph.D. thesis, Dalhousie University, Halifax NS, Canada, 1985.

Wallace, D. W. R., R. M. Moore, and E. Jones, Ventilation of the Arctic Ocean cold halocline: rates of diapycnal and isopycnal transport, oxygen utilization and primary production inferred using chlorofluoromethane distributions, *Deep Sea Research Part A. Oceanographic Research Papers*, *34*, 1957–1979, 1987.

Ward, B. B., Nitrification in marine systems, in *Nitrogen in the Marine Environment*, edited by D. G. Capone, D. A. Bronk, M. R. Mulholland, and E. J. Carpenter, pp. 199–261, Academic Press, San Diego, 2008.

Weigand, M. A., J. Foriel, B. Barnett, S. Oleynik, and D. M. Sigman, Updates to instrumentation and protocols for isotopic analysis of nitrate by the denitrifier method, *Rapid Communications in Mass Spectrometry*, pp. 1365–1383, 2016.

Weiss, R. F., and B. A. Price, Nitrous oxide solubility in water and seawater, *Marine Chemistry*, *8*, 347–359, 1980.

Westley, M. B., B. N. Popp, and T. M. Rust, The calibration of the intramolecular nitrogen isotope distribution in nitrous oxide measured by isotope ratio mass spectrometry, *Rapid Communications in Mass Spectrometry*, *21*, 391–405, 2007.

Wijffels, S. E., E. Firing, and H. Bryden, Direct observations of the Ekman balance at 10°N in the Pacific, *Journal of Physical Oceanography*, *24*, 1666–1679, 1994.

Wijffels, S. E., J. M. Toole, H. H. L. Bryden, R. A. Fine, W. J. Jenkins, and J. L. Bullister, The water masses and circulation at 10°N in the Pacific, *Deep sea research part I: Oceanographic Research Papers*, *43*, 501–544, 1996.

Wu, Y., C. Tang, and C. Hannah, The circulation of eastern Canadian seas, *Progress in Oceanography*, *106*, 28–48, 2012.

Wyrtki, K., An estimate of equatorial upwelling in the Pacific, *Journal of Physical Oceanography*, *11*, 1205–1214, 1981.

Yamagishi, H., N. Yoshida, S. Toyoda, B. N. Popp, M. B. Westley, and S. Watanabe, Contributions of denitrification and mixing on the distribution of nitrous oxide in the North Pacific, *Geophysical Research Letters*, *32*, 2005.

Yamamoto-Kawai, M., E. Carmack, and F. McLaughlin, Nitrogen balance and Arctic throughflow, *Nature*, *443*, 43, 2006.

Yamamoto-Kawai, M., F. A. McLaughlin, E. C. Carmack, S. Nishino, and K. Shimada, Freshwater budget of the Canada Basin, Arctic Ocean, from salinity, δ^{18}O, and nutrients, *Journal of Geophysical Research: Oceans*, *113*, 2008.

Yamamoto-Kawai, M., F. A. McLaughlin, E. C. Carmack, S. Nishino, K. Shimada, and N. Kurita, Surface freshening of the Canada Basin, 2003–2007: River runoff versus sea ice meltwater, *Journal of Geophysical Research: Oceans*, *114*, 2003–2007, 2009.

Yashayaev, I., Hydrographic changes in the Labrador Sea, 1960–2005, *Progress in Oceanography*, *73*, 242–276, 2007.

Yoshida, N., and S. Toyoda, Constraining the atmospheric N_2O budget from intramolecular site preference in N_2O isotopomers, *Nature*, *405*, 330–334, 2000.

Yoshikawa, C., T. Nakatsuka, and H. Kawahata, Transition of lowsalinity water in the Western Pacific Warm Pool recorded in the nitrogen isotopic ratios of settling particles, *Geophysical research letters*, *32*, 2005.

Yoshikawa, C., T. Nakatsuka, and M. Wakatsuchi, Distribution of N* in the Sea of Okhotsk and its use as a biogeochemical tracer of the Okhotsk Sea Intermediate Water formation process, *Journal of Marine Systems*, *63*, 49–62, 2006.

Yoshikawa, C., A. Makabe, T. Shiozaki, S. Toyoda, O. Yoshida, K. Furuya, and N. Yoshida, Nitrogen isotope ratios of nitrate and N* anomalies in the subtropical South Pacific, *Geochemistry, Geophysics, Geosystems*, *16*, 1439–1448, 2015.

Zhan, L., L. Chen, J. Zhang, and Y. Li, A vertical gradient of nitrous oxide below the subsurface of the Canada Basin and its formation mechanisms, *Journal of Geophysical Research: Oceans*, *120*, 2401–2411, 2015.

Zhang, J., L. Zhan, L. Chen, Y. Li, and J. Chen, Coexistence of nitrous oxide undersaturation and oversaturation in the surface and subsurface of the western Arctic Ocean, *Journal of Geophysical Research: Oceans*, *120*, 8392–8401, 2015.

Zweng, M. M., and A. Münchow, Warming and freshening of Baffin Bay, 1916–2003, *Journal of Geophysical Research: Oceans*, *111*, 1–13, 2006.